

Copyright
by
Baris Binici
2003

The Dissertation Committee for Baris Binici certifies that this is the
approved version of the following dissertation:

PUNCHING SHEAR STRENGTHENING OF REINFORCED
CONCRETE SLABS USING FIBER REINFORCED POLYMERS

Committee:

Oguzhan Bayrak, Supervisor

Sharon L. Wood

James O. Jirsa

Michael E. Kreger

Loukas F. Kallivokas

Eric B. Becker

Jack P. Moehle

PUNCHING SHEAR STRENGTHENING OF REINFORCED
CONCRETE SLABS USING FIBER REINFORCED POLYMERS

by

BARIS BINICI, B.Sc., M.S.E.

DISSERTATION

Presented to the Faculty of Graduate School of

The University of Texas at Austin

in Partial Fulfillment

of the Requirements

for the degree of

DOCTOR OF PHILOSOPHY

The University of Texas at Austin

December, 2003

Acknowledgements

The acknowledgments here are for those who made it possible for me to pursue what I wanted and those who helped me to take a step at this endless learning journey.

I am most thankful to my parents, Nihal and Rahmi Binici for their never ending support and their comforting hearts, in which I always find my presence. I thank my sister, Eda, her husband Engin for always remembering me and reminding my only nephew, Can, of my existence.

I would like to thank my supervisor Dr. Oguzhan Bayrak, for his continuous encouragement and support throughout this research. For me, he will always be an example of a passionate engineer and researcher who values practical solutions greatly.

I would like to thank Drs. Wood, Jirsa, Kreger, Kallivokas, Becker and Moehle for serving on my dissertation committee. A detailed review of the dissertation by Dr. Wood is greatly appreciated. Suggestions by Dr. Kreger at various stages of the study and his keen insight on lectures and discussions are acknowledged. Invaluable comments from Dr. Jirsa were very helpful in improving the final version. Advice provided on various issues by Dr. Kallivokas, his friendship and eagerness to help will never be forgotten.

Technical assistance provided by the Ferguson Structural Engineering Laboratory staff is greatly acknowledged.

I would like to thank Dr Wheat for providing me with teaching assistantships for a number of times when I was at need. I am glad to have known him both as a professor and as a great human being.

I would also like to thank other members of the faculty who have contributed to this study in various ways; in lectures and suggestions. These inspiring people make this institution a great place.

Last but not the least; to my wife Canan, my love, my friend, my shoulder to cry on and my companion in this long journey. In a sense, the completion of this work is an evidence of our success as unity. Yes, it is dedicated to you.

Punching Shear Strengthening of Reinforced Concrete Slabs Using Fiber Reinforced Polymers

Publication No. _____

Baris Binici, Ph.D
The University of Texas at Austin, 2003

Supervisor: Oguzhan Bayrak

Reinforced concrete flat plates are widely used structural systems. The absence of beams makes these systems attractive due to advantages such as easier formwork, shorter construction time, less total building height with more clear space, and architectural flexibility. Changes in the force or displacement demands imposed by gravity loads, wind, and earthquakes necessitate the upgrade of slab-column connections that are not provided with shear reinforcement and those that do not comply with integrity steel requirements. This research introduces an upgrading scheme for slab-column connections using externally installed CFRP stirrups. Behavior of 15 slab specimens subjected to shear and combined shear and moment transfer was studied experimentally. Various configurations of strengthening, amounts and details of CFRP installation were investigated. The effectiveness of proposed details of external CFRP reinforcement was evaluated. Simple mechanical models were used to predict punching shear strength, post punching resistance and anchorage strength of CFRPs bonded to concrete. Finite element analyses were conducted to provide further insight to the mechanics of load transfer, cracking and local stress conditions. Proposed upgrade method proved to be successful in strengthening the slab-column connections. Based on the results of the experimental and analytical studies, a procedure, which makes use of punching shear strength provisions of ACI 318-02, was proposed for upgrade design of slab-column connections.

Table of Contents

CHAPTER 1 Introduction	1
1.1 GENERAL	1
1.2 MOTIVATION	5
1.3 OBJECTIVES AND SCOPE	6
1.4 BACKGROUND	7
1.4.1 Research on Punching Shear Resistance.....	8
1.4.1.1 Elstner and Hognestad (1956).....	8
1.4.1.2 Kinnunen and Nylander (1960)	9
1.4.1.3 Moe (1961).....	11
1.4.1.4 Criswell and Hawkins (1974)	13
1.4.1.5 Ghali et. al. (1982, 1992, 1995)	14
1.4.1.6 Broms (1990)	17
1.4.1.7 Menetrey (1996).....	18
1.4.1.8 Theodorakopoulos and Swamy (2002).....	20
1.4.2 Research on Gravity and Lateral Load Behavior of Flat Plates.....	22
1.4.3 Research on Strengthening for Punching Shear Resistance	23
1.4.3.1 Martinez et. al. (1994).....	23
1.4.3.2 Farhey et. al. (1995).....	25
1.4.3.3 Hassanzadeh and Sundqvist (1998)	26
1.4.3.4 Ebead and Marzouk (2002).....	27
1.4.4 Building Code Approaches for Punching Shear Design.....	29
1.4.4.1 ACI 318-02	29
1.4.4.2 Canadian and New Zealand Codes	34
1.4.4.3 European Codes	35
1.5 ORGANIZATION OF DISSERTATION.....	38
CHAPTER 2 Punching Shear Strengthening of Concentrically Loaded RC Flat Plates	39

2.1	GENERAL.....	39
2.2	CHOICE OF STRENGTHENING MATERIAL.....	39
2.3	DESIGN OF TEST SPECIMENS	41
2.4	MATERIAL PROPERTIES	50
2.5	STRENGTHENING METHOD.....	51
2.6	SPECIMEN DETAILS AND TEST PROCEDURE	56
2.6.1	Specimen Details	56
2.6.2	Instrumentation and Testing	58
2.7	TEST RESULTS.....	60
2.7.1	Load Deformation Results	61
2.7.2	Strain Measurements.....	70
2.7.2.1	Steel Strains	70
2.7.2.2	Concrete Strains	78
2.7.2.3	FRP Strains	79
2.7.3	Crack Patterns and Failure Modes	89
2.8	DISCUSSION OF TEST RESULTS.....	95
2.8.1	Stiffness, Strength and Ductility	95
2.8.2	FRP Amount, Efficiency and Detailing.....	98
2.8.3	Effectiveness of Diagonal Stirrups at Outermost CFRP Perimeters.....	103
2.8.4	Anchorage of CFRPs used as Shear Reinforcement.....	107
2.8.4.1	Anchorage Strength of CFRPs bonded to Concrete: Experiments	108
2.8.4.2	Anchorage Strength of CFRPs bonded to Concrete: Analysis	116
2.8.5	Capacity Loss at Punching Failure	122
2.8.6	A Simple Model to Calculate Punching Shear Capacity	129
2.8.6.1	Model by Theodorakopoulos and Swamy (2002).....	129
2.8.6.2	Modified Model	133
2.8.6.3	Comparison of Computed Capacities with Test Results.....	136
CHAPTER 3 Punching Shear Strengthening of Eccentrically Loaded RC Flat Plates		
.....		139

3.1	GENERAL.....	139
3.2	TEST SPECIMENS.....	139
3.3	INSTRUMENTATION AND TESTING.....	143
3.4	TEST RESULTS.....	145
3.4.1	Load-Deformation Results.....	145
3.4.2	Concrete and Steel Strain Measurements.....	149
3.4.3	Crack Patterns and Failure Modes.....	153
3.5	DISCUSSION OF TEST RESULTS.....	156
3.5.1	Stiffness.....	156
3.5.2	Strength and Ductility.....	160
3.6	UNBALANCED MOMENT DEMANDS AT INTERIOR SLAB-COLUMN CONNECTIONS DUE TO GRAVITY LOADS.....	163
3.7	SEISMIC UPGRADE OF SLAB-COLUMN CONNECTIONS.....	170
	CHAPTER 4 Finite Element Analyses of Concentrically Loaded Flat Plates	172
4.1	GENERAL.....	172
4.2	DESCRIPTION OF THE FINITE ELEMENT MODEL.....	173
4.2.1	Concrete Constitutive Model.....	174
4.2.2	Selection of Constitutive Model Parameters for Concrete.....	182
4.2.3	Steel and CFRP Constitutive Model.....	185
4.2.4	Modeling and Analysis Procedure.....	186
4.3	ANALYSIS OF CONCENTRICALLY LOADED RC FLAT PLATES WITHOUT SHEAR REINFORCEMENT.....	189
4.3.1	Control Specimen.....	190
4.3.2	Parametric Studies.....	198
4.3.2.1	Effect of Longitudinal Reinforcement Ratio.....	199
4.3.2.2	Effect of Concrete Tensile Strength.....	200
4.3.2.3	Effect of Concrete Compressive Strength.....	202
4.4	ANALYSIS OF CONCENTRICALLY LOADED RC FLAT PLATES STRENGTHENED WITH CFRP.....	203

4.4.1	Comparisons of Analysis Results with Experimental Results	204
4.4.2	Cracking and Strengthening Mechanism	208
4.4.3	Principal Stresses and Failure Surfaces	212
CHAPTER 5 Evaluation of Code Requirements and Proposed Design Procedure		217
5.1	GENERAL	217
5.2	EXAMINATION OF CODE PROCEDURES AND DESIGN	217
5.2.1	Pure Shear Transfer	217
5.2.1.1	ACI 318-02	218
5.2.1.2	CEB-FIP Model Code 90	219
5.2.1.3	CSA-A23.3-94	220
5.2.1.4	Examination of Code Provisions	222
5.2.1.5	Proposed Design Procedure Using ACI 318-02 Provisions	229
5.2.1.6	Other Considerations	237
5.2.2	Combined Shear and Moment Transfer	240
5.2.2.1	ACI 318-02 Provisions	241
5.2.2.2	Computed and Experimental Capacities	244
5.2.2.3	Proposed Design Procedure Using ACI 318-02 Provisions	245
CHAPTER 6 Summary and Conclusions		248
6.1	GENERAL	248
6.2	SUMMARY	248
6.3	CONCLUSIONS	250
6.4	RECOMMENDATIONS FOR FUTURE RESEARCH	253
APPENDIX A		255
APPENDIX B		256
APPENDIX C		265
APPENDIX D		267
APPENDIX E		269
REFERENCES		271
VITA		284

CHAPTER 1

Introduction

1.1 GENERAL

Reinforced concrete flat plates consist of uniform thickness slabs supported directly on columns. The absence of beams makes these systems attractive due to advantages such as economical formwork, shorter construction time, less total building height with more clear space and architectural flexibility.

The greatest disadvantage of flat plate systems is the risk of brittle punching failure at the slab-column connection due to transfer of shear and unbalanced moment. Vertical loads acting on the floor system and moments transferred from the columns may create excessive shear stresses around the slab-column connection. Unbalanced moments naturally occur at corner and edge slab-column connections. They may also occur at interior connections with unequal vertical loads on adjacent spans, or at any connection due to combined vertical and lateral forces as a result of wind effects or earthquake excitations.

Punching shear failure is defined as the local brittle failure of the slab-column connection in which the column together with a portion of the slab is pushed through the slab. Figure 1.1 shows the elevation view of a slab-column connection transferring shear due to gravity loads. When the slab-column connection is loaded up to its load carrying capacity, the following sequence of events is observed (as reported in CEB-FIP 1985): Flexural cracks are observed as soon as the cracking moment per unit width is reached around the loading area. An inclined shear crack, which makes an angle of 20 to 35° with the

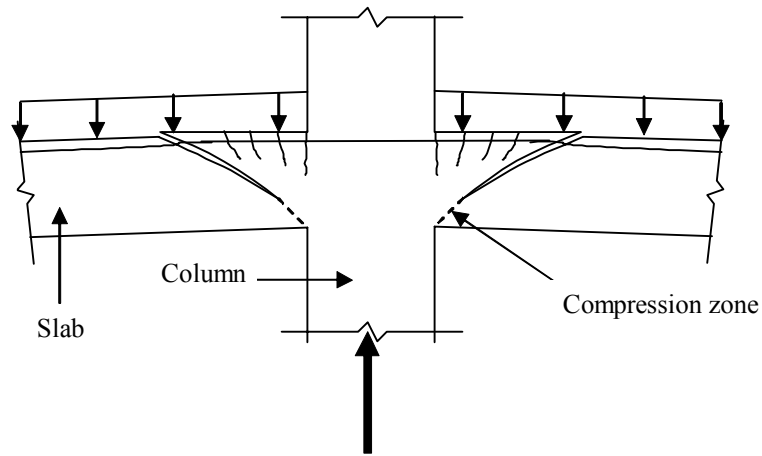


Figure 1.1 Punching Shear Failure Mechanism

tension face of the slab, starts to develop at about 60 to 70% of the ultimate load. The inclined crack is in the form of a truncated cone for the circular columns and pyramid for rectangular columns. At this stage shear is carried by the compression zone and along the surface of the inclined crack by friction and aggregate interlock. The slab-column connection is stable at this point and it can be loaded and unloaded without changing the load carrying capacity. Yielding in the longitudinal reinforcement initiates at the face of the connection and extends along the span. The extent of yielding depends on the reinforcement ratio. As the width of the inclined crack increases, the effects of aggregate interlock and friction decrease whereas the contribution from the dowel action increases. Failure occurs without any warning when the inclined crack tip penetrates into the weakened compression zone.

The sudden and brittle nature of this phenomenon resulted in the progressive collapse of a number of buildings. Sampoong Department Store collapsed in South Korea in 1994 (Figure 1.2). The building was a 5-story flat plate building. The forensic investigations showed that the failure initiated due to distress in the 5th floor slab-column connections after the change of the restaurant

area to a swimming pool (Gardner et. al. 2002). It was also reported that the effects of unbalanced moments in the slab-column connections were neglected during the design of the building. Additional unbalanced moments were created at interior slab column connections when the location of a cooling tower was changed. Noncompliance with the design documents, such as use of concrete with a lower compressive strength, misplacement of longitudinal reinforcement resulting in smaller effective depth, and lack of integrity steel caused significant decreases in the load carrying capacity of individual connections.

Many flat slab structures collapsed in past earthquakes. Punching failures are 44 waffle-slab buildings in the 1985 Mexico City earthquake (Rosenblueth and Meli 1986), Baybridge Office Plaza in the 1989 Loma Prieta earthquake (Mitchell et. al. 1990), Bullocks Department Store in the 1994 Northridge earthquake (Mitchell et. al. 1995) (Figure 1.3). Flat plate systems are allowed in low seismic zones as the primary lateral force resisting system. In high seismic



Figure 1.2 Sampoong Department Store Collapse (Gardner et. al. 2002)



a) Bullocks Department Store- Northridge



b) Waffle Slab- Mexico City

Figure 1.3 Flat Slab Failures due to Earthquakes

zones, they are designed only to carry gravity loads. But, the slab-column connections must possess enough deformability to sustain the deformations imposed by the earthquakes. The failures mentioned above occurred due to the lack of ductility and inadequate post-punching strength of the slab-column connections, which led to the progressive collapse of the structural system.

Flat plate structural systems are one of the most vulnerable systems that are susceptible to damage and collapse unless they are designed and detailed properly. Further problems arise for the existing slab-column connections especially in existing flat plate systems built in the 1960s and 1970s. The poor structural performance expected in these existing structures make them prime candidates for rehabilitation.

1.2 MOTIVATION

Existing flat plate structural systems may require rehabilitation for the following reasons:

- i) *Changes in force and/or displacement demands on the structure and individual components:* The structural system designed and detailed for prescribed forces using a given code at a given time may be subjected to forces and displacements higher than those considered in the initial design during its lifetime. Examples can be the changes in use of the whole or a part of the structural system or changes in the prescribed design forces due to an increased seismicity of the area. These and similar situations increase either strength or deformation demands on the structural elements.
- ii) *Changes in capacity requirements of the structural elements:* There may be situations where the intended design capacity of a structural member may be insufficient. A recent study might have pointed out the fact that the old design and construction practice may have led to unsafe designs (i.e. lack of integrity steel, lack of shear reinforcement etc.). In addition, time dependent deterioration in the structural elements may result in reduced capacities. The particular examples for existing flat plate systems are non-ductile slab-column connections designed only to carry vertical loads and slab-column connections that are deficient with regard to continuous bottom bar requirements that were introduced in the late 1980s.

There has been a tremendous amount of research that has focused on strengthening of existing structural components in the past. However, the evaluation and strengthening of slab-column connections for punching shear resistance in existing flat plate structural systems has not been studied

extensively. Therefore there is a need to establish an effective, reliable and economical strengthening/upgrade method for slab-column connections. The success of the upgrade method should be tested experimentally and it should address various loading conditions that can be encountered in actual systems.

1.3 OBJECTIVES AND SCOPE

The objectives of this research are as follows:

- To develop a reliable and efficient strengthening/upgrade procedure for existing slab-column connections to increase punching shear strength, using fiber reinforced polymers as externally installed stirrups,
- To investigate the effectiveness of the proposed strengthening method for shear and shear combined with unbalanced moment,
- To investigate the shear strengthening mechanism,
- To study the local behavior of the slab-column connections before and after strengthening using simple physical models and numerical simulations,
- To study the post-punching (residual) capacity of the slab-column connections,
- To develop design provisions for upgrading connections and guidelines for shear strengthening.

To achieve these objectives, a combined experimental and analytical study was conducted in Ferguson Structural Engineering Laboratory at The University of Texas at Austin. The experimental program was divided into two phases. Phase 1 consisted of 11-full scale, reinforced concrete flat plate specimens loaded concentrically to simulate pure shear transfer. Phase 2 consisted of 4-half scale, reinforced concrete flat plates loaded eccentrically to simulate shear and moment transfer at the slab-column connections. All of the specimens were

isolated interior slab-column connections without any in-plane or rotational boundary restraints. Only square columns were considered throughout the experimental study. Fiber reinforced polymers (FRPs) were used as the strengthening material for all of the specimens. Three-dimensional nonlinear finite element analyses were performed to simulate the behavior of the concentrically loaded test specimens to understand the local behavior and gain insight about the strengthening mechanism.

1.4 BACKGROUND

There has been a vast amount of experimental and analytical research carried out since the 1950s to understand punching shear resistance of slab-column connections. Four state-of-the-art documents, Shear in Concrete (ACI 1974), Punching Shear in Reinforced Concrete (CEB-FIP 1985), Shear Reinforcement for Slabs (ACI-ASCE-421 1999) and Punching of Structural Concrete Slabs (CEB-FIP 2001) were published on shear in concrete slabs in the last three decades. These documents included the comparisons of various mechanical and numerical models with the experimental results, and different code approaches for design. Repetition of the discussions in these documents is not the intent of this section, important points in these studies are highlighted as they relate to this study.

Although studies on punching shear strength have been conducted for more than 50 years, there is still not a consensus on local failure phenomena and design approaches. This section summarizes the benchmark studies on punching shear resistance and strengthening studies and differing views of researchers and various code approaches.

1.4.1 Research on Punching Shear Resistance

1.4.1.1 *Elstner and Hognestad (1956)*

One of the first experimental studies on punching shear strength of reinforced concrete slabs was carried out by Elstner and Hognestad (1956). The experimental study involved testing of thirty-nine, 6-ft square slabs that were 6-in. thick. The slabs were simply supported at the edges and loaded through a centrally located column stub. Test variables were size of the loading plate (10 and 14 in.), concrete strength (2000 to 7000 psi), support conditions (two sides versus four sides simply supported), and amount of longitudinal reinforcement ratio (0.5 to 3.7%). In addition, two of the specimens were loaded with eccentricities equal to half the size of the loading plate.

Shear and flexure were considered to be a combined problem for slabs subjected to concentrated loads in this study. Based on the experimental results, the following expression was proposed to compute the punching shear strength of slabs:

$$\frac{V_u}{7/8 bd} = 333 \text{ psi} + \frac{0.046 f_c'}{\phi} \quad (1.1)$$

where V_u is the ultimate shear strength of the slab, b is the perimeter of the loaded area, f_c' is the concrete compressive strength in psi, and ϕ is the ratio of the shear capacity to flexural capacity from yield line analysis. It can be observed that the shear strength was assumed to be proportional to f_c' , implying that punching failure is a compression-induced failure.

Furthermore, it was found that concentration of 50% of tension reinforcement directly over the column did not increase the shear capacity of the slab-column connection. It is also interesting that the eccentricity applied and existence of compression reinforcement had no significant effect on the ultimate

shear strength of the test specimens. For slabs that failed in flexure, the measured ultimate capacities were about 10 to 20% greater than those predicted by the yield line theory, and this difference was attributed to membrane action and strain hardening of the reinforcement at large deformations.

The study summarized above presents a large database of test results for rectangular slabs subjected to concentric loads. Effects of parameters such as reinforcement ratio, column size, and concrete strength on punching shear resistance were studied and reported. Elstner and Hognestad (1956) showed that the simple test setup used in the experimental program of their study can be effectively used to investigate the punching shear strength of slabs subjected to concentrated loads or column reactions. In fact, a similar test setup is used in this study to investigate punching shear resistance of the strengthened slabs (Chapter 2). In addition, strength results from their tests are used for evaluating the code expressions in Chapter 5.

1.4.1.2 Kinnunen and Nylander (1960)

The first mechanical model to estimate punching shear capacity considering geometry and equilibrium was proposed by Kinnunen and Nylander (1960). The model was based on the test results of 61 circular slabs supported on circular columns and loaded around the periphery. Test variables were the amount and type of longitudinal reinforcement (axisymmetric and two-way). The mechanical model was based on axisymmetry of the slab and assumed that the slab was separated by radial cracks into segments. Each segmental slab was assumed to be supported on a conical shell between the column and root of the shear crack (Figure 1.4). Equations of equilibrium in the radial and tangential directions were used together with failure criteria to compute the load carrying capacity.

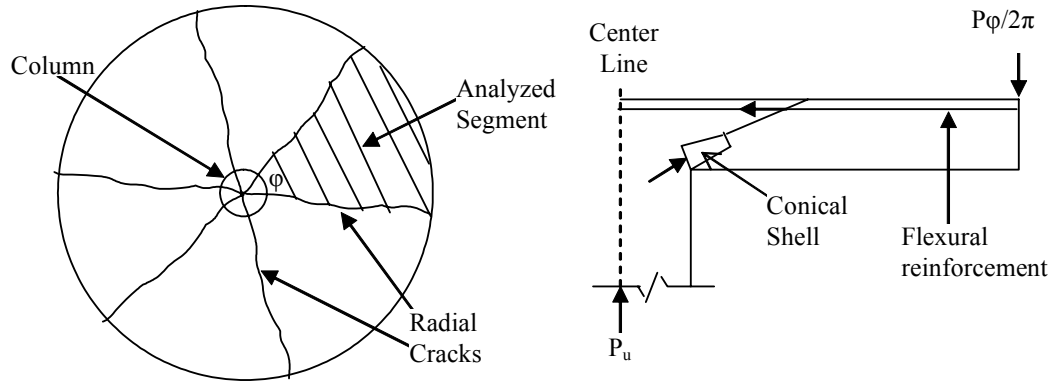


Figure 1.4 Punching Shear Model (Kinnunen and Nylander 1960)

The researchers argued that there was a triaxial state of compression at the conical shell and when a critical tangential strain value was reached at the compression face of the slab, punching shear failure occurred. This critical compressive strain value was obtained from experimental results of the circular slab tests and given as follows:

$$\text{For } 0 < B/h < 2, \quad \varepsilon_{ct} = 0.0035 \left(1 - 0.22 \frac{B}{h} \right) \quad (1.2)$$

$$\text{For } 2 \leq B/h, \quad \varepsilon_{ct} = 0.0019$$

where B is the diameter of the column and h is the slab thickness. The model considered the effect of the flexural reinforcement ratio and was capable of predicting the strength and deformation capacities of slabs failing in shear and flexure. Kinnunen and Nylander (1960) proposed that the limited deformation capacity of the slab adjacent to a column should be taken into account in the design of reinforcement for positive moments in the span. Computation of strength of slab-column connections according to the Kinnunen and Nylander's model was not deemed suitable for practical code procedures as it was an iterative method. In addition, this model is only applicable to slabs with axisymmetric

geometry and loading. On the other hand, it is the first model that explicitly accounts for the local conditions at the root of a shear crack in a slab-column connection and provides a realistic picture of the failure mechanism. This axisymmetric mechanical model was later modified by Kinnunen (1963) to consider two way reinforcement and dowel action and by Andersson (1963) to account for shear reinforcement in circular slabs as reported in CEB-FIP (1985).

1.4.1.3 Moe (1961)

Moe (1961) tested 41 flat plates subjected to pure shear loading at simulated slab-column connections. Based on the experimental results, the following expression was proposed to compute the load carrying capacity of slab-column connections:

$$\frac{V_u}{bd} = \frac{15(1 - 0.075c/d)\sqrt{f'_c}}{1 + \left(\frac{5.25bd\sqrt{f'_c}}{V_{\text{flex}}} \right)} \quad (1.3)$$

where V_{flex} is the flexural capacity based on yield line analysis, b is the perimeter of the loading area, c is the side length of the square column, d is the effective depth of the slab, and f'_c is the concrete compressive strength. Similar to Equation (1.1), this expression considered the interaction between flexural and shear strength of the slab. ACI Committee 326 (1962) further simplified this expression for design, by setting the ratio of shear to flexural capacity equal to one to ensure flexural distress before the shear failure, and consequently the following expression was obtained:

$$\frac{V_u}{bd} = (9.75 - 1.125\frac{c}{d})\sqrt{f'_c} \quad (1.4)$$

It can be observed that Equation (1.4) becomes negative for large values of c/d . In order to address such practical issues, the committee further simplified the

expression and used a lower bound of test results. The resulting expression is as follows:

$$\frac{V_u}{bd} = 4\left(1 + \frac{c}{d}\right)\sqrt{f'_c} \quad (1.5)$$

The validity of increasing the limiting concrete strength above $2\sqrt{f'_c}$ (the value associated with beams) was justified by comparing experimental results of slabs failing in shear against wide beam tests. Furthermore, they noted that for design purposes Equation (1.5) could be simplified using a critical section located $d/2$ away from the rectangular column face. The final form of the equation is as follows:

$$V_u = 4b_o d \sqrt{f'_c} \quad (1.6)$$

in which b_o is the length of the critical perimeter located $d/2$ away from the column face.

Moe's empirical relations calibrated by experimental data form the basis of the ACI-318 provisions for punching shear resistance. There are three important conclusions from Moe's work.

- 1- Punching shear failure is related to tensile failure of concrete, and $\sqrt{f'_c}$ was used to predict the punching shear capacity for the first time.
- 2- Shear strength of concrete slabs acting in two-way action is higher than that of one-way members.
- 3- The interaction between flexural and shear strength of two-way slabs can be incorporated in the shear strength expressions so that flexural distress is ensured.

1.4.1.4 Criswell and Hawkins (1974)

A concise summary of research on methods of analysis and theories for predicting punching shear strength was presented by Criswell and Hawkins (1974). The shear transfer mechanism, the effect of reinforcement ratio, effect of unbalanced moment and test setup limitations on punching shear resistance were discussed in their study. They argued that due to two-way action, the unyielding portions of the slab would restrain the yielding portion and develop in-plane compressive forces. The compressive forces tended to increase the punching shear capacity; therefore isolated slab-column connections would give limited information on the actual capacity of the slab-column connection.

The researchers also discussed the interaction between failures due to flexure and shear depending on the reinforcement ratio. Figure 1.5 shows the changes in behavior of the slabs with different reinforcement ratios. According to this, even when the flexural capacity based on yield line analysis was attained, ductile behavior of the slab was not ensured and punching failure could still occur. The researchers concluded that the increased ultimate load, which was 20 to 25% more than the yield line capacity ensured ductile behavior of the slab-column connections with the formation of a full flexural yield line mechanism. This amount was proposed to be about 10 to 20 % by Elstner and Hognestad (1956) as discussed in Section 1.4.1.1.

Criswell (1974) and Hawkins (1974) reported results of experiments on different forms of shear reinforcement in the form of shear heads, bent bars and stirrups to increase punching shear strength. Shear heads used in their research were made from structural steel sections (I or channel sections) placed in orthogonal directions passing through the slab-column connection. It was found that the shear heads and the slab behaved compositely until an inclined crack spread into the shearhead arms. Beyond this point additional shear was carried by

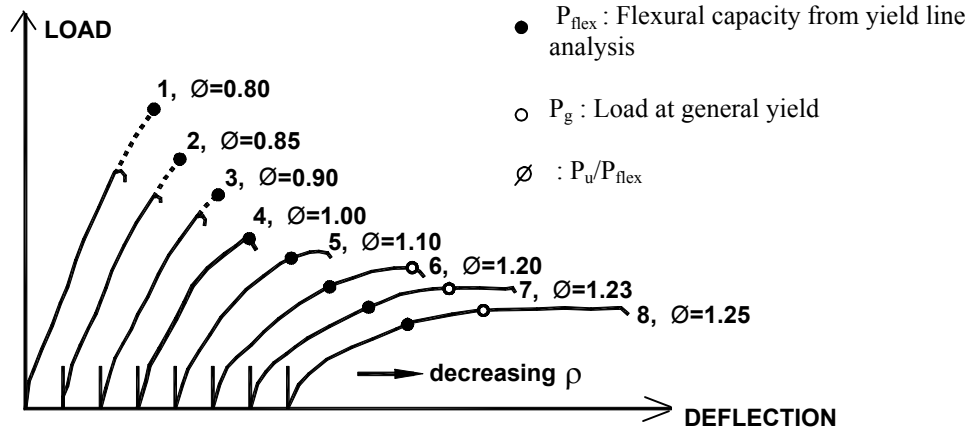


Figure 1.5 Effect of Reinforcement Ratio on Slab Behavior (Criswell 1974)

the shear heads. Use of shear heads was effective in increasing the punching shear capacity of the test specimens; however, it had many drawbacks such as construction inconvenience and cost.

Bent bars and stirrups used as shear reinforcement were found to be effective when shear reinforcement legs were properly anchored. The shear reinforcement contributed to the shear resistance by developing tensile forces in the vertical legs of the shear reinforcement provided that there was no slip. These forces could not develop unless vertical legs of the shear reinforcement were anchored effectively near the top and bottom of the slab. Such anchorage was found to be difficult to achieve in thin slabs. Even small errors in the placement and layout of the shear reinforcement were found to nullify the effectiveness of the shear reinforcement in relatively thin slabs.

1.4.1.5 Ghali et. al. (1982, 1992, 1995)

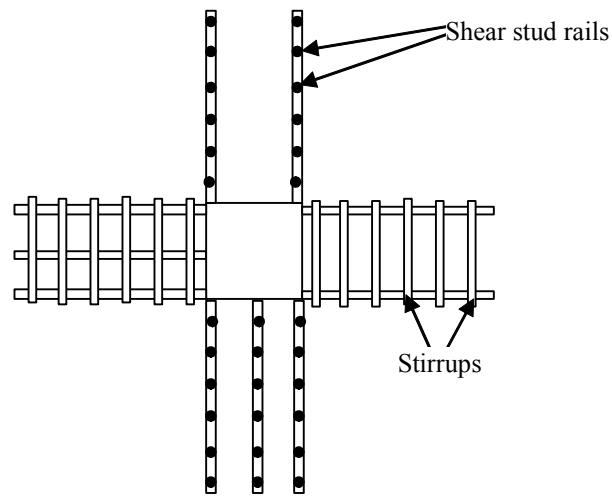
Ghali and his collaborating investigators (Mokhtar 1982, Hammill 1992, Megally 1995) investigated various methods to increase punching shear capacity

of slab-column connections in new construction. They used stirrups, column capitals, and drop panels around the slab-column connection area. They considered interior, exterior, and corner slab-column connections.

The researchers concluded that increasing the slab thickness (drop panel), or increasing the column size around the slab-column connection (column capital) was not an effective way of eliminating punching failure especially under cyclic unbalanced moments. They stated that conventional stirrups had several practical problems. It was claimed that the failure mode of a stirrup was controlled by concrete crushing under the bend and hence stirrup bars typically developed about 70% of yield strength at failure. The researchers reported that significant slip occurred at the corners of the stirrups which caused the vertical legs of the shear reinforcement to be less effective. Moreover, they argued that the corners of the stirrups could significantly reduce the effective height of the shear reinforcement leg.

They proposed the use of preassembled units of shear stud rails (SSR) as shear reinforcement and developed design guidelines to take full advantage of the efficient anchorage of the studs compared to conventional stirrups. SSR relied on mechanical anchorage by heads at both ends of the stem or a mechanical weld at one end and a head at the other end. The steel strip to which the stem was welded to kept the SSR in place during casting. The head of the stirrup could be up to ten times the stem cross-sectional area to develop full yield strength of the bar. Four different stirrup and SSR arrangements used by the researchers are shown prior to casting concrete in Figure 1.6. In addition, layouts of stirrups and studrails are given on the same figure.

The experimental results showed that for concentrically loaded slabs, strength increases compared to a reference specimen were about 80% and 50%



a) Stirrups



b) Shear Stud Rails

Figure 1.6 Arrangements of Shear Stud Rails and Stirrups

with the use of SSR and stirrups as shear reinforcement, respectively. It was also found that yield strength of the stud rails was reached in the tests without loss of anchorage in the vertical legs of shear reinforcement.

Results of their studies provided valuable information on the anchorage requirements of shear reinforcement used in slabs and on the effectiveness and design of SSR as shear reinforcement for new construction.

1.4.1.6 Broms (1990)

Broms (1990) modified the failure criteria in the Kinnunen and Nylander Model (1960) using a tangential strain limit based on microcracking in the compression zone, and a limiting stress in a conical shell under biaxial compressive stresses (Figure 1.7). Based on the behavior of uniaxially compressed cylinder specimens, Broms defined the critical tangential concrete strain as a function of concrete strength and depth of compression zone:

$$\varepsilon_{cpu} = 0.0008 \left(\frac{150}{\alpha x_{pu}} \frac{25}{f'_c} \right)^{1/3} \quad (1.7)$$

where 150 is the diameter of the cylinder specimens in mm., (αx_{pu}) is the height of the equivalent rectangular stress block, and f'_c is the concrete compressive strength in MPa. Using the known critical tangential strain, punching load corresponding to the limiting tangential strain criterion (V_ε) was computed based on linear elastic bending moments of a circular slab loaded around the periphery and on the bilinear section properties for concrete and steel. Moreover, the calculations were performed as a function of reinforcement ratio to account for possible yielding of the reinforcement.

In the radial direction, punching failure was assumed to occur when the compression stress in a conical shell (of a constant thickness and inclination of 15°) reached the critical value of $(1.1 f'_c)$ at the root of the inclined crack (Figure 1.7). Therefore punching shear load V_σ was calculated from the equilibrium of forces in the vertical direction incorporating a size effect factor $(150/0.5y)^{1/3}$:

$$V_\sigma = \left[\pi \left(B + \frac{2y}{\tan 30^\circ} \right) \frac{y \sin 15^\circ}{\sin 30^\circ} (1.1 f'_c) \left(\frac{150}{0.5y} \right)^{1/3} \right] \sin 15^\circ \quad (1.8)$$

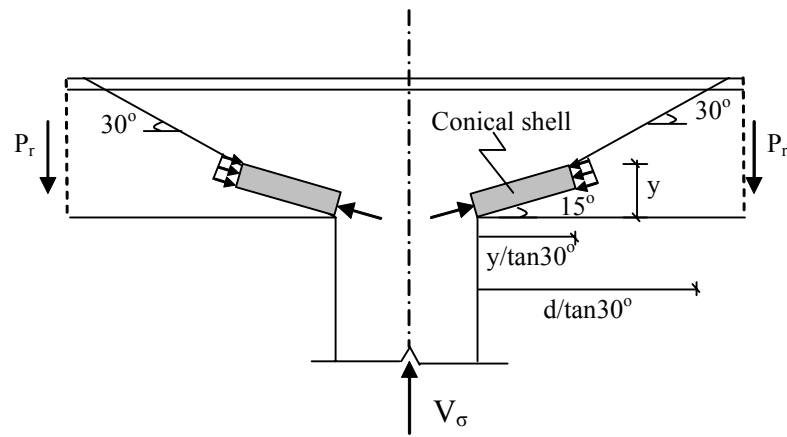


Figure 1.7 High Radial Compression Stress Failure (Broms 1990)

B is the diameter of the circular column and y is the depth of the radial compression zone. The governing punching load was given as the smallest of the capacities V_e and V_σ .

The model proposed by Broms assumed that punching failure occurred at the root of the inclined crack in a compression-shear failure mode. It recognized the size effect and was a function of concrete compressive strength. It was extended to be used in rectangular slab-column connections with the help of an equivalent circular column approach. The extrapolation of the mechanical model assumptions, regarding the local stress conditions, from axisymmetric cases to rectangular column cases are evaluated in Chapter 4 using finite element analysis.

1.4.1.7 Menetrey (1996)

Menetrey (1996) proposed an analytical expression to compute the punching shear capacity based on the results of finite element simulations. The model assumed that punching failure load corresponded to the failure of the concrete tie, and could be obtained by integrating the vertical component of the concrete tensile stress around the punching crack (Figure 1.8). The vertical forces

contributed by reinforcement crossing the inclined crack were included and the following expression was proposed:

$$F_{\text{pun}} = F_{\text{ct}} + F_{\text{dow}} + F_{\text{sw}} + F_{\text{p}} \quad (1.9)$$

where F_{ct} is the vertical component of the concrete tensile force, F_{dow} is the dowel contribution from the flexural reinforcement, F_{sw} is the vertical component of the shear reinforcement, and F_{p} is the vertical component of the force in prestressed tendons. Based on axisymmetric nonlinear finite element simulations, the following expression was derived to compute F_{ct} as a function of reinforcement ratio, ρ , concrete tensile strength, f_t , size effect (η and μ), and radii of punching crack (r_1 , and r_2):

$$F_{\text{ct}} = \pi(r_1 + r_2)f_t^{2/3}\rho\eta\mu \quad (1.10)$$

The contribution of shear reinforcement was computed by taking the vertical component of the yield force in the stirrups. On the other hand, dowel action was given as a function of bar diameter, number of longitudinal bars crossing the

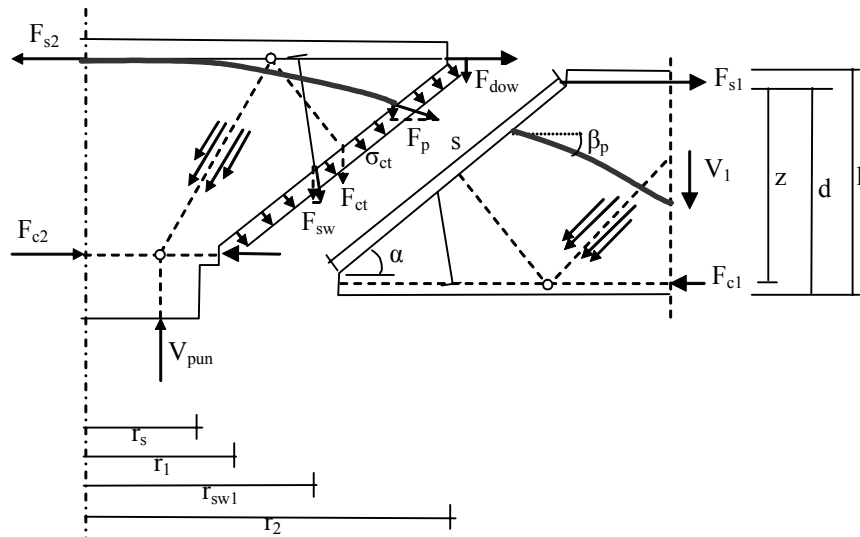


Figure 1.8 Representation of Punching Shear Failure (Menetrey 1996)

punching crack, and axial tensile force in the bars. For slabs with shear reinforcement, punching failure load, F_{pun} , could be predicted inside or outside the shear reinforced area by using Equation (1.9). This work is one of the few studies where the researcher started with the development of a concrete constitutive model, implemented it in a finite element framework, and used it for the analysis of circular slabs for punching shear resistance to develop a mechanical model.

1.4.1.8 Theodorakopoulos and Swamy (2002)

Theodorakopoulos and Swamy (2002) recently proposed a simple engineering model to predict punching shear capacity of slab-column connections without any shear reinforcement. The model considered the free-body diagram around the slab column connection area at the stage where an inclined crack had formed and its propagation was prevented by the compression zone (Figure 1.9). Thus, the total shear resistance of a slab column connection without shear reinforcement was computed by:

$$V_u = V_c + V_a + V_d \quad (1.11)$$

where V_u is the punching shear capacity, V_c is vertical component of the concrete resistance provided in the compression zone, V_a and V_d are the resistances provided by the aggregate interlock and dowel action, respectively. The aggregate interlock force is activated only after the formation of the inclined crack and the model, discussed herein, neglected this because of large separation of the crack faces ($V_a = 0$). The failure was assumed to occur when splitting failure occurred along lines AA' and BB' in the compression zone (Figure 1.9). Thus, the model assumed the punching failure as a result of splitting failure of the compression zone at the ultimate load.

Theodorakopoulos and Swamy (2002) assumed that the dowel action was proportional to the length of the location where dowel action is expected to occur.

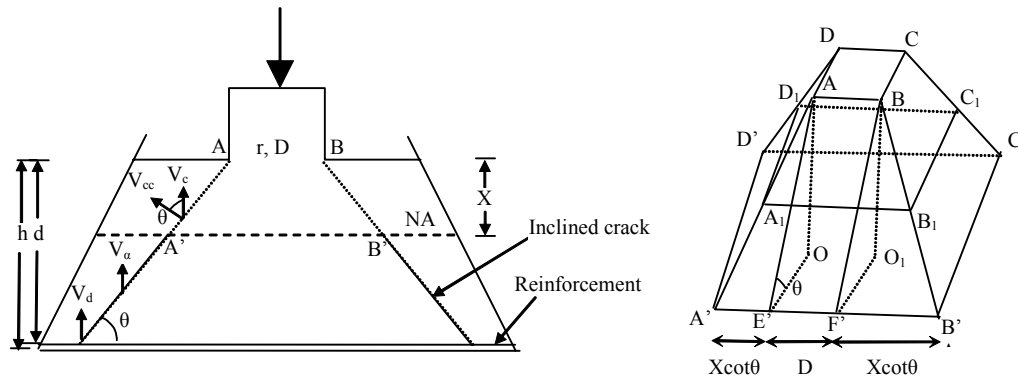


Figure 1.9 Punching Shear Model (Theodorakopoulos and Swamy 2002)

They preferred to combine the two terms V_c and V_d based on an average critical perimeter located $1.5d$ away from the column face (as in British Standard 8110). The resulting expression for the punching shear strength was given as follows:

$$V_c = b_p X \cot \theta f_{ct} \quad (1.12)$$

where b_p is the critical perimeter located $1.5d$ away from the column face, X is the depth of the compression zone, θ is the assumed inclined crack angle (30°), and f_{ct} is the splitting tensile strength taken as $0.27 f_c^{2/3}$ [MPa].

Theodorakopoulos and Swamy (2002) verified their model against concentrically loaded slabs without any shear reinforcement. The average of the ratio of calculated capacity to observed capacity was 0.93 with a standard deviation of 0.135 for 60 specimens tested by various researchers.

From above studies, it can be observed that models to predict punching shear resistance are mainly divided into two categories in terms of the assumption for the failure mode. First category includes models of Elstner and Hognestad (1956), Kinnunen and Nylander (1960), and Broms (1990) in which punching failure is assumed to be a combined compression shear type of failure. On the other hand models of Moe (1961), Menetrey (1996), and Theodorakopoulos and Swamy (2002) assume that punching failure is in fact a tension induced failure.

In this dissertation, the failure mechanism of eleven specimens tested, are explained using the model introduced by Theodorakopoulos and Swamy (2002). The details of the model and its extensions for CFRP strengthened slabs are given Chapter 2.

1.4.2 Research on Gravity and Lateral Load Behavior of Flat Plates

The studies mentioned above mostly focused on the behavior of slab-column connections under concentric loads (pure shear) to investigate punching shear capacity with and without shear reinforcement. There have been a number of other research efforts to understand lateral load behavior of flat plate systems under constant gravity shear. Experiments were conducted on isolated interior and exterior slab-column connections (Islam and Park 1976, Morrison et. al. 1983, Zee and Moehle 1984, Pan and Moehle 1988, Luo and Durrani 1994, Ghali and Megally 1995) and on flat plate sub-assemblages (Robertson and Durrani 1990, Durrani and Du 1995, Hwang and Moehle 1993). The results of the experiments provided information on the lateral stiffness, strength, ductility, and cyclic behavior of the slab-column connections of reinforced concrete flat plate systems. It was found that gravity shear is the most important factor affecting the ductility of the connections under cyclic load reversals. Therefore it was recommended to limit the gravity shear to obtain sufficient ductility in the individual slab-column connections. Effectiveness of shear reinforcement in the form of stirrups, shear stud rails and drop panels to increase punching shear capacity and ductility of the connections were investigated and design guidelines were provided based on the experimental results. Besides the experimental studies, analytical models to idealize strength and stiffness characteristics of flat plates were developed. Equivalent frame (Corley and Jirsa, 1970) and effective beam width models (Pecknold, 1975, Allen and Darvall 1977, Luo and Durrani 1995, Hwang and

Moehle 1993) were developed to analyze flat plate buildings as two dimensional frames. These studies show that there has been an important emphasis on understanding lateral load behavior of flat plate structural systems in the last three decades. The most important reason for this is the highly vulnerable nature of flat plate systems to damage and progressive collapse under earthquake loading.

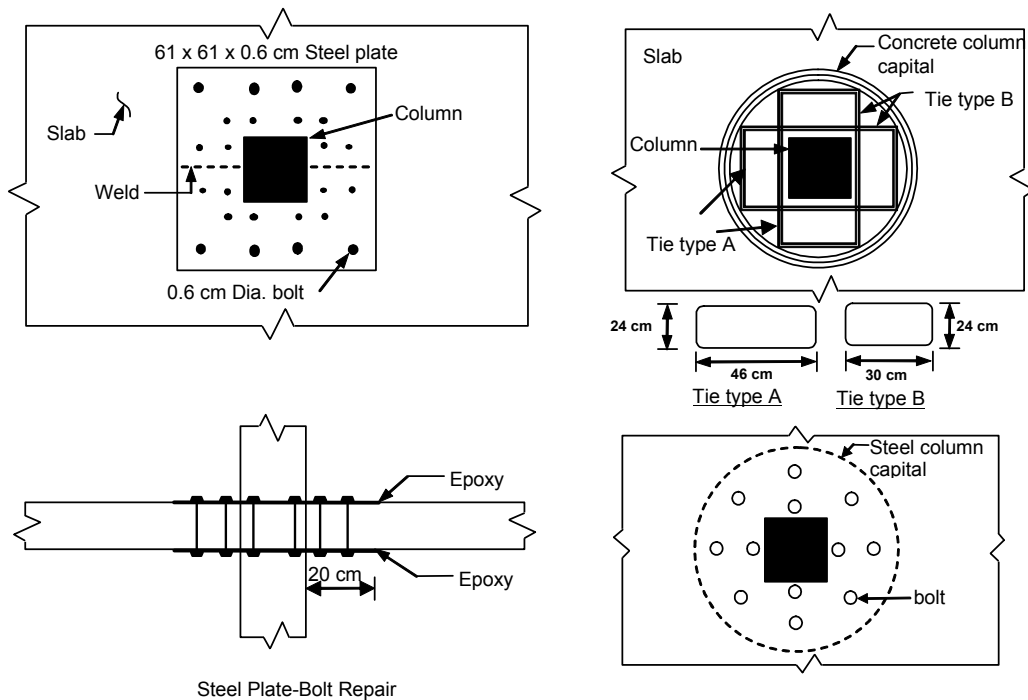
The research summarized above has focused on the issues related to the design and detailing of new flat plate buildings construction. Studies on the strengthening of existing slab-column connections of existing flat plate systems are presented next.

1.4.3 Research on Strengthening for Punching Shear Resistance

There is a limited amount of research on strengthening slab-column connections of flat plates. These studies including the details of the repair and strengthening procedures and experimental results are presented in this section.

1.4.3.1 Martinez et. al. (1994)

Martinez et. al. (1994) employed steel and concrete drop panels added below the slab to increase the punching shear perimeter and therefore the punching shear strength. In addition, test results were reported in which the slab was retrofitted using steel plates on both sides of the slab with through-bolts to act as shear reinforcement (Figure 1.10). A total of 24 bolts were used to act as shear reinforcement, and steel plates were epoxied on the top and bottom of the slab. The concrete column capital was built by chipping out the concrete at the bottom of the slab and recasting the slab with the capital. Specimens were loaded in a



Steel Plate-Bolt Repair

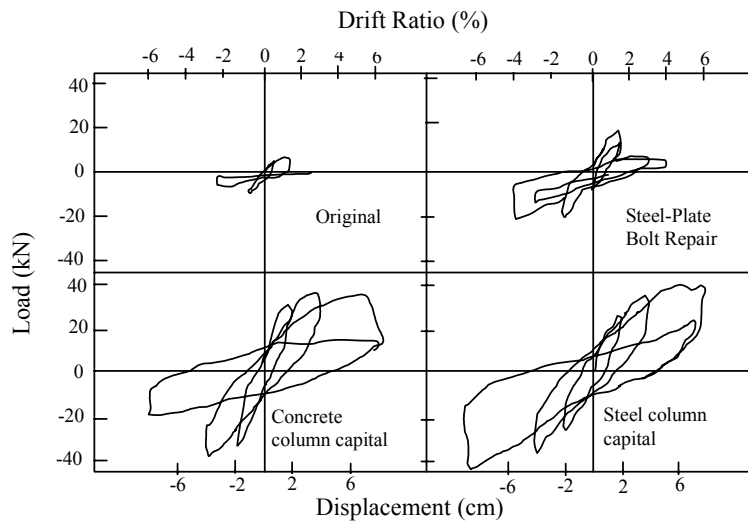


Figure 1.10 Retrofit Scheme of Slab-Column Connections (Martinez et. al. 1994)

reversed cyclic mode under constant gravity shear. The results of load deformation response of the specimens, including the reference specimen with no strengthening, a repair specimen with epoxy injection repair reported by Pan and Moehle (1988), and specimens with concrete and steel column capitals are given in Figure 1.10. It can be observed that lateral load and deformation capacity of the specimens significantly improved. Similar results for load and deformation capacities were obtained for the concrete and steel column capital cases. Both of these specimens experienced punching outside the strengthened zone with a sudden drop in load carrying capacity. It can be seen that column capital solution was effective.

1.4.3.2 Farhey et. al. (1995)

Farhey et. al. (1995) conducted an investigation on epoxy repair RC slab-column connections. Four 2/3 scale interior slab-column connections were tested before and after. Repair was performed by removing the concrete in the damaged zone of the slab-column connection and replacing it with mortar. After curing, holes were drilled in the slab and steel plates were placed at the top and bottom of the repaired region held with bolts (Figure 1.11). High pressure epoxy was injected to fill the cracks. Specimens were tested by applying lateral load reversals under constant gravity shear. Effectiveness of epoxy injection versus mortar patching and thickness of the steel plates were taken as the test parameters. The repair technique resulted in about 2 times the strength and about 4 times the stiffness compared to that of the specimen prior to repair. The ultimate lateral displacement of the repaired specimen did not significantly increase compared to that of the specimen prior to repair. It was found that surface treatment and thickness of the steel plates significantly affected the performance of the test specimens. The results of this study addressed the repair of damaged slab-column

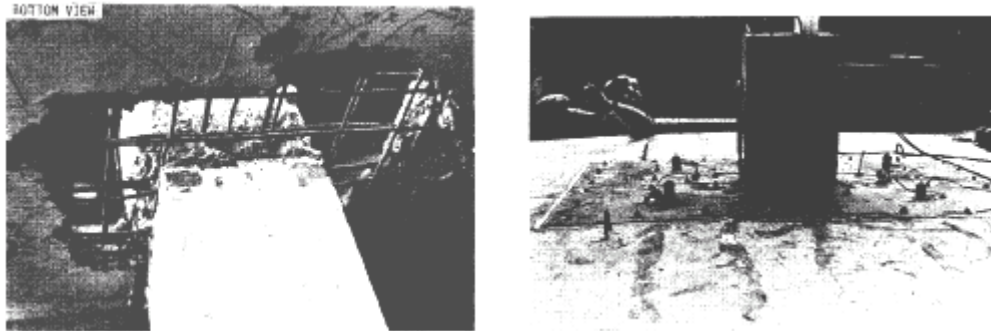


Figure 1.11 Repair of Slab-Column Connections (Farhey et. al. 1995)

connections following an earthquake provided that the slab-column connection remained intact.

1.4.3.3 Hassanzadeh and Sundqvist (1998)

Hassanzadeh and Sundqvist (1998) presented three strengthening methods for bridge slabs supported on columns while the bridge was open to traffic (Figure 1.12). The proposed methods included building a column capital by applying shotcrete, attaching a steel collar to act as a drop panel, and inserting inclined rebars from the bottom of the slab. Specimens were supported on the column and loaded around the periphery of the circular slab during testing. Strength increases of about 60%, 70%, and 55% were obtained for the three methods, respectively, compared to the control specimen with no strengthening. The proposed strengthening methods were successful in terms of increasing the punching shear capacity. However, the authors reported several disadvantages for each of the three methods. The first method involving a shotcrete column capital was found to be expensive, and highly time consuming, and various construction difficulties were encountered during shotcrete application. Although the second method resulted in the highest increase in punching shear capacity, positioning and fixing of the steel collar was found to be difficult for field applications. The insertion of

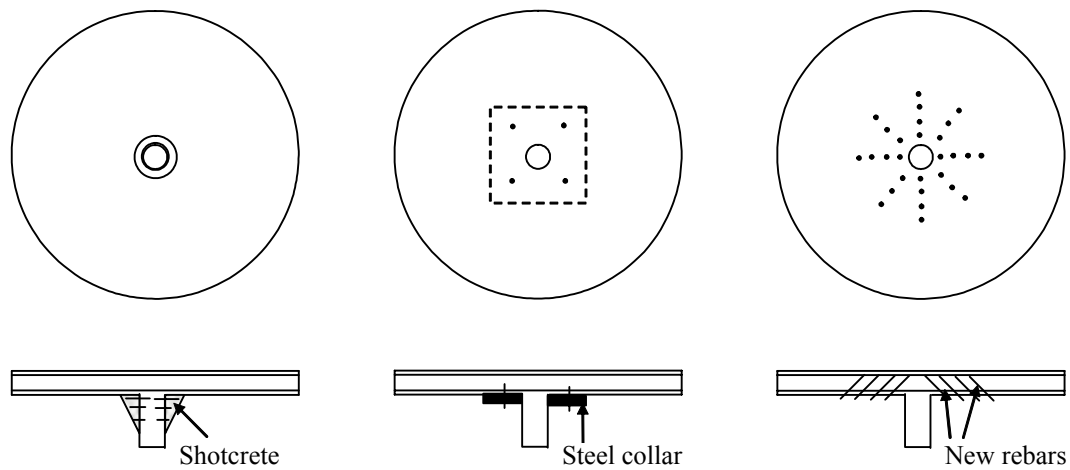


Figure 1.12 Strengthening Methods (Hassanzadeh and Sundqvist 1998)

new rebar as in the third strengthening scheme was the most efficient and inexpensive method among the three methods. However the authors expressed concern regarding the vulnerability of rebar to corrosion and other durability problems.

1.4.3.4 Ebead and Marzouk (2002)

Ebead and Marzouk (2002) recently proposed a strengthening method for slab-column connections using steel bolts and plates that work as a unit. The strengthening procedure started with attaching top and bottom steel plates to surfaces using a two-component epoxy. Following that, bolts were dipped into epoxy, inserted in the drilled holes and pretensioned against the steel plates. Slabs with two different longitudinal reinforcement ratios were subjected to concentric shear loads and combined shear and cyclic unbalanced moments. Load-deformation responses of concentrically loaded specimens with similar reinforcement ratios are presented in Figure 1.13 together with steel plate and bolt

layouts. Strength increases up to about 65% was observed in the concentric load tests, however ductility increases were insignificant as can be seen in Figure 1.13.

For the analysis of concentrically loaded specimens a simple yield line analysis was proposed in which a larger loading area was considered for the strengthened region to compute punching shear capacity. The selection of relatively low slenderness (thickness to span ratio of the slab) for the cyclic tests resulted in higher drifts (~5% for control specimen, 8% for strengthened specimen) than the expected performance of the slab-column connections as reported by Pan and Moehle 1988. In addition, proposed strengthening method resulted in increases in slab thickness and left the steel plates and bolts susceptible to long term durability problems such as corrosion.

It can be observed that the approaches for strengthening slab-column connections presented above are rather intuitive. The amount of vertical shear reinforcement in case of rebars or bolts, the construction and general design guidelines for field applications, and the nature of the strengthening mechanisms have not been reported. Furthermore, fiber reinforced polymers were not used as shear reinforcement in any of the reported tests.

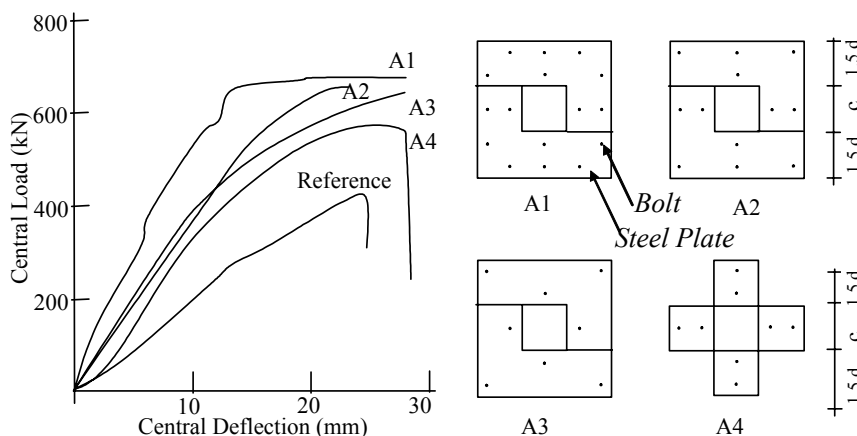


Figure 1.13 Strengthening of Concentrically Loaded Slabs Using Steel Plates and Bolts (Ebead and Marzouk 2002)

1.4.4 Building Code Approaches for Punching Shear Design

North American and European Codes for reinforced concrete design use a critical perimeter approach for punching shear design. Critical section approach was first proposed by Talbot (1913) based on column footing tests. According to this, punching shear capacity is computed by multiplying a shear strength term by the length of the critical perimeter and the depth of the slab. Based on extensive experimental research, building codes modified this concept to include the effect of various parameters. The comparisons of the codes with the experimental database can be found elsewhere (CEB-FIP 2001). A brief summary of code provisions for punching shear resistance are given in this section as the code provisions summarized in this section are later used in assessing the strength of the specimens tested in this study. The code expressions are given in U.S Customary Units unless otherwise stated in the following sections.

1.4.4.1 ACI 318-02

ACI code defines the punching shear strength for slabs without any shear reinforcement as follows:

$$v_c = \min \left\{ 4\sqrt{f'_c} ; \left(\frac{\alpha_s}{(b_o/d)} + \frac{1}{2} \right) 4\sqrt{f'_c} ; \left(\frac{1}{2} + \frac{1}{B} \right) 4\sqrt{f'_c} \right\} \quad (1.13)$$

where v_c is the concrete shear strength, f'_c is the concrete compressive strength, b_o is the length of the perimeter on which shear is considered to act as shown in Figure 1.14.a, d is the effective depth of the slab, α_s is 10 for interior connections, and B is the aspect ratio of the column section ($B \geq 1.0$). As the length of the critical perimeter to effective depth ratio, b_o/d , or column size aspect ratio, B , increases, shear strength, v_c approaches the one-way shear strength. The

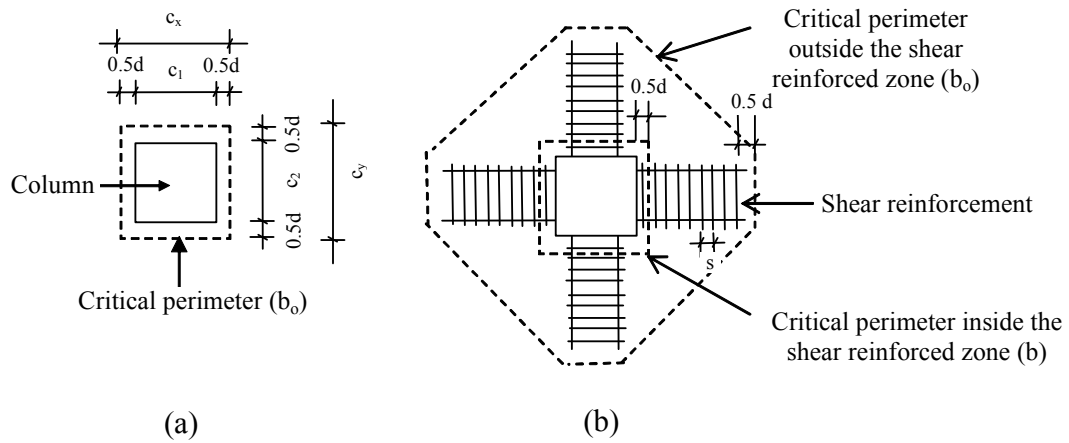


Figure 1.14 Critical Perimeters According to ACI 318-02

ultimate load carrying capacity of the slab-column connection is then computed by:

$$V_c = v_c b_o d \quad (1.14)$$

For slab-column connections where the computed punching shear capacity is smaller than that demanded by the loads; drop panels, column capitals or shear reinforcement in the form of stirrups or shear stud rails can be used. In reinforced slab-column connections, the punching shear capacity, V_n , can be calculated as the smallest of the capacity inside the shear reinforced zone (or inside drop panel, if any), V_n^i , and outside the shear reinforced zone (or outside the drop panel, if any), V_n^o . The capacity inside the shear reinforced zone is computed by:

$$V_n^i = 2\sqrt{f_c'} bd + \frac{A_{sv} f_y d}{s} \leq 6\sqrt{f_c'} bd \quad (1.15)$$

where d is the effective depth of the slab, A_{sv} is total area of SSR or stirrup legs along the perimeter, s is the spacing of the shear reinforcement ($s \leq d/2$), and b is the length of the critical perimeter constructed $d/2$ away from the face of the

column (Figure 1.14.b). The capacity outside the shear reinforced zone is computed by:

$$V_n^o = v_c b_o d \quad (1.16)$$

where v_c can be calculated using Equation (1.13), b_o is the critical perimeter located $d/2$ away from the outermost shear reinforcement (Figure 1.14.b). ACI 318-02 requires that punching shear capacity modified with a resistance factor, ϕ , should be greater than the factored shear force, V_u , in the slab-column connections:

$$\phi V_n \geq V_u \quad (1.17)$$

In the case of combined shear and unbalanced moment, shear stress at a critical perimeter located $d/2$ away from the column face is computed using the following code equation that is based on research reported by Di Stassio and Van Buren (1960):

$$v_u = \frac{V_u}{b_o d} + \frac{\gamma_{vx} M_{ux}}{(J_x / c_x)} + \frac{\gamma_{vy} M_{uy}}{(J_y / c_y)} \quad (1.18)$$

where V_u is the gravity shear, M_{ux} and M_{uy} are the unbalanced moments acting on the connection in x and y directions respectively, and c_x and c_y are as shown in (Figure 1.14.a). The terms J_x and J_y are analogous to the polar moment of inertia and given as follows for square columns:

$$J = \frac{d(c+d)^3}{6} + \frac{(c+d)d^3}{6} + \frac{d(c+d)^3}{2} \quad (1.19)$$

where c is the side length of the column and d is the effective depth of the slab. ACI Code assumes that part of the unbalanced moment, $\gamma_f M_u$ is resisted by flexure within the strip with width $c+3h$ along the direction of moment transfer,

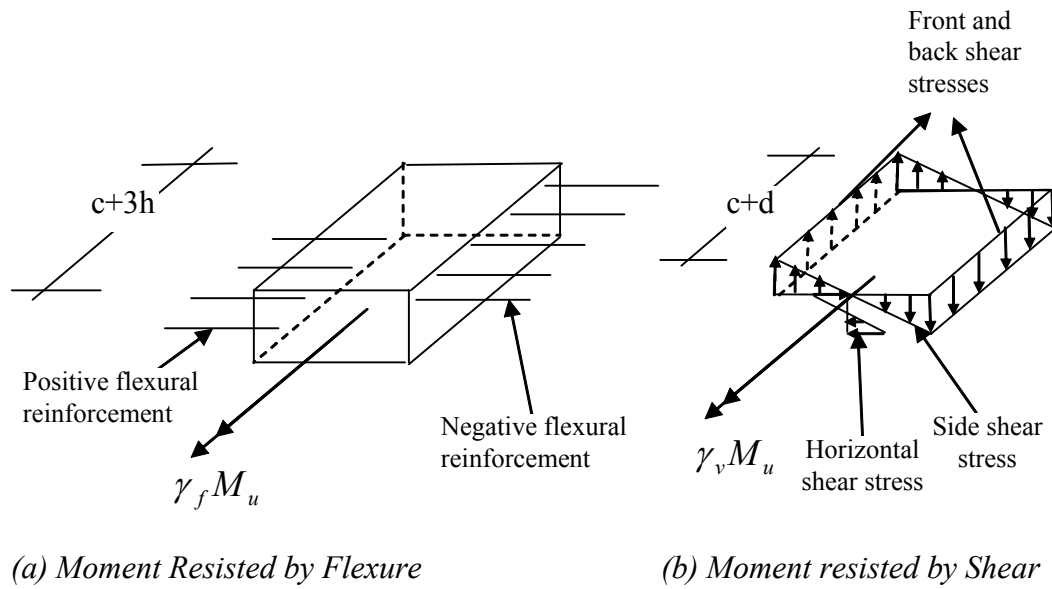


Figure 1.15 Resistance Model for Unbalanced Moment

where h is the thickness of the slab, and $\gamma_v M_u$ by eccentricity of shear in both directions as shown schematically in Figure 1.15. This assumption requires that:

$$\gamma_v + \gamma_f = 1 \tag{1.20}$$

The γ_v factor for computing the fraction of the unbalanced moment transferred by eccentricity of shear is given by:

$$\gamma_v = 1 - \frac{1}{2/3 + \sqrt{c_x/c_y}} \tag{1.21}$$

Punching failure is assumed to occur when the critical shear stress computed from Equation (1.18) (given as the summation of average shear stresses due to gravity shear and unbalanced moments) exceeds the shear strength, ϕv_n . In the absence of shear reinforcement, v_n is computed from Equation (1.13). For slabs with shear reinforcement in the form of stirrups or SSR a similar approach to Equation (1.15) is followed to calculate v_n :

$$v_n = v_c + v_s = 2\sqrt{f'_c} + \frac{A_{sv}f_y}{b_s} \leq 6\sqrt{f'_c} \quad (1.22)$$

where b is the length of the critical perimeter located $d/2$ away from the column face, s is the spacing of the shear reinforcement in the form of stirrups, and A_{sv} is total area of stirrup legs along the perimeter.

An important detailing provision for flat-plate buildings is the structural integrity steel requirement in ACI-318 Code. In this context ACI 318-02 requires that all bottom bars (compressive reinforcement) in each direction shall be continuous and at least two of the bottom bars shall pass through the column core and be anchored at exterior supports. This provision was based on research results reported by Mitchell and Cook (1984) and included in ACI 318-89 for the first time. Mitchell and Cook pointed out that continuous column strip bottom bars provide some residual capacity in case of single slab-column connection damage. The two well anchored bottom bars passing through the column core were labeled integrity steel and were recommended for reducing potential for progressive failure of a flat-plate building when a punching failure occurs at a slab-column connection. This is shown schematically in Figure 1.16. In the absence of continuous bottom bars top steel can rip out following a punching failure and catastrophic progressive collapse may be unavoidable. When well anchored continuous bottom bars are used in the slab- column connection, they can act as a safety net to hold the slab in place.

Slab column connections of older flat plate buildings generally lack the shear reinforcement and/or integrity steel which were is required by building codes since the late 1980s. Hence, slab-column connections of existing flat plate buildings may need to be strengthened both to increase the punching shear capacity and the residual capacity following a punching failure (i.e. to eliminate the deficiency associated with the lack of integrity steel).

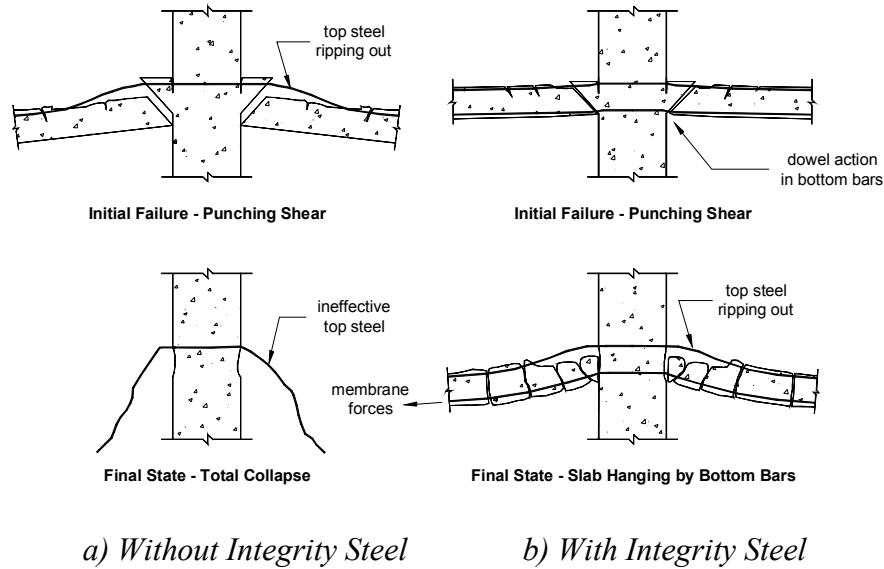


Figure 1.16 Effectiveness of Integrity Steel (Mitchell and Cook 1984)

1.4.4.2 Canadian and New Zealand Codes

Canadian Building Code CSA-A23.3-94 uses the same concept as ACI 318-02 Code. The concrete shear strength given in Equation (1.13) according to ACI 318-02 is replaced with the following expression:

$$v_c = \min \left\{ 4.8\lambda\sqrt{f'_c}; \quad \left(\frac{\alpha_s}{(b_o/d)} + \frac{1}{2} \right) 4.8\lambda\sqrt{f'_c}; \quad \left(\frac{1}{2} + \frac{1}{B} \right) 4.8\lambda\sqrt{f'_c} \right\} \quad (1.23)$$

where λ is 1.0, 0.85, and 0.6 for normal weight, semi-lightweight and lightweight concrete, respectively. The contribution of stirrups to punching shear resistance inside the shear reinforced zone can be calculated similarly to that given by ACI 318-02. The capacity inside the shear reinforced zone is computed as follows:

$$V_n^i = 2.4\lambda\sqrt{f'_c}bd + \frac{A_{sv}f_yd}{s} \leq 7.2\lambda\sqrt{f'_c}bd \quad (1.24)$$

where b is the length of the critical perimeter located $d/2$ away from the column face, d , A_{sv} , f_y , s were previously defined for Equation (1.15).

New Zealand Code (NZS 3101-95) employs the same equations and design procedure that are given in ACI 318-02 for punching shear design. The details explained in Section 1.4.4.1 are valid for design according to this code.

1.4.4.3 European Codes

Different approaches of CEB-FIP Model Code-90 (1990) and British Standard 8110 (BS 8110-97, 1997) for punching shear resistance are discussed in this section. According to ACI 318-02 punching shear resistance is a function of the square root of concrete compressive strength, the ratio b_o/d , and aspect ratio of the column section, B . On the other hand, CEB-FIP MC 90 and BS 8110-97 consider the punching shear resistance as a function of cubic root of concrete compressive strength, size effect, and longitudinal reinforcement ratio. The punching shear capacity is given with the following expressions in CEB-FIP MC90:

$$V_c = \frac{0.18}{\gamma} \xi (100 \rho f_c')^{1/3} u d \quad [\text{N-mm}] \quad (1.25)$$

$$\xi = 1 + \sqrt{\frac{200}{d}} \quad [\text{mm}] \quad (1.26)$$

where ξ is the factor to account for size effect, ρ is the reinforcement ratio, f_c' is the concrete compressive strength, d is the effective depth of the slab, γ is the partial safety factor, and u is the length of the critical perimeter constructed $2d$ away from the column face (Figure 1.17).

The concrete contribution to punching shear capacity of slab-column connections according to BS 8110-97 is as follows:

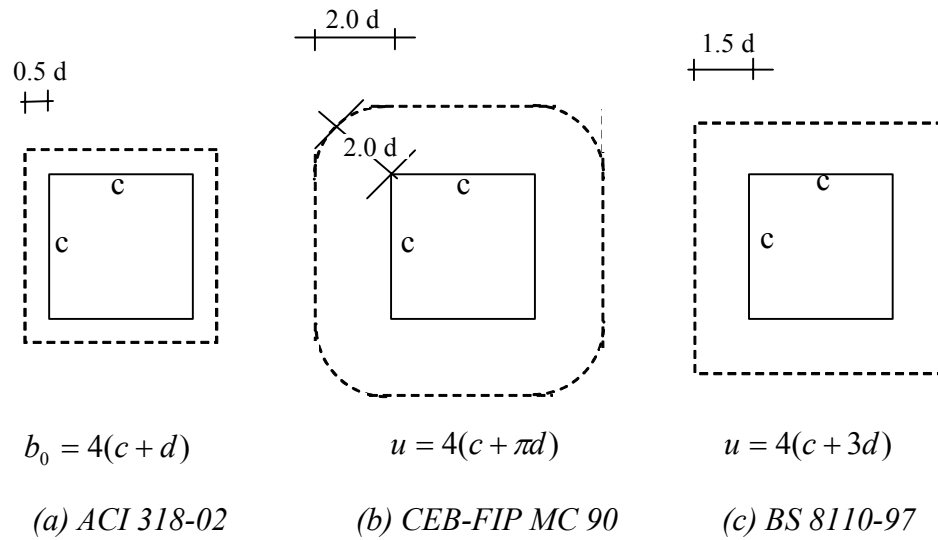


Figure 1.17 Critical Perimeters Defined by Different Codes

$$V_c = \frac{1.5d}{a_v} \frac{0.34}{\gamma} k (100 \rho f_c')^{1/3} u d \quad [\text{N-mm}] \quad (1.27)$$

$$k = \sqrt[4]{\frac{400}{d}} \quad [\text{mm}] \quad (1.28)$$

where a_v is the distance between the control perimeter and the column face, k is the factor to account for size effect, ρ is the reinforcement ratio, f_c' is the concrete cylinder compressive strength, d is the effective depth of the slab, γ is the partial safety factor, and u is the length of the critical perimeter constructed $1.5d$ away from the column face (Figure 1.17).

CEB-FIP MC90 considers a critical perimeter $2d$ away from the column face and suggests the use of one-way shear strength similar to that used for beams. On the other hand ACI 318-02 recommends the use of two times the one-way shear strength with a critical perimeter located $0.5d$ away from the column face for connections with square columns. Both CEB-FIP MC 90 and BS 8110-97 consider the beneficial effect of increasing longitudinal reinforcement ratio, which results in increased punching shear capacity. However ACI 318-02 neglects the

effect of reinforcement ratio on punching shear capacity recognizing that for most practical cases, a ρ value of 0.5 to 1.2% does not change the concrete contribution to punching shear capacity significantly. In addition, ACI 318-02 recognizes the decrease in shear strength with increasing length of the critical perimeter, and aspect ratio of the column sides. CEB-FIP MC 90 provisions neglect this effect and suggests using the same shear strength for any b_o/d ratio. On the other hand BS-8110-97 incorporates this effect with the use a_v factor in Equation (1.27).

The maximum punching shear capacity associated with the crushing of concrete at the column face is given by the following equation for CEB-FIP MC90 (in N-mm):

$$V_{\max} = 0.6 (0.5 f'_c) \left(1 - \frac{f'_c}{250}\right) (f'_c) u_o d \quad [\text{N-mm}] \quad (1.29)$$

The perimeter of the loading area (i.e. the column), u_o is used in Equation (1.29).

CEB-FIP MC90 gives the punching shear capacity inside the shear reinforced zone similar to Equation (1.15):

$$V_n^i = 0.75 V_c + \frac{A_{sv} f_y d}{s} \leq V_{\max} \quad (1.30)$$

V_c can be calculated using Equation (1.25), and $A_{sv} f_y$, and s are the total cross-sectional area of the shear reinforcement along the periphery, yield strength and spacing of the shear reinforcement, respectively.

In addition, punching shear capacity outside the shear reinforced zone can be computed by using Equation (1.25) with a critical perimeter constructed $2d$ away from the outermost shear reinforcement. In calculating the capacity, CEB-FIP Code recommends not considering a portion of the critical perimeter in capacity calculations where the tangential spacing of shear reinforcement exceeds $2d$. The details of calculating punching shear capacity with shear reinforcement for BS 8110-97 are similar to those in CEB-FIP MC90 requirements.

In short, the provisions of two European codes considered above and ACI 318-02 for punching shear resistance are conceptually similar. However, there are some differences in terms of the parameters considered in the shear capacity calculations. Most of the European research encountered in the technical literature is on concentrically loaded circular slab-column connections. Related code provisions are calibrated with experiments and provide more detailed treatment of the concentric punching shear capacity especially for cases without any shear reinforcement. On the other hand, ACI Code provisions for punching shear are simpler and easier for use in design and address practical issues with a more general look at the overall performance of the slab-column connections.

1.5 ORGANIZATION OF DISSERTATION

This dissertation describes the development of a rational method to strengthen existing slab-column connections under the actions of shear and unbalanced moment. Experimental work on concentrically loaded flat plates is presented in Chapter 2. Experimental program on flat plates subjected to eccentric shear forces is presented in Chapter 3. In order to study the mechanics of the load transfer, three dimensional nonlinear finite element analyses were conducted. Results of these numerical simulations are presented in Chapter 4. A synthesis of experimental findings and analytical studies facilitated the development of punching shear upgrade design guidelines. These recommendations are presented in Chapter 5. A summary of this research, conclusions and recommendations for future investigations can be found in Chapter 6.

CHAPTER 2

Punching Shear Strengthening of Concentrically Loaded RC Flat Plates

2.1 GENERAL

The development of a strengthening method to increase punching shear capacity of interior slab-column connections subjected to concentric forces is presented in this chapter. For this purpose, an experimental program was conducted on eleven full scale reinforced concrete flat plates loaded concentrically at the center. The objectives of the experimental program were:

- To propose a punching shear strengthening method that employs Carbon Fiber Reinforced Polymers (CFRPs) used as externally bonded shear reinforcement,
- To study the effectiveness of different shear reinforcement patterns and detailing,
- To evaluate the optimum amount of CFRP reinforcement to enhance slab-column connection behavior,
- To investigate the mechanics of load transfer in strengthened specimens,
- To propose design guidelines for the strengthening of slab-column connections using CFRPs.

2.2 CHOICE OF STRENGTHENING MATERIAL

Fiber reinforced polymers (FRPs) have long been successfully used by the aerospace and defense industries. Their use in strengthening and retrofit of reinforced concrete members is established in the last decade. Some advantages

include ease of installation on site, high strength to weight ratio, and improved durability of the composite materials.

Strengthening research using composite materials concentrated on the upgrade of beams, columns, and one-way slabs for concrete structural elements. Fiber reinforced polymer (FRP) products have been used to strengthen beams and columns for flexure (Grace et. al. 1999; Arduini and Nanni 1997) and shear (Triantafillou 1999; Malek and Saasatmanesh 1998). Design guidelines have been established by ACI 440 (2002), ISIS (2001) and JSCE (1999) for the use of FRP products for strengthening. In the literature examined, there was no reported use of fiber reinforced polymers as shear reinforcement in existing reinforced concrete flat plates.

Use of fiber reinforced polymers as external shear reinforcement for punching shear strengthening has many advantages over other strengthening methods such as use of bolts, rebars acting as shear reinforcement or, externally built drop panels and capitals. The greatest advantages are due to favorable material properties such as light weight, high strength and ease of handling and applications. In addition, use of fiber reinforced polymers has previously proven to be successful in flexure and shear strengthening of beams and columns. Superior material properties of these materials and ease of application (i.e. reduced labor costs) have led to the increased popularity of FRPs for strengthening and rehabilitation of structural components. Besides the advantages outlined above, there are additional advantages for their utilization in strengthening slab-column connections.

As flat-plate structural systems are preferred for to their versatile characteristics due to absence of beams, upgrade procedure should be such that flexible and aesthetic aspects of these systems are preserved after rehabilitation. Local increases in slab thickness or column size around the connection area may

not be tolerated and they may bring additional costs in addition to rehabilitation costs. When FRPs are used for punching shear strengthening, slab thickness does not increase as a result of the application. Another advantage is the ease of detailing of FRP strips to form closed stirrups. During the application, FRP strips are saturated with bonding agent and the composite matrix is then applied to the concrete surface. At this stage of application, the composite material is flexible, easy to work with and it can be formed into any given shape for detailing purposes. For applications where FRPs are used as shear reinforcement, flexible nature of the material allows them to be wrapped around any shape, to be anchored by FRP overlaps, and to form closed loops as stirrups. Considering these advantages, the use of FRP as shear reinforcement for punching shear strength increase of reinforced concrete flat-plates was adopted in this study. However, it is well appreciated that somewhat lower stiffness of this costly material needs to be considered in punching shear upgrades.

2.3 DESIGN OF TEST SPECIMENS

The most realistic laboratory simulation of flat plate systems would be the use of full-scale multi-bay and perhaps multi-story sub-assemblages. Since these tests are expensive and time consuming, scaled floor systems can be used (Moehle and Diebold 1984, Aghayere and Macgregor 1990). Another approach is to select a prototype floor system, and consider a full-scale isolated flat-plate system with appropriate boundary conditions. As mentioned in Section 2.1, there are a number of parameters under investigation that have not been previously investigated and this requires a number of tests to be performed. Therefore, the second approach is preferred with the prototype floor system shown in Figure 2.1.

The specimen size (6''x78''x78'') was selected based on the lines of contraflexure (zero moment locations) around the slab-column connection area

from the prototype floor system. The test specimen size simulates the test zone from a full-scale model of the prototype floor with a 16' span and 6 in. slab thickness (Figure 2.1). In addition, the test specimen size is also valid for the test zone of a 3/4 scaled model for the prototype floor with a 20' span and 8 in. slab thickness (Figure 2.1). A simple yield line analysis was used to compute the approximate flexural capacity, and ACI 318-02 design provisions were used to estimate the punching shear strength of the specimens. The yield line mechanism

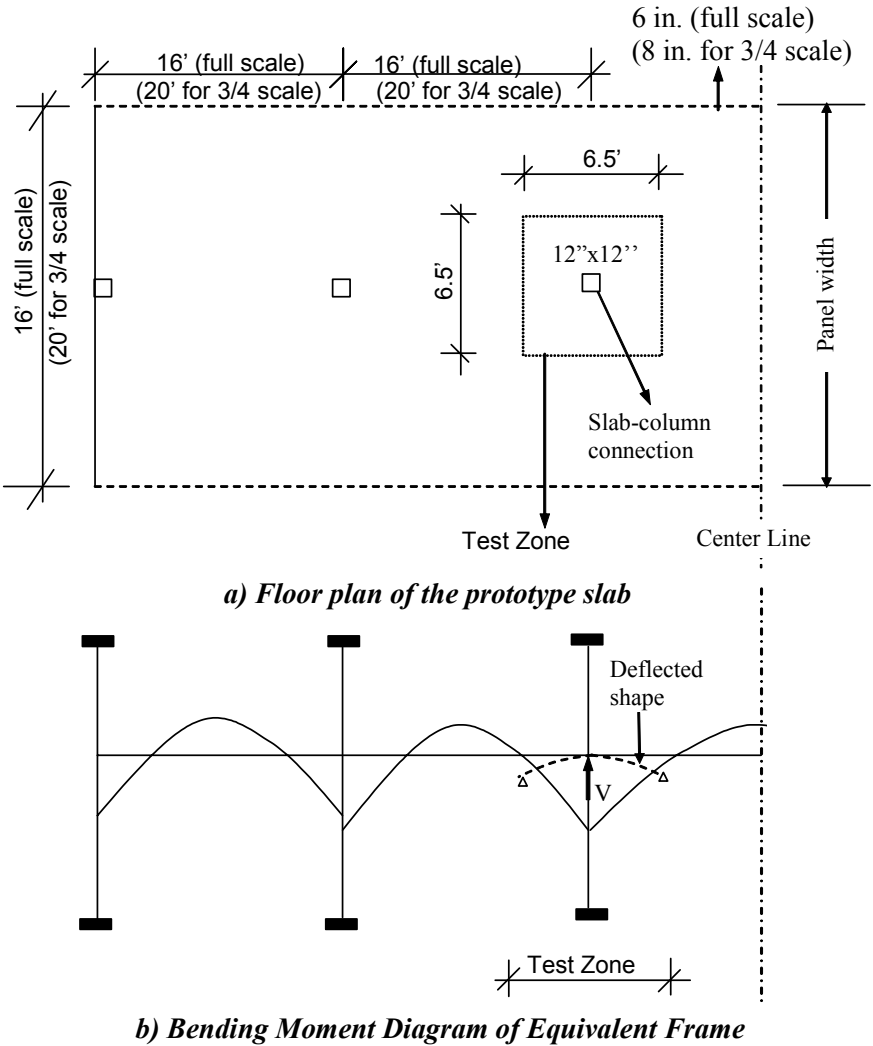
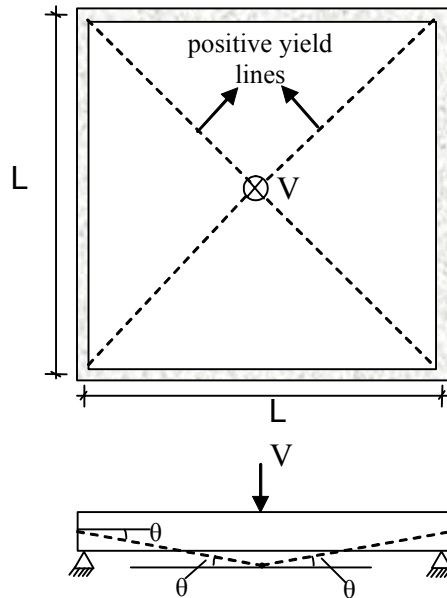


Figure 2.1 Details of Prototype Floor and Selection of Test Zone



Int. Virtual Work = Ext. Virtual Work

$$4(m_u L)\theta = V_{flex} \theta \frac{L}{2}$$

$$V_{flex} = 8 m_u$$

(Neglecting self weight
and size of loading area)

Figure 2.2 Simple Yield Line Analysis to Compute Flexural Capacity

considered for a square slab loaded with a point loaded at the center is shown in Figure 2.2. Punching shear capacity of the control-specimens, i.e. specimens without any strengthening was computed using ACI 318-02 expressions (Equations (1.13) and (1.16) given in Section 1.4.4.1). In the initial design of the test specimens, the arrangement of the shear reinforcement for the strengthened specimens was based on stirrup and shear stud rail arrangements shown in Figure 1.6 that are commonly used in new construction. In order to eliminate the punching failure due to an inclined shear crack at the face of the loaded area, shear reinforcement in the form of CFRPs should span the inclined crack and help to carry the shear as shown in Figure 2.3 schematically. For existing slabs, this can be achieved by drilling holes along the depth of the slab, and providing CFRPs in the vertical direction to pass through the expected failure plane. It was

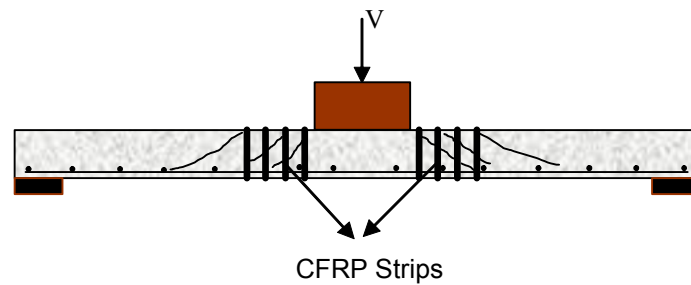


Figure 2.3 Postulated Shear Response

hypothesized that as the inclined crack forms around the concentrically loaded area, closest CFRP stirrups start carrying forces and the critical perimeter is shifted to the next set of CFRP stirrups with the formation of a new inclined crack. In this way, the length of the shear critical section can be increased resulting in an increased punching shear capacity of the slab-column connection. Based on this hypothesis, failure can take place i) inside the shear reinforced region due to sudden loss of load carrying capacity as a result of CFRP rupture, ii) outside the shear reinforced zone due to an inclined crack that develops outside the shear reinforced zone, iii) in flexure. Considering these failure modes, the number of CFRP perimeters and the amount of CFRP per hole are the two important test parameters. In addition, different configurations of holes resulting in different CFRP patterns in the plan of a slab specimen is considered as shown in Figure 2.4 for similar number of holes extending from the loading area. Pattern A is similar to the layout of shear stud rail arrangement shown in Figure 1.6. On the other hand Pattern B is similar to a radial shear stud rail arrangement as suggested by Gomes and Regan (1999). Patterns C and D are different forms of Pattern B where a smaller number of discrete shear reinforcement legs with a larger tangential spacing are used per perimeter. For patterns C and D, shear reinforcement legs extend from the face and corner of the column, respectively (Figure 2.4). Two problems can arise for these two patterns:

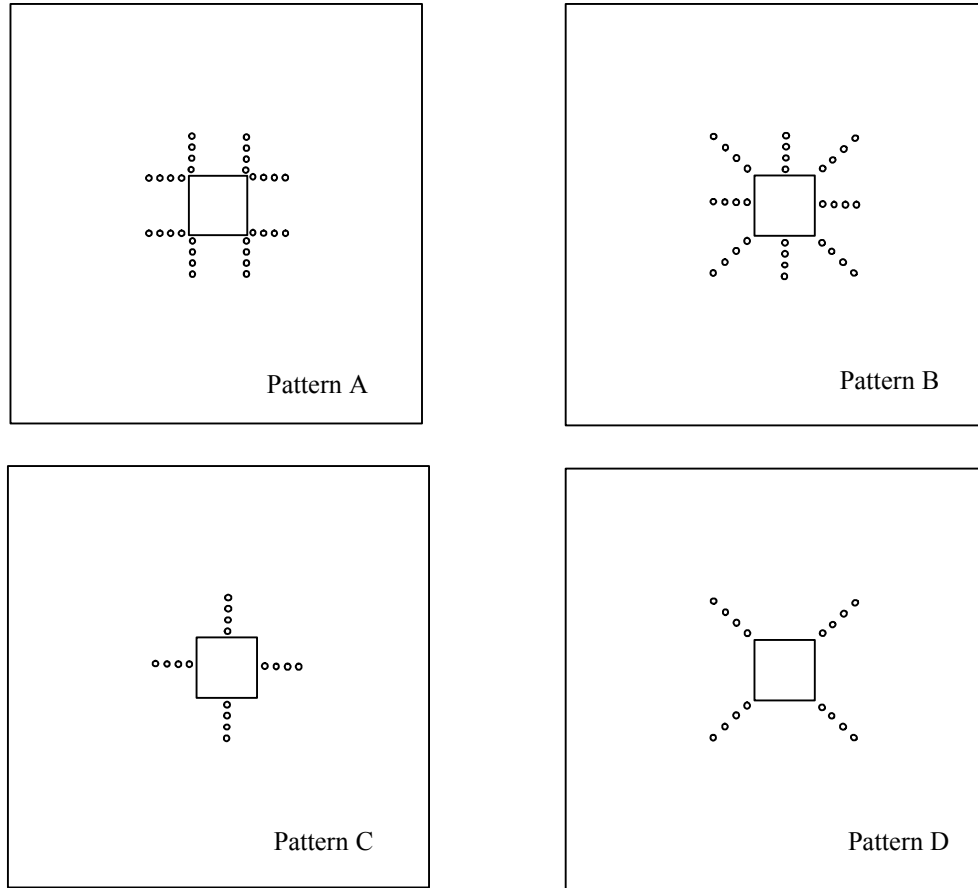


Figure 2.4 Possible Shear Reinforcement Patterns (Plan View)

i) The postulated shear response (i.e. first CFRP perimeter contributing to shear resistance and shifting the weaker plane outside the shear reinforced zone) may be violated with the failure inside the shear reinforced zone. This may occur due to the large lateral spacing of the shear reinforcement legs. The inclined crack in the form of a pyramid in three dimensions may penetrate into the shear reinforced zone from the corners for Pattern C and from the face for Pattern D.

This results in a premature failure before reaching the maximum available punching shear capacity outside the shear reinforced zone.

ii) Bonding of CFRP to the concrete surface may be a problem. The feasible anchorage with optimum material use for these patterns (patterns C and D) is bonding the CFRP strips to the top and bottom of slab surfaces. Compared to CFRP overlap anchorage in the form of closed loops, this alternative is less likely to be successful as the anchorage of the vertical CFRP strips are solely provided by the concrete to CFRP bond. A detailed investigation on anchorage of CFRP reinforcement is presented in Section 2.8.4.

The following parameters are studied during the course of the experimental program:

- Number of shear reinforcement perimeters (4, 6, and 8),
- Amount of vertical shear reinforcement,
- Shear reinforcement patterns (Patterns A and B),
- Detailing of wrapping scheme for optimum performance,
- Presence and absence of integrity steel.

ACI 318-02 design provisions summarized in Section 1.4.4 were used to estimate the load carrying capacity with the assumption of failure outside the shear reinforced zone. Punching shear capacity, V_n^o , was computed based on critical perimeters constructed $d/2$ away from the shear reinforced zone similar to Figure 1.14 for specimens with Pattern A. On the other hand, for specimens with pattern B, a rectangular critical perimeter located $d/2$ away from the outermost shear reinforcement was used.

The control specimens were designed to fail through punching shear. For the strengthened specimens, it was intended to shift the failure mode from punching to flexure with increasing area of shear reinforced zone. For this purpose it is necessary to use a high longitudinal reinforcement ratio such that the

Table 2.1 Design of Test Specimens

$f'_c = 4000 \text{ psi}$ (Target concrete strength) $m_u = 18.2 \text{ k-in/in}$ (Moment capacity)
 $d = 4.5 \text{ in}$ (Effective slab depth) $V_{flex} = 146 \text{ k}$ (Yield Line capacity)
 $A_s = 0.44 \text{ in}^2$ (#6 Rebar) $c = 12 \text{ in}$. (Column size)
 $s = 5.5 \text{ in}$. (Rebar spacing) $f_{FRP} = 127 \text{ ksi}$ (Ultimate strength of FRP)
 $A_{FRP} = \frac{V_n^o}{n f_{FRP}}$ (Area of FRP required per hole) $f_y = 60 \text{ ksi}$ (Yield strength of steel)

Pattern	# of Perimeters	Specimen Name	b_1 (in.)	v_c (psi)	V_n^o (k)	V_n^o / V_{flex}	A_{FRP} (in ²)
-	-	Control	66	253	75	0.51	-
A	4	A4*	105	235	111	0.76	0.11
A	6	A6	131	214	126	0.86	0.12
A	8	A8	156	199	140	0.96	0.14
B	4	B4	129	215	125	0.85	0.12
B	6	B6	165	195	145	0.99	0.14
B	8	B8	201	183	166	1.13	0.16

All A4 specimens have the same capacity outside the shear reinforced zone.

V_n^o : Capacity computed based on shear strength outside the reinforced zone

flexural capacity is significantly greater than the shear capacity for specimens without any strengthening. Table 2.1 summarizes the load carrying strengthening A and B and with 4, 6, and 8 perimeters of shear reinforcement. The estimated capacity compared with the flexural capacity based on yield analysis is also presented. It can be observed that as the number of perimeters was increased the punching shear capacity was expected to increase and the failure mode to shift from shear to flexure. The most important assumption in these calculations was the punching failure taking place outside the shear reinforced zone without any premature failure inside the CFRP reinforced zone. The validity of this assumption and the optimum amount of vertical CFRP reinforcement can only be found from the results of experiments.

The preliminary design and detailing of externally bonded CFRP reinforcement per hole was based on a “worst case scenario” of concrete contribution inside the shear reinforced zone being negligible. Then the punching shear capacity, V_n^o was used to compute the amount of CFRP as follows:

$$V_n^o = V_n^i = nA_{FRP}f_{FRP} \quad (2.1)$$

where n is the number of vertical legs considered in a perimeter, A_{FRP} is the area of CFRP per vertical legs, and f_{FRP} is the tensile strength of CFRP.

Table 2.1 shows the CFRP cross sectional areas required for each specimen at the corresponding ultimate load. In order to isolate and study this parameter, 4 specimens with Pattern A consisting of 4 perimeters of shear reinforcement were selected. Amount of CFRP and configuration details were taken as the only test variables in these specimens. Based on the test results of these A4 specimens, the detailing and amount of CFRPs for the rest of the specimens were later revised as required.

In addition to the test parameters associated with the strengthening scheme, one additional parameter, the effect of integrity steel, was studied in the experimental program. To achieve this, two control specimens without any strengthening were considered, one with the two continuous compression bars in each direction (as discussed in Section 1.4.4.1), and one without any compression reinforcement. It is important to note that all of the strengthened specimens were similar to the control specimen without any integrity steel. The specimen with the integrity steel not only provided information on the effectiveness of the ACI 318-02 requirements on integrity steel, but also provided a basis of comparison for the residual capacity of the strengthened specimens with code compliant specimen.

Figure 2.5 shows the different CFRP installation patterns used in this study. Details of the strengthening procedure are presented later in this chapter (Section 2.5). Table 2.2 summarizes the details of the test matrix considering all the test variables. In addition, the actual amount of vertical CFRP shear reinforcement per hole at every perimeter is given in Table 2.3. The amount of CFRPs varied from perimeter to perimeter for some of the specimens in order to accommodate various details and patterns shown in Figure 2.5.

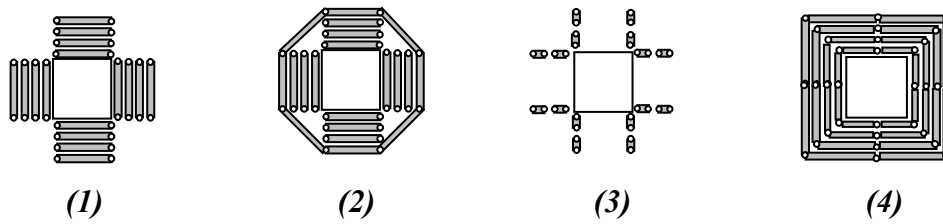


Figure 2.5 Detailing of CFRP reinforcement (Plan View)

Table 2.2 Test Matrix

TEST MATRIX	Test Specimens										
	Control-1	Control-2	A4-1	A4-2	A4-3	A4-4	A6	A8	B4	B6	B8
CFRP Pattern ¹	-	-	A	A	A	A	A	A	B	B	B
CFRP Detailing ²	-	-	1	2	2	3	2	2	4	4	4
Number of CFRP Layers per Hole ³	-	-	4	2	1	2	3	3	3	4	4
Number of CFRP Perimeters ⁴	-	-	4	4	4	4	6	8	4	6	8
Integrity Steel ⁵	NO	YES	NO	NO	NO	NO	NO	NO	NO	NO	NO

- 1: CFRP patterns as shown in Figure 2.4
 2: CFRP wrapping scheme as shown in Figure 2.5
 3: Minimum amount of CFRP per leg (1" width 0.04" thickness)
 4: CFRP perimeters extending from the face of the loading area
 5: Two continuous compressive bars

Table 2.3 Vertical CFRP Amount Used as Shear Reinforcement

Specimen Name	Number of CFRP Layers* at Different Perimeters							
	1	2	3	4	5	6	7	8
A 4 - 1	4	4	4	4	-	-	-	-
A 4 - 2	2	2	2	3	-	-	-	-
A 4 - 3	1	1	1	2	-	-	-	-
A 4 - 4	2	2	2	2	-	-	-	-
A6	3	5	3	5	3	5	-	-
A8	3	5	3	5	3	5	3	5
B4	3	4	4	3	-	-	-	-
B6	5	4	4	4	4	5	-	-
B8	5	4	4	4	4	4	4	5

*: 1 layer correspond to 1 in. wide 0.04 in. thick CFRP strips

2.4 MATERIAL PROPERTIES

The concrete mixture used was designed for a target compressive strength of 4000 psi to simulate the concrete strength in existing reinforced concrete flat-plate systems. 3/8 in. siliceous river gravel was used as the aggregate in the concrete mix. Concrete cylinders were cured under same conditions as those of the test specimens. Actual mean compressive strength from compressive cylinder tests is shown in Table 2.4. The steel reinforcement was Grade 60 deformed bars with mean yield strength of 65 ksi obtained from uniaxial tension tests.

In this study, a custom stitched unidirectional carbon fabric with aramid cross fibers (Tyfo SCH-41S) was used as the strengthening material. Carbon fiber reinforced polymers (CFRPs) were chosen over other types of composites such as glass fiber reinforced polymers due to their higher strength and stiffness. These properties of FRPs are important in controlling the width of inclined cracks when used as shear reinforcement. However, it is believed that other types of FRPs can be used in a similar fashion to strengthen flat plates upon experimental verification prior to their use in practice. A two-component epoxy matrix material was used to bond CFRP to concrete. The material properties of the CFRP and epoxy used in the strengthening design reported by the manufacturer are summarized in Table 2.4. Uniaxial tensile stress-strain response of steel, epoxy

Table 2.4 Material Properties

Materials	Elastic Modulus (ksi)	Compressive Strength (psi)	Yield Stress (ksi)	Yield Strain (in/in)	Ultimate Tensile Stress (ksi)	Ultimate Tensile Strain (in/in)
Concrete	-	4100	-	-	-	-
Steel	29580	-	65	0.0022	102	0.115
CFRP	10500	-	-	-	127	0.012
Epoxy	461	-	-	-	11	0.050

and CFRP are compared in Figure 2.6. It can be observed that CFRP has higher strength but lower elastic modulus than steel. In order to verify the manufacturer's reported values of strength and stiffness, 8.00" x 1.00" x 0.04" CFRP coupons were tested at the Ferguson Structural Engineering Laboratory. Results of the uniaxial tension tests of CFRP-epoxy composite coupons are presented in Table 2.5. The strains in the CFRP were measured with strain gauges attached at the center of the coupons. Based on these results, average rupture strain was found to be similar to the value reported by the manufacturer. However, the actual strength of CFRP composite was about 9% lower than the value reported by the manufacturer. The wide of range of Modulus of Elasticity values obtained for CFRP coupons is an indication of uncertainty associated with carbon fiber to epoxy volume ratio during impregnation. In addition, non-uniform stresses that might be induced at the strain gauge locations due to difficulties in gripping the CFRP coupons resulted in a high standard deviation.

2.5 STRENGTHENING METHOD

A total of nine specimens were strengthened using CFRPs in this phase of the experimental program. Vertical holes were positioned around the loading area

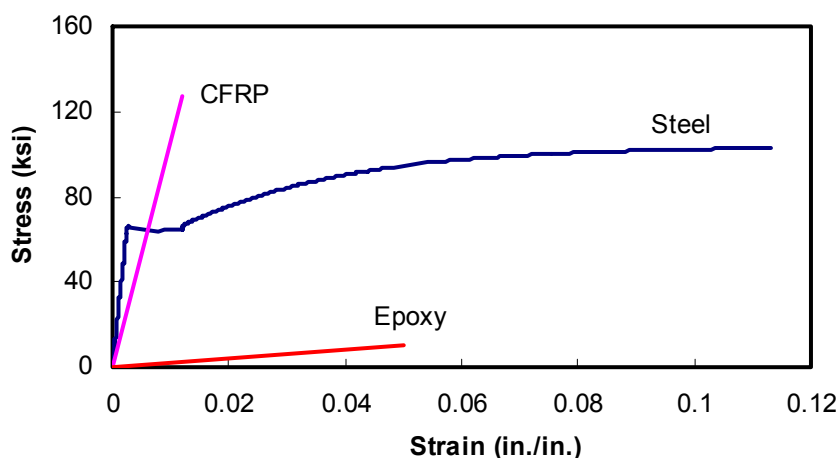
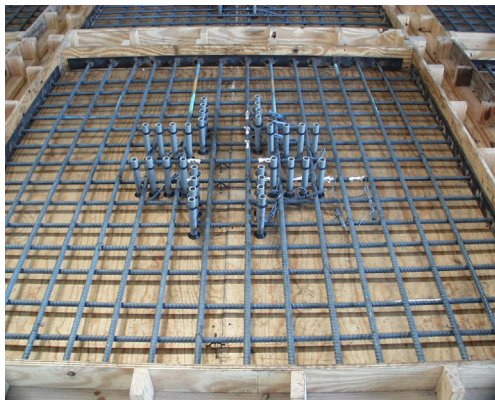


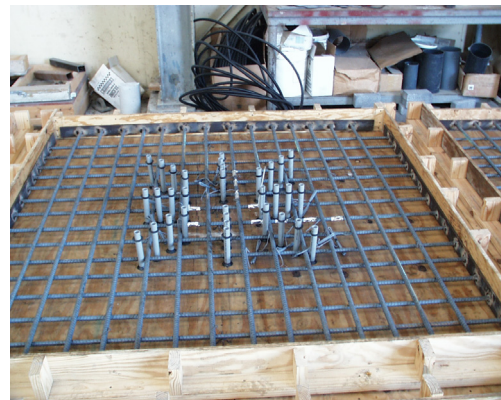
Figure 2.6 Comparison of Uniaxial Tensile Stress-Strain Response

Table 2.5 Results of CFRP Coupon Tests

CFRP Coupon	Tensile Strength (ksi)	Rupture Strain	Stiffness (ksi)
1	128	0.008	16031
2	96	0.012	7903
3	110	0.017	6682
4	101	0.015	6983
5	111	0.010	11075
6	115	0.014	8315
7	155	0.014	10957
8	98	0.015	6692
9	126	0.007	18493
Mean :	116	0.012	10348
St. Dev.	18	0.003	4298



(a) Pattern A



(b) Pattern B

Figure 2.7 Positioning of Holes around the Loading Area

using PVC pipes with $\frac{3}{4}$ " diameter prior to casting. Sharp corners around the holes, which may cause premature rupture of CFRP strips, were avoided by using tapered rubber washers prior to casting and chamfering the ends of the holes after casting (Figure 2.7). This simulates drilling of the holes in an actual flat plate and cleaning and smoothing of slab surfaces and rounding the edges of the holes. In

practice, rebar locators need to be used to avoid drilling through the flexural reinforcement. The additional damage to the flexural reinforcement, if any, will necessitate further strengthening of the slab in flexure by providing FRP sheets at the tension side, which has been studied previously by Mosallam et. al. (2000), in which they conducted experiments on strengthening two-way slabs for flexure by bonding FRP sheets on the tension face of the slab. Therefore, flexural strengthening of slabs is considered to be outside the scope of the current study. Although drilling of the holes with proper spacing may be difficult in existing structures, it remains more practical than other alternatives such as increasing column size with jacketing or casting an external drop panel.

The number of holes (CFRP shear reinforcement leg locations) on a line extending from the face of the loading plate was four for five specimens, and six and eight for two specimens, respectively (Table 2.2). The specimens were named according to CFRP perimeters extending from the face of the loading plate. A second number following the CFRP perimeter number was used to distinguish between specimens with same number of shear reinforcement perimeters (Table 2.2). The holes were arranged such that first hole was located $1\text{-}1/8$ in. ($d/4$) from the loading plate, and the spacing of the holes in both directions was $2\text{-}1/4$ in. ($d/2$). After curing of concrete, PVC pipes were removed from their locations by pulling them out. Then, specimens were placed on an elevated platform for strengthening. CFRP strips cut to 1 in. width and appropriate length were impregnated with epoxy. Then the strips were stitched through the holes and wrapped around to form closed stirrups (Figure 2.8). CFRP overlaps at the top slab surface complied with the minimum CFRP to CFRP anchorage length of 6 in. (as recommended by the manufacturer). Figure 2.9 illustrates the CFRP patterns and amounts used in strengthened specimens. After completion of CFRP stirrup placement, additional CFRP plates were bonded to the bottom of the slab to act as

closures for the holes so that the holes could be filled with epoxy. The CFRP bottom plates were kept short enough in order not to strengthen the slabs in flexure. No CFRP plates were used for the concrete bottom surface right below the loading plate, since this area is the column location in a flat plate structure.

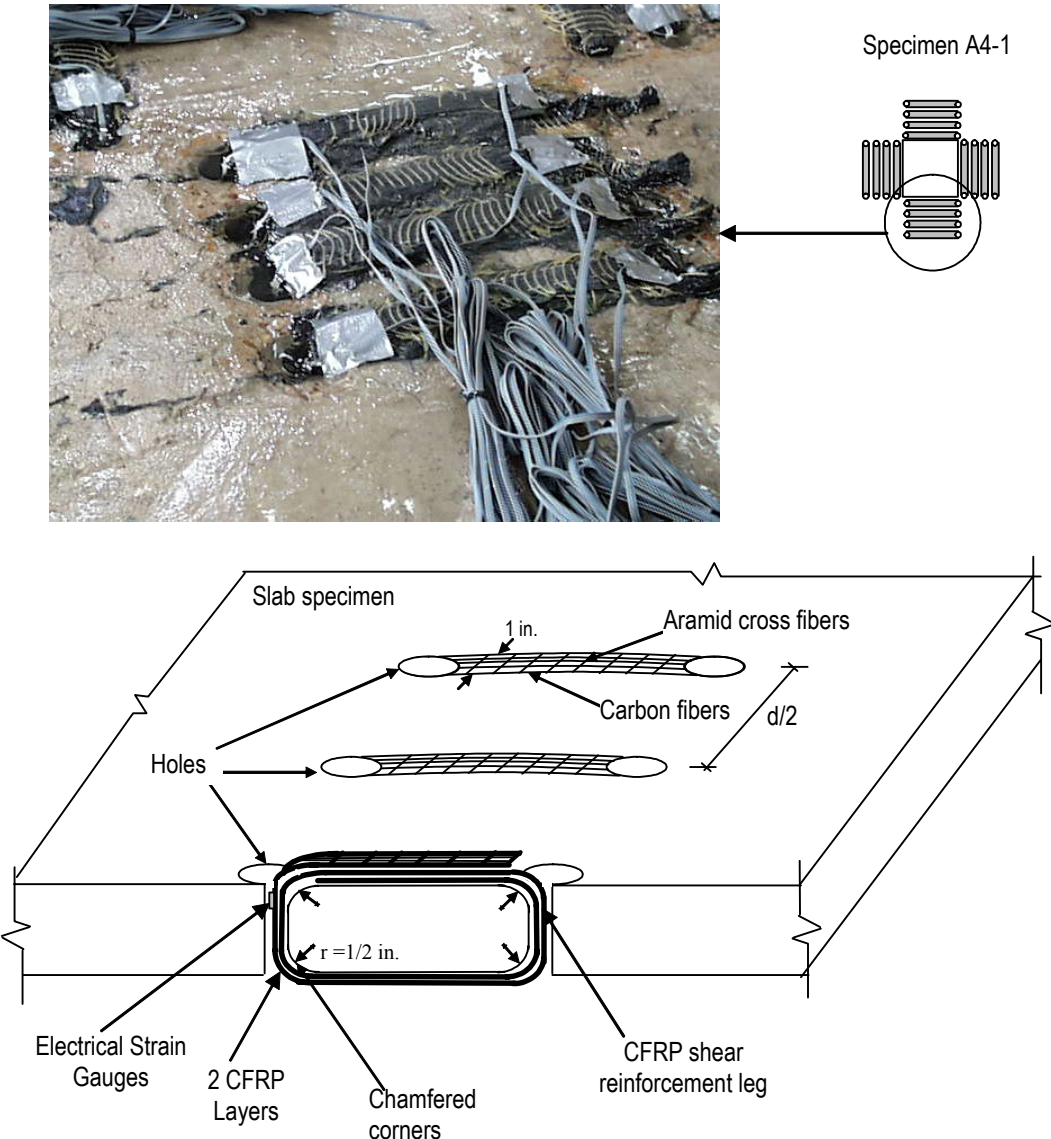
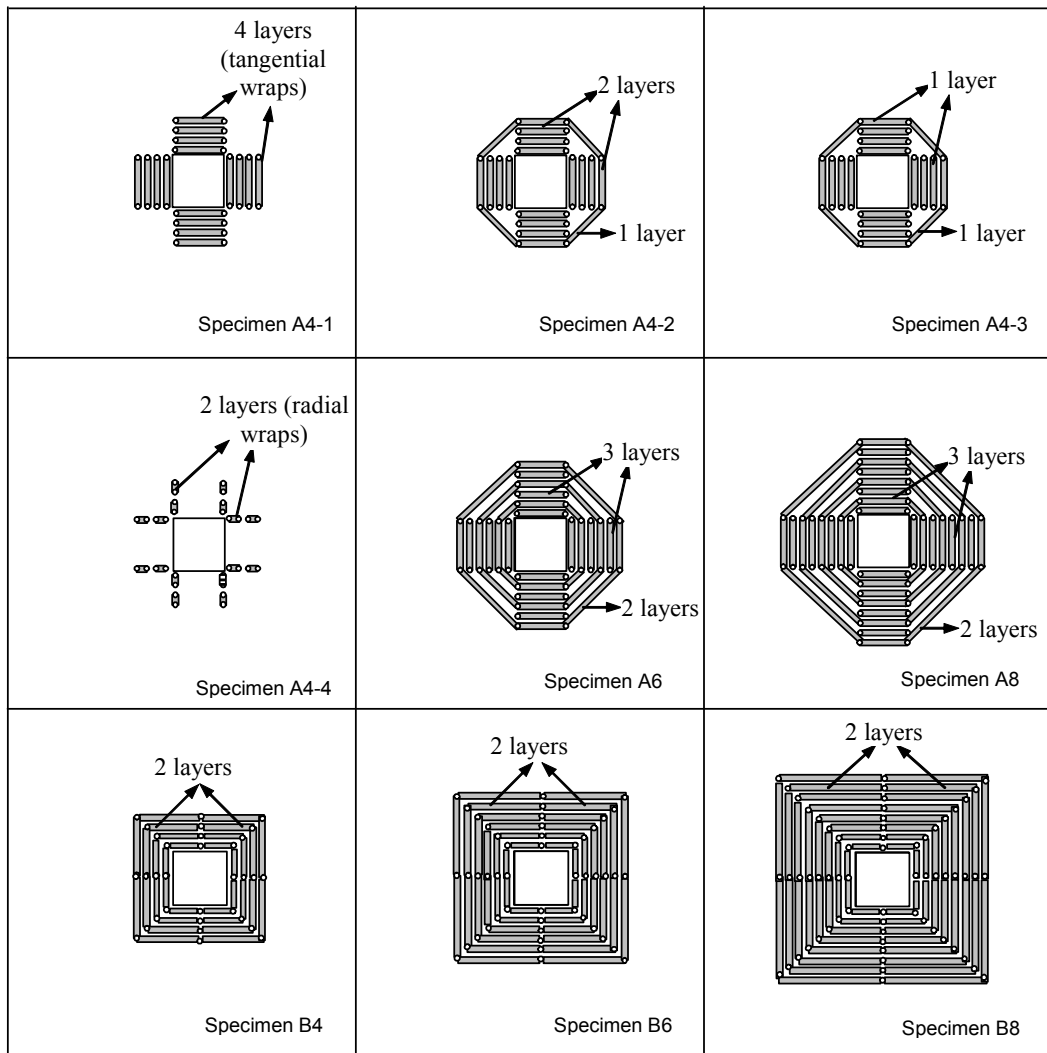


Figure 2.8 Application of CFRP Layers as Shear Reinforcement



— : CFRP strips ◦ : Location of holes and shear reinforcement legs

□ : Loading plate

1 layer corresponds to 1 in. wide and 0.04 in. thick CFRP strip.

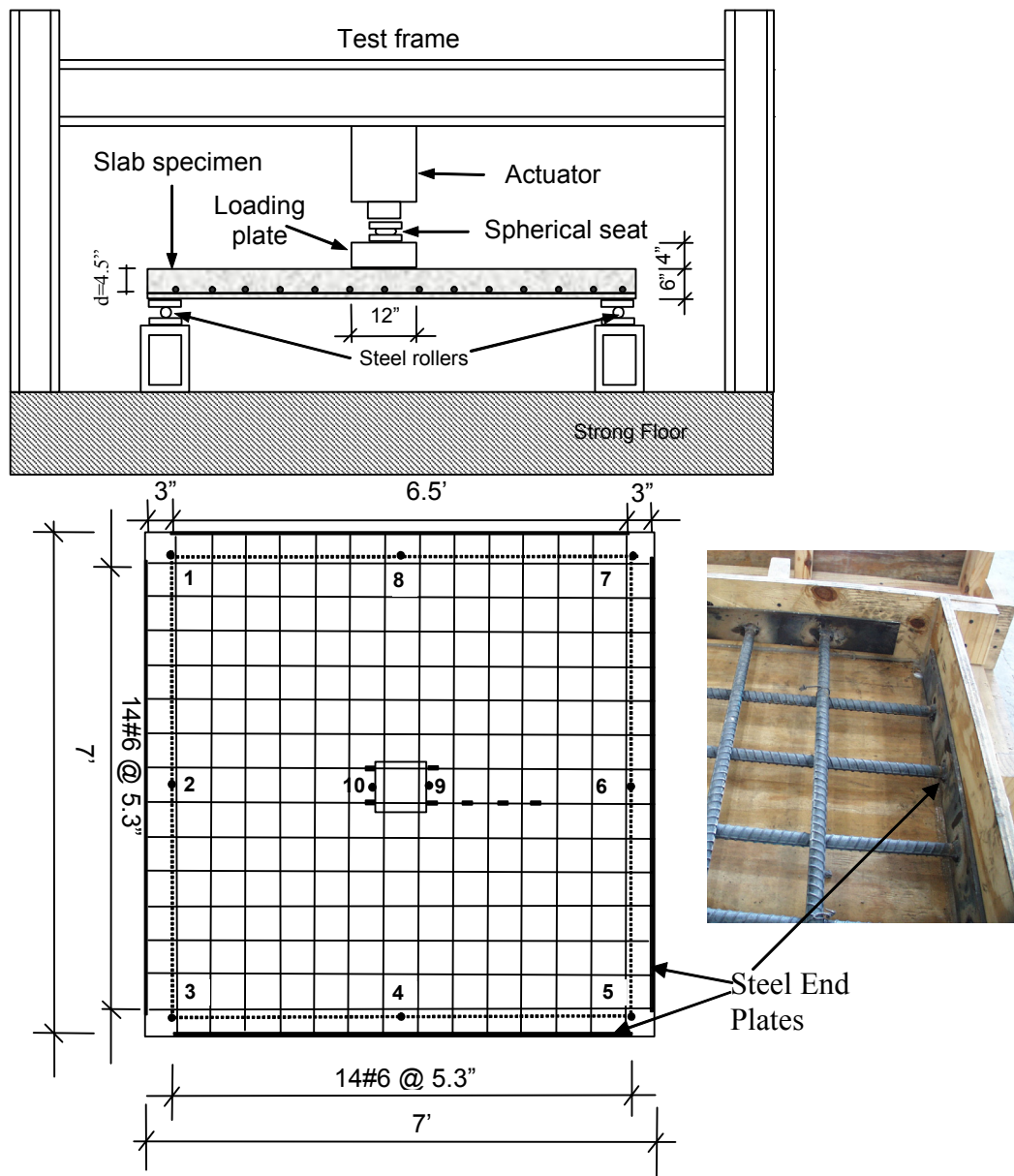
Figure 2.9 Strengthened Specimens (Plan View)

2.6 SPECIMEN DETAILS AND TEST PROCEDURE

2.6.1 Specimen Details

Slab dimensions (84 in. x 84 in. x 6 in.) and flexural steel reinforcement details were kept the same for all the specimens. The main flexural reinforcement was 14-No.6 bars spaced approximately at 5-1/4 in. (Figure 2.10) and arranged to give an average effective depth (d) of 4-1/2 in. The anchorage of these bars was provided by welding 1/4 in. thick steel end plates to the bars except specimen A4-4. This ensured that longitudinal bars were properly anchored to simulate realistic conditions in multi-span flat plate floors. All the slabs contained the same amount of tensile reinforcement (1.76%), and only one of the control specimens (Control-2) had two continuous compression bars with the same mechanical properties as the tensile reinforcement. Two reference specimens with no strengthening were named as Control-1 and Control-2. Control-1 complied with the relevant provisions of ACI 318-63, simulating an existing reinforced concrete flat-plate connection requiring upgrade. Control-2 was designed using the provisions of ACI 318-02 for integrity steel, providing valuable information about the behavior of a typical slab-column connection without shear reinforcement. The two compression bars used in specimen Control-2 provided approximately 0.82% reinforcement ratio under the loading plate region. Names and CFRP details for upgraded specimens are presented in Section 2.5 (Figure 2.9).

A square steel loading plate (12 in. x 12 in. x 4 in.) simulating a column was used to apply the concentrated load. The absence of a concrete column does not realistically simulate the joint region. However, provided that the punching failure occurs outside the joint region and the slab under the loading plate does not suffer any significant damage, the results of the experimental program are not believed to be affected in the absence of a reinforced concrete column.



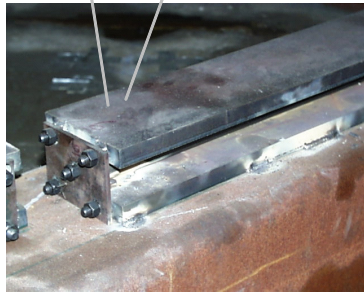
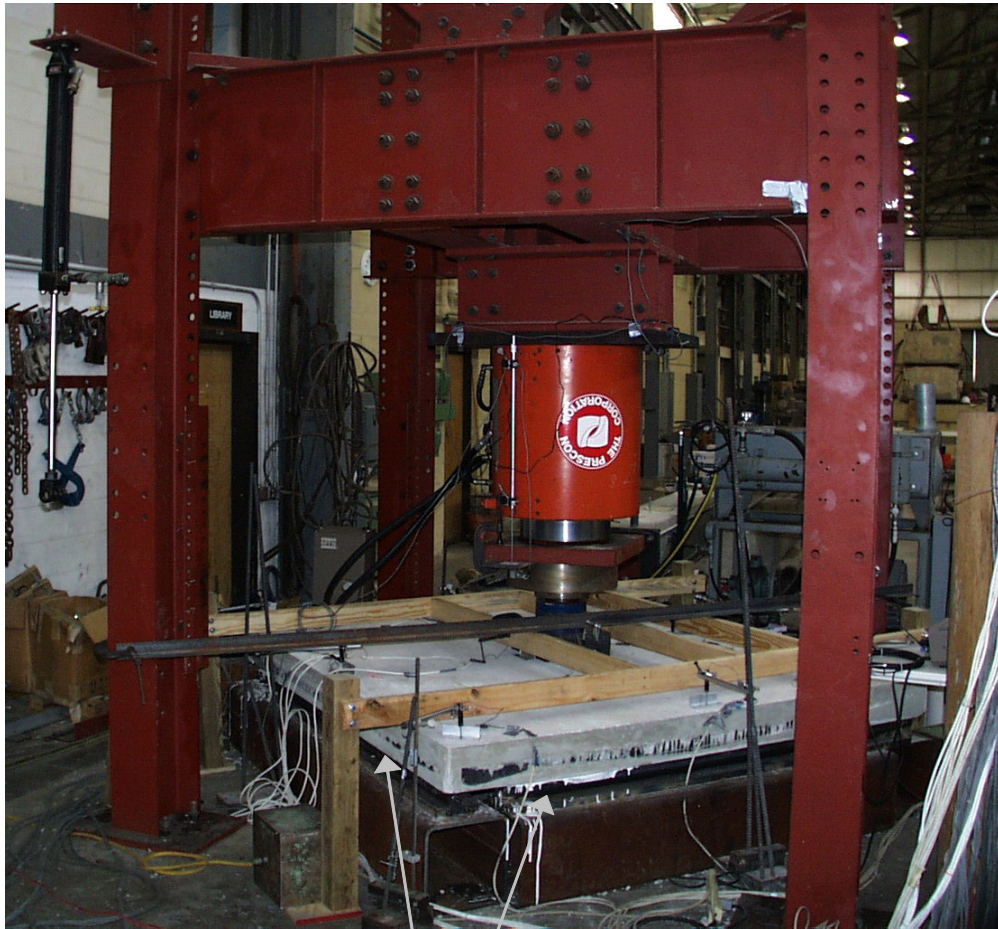
- Linear-potentiometer locations on slab surface
- Steel strain gauge locations
- Support centerline

Figure 2.10 Details of Test Specimens, Instrumentation and Test Setup

Prior to testing, all the specimens were set on steel plates resting on steel rollers along their four sides, leaving the corners free to uplift (Figure 2.10 and Figure 2.11). The studies on the effect of boundary conditions are well described in the document prepared by CEB-FIP (2001) based on experimental findings of various researchers. It is known that the in-plane and rotational restraint provided by the portion of the slab beyond the lines of contra-flexure in an actual flat plate system enhance the punching shear capacity. However, it is difficult to quantify the magnitude of restraint provided in the test zone especially at large inelastic deformations. The boundary conditions from plate theory for a simply-supported plate, where discrete corner forces are observed, also do not realistically model an actual flat plate system. Therefore, it was preferred to be consistent with the control and strengthened specimens in terms of the boundary conditions and to study the percentage increases in the load carrying capacity and ductility. The actual values of load carrying capacity, deformation at failure and stiffness after first cracking may change depending on the selection of the boundary conditions. However it is believed that percentage increases in capacity (strength and ductility) with different boundary conditions should remain similar. The use of different boundary conditions may slightly alter the improvements in load and deformation capacities of the upgraded specimens; but these small differences should not change the results of the study presented herein.

2.6.2 Instrumentation and Testing

A stiff reaction frame was used in the testing of all specimens (Figure 2.11). A spherical seat was placed between the actuator and the steel plate to avoid uneven application of the load. Load measurements were taken through the load cell connected to the actuator. Specimens were tested in a displacement controlled mode with an average displacement rate of approximately 0.01 mm/sec



Support Detail

Figure 2.11 Test Setup

through the use of an MTS 407 controller. A stiff instrumentation frame was used and this frame was fixed at the base by placing steel weights (Figure 2.11). Linear potentiometers were used to measure the displacement of the slab at every

displacement increment. Electrical resistance strain gages attached to reinforcing bars, vertical CFRP legs and concrete surface were used to monitor the strains. FLA-5-11-3LT gauges for steel strains, special composite gauges, BFLA-5-3LT, for CFRP strains and PL-3LT gauges for concrete strains were used. Quick drying adhesive (CN-Y) was used to ensure the bond between the CFRP gauges and the composite material. A smooth surface was obtained for concrete and FRP gauges by applying PS-2 adhesive on concrete and CFRP surface respectively. After completion of the CFRP stitching, strain gauges were bonded to vertical CFRP legs (Figure 2.8). All the gauges were water-proofed using M-Coat D. Concrete strains were also measured for specimen Control-2 on the slab compressive surface within a distance of about 15 in. from the loading plate both in the radial and tangential directions. The locations of steel strain gauges and linear potentiometers are given in Figure 2.10. The locations of CFRP and concrete strain gauges are introduced in the upcoming sections (Sections 2.7.2.2 and 2.7.2.3) while presenting the results of the measurements.

Data were acquired through a Hewlett-Packard 3852 Scanner. Analog to digital signal conversion was performed by using a National Instruments Data Acquisition Card in a Windows based environment, running under Measure, a National Instrument add-in for the Microsoft Excel spreadsheet program.

2.7 TEST RESULTS

The results of the experiments on concentrically loaded flat plate tests are presented in this section. Load-deformation characteristics, measured strains on concrete surface, steel and CFRP reinforcement, and observed crack patterns are given. The detailed discussions of test results are presented in Section 2.8.

2.7.1 Load Deformation Results

The central deflection is calculated by subtracting the average displacements from linear potentiometers 2, 4, 6, and 8 from the average displacements from linear potentiometers 9 and 10 (Figure 2.10). Applied load versus relative central deflection plots for the test specimens are given in Figure 2.12 to Figure 2.14. The solid line shown in these figures, which can also be classified as initial tangents, are the results of elastic analysis of a simply-supported plate with gross section properties, measured material properties, and patch loaded at the center. Navier's type double series solution is used for the analysis of the simply supported plate loaded with a square patch load at the center (Reddy, 1998). This analytical solution does not allow the uplift of the corners. Therefore a linear elastic finite element analysis considering the support uplift was performed to compare the stiffness of the more accurate model. It was found that the stiffness of the system differed by about 8%, the finite element solution being more flexible. Based on these two analyses, it is possible to say that analytical solution from elastic plate theory provided a reasonable approximation of the stiffness of the plate.

It is important to note that until first cracking the slopes of the measured responses were in good agreement with the elastic response. Since it was not possible to observe visually first cracking on the underside of the specimens, the point where the load-deflection response deviated from the initial elastic response gives an indication of the point of first cracking.

Comparisons of the behavior of pattern A and pattern B specimens are shown in Figures 2.15 and 2.16, respectively. Load deflection behavior of specimens with 4 perimeters, A4-1, A4-2, A4-3, A4-4, B4, and specimen Control-1 are compared in Figure 2.17. In addition, post-punching load carrying capacities of control specimens with and without integrity steel are shown with dotted lines

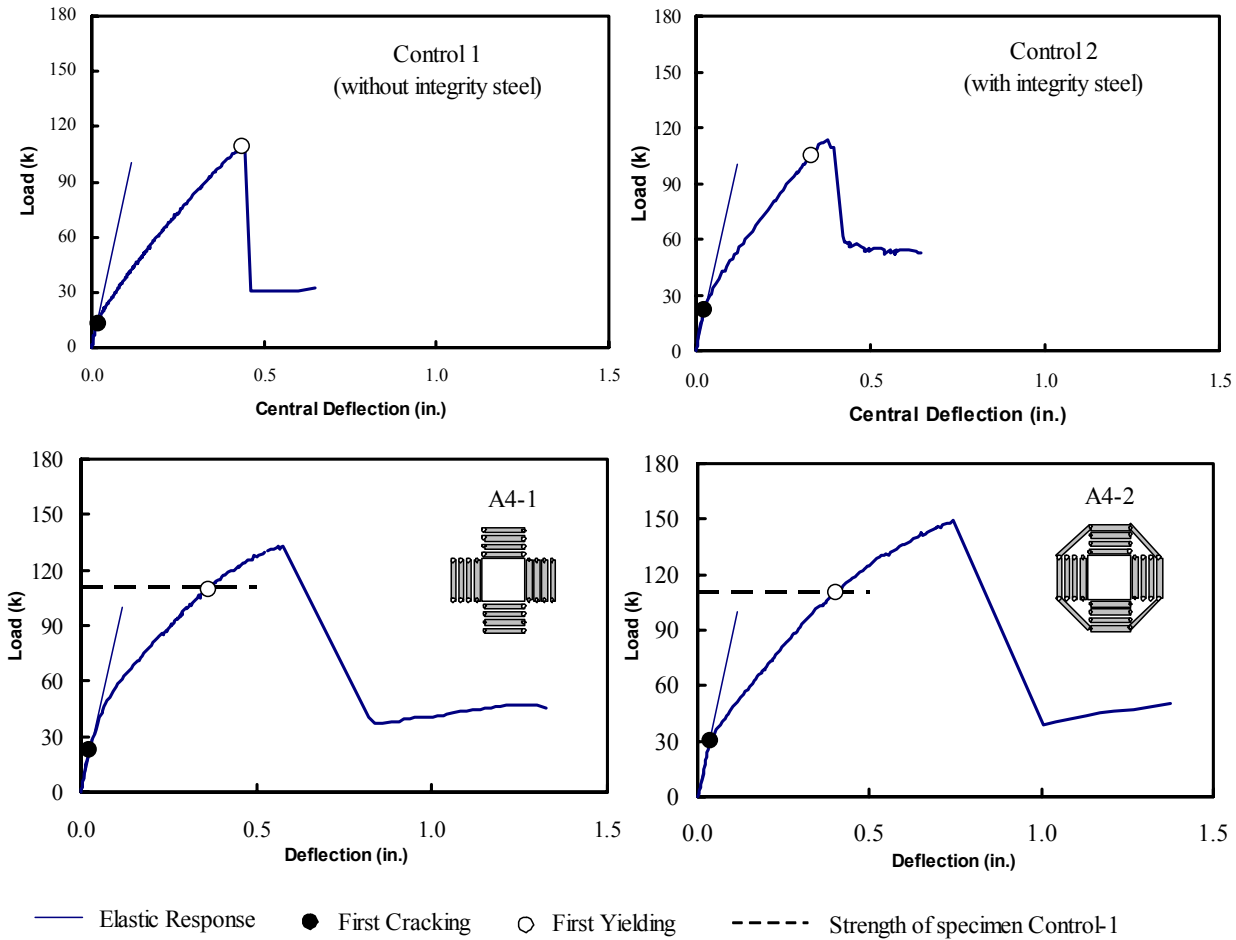


Figure 2.12 Load Deformation Behavior of Specimens Control-1, Control-2, A4-1 and A4-2

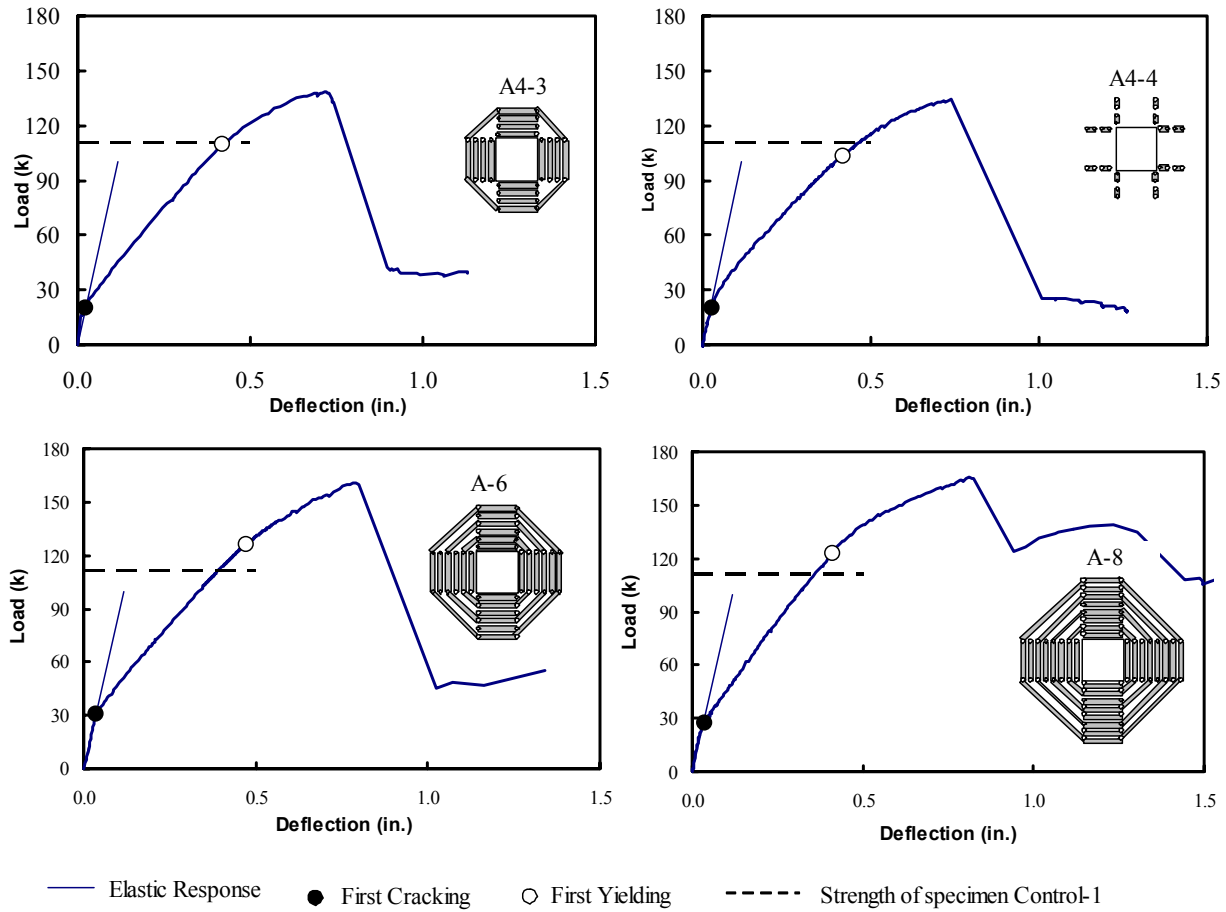


Figure 2.13 Load Deformation Behavior of Specimen A4-3 and A4-4, A6, and A-8

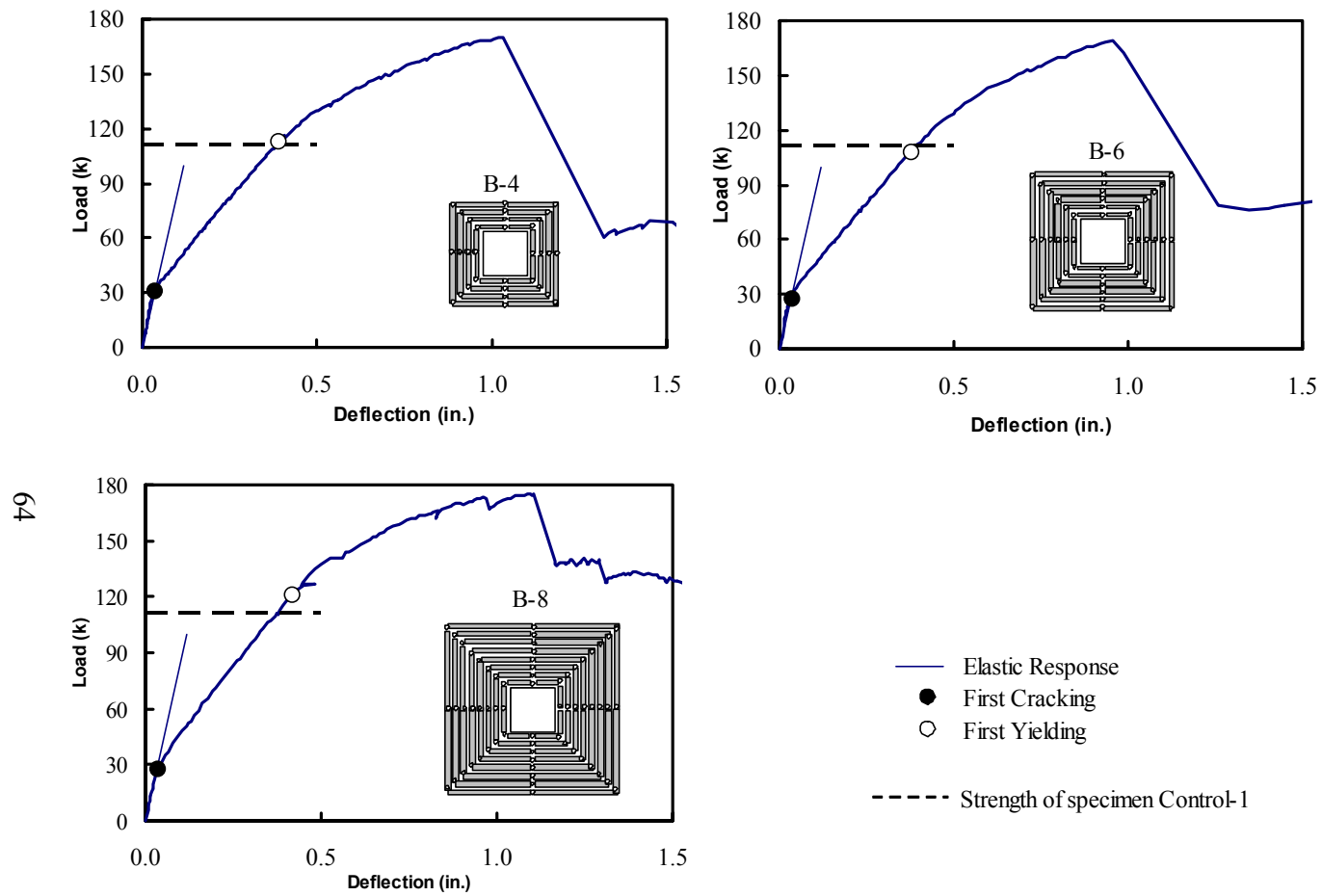


Figure 2.14 Load Deformation Behavior of Specimens B-4, B-6 and B-8

in Figure 2.15 and Figure 2.16.

The flexural capacity of the specimens, V_{flex} , was computed using a more detailed yield line than that previously shown in Figure 2.2, which was used in the design of the test specimens. This pattern consists of two lines extending from each column corner forming corner levers (Elstner and Hognestad 1956; Criswell 1974) to account for the uplift observed in slab corners (Figure 2.18). Load deformation behavior of test specimens (Figures 2.15 and 2.16) shows that CFRP reinforcement has negligible effect on initial stiffness and cracked stiffness. This is an indication of CFRPs having an insignificant effect on flexural capacities of test specimens. Therefore, it is believed that yield line analysis shown in Figure 2.18 provides a reasonable estimate of flexural capacity for all of the specimens.

Table 2.6 summarizes the results of load-deflection measurements for all specimens. The cracking load for the specimens ranged from 13 k to 31 k (Table 2.6). The load at the initiation of yielding in flexural reinforcement at the face of the loaded area ranged from 104 k to 126 k for the specimens. The load carrying capacity of specimen Control-2 was 3% higher than that of specimen Control-1. This shows that there was a negligible effect of the compression steel on the load carrying capacity. The strength of specimens upgraded with pattern A ranged from 1.2 to 1.5 times the strength of specimen Control-1. The strength of specimens upgraded with Pattern B ranged from 1.5 to 1.6 times the strength of the control specimen.

The ratio of maximum measured loads, V_u , to calculated flexural capacity, V_{flex} , increased from approximately 0.7 for the control specimens to about 1.0 for specimens A6 and A8 (Table 2.6). Although flexural capacity according to the yield line method was reached for specimens A6 and A8, extensive yielding did not occur, and punching failures occurred after some yielding in the repaired zone. Similarly, although specimens B4, B6 and B8 reached their computed

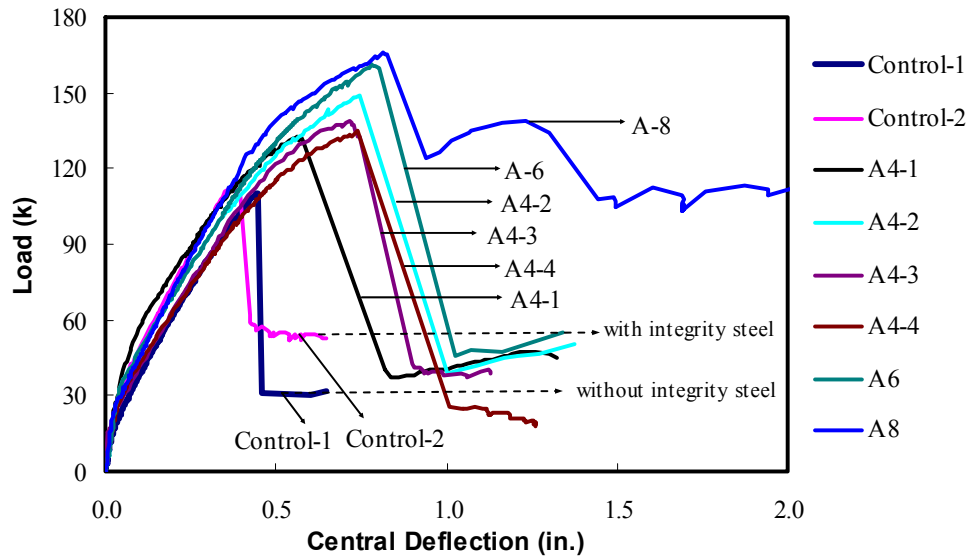


Figure 2.15 Load Deformation Comparison of Pattern- A Specimens

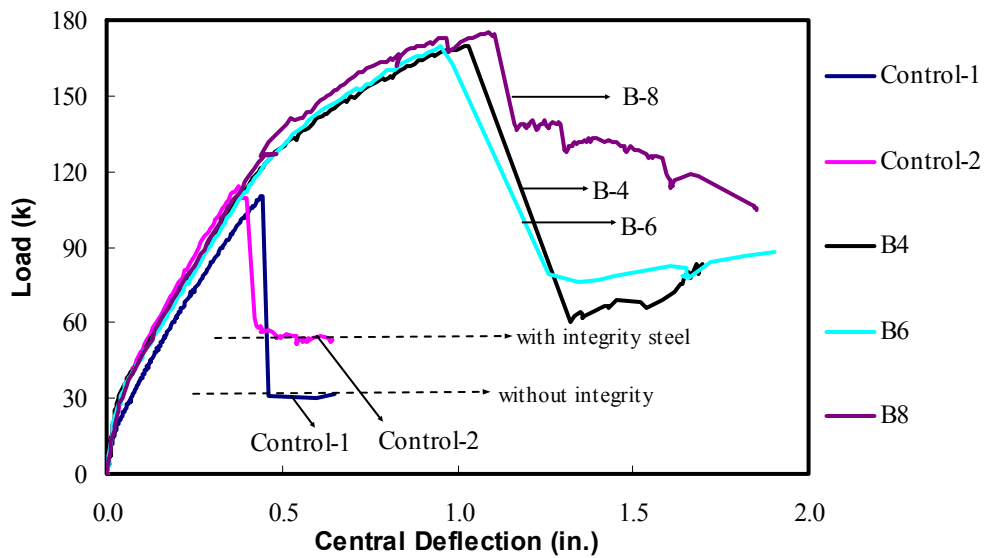


Figure 2.16 Load Deformation Comparison of Pattern- B Specimens

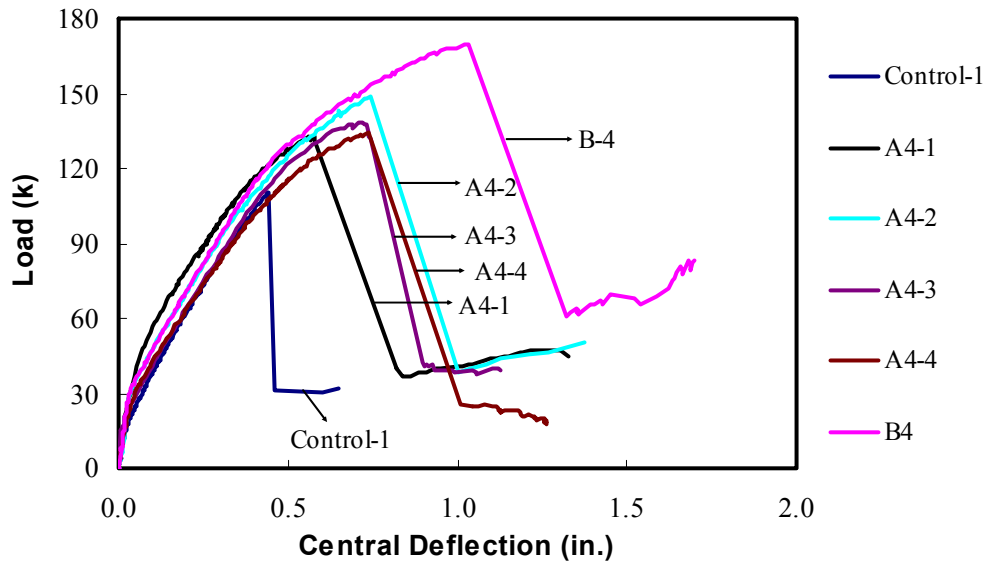


Figure 2.17 Load-Deformation Comparison for A4, B4, and Control Specimens

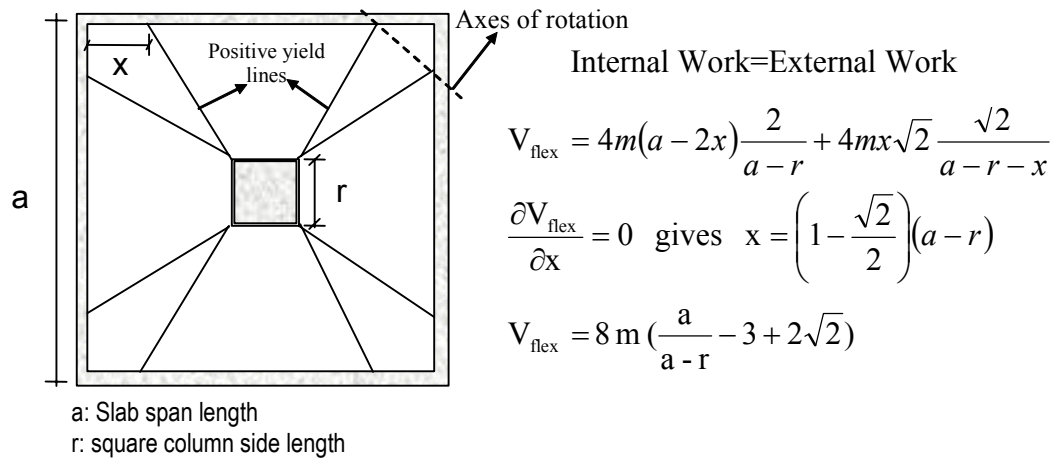


Figure 2.18 Refined Yield Line Analysis Considering Corner Uplift

flexural capacities, a complete ductile behavior with a yield plateau was not achieved. This agrees with research results reported by Elstner and Hognestad (1956) and Criswell (1974). These researchers observed that although yield line

strengths of the slabs were attained, punching failure took place due to the lack of over-strength (reserve strength) and ductility needed for a yield mechanism to occur. The ultimate loads for flexural mechanisms were observed to be about 10 to 25% above the yield line loads in their experiments (Elstner and Hognestad (1956) and Criswell (1974)). This difference was attributed to the possible strain hardening and membrane action that occur during a flexural mechanism but are not accounted for in the yield line analysis (Sections 1.4.1.1 and 1.4.1.4).

The ratios of post cracking stiffness to the initial stiffness of the specimens are also presented in Table 2.6. This ratio was between 0.24 and 0.30 and showed very little variation from specimen to specimen.

The capacity immediately following the punching failure (V_{pp}) of specimen Control-2 was about 1.9 times that of Control-1 (Table 2.6). The values of V_{pp} for specimens A4-1, A4-2, 4-3 and A6 were higher than that of Control-1 however smaller than V_{pp} of Control-2. The capacity losses at punching failure for specimens A-8, B-4, B-6, and B-8 were smaller in comparison to that of specimen Control-2. For specimens B-8 and A-8, V_{pp} values in the tests were actually higher than the load carrying capacities of the control specimens.

Displacement ductilities (Δ_u/Δ_y), defined as the ratio of deflection at the ultimate load divided by the deflection at first yield was about 1.0 for Control specimens. For specimens with pattern A, displacement ductility ranged from about 1.5 to 2.0. On the other hand, higher displacement ductilities (from 2.5 to 2.7) were observed for specimens strengthened with Pattern B. It was also possible to see that as the area of the CFRP strengthened zone increased, the maximum load carrying capacity and displacement ductility tended to increase.

Table 2.6 Summary of Test Results

Specimen Name	Maximum Measured Load, V_u (k)	Punching Failure Location	V_u/V_{flex}	Load at First Cracking, V_{cr} (k)	Load at First Yield, V_y (k)	Post-Punching Load, V_{pp} (k)	Ratio of post cracking stiffness to initial stiffness, K_{cr}/K_i	% Increase in Ultimate Load with respect to Control 1	Deflection at First Cracking, Δ_{cr} (in)	Deflection at First Yield, Δ_y (in)	Deflection at Ultimate Load, Δ_u (in)	% Increase in Displacement with respect to Control 1	Displacement Ductility, Δ_u/Δ_y
Control 1	110	-	0.67	13	109	31	0.27	-	0.017	0.43	0.44	-	1.03
Control 2	114	-	0.69	23	105	56	0.30	-	0.024	0.33	0.38	-	1.15
A4-1	133	Inside / Outside	0.81	23	110	37	0.28	20	0.023	0.36	0.56	26.1	1.56
A4-2	149	Outside	0.91	31	111	39	0.26	35	0.037	0.40	0.74	67.6	1.85
A4-3	139	Inside	0.85	20	110	39	0.26	26	0.020	0.42	0.71	59.8	1.69
A4-4	135	Inside	0.82	21	104	26	0.24	22	0.027	0.42	0.74	66.6	1.78
A6	161	Outside	0.98	31	126	46	0.25	46	0.036	0.46	0.78	75.8	1.70
A8	166	Outside	1.01	28	123	125	0.30	50	0.035	0.41	0.81	83.1	1.98
B4	170	Outside	1.04	31	113	61	0.27	54	0.035	0.39	1.03	131.9	2.64
B6	169	Outside	1.03	28	108	79	0.27	53	0.037	0.38	0.95	113.9	2.53
B8	175.0	Outside	1.07	27	121	131	0.28	59	0.036	0.42	1.09	144.5	2.59

2.7.2 Strain Measurements

This section summarizes the results of strain measurements on steel reinforcement, CFRP strips, and concrete surface. Locations of steel strain gauges are shown in Figure 2.10, whereas locations of CFRP and concrete gauges are introduced in the upcoming sections. CFRP and concrete gauge designations are based on their distances from the face of the loading plate. Additional results are also presented such as comparisons of estimated moments based on elastic plate theory against those obtained from measured strains, and concrete and CFRP contributions that are based on strain measurements.

2.7.2.1 Steel Strains

Steel strain profiles are shown in Figure 2.19 for rebars passing under the loaded area at the ultimate loads of the specimens. The horizontal line in this figure illustrates the yield strain for reinforcing bars, determined as 2240 microstrain from uniaxial tension tests. Steel strains decreased with increasing distances from the loading plate. Yielding distance was calculated by linear interpolation between strain measurements. According to this, yielding distance increased from about 0.8 in. from the face of the loading plate for Control-1 to about 5 in. for A8 and for all pattern B specimens. To put this in perspective, the ratios of the plan areas of the slab in which the flexural reinforcement yielded can be examined. Figure 2.20 shows the assumed rectangular zone of yielding. Although strain gauges were not located at the corners of this area it is reasonable to assume this zone to be rectangular for the sake of comparisons. According to this, the ratio of the areas in which the reinforcement yielded for Specimen A8, B4, B6, and B8 to that of Control-1 was about 2.5 (Figure 2.20). However, when the size of the zone where flexural reinforcement yielding was experienced is compared to the size of the test specimen, it can be seen that the zone of yielding was limited to 8% of the

test specimen. It should be noted that even if the yielding zone is assumed to be a circular a similar ratio is obtained for the ratio of yielding zone to test specimen size.

A systematic increase was observed in the ultimate strains reached in steel reinforcement with increasing load carrying capacities. Measured steel strains support the aforementioned relation between flexural capacity from yield line analysis and the punching loads; that is initiation of yielding of flexural reinforcement does not guarantee a flexural failure mode (formation of a collapse mechanism through flexural yielding). Although high strain levels in flexural reinforcement were reached for strengthened specimens, it was not possible to change the failure mode completely to flexure. Punching failure mechanism initiated once the shear strength of the unreinforced region was reached.

Figure 2.21 and 2.22 show the strain profiles of the test specimens at loads corresponding to $\frac{1}{4}$, $\frac{1}{2}$, $\frac{3}{4}$ and 1 times their load carrying capacities. It was observed that the increase in steel strains were almost proportional until first yielding at the face of the loading plate. Punching failure took place soon after the yielding of steel for specimens Control-1 and A4-2 (similar to other A4 specimens). For specimens A6, A8, B-4, B6 and B-8 first yielding of the flexural reinforcement was observed at about $\frac{3}{4}$ of the loads. After this load stage, strain localization occurred at the face of the loading plate, and strains almost 3 times yielding strain of steel were reached. However, second strain gauges located 5 in. away from this gauge barely reached the yielding strain. Punching failure took place before yielding occurred beyond about 5 in. away from the face of the loading area. There are two main reasons for this situation:

(i) The section was heavily reinforced (1.76%), and moment demands on the section were rapidly decreasing for a given applied load. Figure 2.23 shows

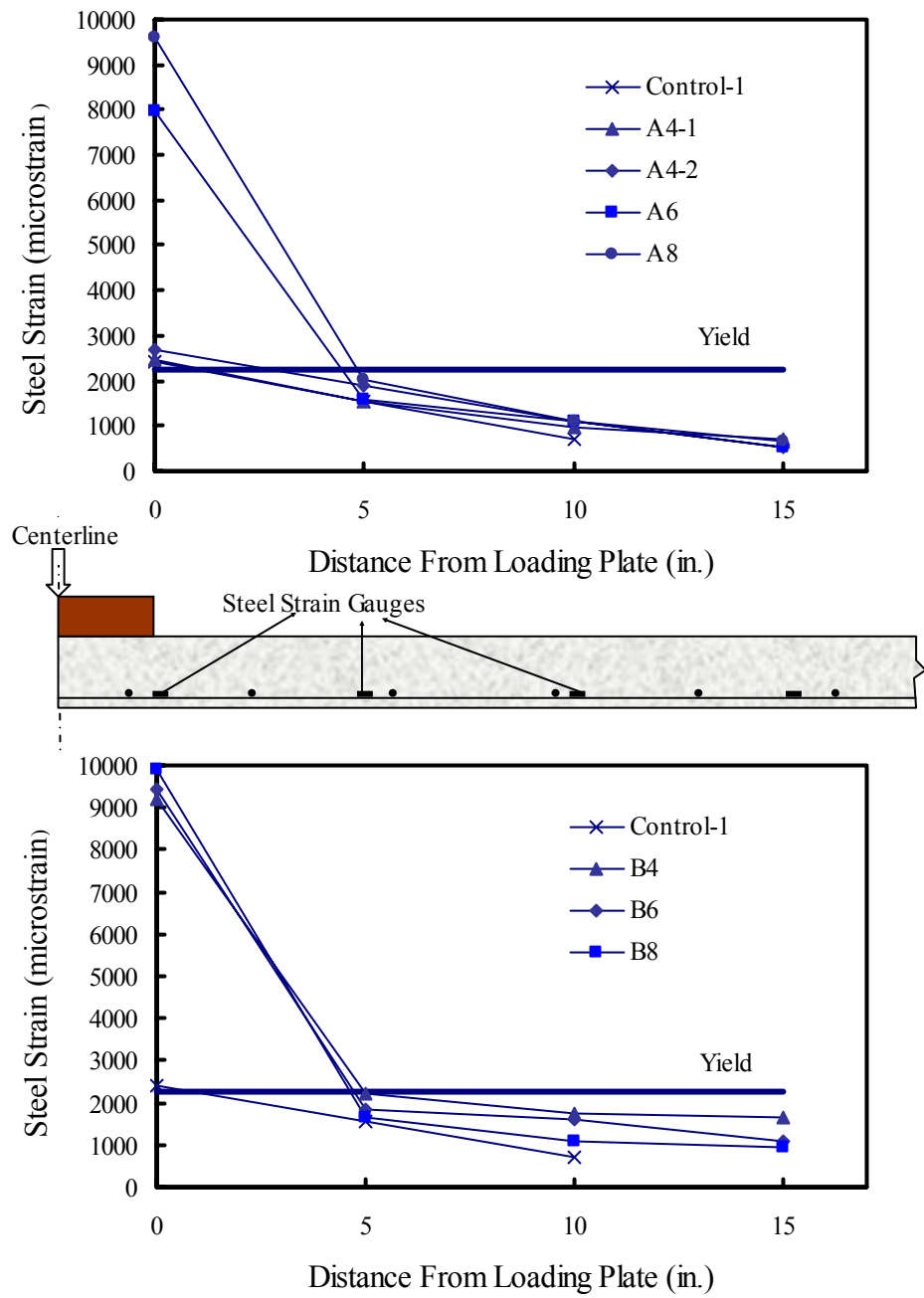


Figure 2.19 Steel Strain Profiles

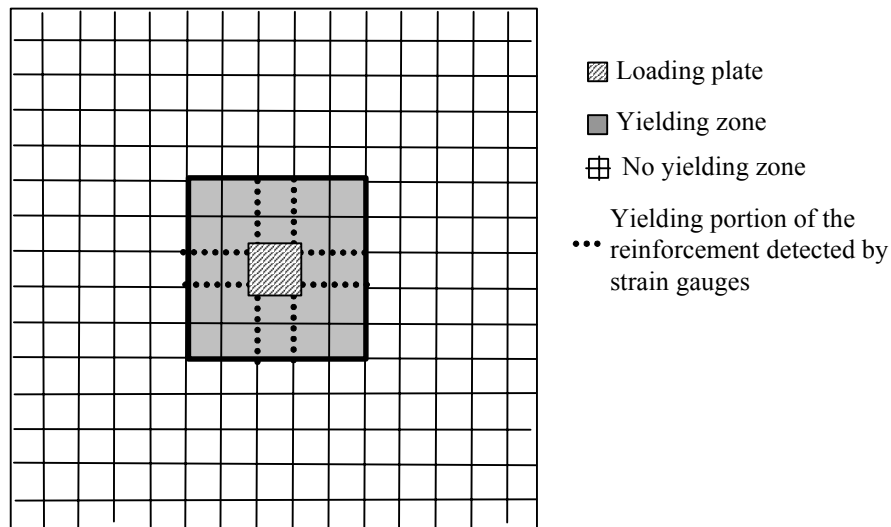


Figure 2.20 Yielding Zone of Flexural Reinforcement in Test Specimens

the moment diagram across the centerline of the slab for an applied load of 100 k, calculated using the material properties and dimensions from the test specimens using the elastic plate theory. The moments per unit length, M_x and M_y at the center of the slab are equal due to symmetry of the loading and geometry. It can be seen that the moment on the section 5 in. away from the face of the loading plate is about 55% of the moment at the face of the loaded area. This shows that prior to reaching strain levels several times larger than the yield strain, spreading of yielding, i.e. a flexural failure mechanism, can not be obtained. However, it is shown in Chapter 3 that for realistic levels of flexural reinforcement used in existing flat plate systems (0.5-1.2%), more ductile behavior can be obtained with the use of proper shear reinforcement.

(ii) There exists a weaker zone that is susceptible to shear failure outside the shear reinforced zone prior to a flexural mechanism. High strains in steel reinforcement are reached at the face of the loading area. Before yielding in the longitudinal reinforcement can extend away from this location, punching failure occurs by reaching the capacity outside the shear reinforced zone.

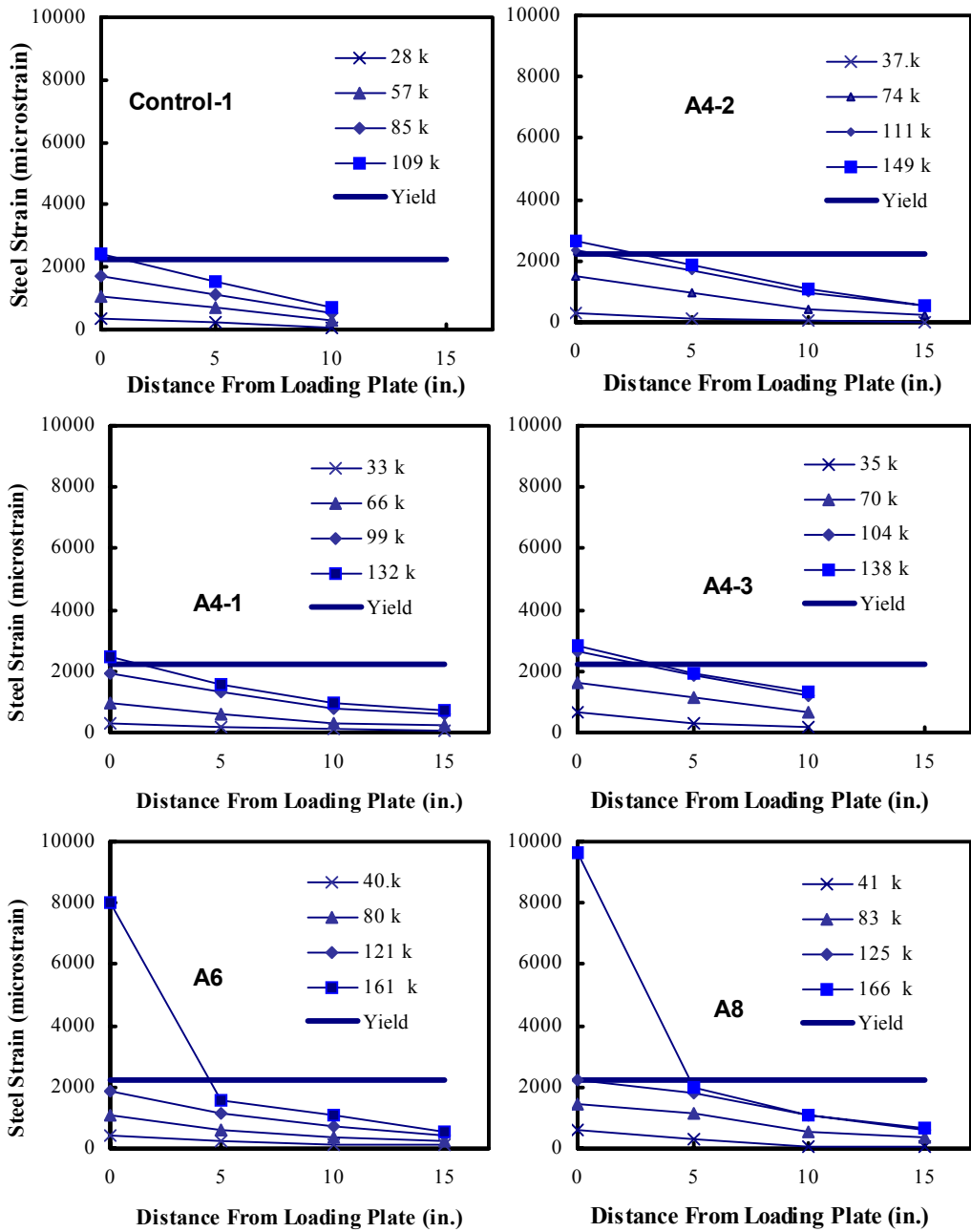


Figure 2.21 Steel Strain Profiles at Various Load Levels (Specimens Control-1, A4-1, A4-2, A4-3, A6, A8)

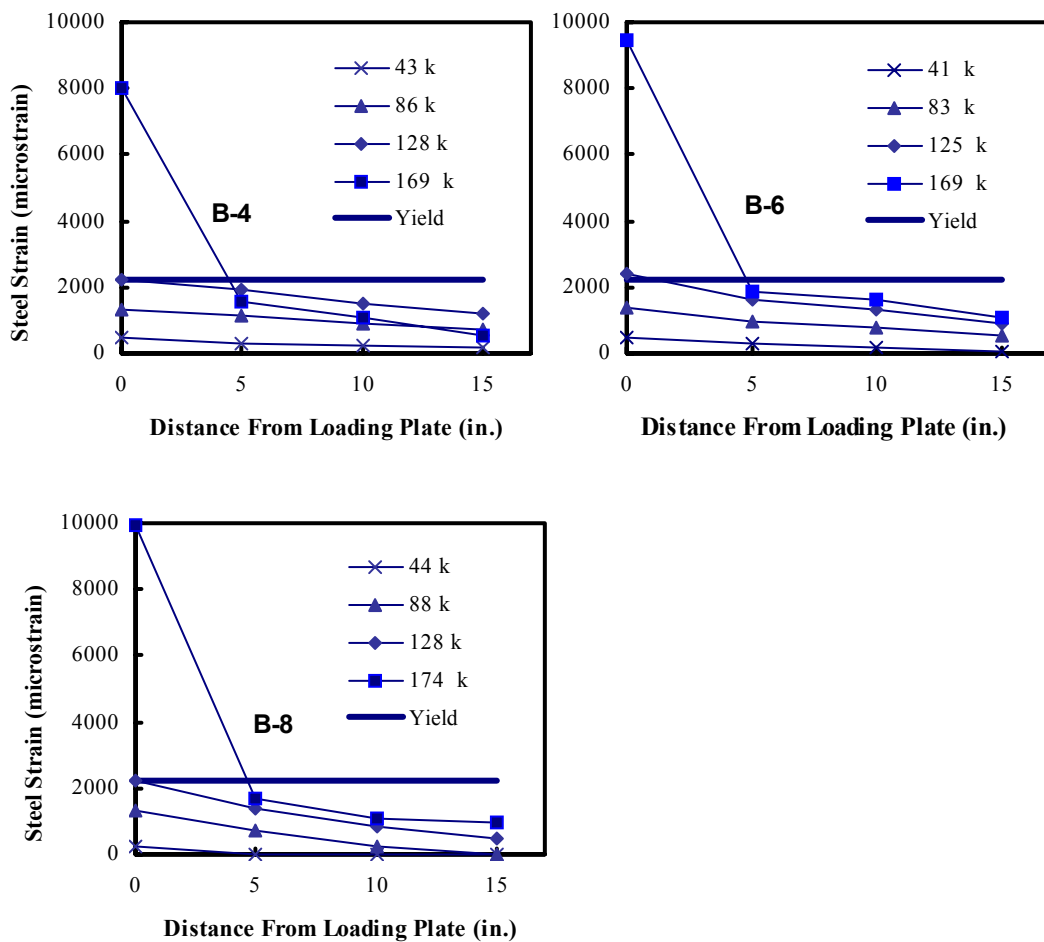


Figure 2.22 Steel Strain Profiles at Various Load Levels (Specimens B-4, B-6 and B-8)

In order to gain more confidence on the measured steel strains, the moments calculated using measured steel strains were compared with those computed using elastic plate theory. The procedure can be summarized as follows: First, moment versus steel-strain curve was developed for a unit width of concrete section similar to that of the slab section using sectional analysis (Figure 2.24). This curve can be used to evaluate the sectional moment for a given level of steel strain. Sectional moments at gauge locations were determined by simply

using this relationship. In addition, it is possible to compute the elastic sectional moment for a given level of applied load using elastic plate solution (previously used in Section 2.7.1 to compute the elastic stiffness of the slab). The load corresponding to the measured strains was used with elastic plate analysis to compute the elastic sectional moment. It is important to note that this procedure assumes that strains in the flexural reinforcement are primarily due to the bending moments about an axis perpendicular to the direction of the reinforcement.

Figure 2.25 shows the comparisons of analytical moments from elastic analysis to the computed moments from measured strains at different load levels. It can be observed that a good agreement was obtained, validating the steel strains with the elastic theory at load levels less than $\frac{1}{2}$ of the load carrying capacity. Extensive cracking and possible yielding in the reinforcement caused redistribution along the width of the slab, and elastic moments deviated from the moments in the cracked portions of the slab. Plasticity methods, such as the yield line analysis, are more appropriate for use after extensive yielding. Therefore, calculations from first yielding up to the load carrying capacity can not yield accurate results using the procedure described above.

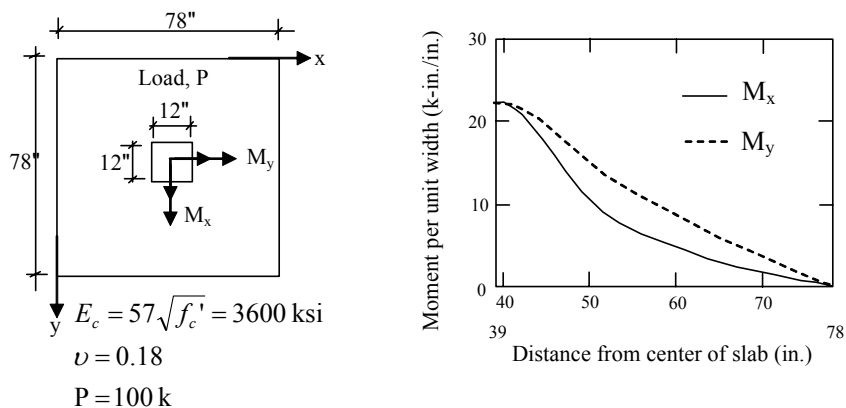


Figure 2.23 Elastic Moments for a Centrally Loaded Plate with Four Sides Simply Supported

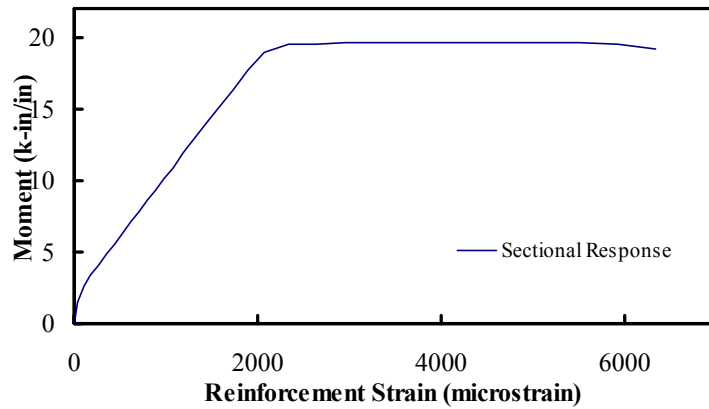


Figure 2.24 Moment versus Steel Strain Response of RC Slab Section

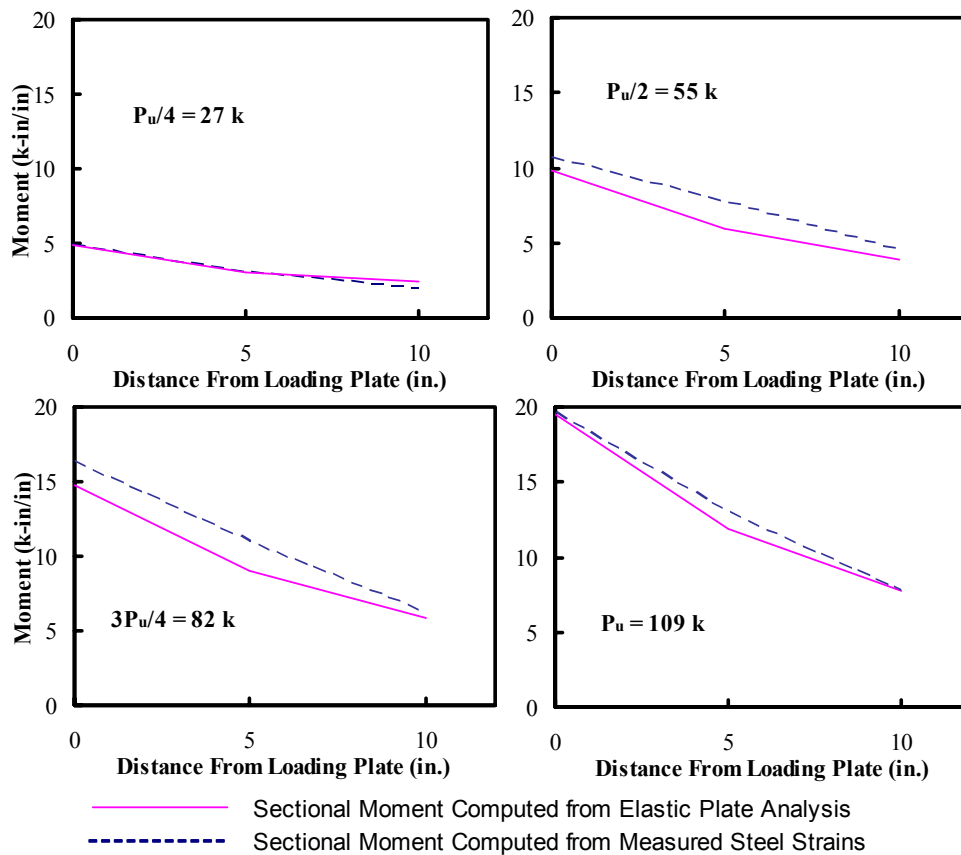


Figure 2.25 Comparisons of Calculated Sectional Moments from Strain Gauge Readings against Elastic Sectional Moments

2.7.2.2 Concrete Strains

Concrete strains were measured on the top surface of specimen Control-2 to observe the strain levels at punching. Radial and tangential strains were measured at various locations. Figure 2.26 shows the measured compressive radial and tangential strains versus the distance from the face of the loading plate. Both the tangential and the radial strains at ultimate load decreased with increasing distance from the loading plate. In addition, with increasing distance from the loading plate there was a more rapid decrease in the radial strains, which were always smaller than the tangential strains.

The highest tangential strain measured was about 1800 microstrain, which corresponds approximately to a biaxial confining stress of $0.95f_c'$. Existence of high tangential strains (and lower radial strains) at the face of the loading plate was an indication of one of the following two failure modes:

- 1- Failure of the compression zone due to splitting failure through the thickness,
- 2- Failure due to shear-compression failure of the compression zone.

As explained previously in Section 1.4.1, it is possible to find models in the literature that are based on one of these two failure modes. In light of the strain measurements at the face of the loading plate, it is more likely that punching shear failure is a tension induced failure due to the splitting of the compression zone, since no crushing of concrete was observed in any of the test specimens. A simple model using this approach is presented in Section 2.8.6 to predict punching shear capacity of the test specimens. In addition, results of the finite element analyses are presented in Chapter 4 to show the validity of this failure mode at the face of the loading area.

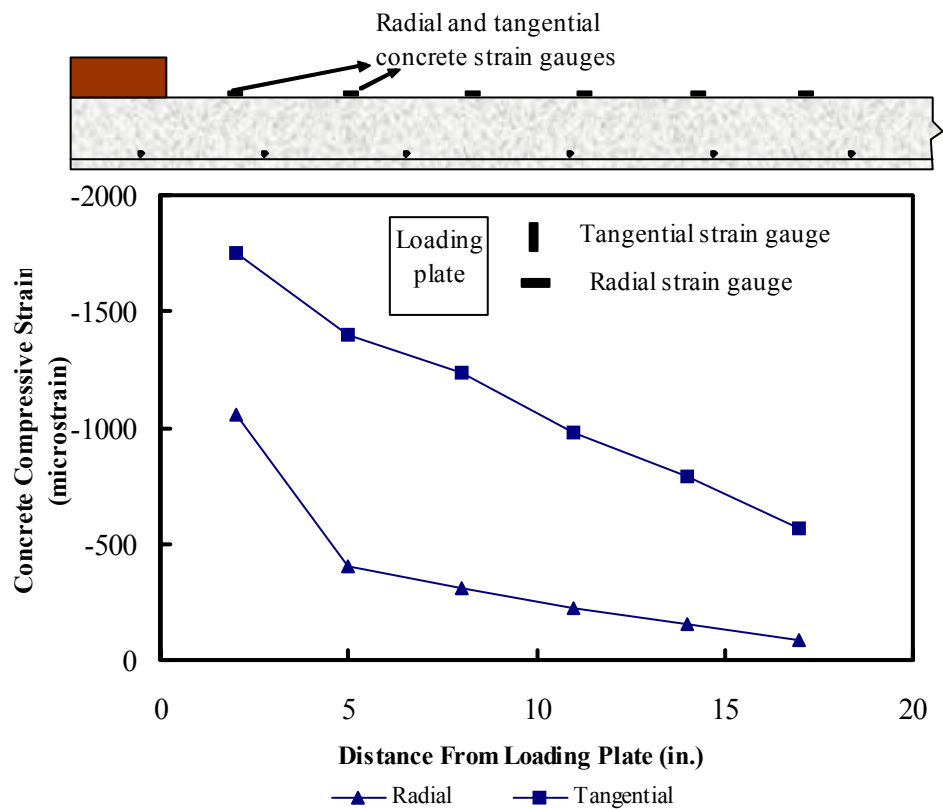


Figure 2.26 Concrete Strain Profiles for Control-2 Specimen

2.7.2.3 FRP Strains

CFRP strains in the vertical direction were measured using the gauges attached on FRP strips inside the hole (Figure 2.8), starting from the first CFRP stirrup perimeter $d/4$ away from the loading plate to the outermost perimeter. CFRP perimeters referred to in this section are shown in Figure 2.27. Vertical CFRP strain measurements versus distance from the loading plate are given in Figure 2.28. Vertical CFRP strains were not available for specimen A4-4, since no reliable data were collected from attached gauges due to their malfunctioning.

Highest strains were observed in the second perimeter for all specimens except specimen B8. At the outermost perimeter, a slight increase in CFRP strains

was observed due to the proximity of punching failure just outside the shear reinforced zone. Each measured strain on these plots corresponds to the location of a hole through which CFRP strips were inserted as shear reinforcement. Table 2.7 summarizes the FRP amount and measured maximum strains for the strengthened specimens. Appendix A shows the vertical strains measured at various locations of CFRP legs for specimen A4-2. The highest vertical strain in CFRP strips was observed in specimen A4-3. This strain level was about 80% of the strain capacity of the CFRP coupons. Rupture of CFRP strips initiating from the corner of the shear reinforcement legs was observed in this specimen.

Contribution of FRP and concrete throughout the loading was calculated using FRP strain measurements. Since CFRP stress-strain behavior is linear, CFRP forces can be computed by multiplying the measured strain with area and elastic modulus. Assuming a 45 degree inclined crack (to be consistent with the ACI 318-02 approach), the concrete contribution was computed by subtracting the summation of CFRP forces from the ultimate load. Figure 2.29 shows the portion of the load carried by CFRP reinforcement and concrete for specimens A4-1 and A4-2. The concrete contribution for all the test specimens at their ultimate loads normalized with respect to the load carrying capacity of specimen Control-1 are

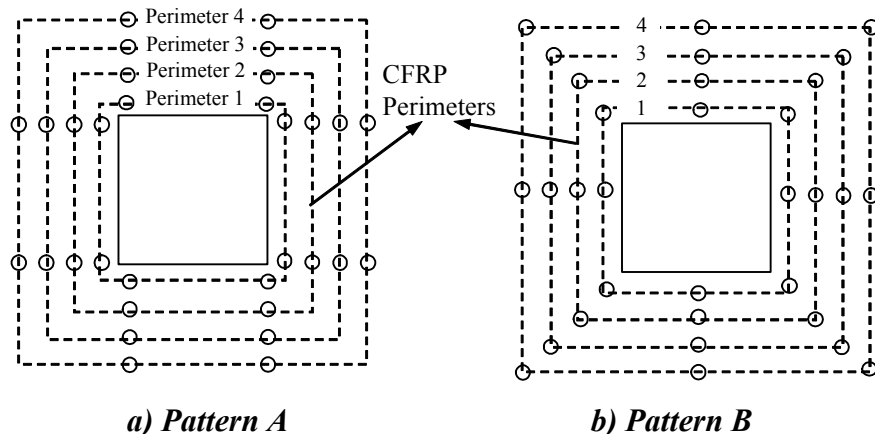


Figure 2.27 CFRP Perimeters

presented in Table 2.8. For the control specimen, the load carrying capacity was solely provided by, V_c , since no CFRP shear reinforcement was used. Table 2.8 shows that the concrete contribution inside the shear reinforced zone, V_c , in strengthened specimens was similar to those of control specimens.

When the inclined crack is assumed to cross only one set of CFRP vertical legs at a given perimeter, concrete shear resistance per perimeter inside the shear reinforced zone, v_c^i can be calculated using Equation 2.2. This is equivalent to assuming that 45 degree inclined crack crosses the CFRP vertical legs perfectly at the center and only one CFRP perimeter contributes to carry vertical force.

$$v_c^i = \frac{V_u - \varepsilon_{FRP} E_{FRP} A_{FRP}}{bd} \quad (2.2)$$

where V_u is the ultimate load carrying capacity, ε_{FRP} is the average measured strain in CFRP, E_{FRP} is the Modulus of Elasticity of CFRP, A_{FRP} is the total area of CFRP per perimeter, b is the length of the CFRP perimeter under consideration, as shown in Figure 2.27. The shear strength of concrete inside the shear reinforced zone plotted against the distance from the face of the loading plate is shown in Figure 2.30. This figure illustrates that concrete contribution decreased as the distance from the loading plate increased for CFRP perimeters. The information on concrete contribution inside the shear reinforced zone presented above is invaluable and is used in Chapter 5 while proposing design expressions for the strengthening procedure.

Figure 2.31 and 2.32 show the applied concentrated load versus the maximum measured CFRP strains for strengthened specimens. It was observed that CFRP strains were extremely small up to a certain applied external load. On average, CFRP stirrups were not active up to about 60% of the ultimate load of the slabs (Table 2.9). Up to this load level, shear stresses were mostly carried by the concrete. Starting at this point, CFRP strips engaged and carried the shear

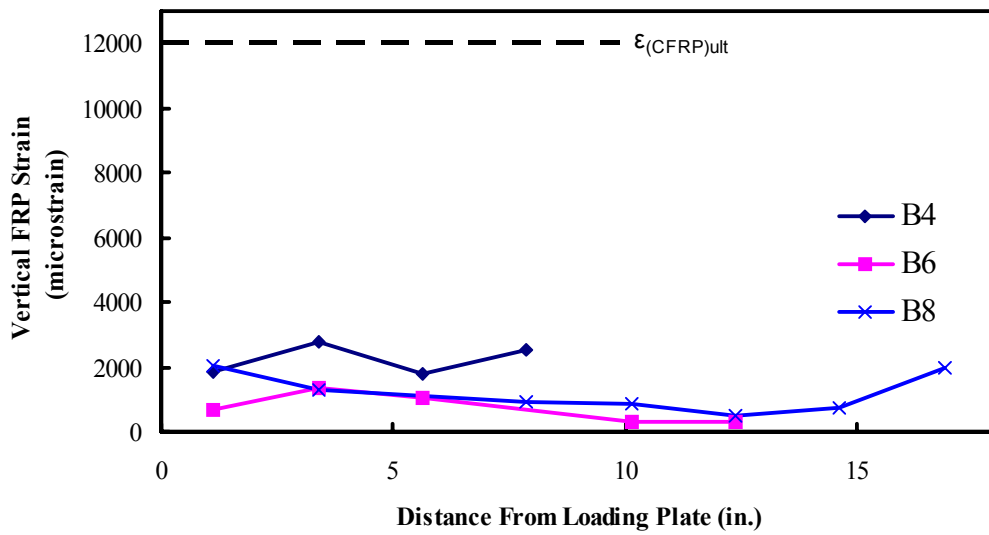
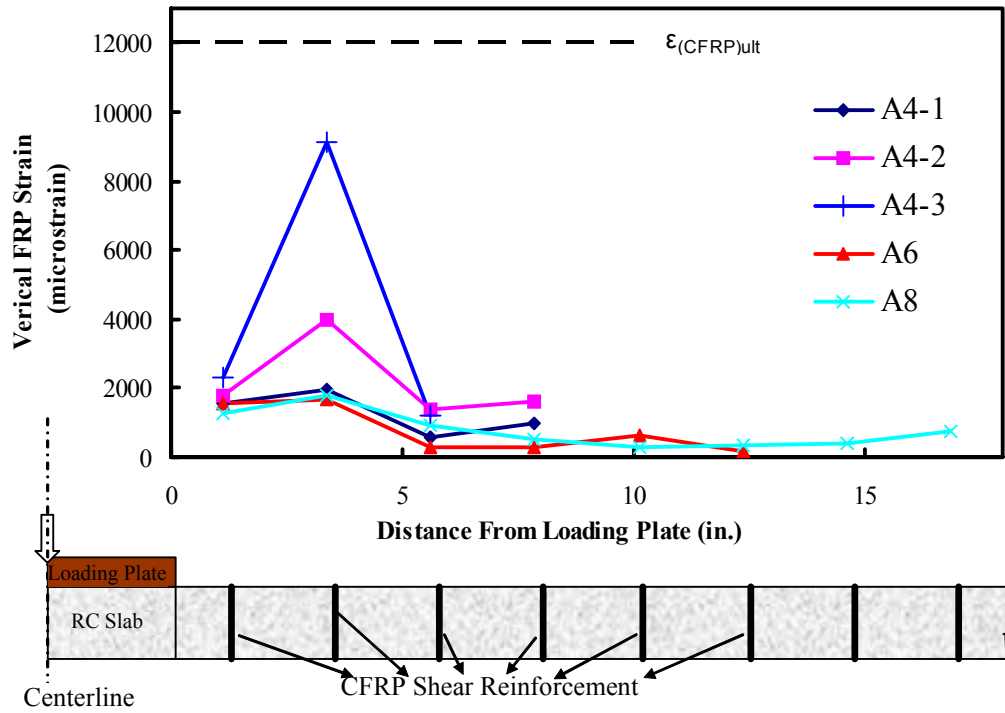


Figure 2.28 Vertical FRP Strain for Test Specimens

Table 2.7 Summary of Vertical CFRP Strain Results

Specimen Name	Number of CFRP Perimeters	CFRP Layer per Hole*	Average A_{FRP} per hole (in ²)	Average A_{FRP} per perimeter (in ²)	$\epsilon_{(FRP)max}$	$\epsilon_{(FRP)max} / \epsilon_{(FRP)ult}$	Punching Failure Mode
A 4 -1	4	4	0.16	1.28	0.0019	0.16	Inside/Outside
A 4 -2	4	2	0.08	0.64	0.0040	0.33	Outside
A 4 -3	4	1	0.04	0.32	0.0091	0.76	Inside
A 4 -4	4	2	-	-	-	-	Inside
A6	6	4 (3-5)	0.16	1.28	0.0017	0.14	Outside
A8	8	4 (3-5)	0.16	1.28	0.0018	0.15	Outside
B4	4	3.5 (3-4)	0.14	1.12	0.0028	0.23	Outside
B6	6	4.5 (5-4)	0.18	1.44	0.0014	0.11	Outside
B8	8	4.5 (5-4)	0.18	1.44	0.0021	0.17	Outside

*: CFRP Layers in the first two perimeters are shown.

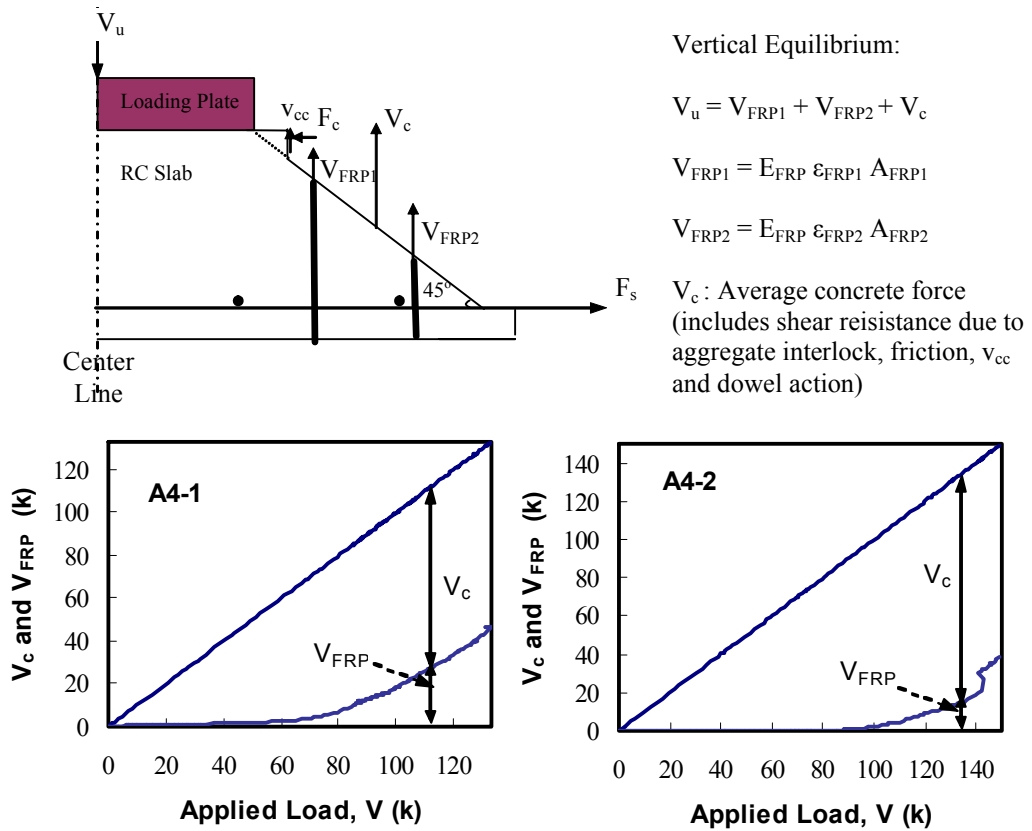


Figure 2.29 FRP and Concrete Contributions Obtained from Strain Measurements

Table 2.8 Summary of FRP and Concrete Contributions

Specimen Name	V _u (k)	Perimeter	$\epsilon_{(FRP)max}$ (microstrain)	V _{FRP} (k)	V _{FRP} =V _{FRP1} +V _{FRP2} (Assumes 45 degree failure plane)	V _c (k)	V _c / V _{ucontrol}																																																																																																			
A 4 -1	133	1	1587	21.3	47.4	85.6	0.75																																																																																																			
		2	1939	26.1				A 4-2	149	1	1770	11.9	38.8	110.2	0.97	2	4008	26.9	A 4-3	139	1	2316	7.8	38.4	110.6	0.97	2	9107	30.6	A 4-4	135	1	-	-	-	-	-	2	-	-	A6	161	1	1531	15.4	43.6	117.4	1.03	2	1677	28.2	A8	166	1	1271	12.8	43.1	122.9	1.08	2	1803	30.3	B4	170	1	1823	18.4	55.7	114.3	1.00	2	2779	37.3	B6	169	1	684	11.5	29.9	139.1	1.22	2	1366	18.4	B8	176	1	2052	34.5	52.1	123.9	1.09	2	1313	17.6							Mean :	1.02			
A 4-2	149	1	1770	11.9	38.8	110.2	0.97																																																																																																			
		2	4008	26.9				A 4-3	139	1	2316	7.8	38.4	110.6	0.97	2	9107	30.6	A 4-4	135	1	-	-	-	-	-	2	-	-	A6	161	1	1531	15.4	43.6	117.4	1.03	2	1677	28.2	A8	166	1	1271	12.8	43.1	122.9	1.08	2	1803	30.3	B4	170	1	1823	18.4	55.7	114.3	1.00	2	2779	37.3	B6	169	1	684	11.5	29.9	139.1	1.22	2	1366	18.4	B8	176	1	2052	34.5	52.1	123.9	1.09	2	1313	17.6							Mean :	1.02							Stdev:	0.15						
A 4-3	139	1	2316	7.8	38.4	110.6	0.97																																																																																																			
		2	9107	30.6				A 4-4	135	1	-	-	-	-	-	2	-	-	A6	161	1	1531	15.4	43.6	117.4	1.03	2	1677	28.2	A8	166	1	1271	12.8	43.1	122.9	1.08	2	1803	30.3	B4	170	1	1823	18.4	55.7	114.3	1.00	2	2779	37.3	B6	169	1	684	11.5	29.9	139.1	1.22	2	1366	18.4	B8	176	1	2052	34.5	52.1	123.9	1.09	2	1313	17.6							Mean :	1.02							Stdev:	0.15																	
A 4-4	135	1	-	-	-	-	-																																																																																																			
		2	-	-				A6	161	1	1531	15.4	43.6	117.4	1.03	2	1677	28.2	A8	166	1	1271	12.8	43.1	122.9	1.08	2	1803	30.3	B4	170	1	1823	18.4	55.7	114.3	1.00	2	2779	37.3	B6	169	1	684	11.5	29.9	139.1	1.22	2	1366	18.4	B8	176	1	2052	34.5	52.1	123.9	1.09	2	1313	17.6							Mean :	1.02							Stdev:	0.15																												
A6	161	1	1531	15.4	43.6	117.4	1.03																																																																																																			
		2	1677	28.2				A8	166	1	1271	12.8	43.1	122.9	1.08	2	1803	30.3	B4	170	1	1823	18.4	55.7	114.3	1.00	2	2779	37.3	B6	169	1	684	11.5	29.9	139.1	1.22	2	1366	18.4	B8	176	1	2052	34.5	52.1	123.9	1.09	2	1313	17.6							Mean :	1.02							Stdev:	0.15																																							
A8	166	1	1271	12.8	43.1	122.9	1.08																																																																																																			
		2	1803	30.3				B4	170	1	1823	18.4	55.7	114.3	1.00	2	2779	37.3	B6	169	1	684	11.5	29.9	139.1	1.22	2	1366	18.4	B8	176	1	2052	34.5	52.1	123.9	1.09	2	1313	17.6							Mean :	1.02							Stdev:	0.15																																																		
B4	170	1	1823	18.4	55.7	114.3	1.00																																																																																																			
		2	2779	37.3				B6	169	1	684	11.5	29.9	139.1	1.22	2	1366	18.4	B8	176	1	2052	34.5	52.1	123.9	1.09	2	1313	17.6							Mean :	1.02							Stdev:	0.15																																																													
B6	169	1	684	11.5	29.9	139.1	1.22																																																																																																			
		2	1366	18.4				B8	176	1	2052	34.5	52.1	123.9	1.09	2	1313	17.6							Mean :	1.02							Stdev:	0.15																																																																								
B8	176	1	2052	34.5	52.1	123.9	1.09																																																																																																			
		2	1313	17.6										Mean :	1.02							Stdev:	0.15																																																																																			
						Mean :	1.02																																																																																																			
						Stdev:	0.15																																																																																																			

forces upon formation of inclined cracks. This shows that the contribution from concrete and CFRP started taking place at different times.

Strains on the CFRP diagonal strips bonded to the compressive face of the slab were also recorded to study the effectiveness of CFRP stirrups placed diagonally. Figure 2.33 shows the locations of the strain gauges and measurements for specimens A6 and A8. This figure demonstrates that as the load applied on the slab was increased, the strips on the top surface were mainly in compression due to bending. Compressive strain in the first diagonal strip (located in the second perimeter) of specimen A6 started decreasing at about 3/4 of the ultimate load. Similarly for specimen A8, slope of the strain versus load response

(strain gradient) of the first and second diagonal strips changed direction at about 55% and 84% of the ultimate load, respectively. Locations of changes in the strain gradients of diagonal strips are shown with dashed lines for both specimens. The strains in second and third diagonal strips of specimen A6 monotonically increased in the compressive direction up to the failure of the specimens.

The change in the slopes of the load versus strain responses shown in Figure 2.33 can be explained with the following sequence of events: In the elastic stage, CFRP strips on the top surface were in compression whereas the CFRP strips on the bottom side of the slab were in tension (Figure 2.34). After the formation of flexural cracks, cracking in the epoxy occurred close to the tension side. The forces carried by the vertical CFRP legs were almost zero in these two stages since no inclined cracking initiated. After inclined cracks formed, vertical CFRP legs contributed in carrying the excessive shear forces. Since vertical legs were anchored to the compressive face of the slab, they started imposing tensile forces on the CFRP strips bonded to slab surface. These tensile forces counteracted the effect of compressive strains due to bending, resulting in slope changes as shown in Figure 2.33. This phenomenon is schematically illustrated in Figure 2.34. In addition, stress concentrations were imposed on CFRP strips at the corners of the vertical holes. Although the stress concentrations are a function of the radius of the chamfer, this radius was kept constant at 1/2 in. in this study.

For strain gauges located at the center of diagonal strips 2 and 3 (Figure 2.33), compressive strains were measured throughout the test without a significant change in strain gradient. It is important to note that the tensile forces imposed by the vertical legs decayed along the length of the diagonal strips. The strain readings show that at the center of the second and third diagonals in Specimen A6 (Figure 2.33) tensile forces were negligible indicating that the length of these diagonals were sufficient to ensure proper anchorage of the vertical legs. A more

detailed discussion of proper anchorage of vertical CFRP legs is presented in Section 2.8.4.

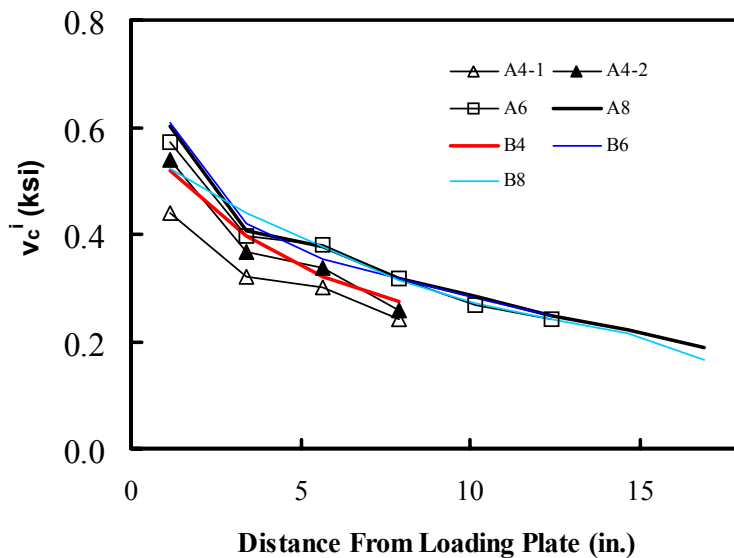


Figure 2.30 Average Concrete Shear Resistance at Different Perimeters

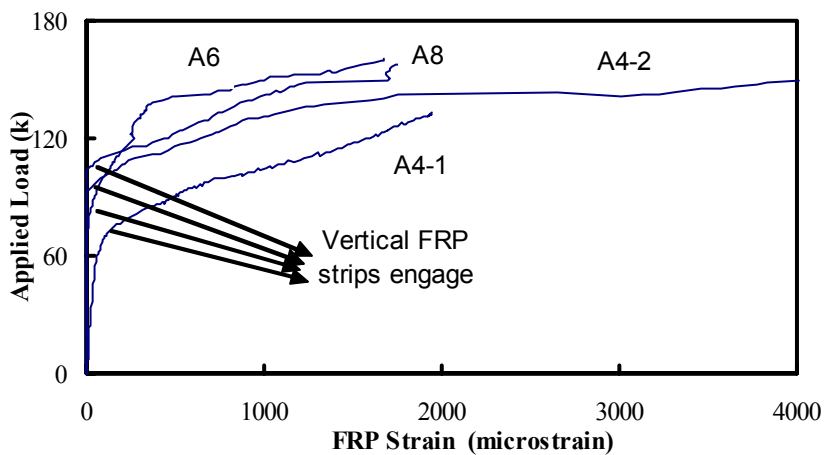


Figure 2.31 Applied Load-Vertical CFRP Strain Relationships, (Pattern A)

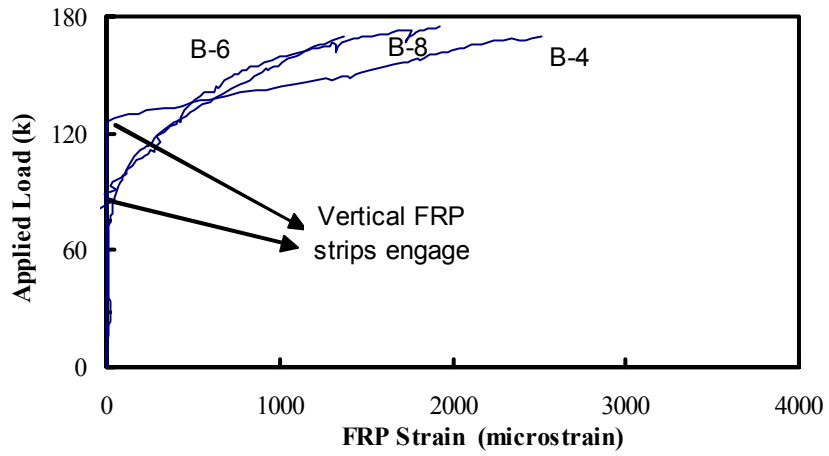


Figure 2.32 Applied Load-Vertical CFRP Strain Relationships (Pattern B)

Table 2.9 Load Corresponding to First Significant Vertical CFRP Strains

Specimens	V_u (k)	Load at FRP engagement, V_{engage} (k)	V_{engage} / V_u
A4-1	133	74	0.56
A4-2	149	92	0.62
A4-3	139	80	0.58
A6	161	86	0.53
A8	166	100	0.60
B4	170	127	0.75
B6	169	75	0.44
B8	175	87	0.50
		Mean =	0.57
		St. Dev. =	0.09

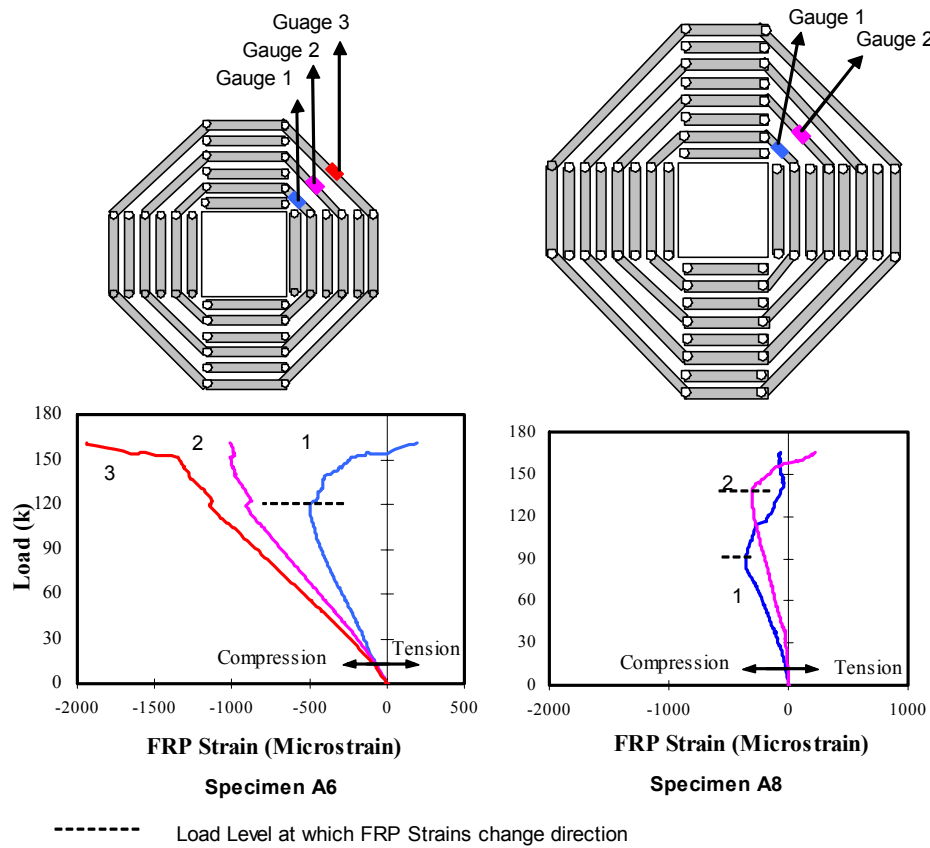


Figure 2.33 Applied Load versus Diagonal CFRP Strain Relationships

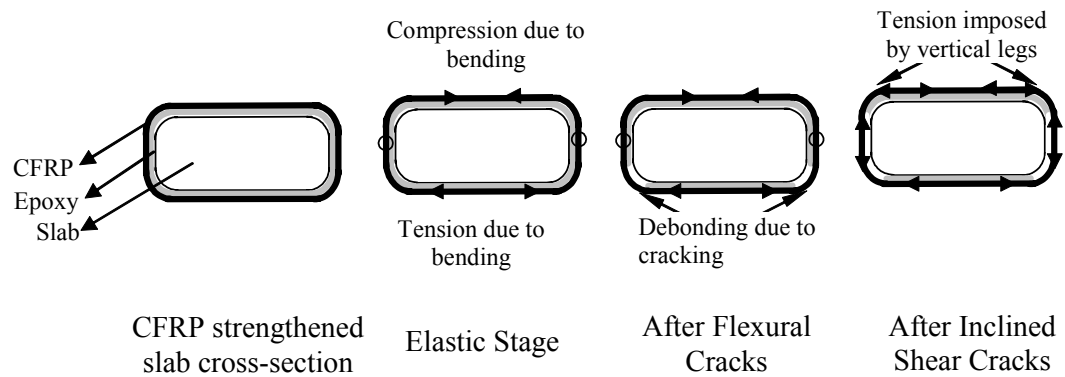


Figure 2.34 Events Leading to Tensile Forces on CFRP Strips

2.7.3 Crack Patterns and Failure Modes

All the specimens failed in a punching failure mode with different levels of ductility as presented in Table 2.6. The specimens, A4-1, A4-2, A6, A8, B4 and B6 were cut through close to the centerline and through the vertical CFRP strips, whereas Control-1 was cut exactly at centerline of the slab to observe the inclined crack patterns after the tests. Figures 2.35 to Figure 2.39 show the failed top surfaces together with the cross sections of these specimens after failure. For A4-1, it was observed that the failure surface started outside the shear reinforced zone followed by the penetration of failure inside the shear reinforced zone (Figure 2.35). In order to avoid failure inside the shear reinforced zone, diagonal stirrups, spanning between the holes located on adjacent sides of the loading plate at the outermost perimeter of specimen A4-2, were used (Figure 2.36). In this way, stirrups with alternative anchorage paths were provided and integrity within the shear reinforced zone was achieved. The effectiveness of CFRP diagonals are examined in detail in Section 2.8.3. Likewise, a similar strategy was used in specimens A6 and A8 with the use of diagonal strips. Specimen A4-3, which had half the amount of vertical CFRP area compared to A4-2, experienced punching failure inside the shear reinforced zone and failure of external CFRP stirrups due to high strain demands. Specimen A4-4, which had the same amount of CFRP compared to A4-2 but wrapped in the radial direction, experienced punching failure initiating outside the shear reinforced zone (Figure 2.37). However, failure occurred inside the shear reinforced zone, since there was no CFRP reinforcement to intercept these cracks and stop the penetration of the failure surface into this zone. Failure of pattern B specimens was governed by the strength of the concrete outside the shear reinforced zone with asymmetric failure surfaces (Figure 2.38 and Figure 2.39). The proximity of slab boundaries is believed to result in these asymmetric failure surfaces. The effects of slab boundaries on specimen behavior

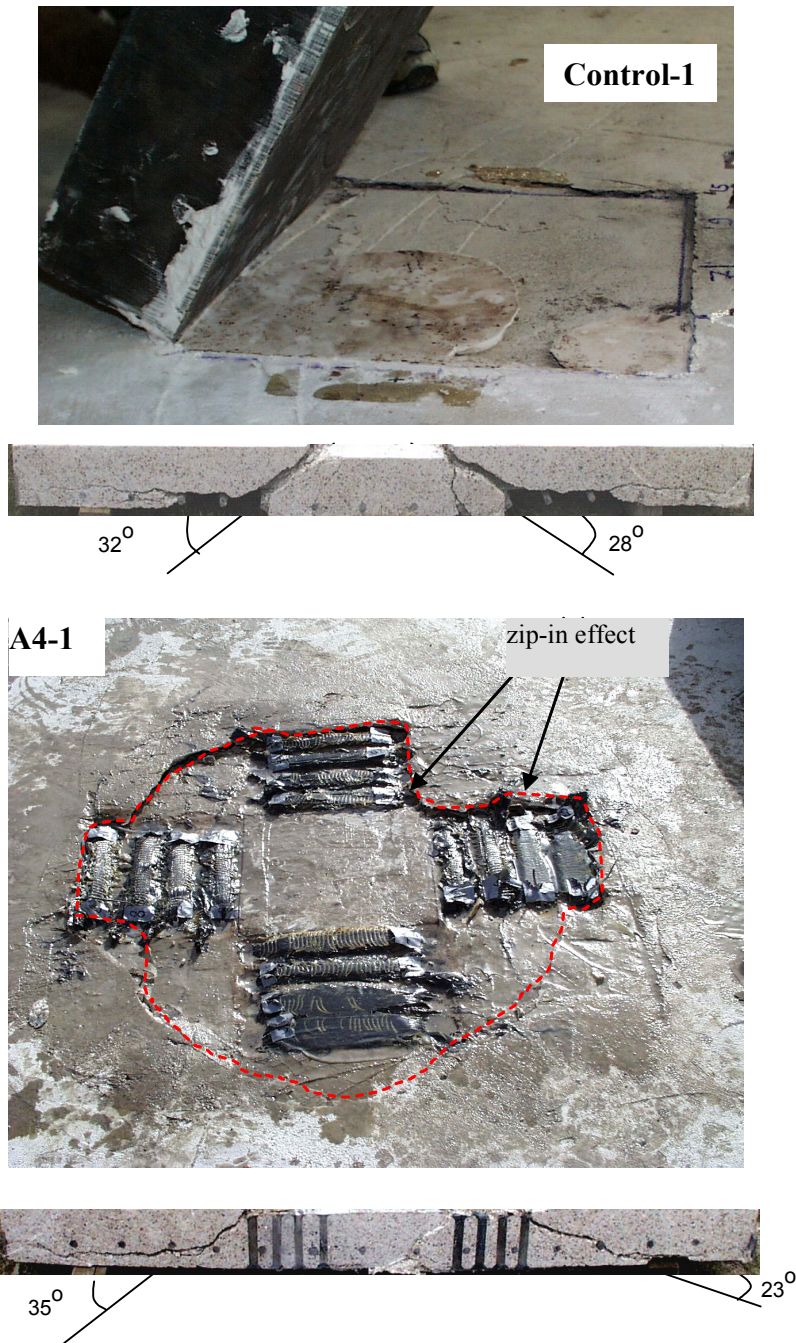


Figure 2.35 Failed Surfaces and Inclined Cracks for Control-1 and A4-1

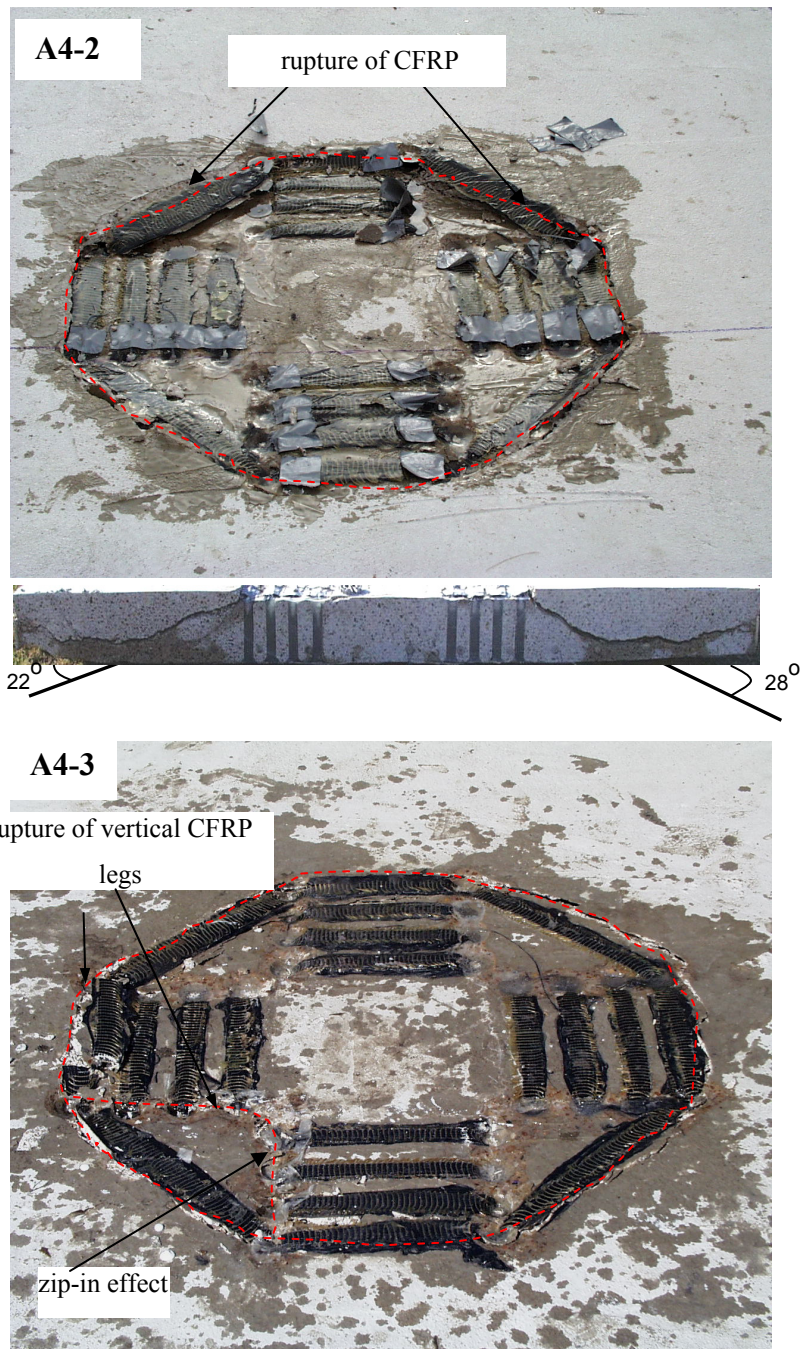


Figure 2.36 Failed Surfaces and Inclined Cracks for A4-2 and A4-3

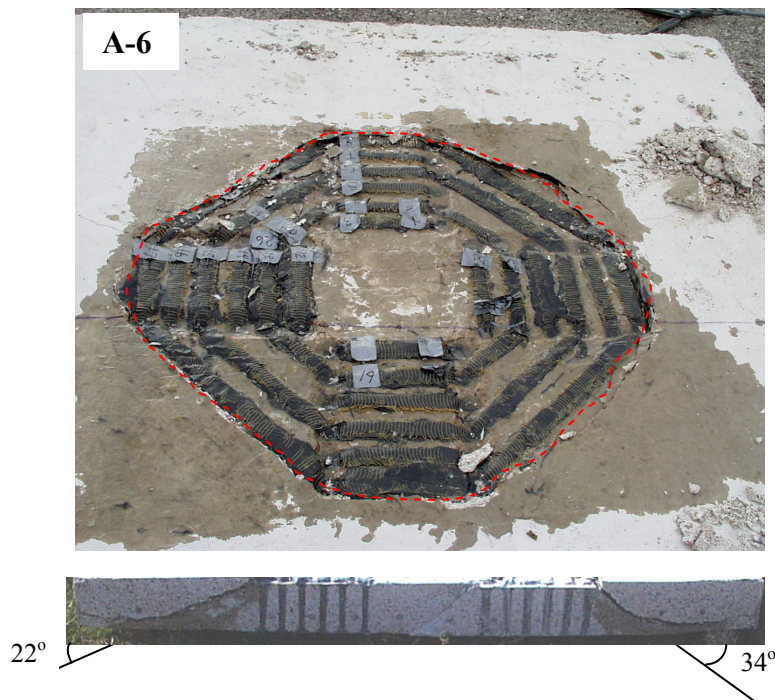
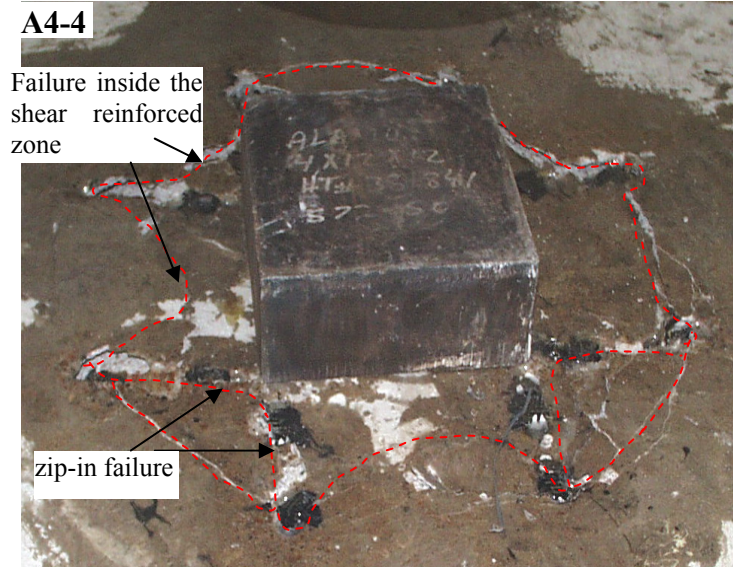


Figure 2.37 Failed Surfaces and Inclined Cracks for A4-4 and A4-6

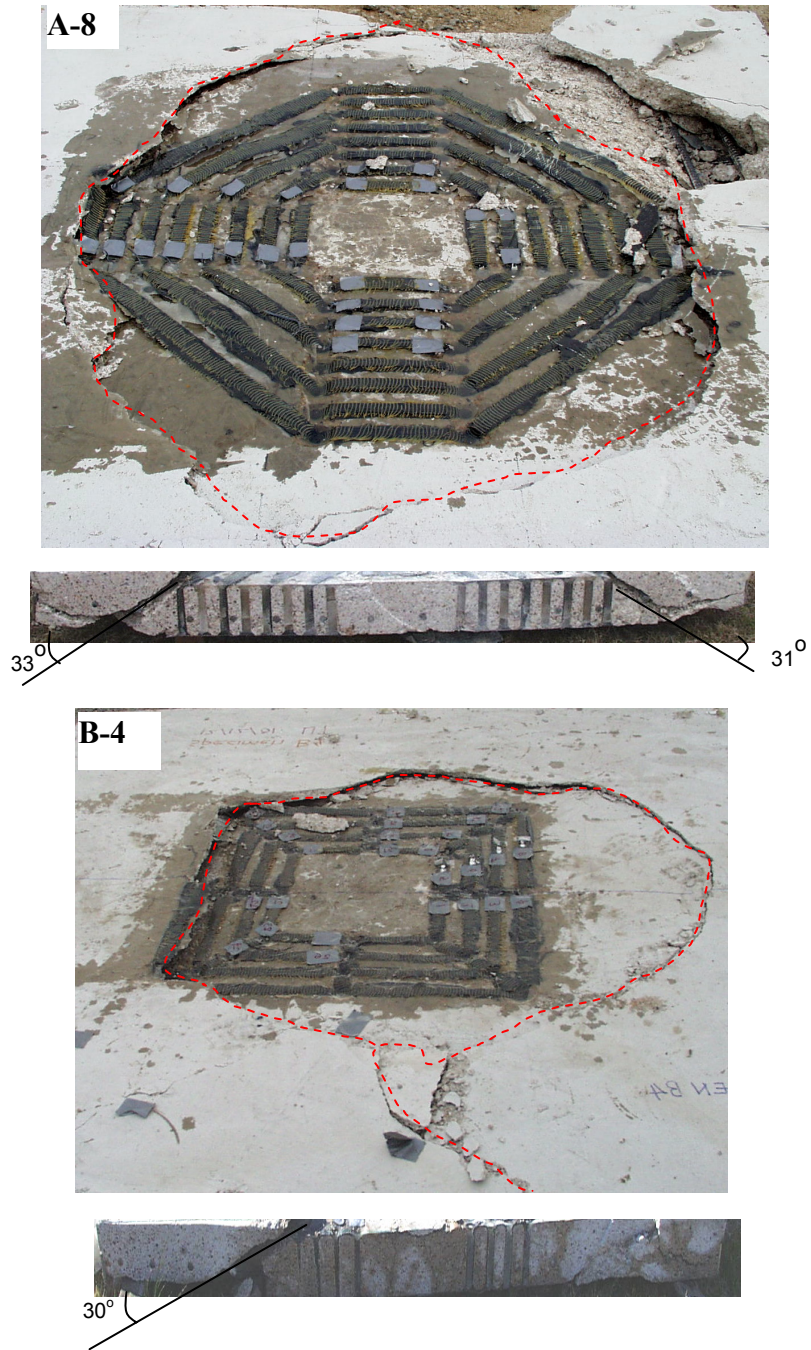


Figure 2.38 Failed Surfaces and Inclined Cracks for A-8 and B-4

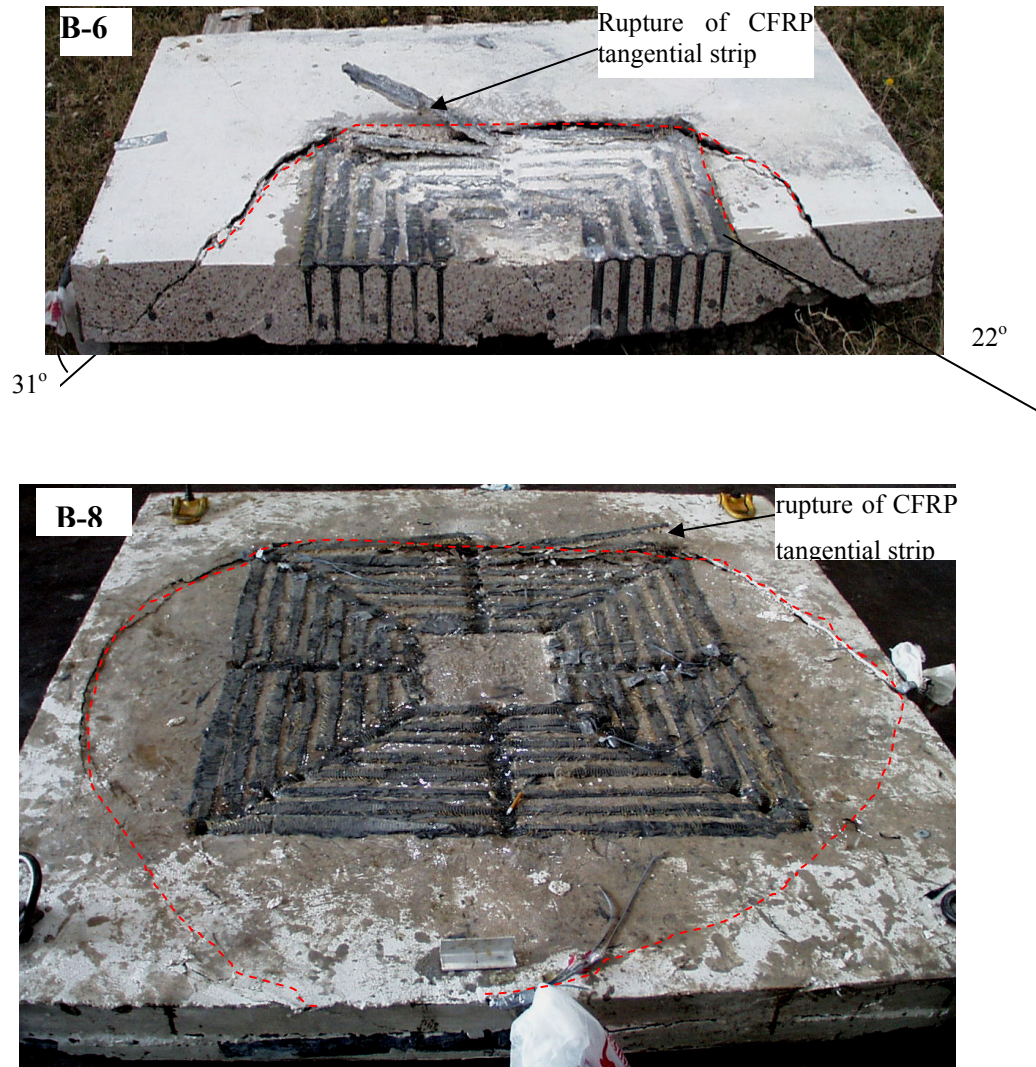


Figure 2.39 Failed Surfaces and Inclined Cracks for B-6 and B-8

are discussed in Section 2.8.5. No visible dominant inclined shear cracks were observed in the CFRP reinforced region for specimens A4-2, A6 and A8, B4, B6 and B8, instead punching failure occurred outside the shear reinforced region. In other words, for all specimens where CFRP loops were formed in the plan view in addition to the vertical legs, the inclined shear crack did not cause failure inside the zone of efficiently knit CFRP stitching system.

It is important to note that the angle of the punching cone was 30° on average for Control-1 (Figure 2.35) and ranged approximately from 22° to 35° for the strengthened specimens that were cut with an average of about 28° . This shows that the formation of the inclined crack leading to a punching failure was similar for the properly detailed strengthened specimens as for the control specimen, the only difference being the location of the failure surface.

2.8 DISCUSSION OF TEST RESULTS

2.8.1 Stiffness, Strength and Ductility

The initial stiffness of all the test specimens agreed well with the elastic analysis results obtained using elastic plate analysis (Figure 2.12 to Figure 2.14). After cracking, stiffness of the specimens reduced to their cracked values as listed in Table 2.6. The stiffness of the cracked specimens ranged between 24 and 30% of the initial elastic stiffness values. This shows that post cracking stiffnesses of the specimens were consistent, indicating that the shear strengthening scheme did not have a significant influence on cracking moments and stiffnesses after cracking. Based on this, the portion of load-deflection response for all of the specimens up to the first yielding can be idealized using the initial stiffness up to cracking, and the post cracking stiffness ($\sim 25\%$ of the initial stiffness) up to first yielding. The load at first cracking and first yielding can be estimated by elastic analysis such that the maximum sectional moment on the plate reaches the

cracking and yielding moments, respectively. Then the corresponding displacements, that is cracking and yielding displacements, can be found using the initial elastic stiffness and a post cracking stiffness, respectively. After the longitudinal reinforcement yielding initiates, stiffness of the slab progressively decreases as the load-deflection curve flattens (Figure 1.5). Beyond first yielding, sectional moments can no longer be used to estimate load deformation characteristics of the specimens due to redistribution of moments and progressive cracking and yielding within the slab. This procedure can be used to estimate deformations up to first yielding of the test specimens.

The load carrying capacities of all specimens normalized with respect to specimen Control-1 are shown in Figure 2.40. It can be observed that most efficient specimen among A4 patterns was specimen A4-2 with two layers of CFRP used as shear reinforcement per hole. Specimens A8, B4, B6 and B8 reached the flexural capacity computed based on yield line analysis (Figure 2.18). However, punching failure occurred when the shear capacity outside the shear reinforced zone was reached. As explained in Section 2.6.2.1, although strain localization in the longitudinal reinforcement occurred at the face of the loading

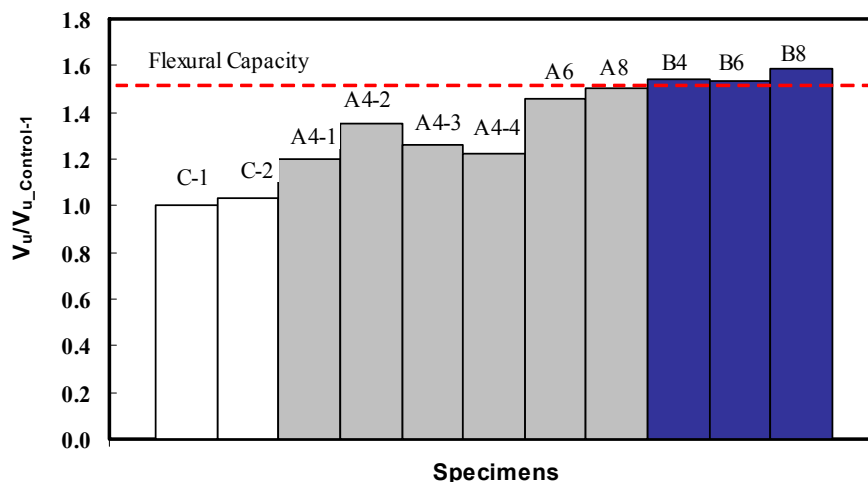
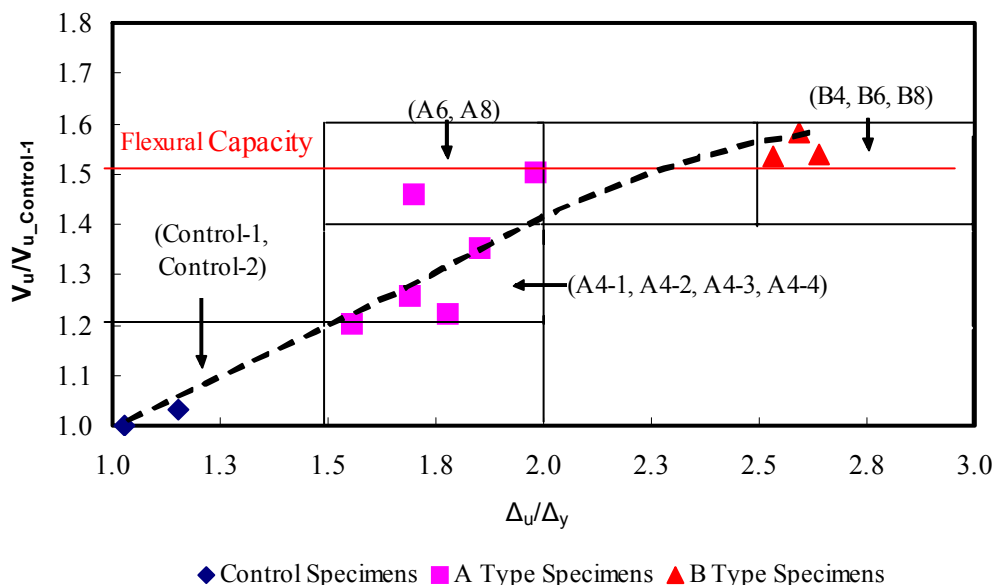


Figure 2.40 Comparison of Load Carrying Capacity of Specimens

area, extensive yielding was not observed, and failure mode was still brittle punching. Strength increases between 20 and 60% were observed in the strengthened specimens. The strength increases were limited to the flexural capacity of the slabs. Most existing flat plate systems have lower longitudinal reinforcement ratios (0.5 to 1.2%) compared with that used in this study (1.76%). For those systems, the ratio of punching shear capacity of the slab column connection to the flexural capacity of the slab is smaller than this ratio for the control specimen (~1.5). Therefore, the range of strength increases obtained in the experiments is likely to be sufficient to ensure that failure mode will be more ductile where there is a potential risk of punching failure due to high gravity loads. The results of the experiments that are presented in Chapter 3 support this argument.



Δ_u : Central displacement at ultimate load
 Δ_y : Central displacement at first yielding of steel reinforcement

Figure 2.41 Strength Increases versus Ductility Increases for Specimens

Strength increases in specimens with respect to specimen Control-1 versus the ratio of displacement at ultimate load to displacement at first yielding of steel reinforcement (detected by strain gauges), Δ_u/Δ_y , are plotted in Figure 2.41. Increase of Δ_u/Δ_y values were observed with increased strength. The dashed line shows the trend observed in this plot. Initially the relationship is proportional. As the flexural capacities of the specimens are reached relationship approaches to a multiple of flexure capacity divided by the shear capacity (~1.25 according to Criswell 1974, 1.1 to 1.2 according to Hognestad 1956). When this limit is reached, further increase in Δ_u/Δ_y values without significant increase in strength is likely to be observed and change of failure mode from punching shear to flexure takes place.

Figure 2.41 shows that based on the desired performance level (strength and ductility) a specific strengthening procedure can be selected. It is important to note that Figure 2.41 is valid for a given reinforcement ratio (1.76%) which corresponds to a flexural capacity of about 50% more than that governed by punching shear strength. Hence the performance based upgrade design of lightly reinforced flat plates may require different amounts of CFRP reinforcement and configuration than what is shown in Figure 2.41.

2.8.2 FRP Amount, Efficiency and Detailing

The test variable for specimens A4-1, A4-2, and A4-3 was the cross sectional area of CFRPs, where 4, 2, and 1 layers of CFRP were used per vertical leg, respectively. On the other hand, similar amounts of CFRP were used in specimens A4-4 and A4-2 with two different stirrup configurations, tangential wrapping (A4-2, Figure 2.36) and radial wrapping (A4-4, Figure 2.37) between the vertical legs (Figure 2.9). Figure 2.42 illustrates a comparison of pattern A4 specimens.

Properties/Specimen	A4-1	A4-2	A4-3	A4-4
Detailing				
Vertical CFRP layer per leg	4	2	1	2
Maximum vertical CFRP strain	0.0019	0.004*	0.0091	-

*: Based on readings from three strain gauges as shown in Appendix A.

Figure 2.42 Comparison of A4 Specimens

Figures 2.35, 2.36, and 2.37 illustrate the failed top surfaces of the A4 specimens after failure. According to these figures, all A4 specimens except A4-2 experienced punching failure inside the shear reinforced zone. For specimen A4-1, failure occurred by the so called “zip-in” failure mode, where the punching shear failure penetrated into the CFRP reinforced zone as shown in Figure 2.36. The same phenomenon was observed during the test of specimen A4-4, where shear cracks in between the legs of CFRP reinforcement and at the corner of the loading area was noted. The penetration of shear crack into the upgraded zone was eliminated in specimens where the CFRP hoops were installed diagonally to work as secondary stirrups. This increased the redundancy of the knit system and helped to intercept the shear crack. A detailed discussion on the effectiveness of diagonal stirrups is presented in Section 2.8.3.

Specimen A4-3 failed inside the shear reinforced zone due to rupture of CFRP strips at the corners. The measured maximum vertical CFRP strain (~ 0.009) was about 80% of the measured tensile strain capacity of CFRP strips from uniaxial tension tests. This high strain level in the vertical direction is an

indication of stress concentrations experienced at the corners of CFRP strips which are vulnerable to rupture. Based on the assumption of similar strains in concrete and CFRP (vertical strain compatibility), it is possible to say that concrete contribution inside the shear reinforced zone vanishes under strains almost 2.5 times that of the crushing strain of concrete ($\sim 0.003-0.004$). This shows that shear reinforced zone can not successfully sustain large strains without loss of concrete contribution and CFRP rupture. Measured maximum vertical CFRP strain was about 0.004 for specimen A4-2 (see also Appendix A). When maximum measured vertical CFRP strains were equal to or smaller than 0.004 in specimens A4-2, A6, A8, B4, B6, and B-8, failure inside the shear reinforced zone or rupture of CFRPs at the corners were not observed. Therefore, the CFRP strain level, 0.004, can be accepted as the maximum attainable strain level in vertical CFRP strips without any significant damage in the shear reinforced zone.

The proposed effective strain limit (0.004) for CFRP vertical legs is based on the experimental results presented in this study. In these experiments only carbon fiber reinforced polymers were considered. It is known that glass and aramid fiber products are also commonly used in the strengthening applications. These types of FRPs have generally lower strength and higher tensile strain capacities ($\sim 2\%$). The proposed effective strain limit could be higher for different types of FRP products depending on the amount and material properties. At this point, it is possible to hypothesize that the proposed strain limit can safely be used with low strength and stiffness FRP products as well. Further experimental verification using different FRP products is necessary if an increase in the vertical strain limit is desired.

The performance of specimens with different number of CFRP perimeters is shown in Figure 2.43 where number of CFRP perimeters is plotted against the obtained strength increases. This figure indicates that there was a trend of increase

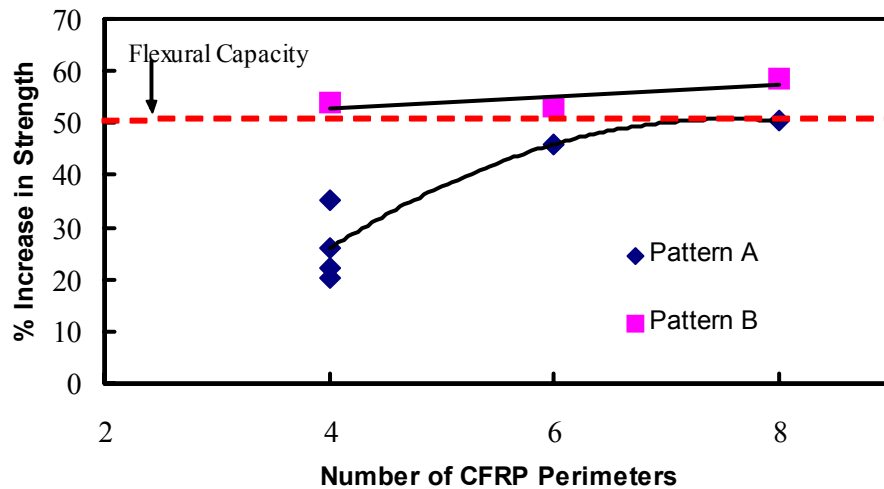


Figure 2.43 Effect of Number of Perimeters on Strength

in strength with increase in the number of CFRP perimeters used for both patterns. For pattern B specimens, increase in the number of CFRP perimeters resulted in smaller strength increases compared to those obtained using pattern A specimens. Use of only four CFRP perimeters with pattern B enhanced the punching shear capacity to a level above the computed flexural capacity. Therefore, further increase in the number of CFRP perimeters resulted in marginal increases in strength. As the length of the perimeter outside the shear reinforced zone increased, higher strength increases were observed. The reason was the increased concrete shear resistance outside the shear reinforced zone with increasing number of CFRP perimeters. For A4 specimens, using the optimum amount and detailing of vertical CFRP shear reinforcement provided increased capacities within the range of 20 to 35%. Substantial increase in capacity was achieved by increasing the number of stirrup perimeters (up to 60%). However the trend line shown in Figure 2.43 became almost parallel to the flexural capacity of the specimen as the number of perimeters was increased. An important aspect for obtaining increased capacities with this scheme is the selection of correct

number of perimeters, which influences the capacity outside the shear reinforced zone. In addition, the ultimate load carrying capacity is always limited to the flexural capacity of the flat plate.

A practical issue for site applications of the proposed procedure is the efficiency which can be defined as the cost versus benefit. The actual cost of the strengthening scheme varies from place to place depending on the material and labor costs. For simplicity, it is assumed that labor cost for strengthening of a single slab-column connection is approximately proportional to the amount of material used. Based on this assumption, total area of CFRP used in a specimen can be accepted as a measure of cost. Figure 2.44 shows the measure of cost against the obtained increases in strength. For the measure of cost, CFRP sheet area used in the experiments are calculated for each specimen. It can be seen that, higher strength increases were obtained with strengthening patterns with higher costs. This relationship together with the desired performance level as shown in Figure 2.41 is very important in the selection of the pattern, detailing, and number of perimeters for the strengthening procedure.

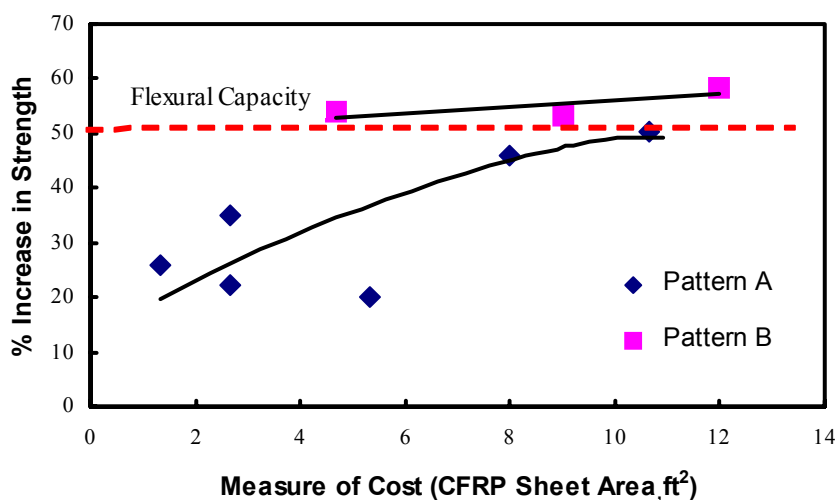


Figure 2.44 Cost Effectiveness of Test Specimens

2.8.3 Effectiveness of Diagonal Stirrups at Outermost CFRP Perimeters

The effectiveness of diagonal stirrups in eliminating punching shear failure inside the shear reinforced zone was briefly discussed in Sections 2.7 and 2.8.2. Specimen A4-1, with 4 layers of CFRP per hole, experienced punching failure inside the CFRP reinforced zone. However, specimen A4-2, with 2 layers of CFRP, did not fail inside the shear reinforced zone, but punching shear failure occurred outside the shear reinforced region. The mechanism for the effectiveness of the diagonals is explained below by comparing behavior of specimens A4-1 and A4-2.

Figure 2.45 illustrates the region outside the shear reinforced zone along the loading area just before the punching failure occurs. The inclined crack outside the shear reinforced and relatively undamaged shear reinforced area can be seen in this figure. The compression zone at the front face (arrow in Figure 2.45) is under a biaxial state of stress ($\sigma_2 < \sigma_3 < 0 < \sigma_1$, negative sign is compression, see also Figure 4.18). The inclined compressive force (similar to the force acting on the conical shell in Figures 1.4 and 1.7) in this zone bears on the CFRP strip bonded to the compressive surface (Figure 2.45). This inclined force effectively pushes these strips. Following that, CFRPs on the compressive face start to debond at the corners due to stress concentrations. In other words, the outermost CFRP stirrup becomes ineffective as the vertical legs lose their anchorage on the top surface. Following this event punching shear failure can occur in one of the following two ways:

i) In the absence of diagonal stirrups (Figure 2.46): The inclined cracks that have developed on the sides of vertical CFRP legs cause the punching failure to initiate inside the shear reinforced zone due to the anchorage failure of the last CFRP strip. The inclined crack instantly penetrates laterally to the corner of the loading area and a “zip-in” failure mode takes place.

ii) In the presence of diagonal stirrups (Figure 2.46): The outermost CFRP stirrups anchored on the compression side may become ineffective. However, vertical legs of CFRP stirrups anchored with the use the diagonals can still carry the excessive shear stresses and prevent failure inside the shear reinforced zone. Further load can be sustained until punching shear failure occurs outside the shear reinforced region due to the penetration of the inclined crack into the compression zone along the octagonal perimeter. The diagonal stirrups serve as alternatively anchored shear reinforcement upon anchorage failure of the front face CFRP legs. Simultaneously, the presence of vertical legs of the diagonally positioned stirrups reduces the strain demand on the primary CFRP stirrup located at the front face. When punching failure occurs outside the shear reinforced zone, the inclined crack tip penetrates into the compression zone. This results in rupture of CFRPs at the outermost shear reinforcement perimeter (Figure 2.36).

This mechanism, postulated based on the loss of CFRP anchorage, necessitates the use of secondary CFRP stirrups in the diagonal directions. These diagonal stirrups act as backup shear reinforcement in the outermost CFRP perimeter. In short, a second vertical strip that is anchored in an alternative direction (compared to the primary shear reinforcement located at the front face) is crucial to achieve optimum performance of the strengthened specimens. This alternative direction was along the diagonals in this study. It is likely that other alternative anchorage directions can work in a similar manner upon experimental verification.

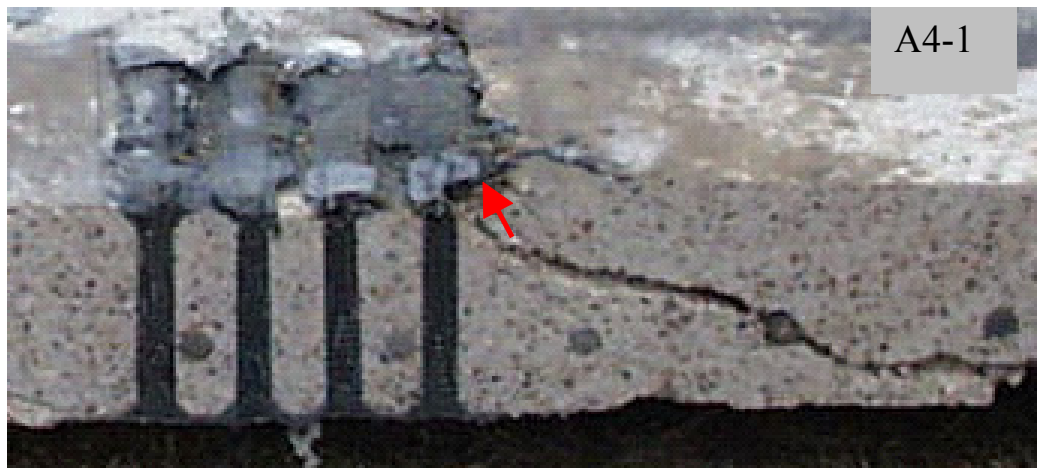
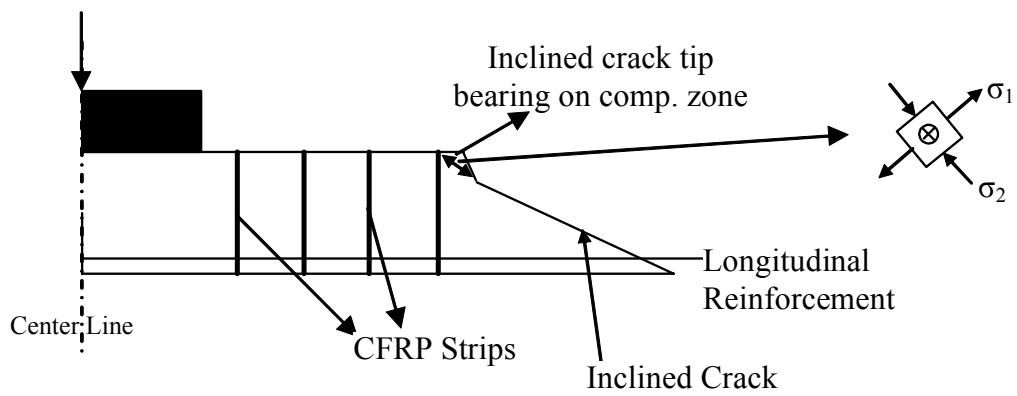
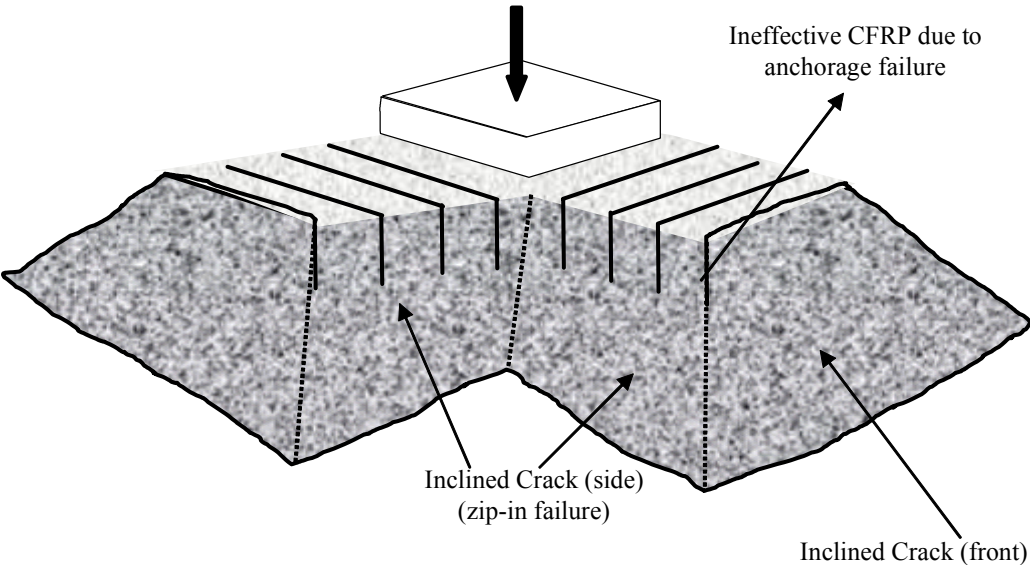
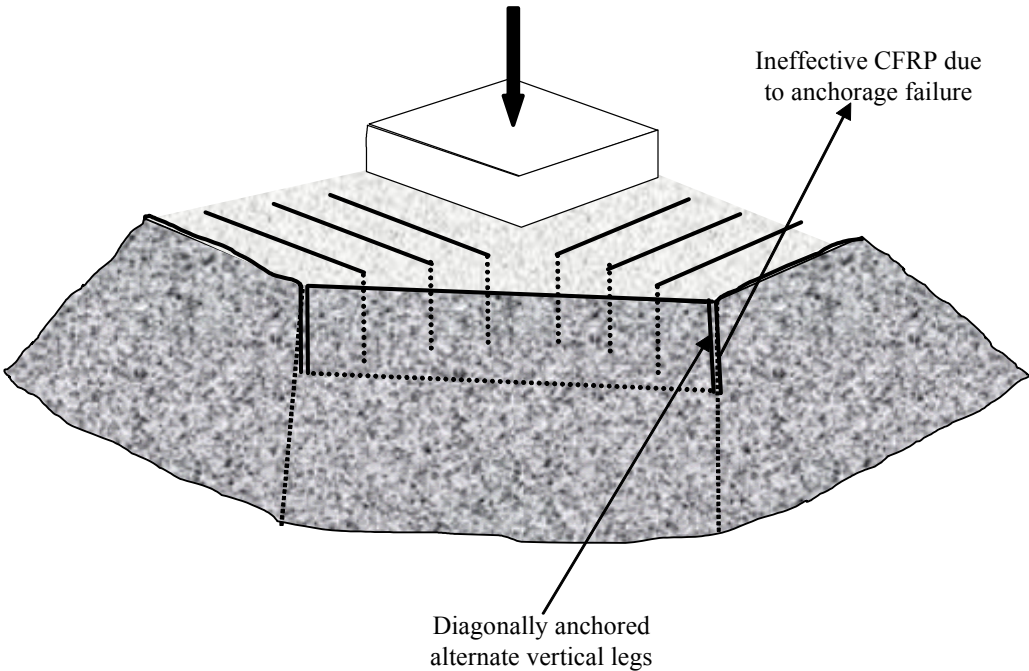


Figure 2.45 Failure of Outermost CFRP Reinforcement



CFRP reinforced zone without diagonals



CFRP reinforced zone with diagonals

Figure 2.46 Effectiveness of Diagonals

2.8.4 Anchorage of CFRPs used as Shear Reinforcement

As explained in Section 2.5, CFRPs were used in the form of continuous closed stirrups for all the strengthened specimens. By using closed loops, vertical CFRP legs were well anchored on the compressive and tensile faces of the slabs (Figure 2.47).

The events that led to the activation of CFRP vertical legs were shown in Figure 2.34 based on the measured vertical CFRP strains (Figure 2.32 and Figure 2.33). According to Figure 2.34, vertical CFRP strips start carrying forces following the formation of inclined cracks crossing them. These forces are transferred to the horizontal parts of CFRP stirrups bonded to the slab surface (CFRP anchors) when the corners are smooth and rounded off to eliminate sharp corners as was the case in all test specimens.

The ultimate strength of the CFRP anchors should be such that the maximum allowable force on the vertical legs can be carried. When closed loops were used, anchorage strength was not critical since no anchorage failure was observed in the tests. This is due to the fact that both bond of concrete to CFRP and overlap of the CFRP strips provided the anchorage strength. In addition, due to the continuity of the CFRP anchors, slip in the CFRPs was negligibly small. These factors together with the experimental evidence show that use of CFRP closed loops was an efficient anchorage method for the vertical legs (Figure 2.47). Even in the presence of additional tensile forces acting on the CFRP anchors due to bending of the section, the anchorage strength was not jeopardized when closed loops were used.

At this point, following question can be raised: “Is it possible to anchor CFRPs other than closed loops?” Bonding of CFRP anchors on the slab surface without making closed loops (Figure 2.48) may be considered as an alternative.

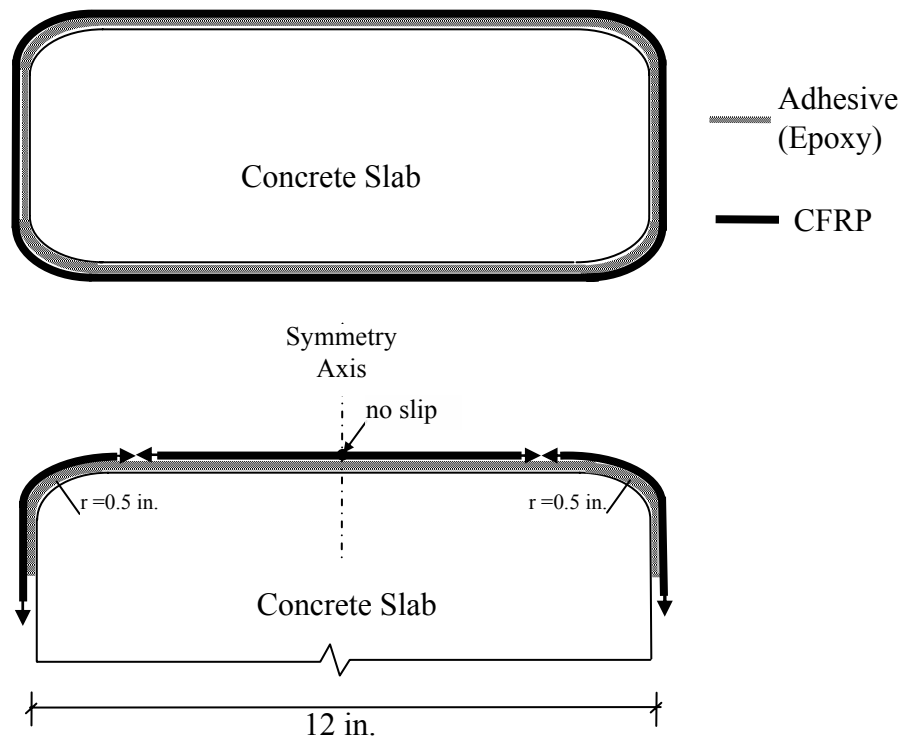


Figure 2.47 Closed CFRP Loops Used as Shear Reinforcement

This kind of shear reinforcement in the form of a “C-Shape” can be used only if the required anchorage length is known. This alternative is explored next.

2.8.4.1 Anchorage Strength of CFRPs bonded to Concrete: Experiments

It is not feasible to determine the required anchorage length of the CFRP shear reinforcement in the form “C-Shape” by repeating the slab tests previously presented. However, the problem can safely be simplified to an anchorage issue as shown in Figure 2.49. The force that needs to be carried by the vertical legs of CFRP strips for optimal performance of the strengthening method is known from the full scale slab tests ($\sim 1/3$ of CFRP uniaxial tensile strength). Hence, the anchorage length that provides the required strength is the only unknown. Results from a number of anchorage tests have been reported in the technical literature.

CFRPs, GFRPs, and steel plates were employed in those tests. However, it is important to determine the required anchorage length using the same kind of CFRP, epoxy and application procedure that were used in the slab tests described in Sections 2.4 and 2.5.

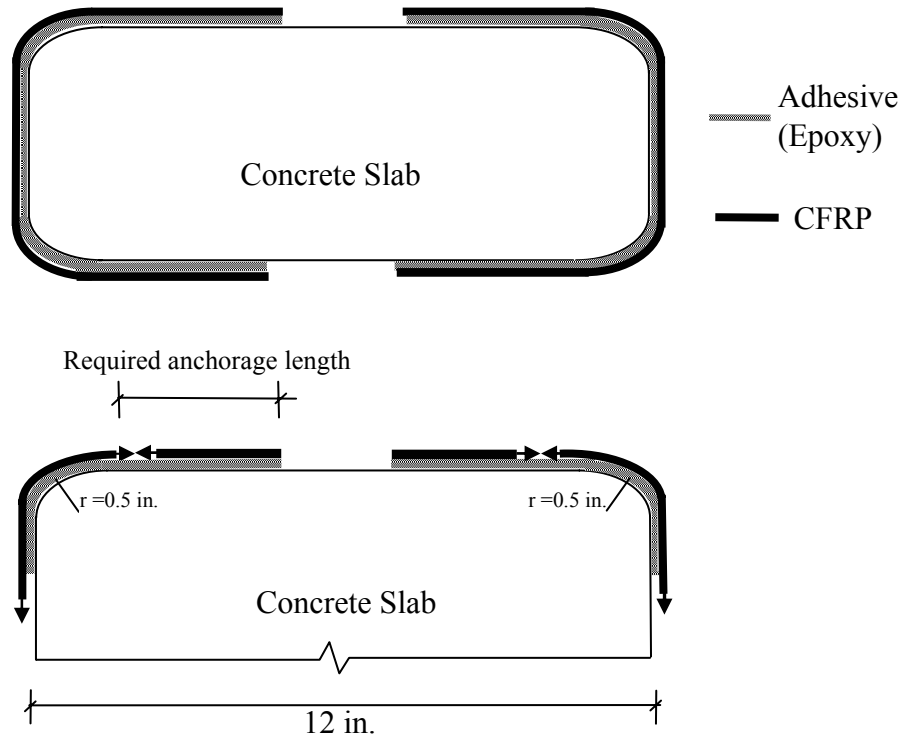


Figure 2.48 “C-Shape” CFRP Strips Used as Shear Reinforcement

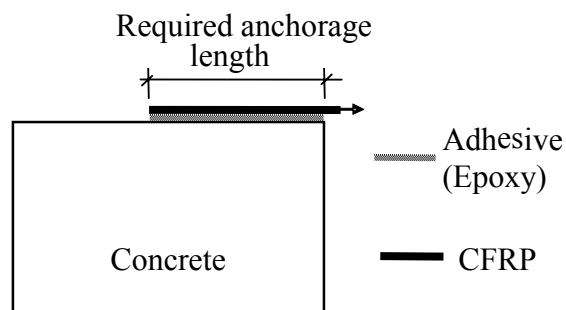


Figure 2.49 Simplified Model to Investigate Anchorage Strength

In order to determine the required anchorage length, double shear push-out tests were performed. The schematic of the test setup is shown in Figure 2.50. Two series of tests were conducted. In the first set of tests, CFRP strips were bonded to the sides of concrete cylinders. Four different CFRP anchor lengths were tested. The details of the specimens including anchorage lengths and widths are given in Table 2.10. Specimens C-3, C-7, C-12 had anchorage lengths of 3.5 in., 7 in., and 12 in. respectively. On the other hand, specimen C-12CL had 12 in. of anchorage length on the sides, but CFRP strips were bent and overlapped at the base of the cylinders. In the second series of tests concrete prisms were used instead of cylinders. Seven different anchorage lengths were tested. Specimens P-3, P-6, P-9, P-12, P-15, P-18, P-24 had anchorage lengths of 3-1/4 in., 6-1/2 in., 9 in., 12 in., 15 in., 18 in., and 24 in., respectively. For concrete prisms additional CFRP patches (6 in. x 6 in.) were attached on three surfaces of CFRP anchors in order to force the failure of the fourth anchorage without any CFRP patches. In this way, it was possible to closely observe the behavior of the critical anchorage. The width of all the CFRP strips were intended to be approximately 1 in. simulating the CFRP strips used in the slab tests. Actual widths of CFRP strips after impregnation and installation were measured using a caliper at anchorage locations in order to obtain the precise widths of CFRP strips. The widths listed in Table 2.10 were the average of three measurements for each test specimen.

Upon curing of the epoxy, a hydraulic ram was positioned at the center lines of the specimens. In the self-contained system illustrated in Figure 2.50, load was applied through a hydraulic ram which pushed the concrete cylinders (or prisms) from each other. Relative displacements of the concrete prisms (slip displacement) in the second series were measured by attaching a linear potentiometer parallel to the loading direction (Figure 2.50). The ultimate loads and maximum slip displacements measured in each test are given in Table 2.10.

In addition, the ultimate load normalized with respect to the ultimate load carrying capacity of CFRP based on coupon tests are also presented in this table. Typical pictures of the specimens after failure are shown in Figure 2.51 and Figure 2.52.

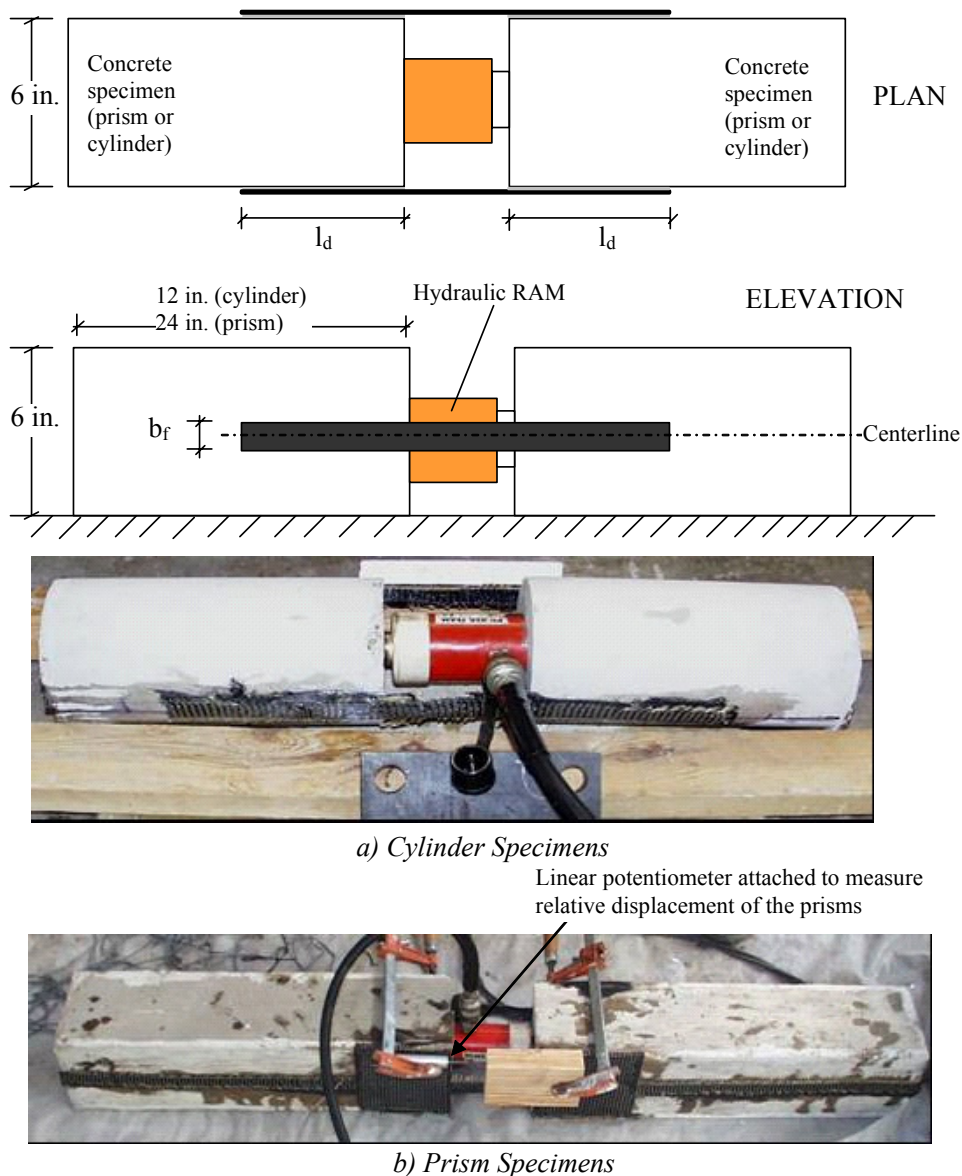


Figure 2.50 Double Shear Push-Out Tests

Table 2.10 Specimen Details and Test Results for Anchorage Strength Experiments

Specimen Name	CFRP Width, b_f (in.)	f'_c (psi)	$f_{ct} = 6\sqrt{f'_c}$ (ksi)	Anchorage Length, l_d (in.)	Ultimate Load P_{exp} (k)	P_{exp} / P_u	Maximum Slip Displacement u^* , (in.)
C-3.5	0.95	4500	0.4	3.5	1.0	0.23	-
C-7	1.06	4500	0.4	7.0	1.2	0.23	-
C-12	1.05	4500	0.4	12.0	2.6	0.52	-
C-12CL	0.71	4500	0.4	12.0	1.7	0.51	-
P-3	1.48	2500	0.3	3.3	1.5	0.21	0.04
P-6	1.37	2500	0.3	6.5	2.6	0.40	0.07
P-9	1.05	2500	0.3	9.0	2.1	0.42	0.03
P-12	1.14	2500	0.3	12.5	2.5	0.46	0.05
P-15	1.11	2500	0.3	15.0	2.7	0.51	0.02
P-18	0.97	2500	0.3	18.0	2.6	0.56	0.06
P-24	1.00	2500	0.3	24.0	2.2	0.47	0.05

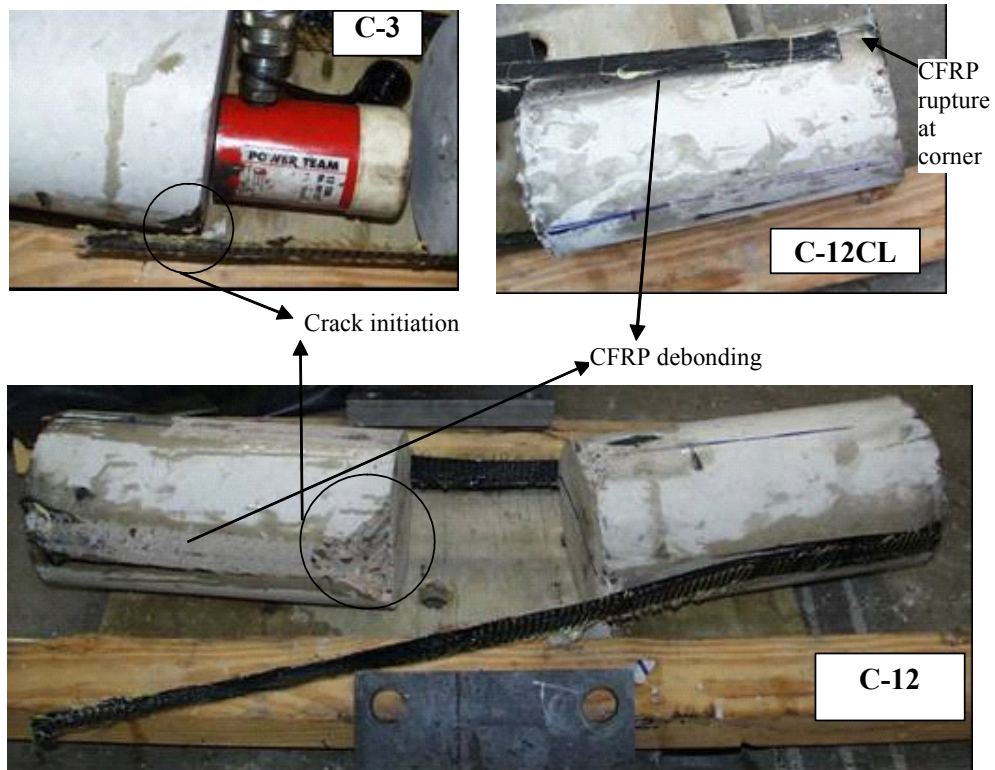


Figure 2.51 Failure of Anchorage Specimens (C-Series)

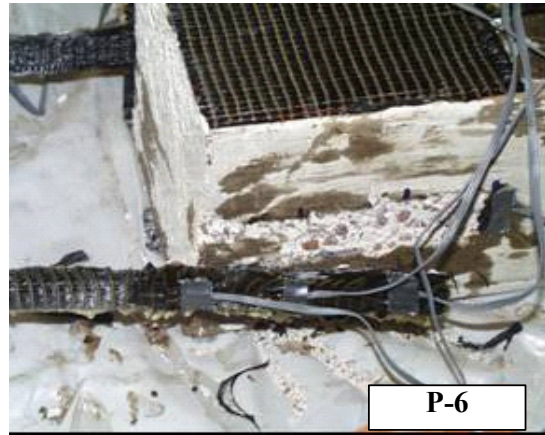
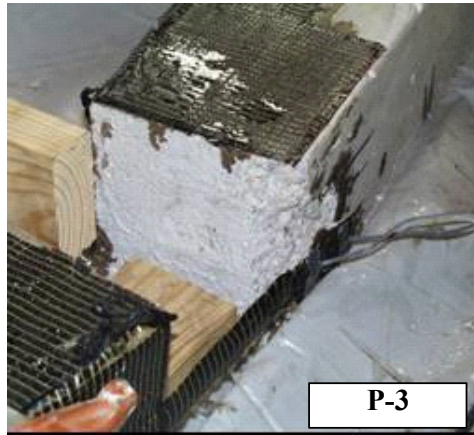


Figure 2.52 Failure Anchorage Specimens (P Series)

All specimens failed in a brittle manner by initiation of a crack in concrete prism (or cylinder) close to the free edge of CFRP-concrete interface followed by rapid-progressive debonding of the CFRP strips along the anchorage length. A thin layer of concrete remained attached to the CFRP strips during CFRP debonding. Specimens C-3 and C-7 carried only about 20% of the load carrying capacity of the CFRP (Table 2.10). Specimens with 12 in. of anchorage length (C-12 and C-12CL) carried about 50% of the load carrying capacity of the CFRP. Specimen C-12CL failed by debonding of CFRP strip from concrete surface followed by the rupture of the CFRP strip at the wrapped edge due to the existence of the sharp corner (Figure 2.51).

The failure modes of prism specimens were similar to those observed in anchorage tests performed using concrete cylinders. Failure initiated with concrete cracking at the edge of the anchorage, followed by debonding of CFRP together with a thin layer of concrete attached to the CFRP strips occurred (Figure 2.52). Beyond an anchorage length of about 9 in. only marginal strength increases were obtained (Table 2.10). Test results showed that load carrying capacity of the anchorage specimens was limited to about 50% of the load carrying capacity of the CFRP strips in uniaxial tension. The results of anchorage strength values for different anchorage lengths are shown in Figure 2.53. This figure shows that the anchorage strength was proportional to anchorage length up to a certain length (9 to 12 in.) beyond which the strength of the anchorage remained constant for all practical purposes.

In Section 2.7 it was shown that the maximum CFRP strain in the vertical legs of CFRP stirrups was about 0.004 without failure of the shear reinforced zone. In fact, this CFRP strain limit is used in Chapter 5 to propose a design procedure. Bearing in mind that ultimate strain of CFRP at rupture in uniaxial tension is about 0.012, a strain value of 0.004 approximately corresponds to $1/3^{\text{rd}}$

of the ultimate strength of CFRP strips. If a similar level of stress acts on the CFRP anchor, an anchorage length of about 12 in. can ensure proper anchorage. In this way CFRP force that corresponds to a strain of 0.004 can be carried safely by the anchorage. It is interesting to note that for pattern A specimens, the distance between the holes (i.e. the length of the horizontal legs of CFRP stirrups) are approximately 12 in. Therefore the required anchorage length upon use of “C-Shape” CFRP shear reinforcement is very similar to that provided by the closed loops. This shows that minimal cost saving from material can be achieved by using “C-Shaped” CFRPs. In fact it is easier and more practical to use closed loops with better anchorage performance. On the tension face of the slab, the force in the CFRP anchor will be higher than that imposed by the vertical leg due to bending of the section and stress concentrations imposed at flexural crack locations. Therefore peeling of the CFRP anchors may cause early failure of the vertical legs, which can initiate a failure inside the shear reinforced zone prior to reaching the shear capacity of the upgraded connection outside the shear reinforced zone.

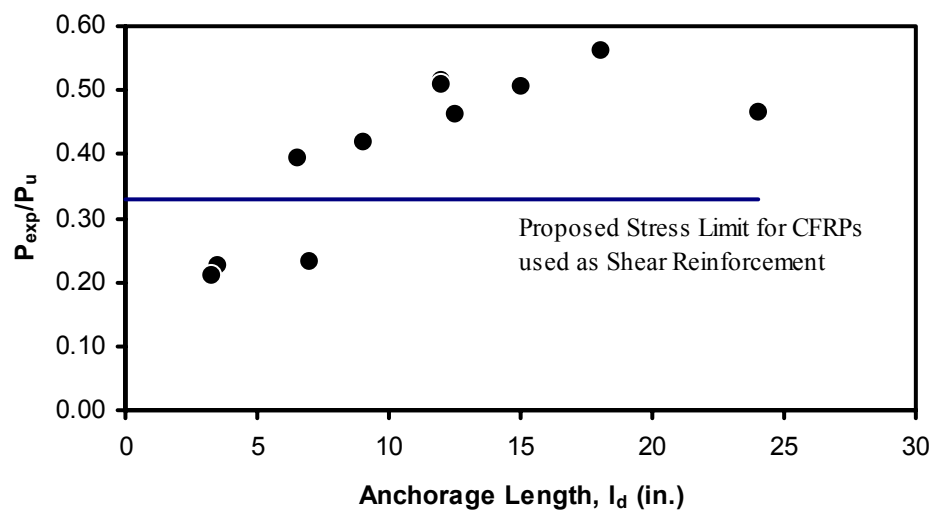


Figure 2.53 Normalized Anchorage Strength vs. Provided Anchorage Length

2.8.4.2 Anchorage Strength of CFRPs bonded to Concrete: Analysis

The test results presented in Section 2.8.4.1 and results from other researchers (Taljsten 1997, Maeda 1998) are examined in this section. In addition, a model presented in Appendix B to determine the strength of CFRP-adhesive-concrete system is employed herein.

The results of single (Taljsten 1997) and double shear tests (Maeda 1998) using CFRPs are presented in Table 2.11 together with the results of the tests conducted in this study. An examination of Table 2.11 indicates that a wide range of CFRP, adhesive and concrete compressive strength was employed in these tests. The experimental anchorage capacities and the ratio of these capacities to the load carrying capacity of CFRPs (as determined by coupon tests) are also given in Table 2.11. Although anchorage lengths up to about 28 in. were used, the strength of the anchorage system did not increase proportionally to the anchorage length. The normalized ultimate loads are plotted against the anchorage length in Figure 2.54. There is a large scatter in the data however it is still possible to observe a similar trend as shown in Figure 2.53. The anchorage strength is proportional to the provided anchorage length up to a certain anchorage length and beyond this length it does not change significantly with increasing anchorage length. From the tests of Maeda and current study it is possible to observe that capacity of the anchorage is limited to about half the load carrying capacity of the CFRP strip in uniaxial tension.

The theory presented in Appendix B postulates that failure occurs at the concrete FRP interface due to high shear stress transfer from FRP to concrete. Even though the anchorage length may be long, failure occurs when a “critical” deformation limit is reached. At this deformation level, concrete cracking takes place along the bonded length. For shorter lengths, the anchorage strength is proportional to the anchorage length. The detailed description of this model

Table 2.11 Tests on Anchorage Strength of CFRPs

Researcher		Adhesive			CFRP				Concrete		Anchorage Length	Results	
Name	Specimen	Young's Modulus E_a (ksi)	Shear Modulus G_a (ksi)	Thickness t_a (in.)	Young's Modulus E_f (ksi)	Thickness t_f (in.)	Ultimate Strength f_u (ksi)	Width b_f (in.)	f'_c (psi)	f_{ct} (ksi)	l_d (in.)	P_{exp} (k)	P_{exp}/P_u
Tajlsten	C100 50 A	972	374	0.08	24656	0.05	362	1.97	-	0.57	4.0	3.89	0.11
	C200 50 A	972	374	0.08	24656	0.05	362	1.97	-	0.59	8.0	6.18	0.18
	C300 50 A	972	374	0.08	24656	0.05	362	1.97	-	0.62	12.0	7.89	0.22
Maeda et. al.	M1	725	279	0.04	33358	0.004	508	1.97	-	0.46	3.0	1.30	0.30
	M2	725	279	0.04	33358	0.004	508	1.97	-	0.46	6.0	2.07	0.48
	M3	725	279	0.04	33358	0.00	508	1.97	-	0.48	12.0	2.69	0.62
	M4	725	279	0.04	55112	0.01	435	1.97	-	0.47	3.0	2.25	0.40
	M5	725	279	0.04	55112	0.01	435	1.97	-	0.47	6.0	1.64	0.29
	M6	725	279	0.04	33358	0.01	508	1.97	-	0.47	3.0	2.15	0.25
	M7	725	279	0.04	33358	0.01	508	1.97	-	0.47	6.0	3.65	0.42
	M8	725	279	0.04	33358	0.00	508	1.97	-	0.48	27.5	2.25	0.52
Binici	C-3	461	177	0.04	10500	0.04	120	0.95	4500	0.40	3.5	1.04	0.23
	C-7	461	177	0.04	10500	0.04	120	1.06	4500	0.40	7.0	1.19	0.23
	C-12	461	177	0.04	10500	0.04	120	1.05	4500	0.40	12.0	2.59	0.52
	C-12CL	461	177	0.04	10500	0.04	120	0.71	4500	0.40	12.0	1.74	0.51
	P-3	461	177	0.04	10500	0.04	120	1.48	2500	0.30	3.3	1.50	0.21
	P-6	461	177	0.04	10500	0.04	120	1.37	2500	0.30	6.5	2.60	0.40
	P-9	461	177	0.04	10500	0.04	120	1.05	2500	0.30	9.0	2.12	0.42
	P-12	461	177	0.04	10500	0.04	120	1.14	2500	0.30	12.5	2.53	0.46
	P-15	461	177	0.04	10500	0.04	120	1.11	2500	0.30	15.0	2.70	0.51
	P-18	461	177	0.04	10500	0.04	120	0.97	2500	0.30	18.0	2.63	0.56
P-24	461	177	0.04	10500	0.04	120	1.00	2500	0.30	24.0	2.25	0.47	

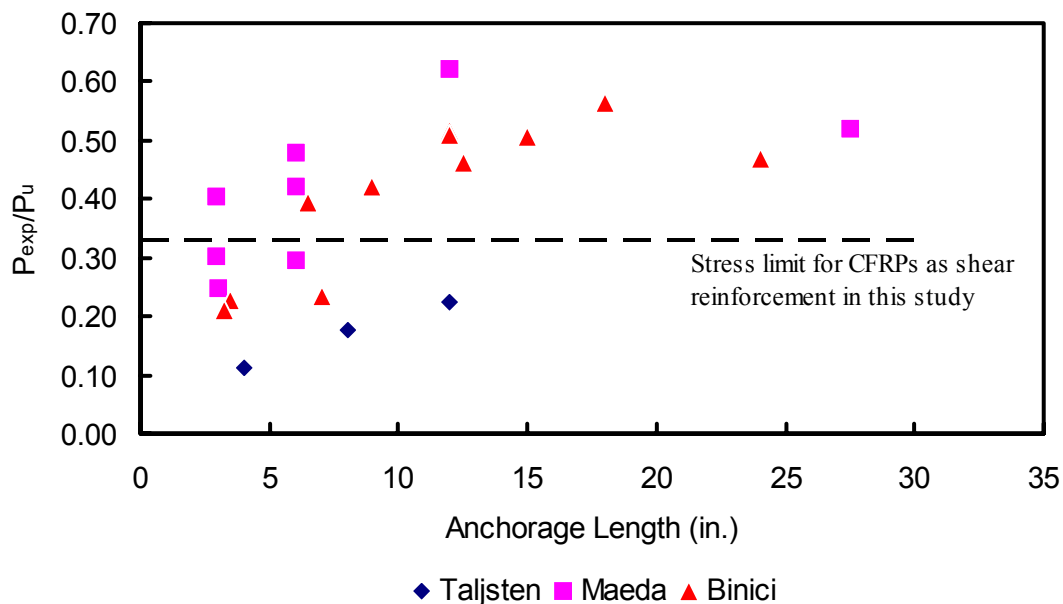


Figure 2.54 Anchorage Strengths for Different Anchorage Lengths of CFRPs

is given in Appendix B. Only relevant expressions are reviewed herein.

For a given anchorage length, material properties of CFRP, adhesive and concrete, the capacity of the anchorage can be computed by using the following expression:

$$T = \left(\frac{f_{ct} b_f}{w} + \frac{f_{ct} b_f L_{eff}}{2} \right) \quad (2.3)$$

where f_{ct} is the limiting strength of concrete and taken as the tensile strength of concrete, b_f is the width of CFRP, w and L_{eff} are given as:

$$w^2 = \frac{G_a}{E_f t_a t_f} \quad (2.4)$$

$$L_{eff} = \min (l_d , l_{cr}) = \min \left(l_d , \frac{3}{2} \left[\sqrt{\frac{4 u^* E_f t_f}{3 f_{ct}} + \frac{1}{w^2}} + \frac{1}{w} \right] \right) \quad (2.5)$$

where l_d is the supplied anchorage length, l_{cr} is the critical anchorage length computed based on a deformation limit, L_{eff} is the effective anchorage length, u^* is the critical slip displacement, E_f is the Modulus of Elasticity of CFRP, t_f is the thickness of CFRP and f_{ct} is the concrete tensile strength as determined by split cylinder tests.

It can be observed that the critical length l_{cr} limits the ultimate load carrying capacity based on a critical slip displacement, u^* . The predictions obtained through the use of the model are given in Figure 2.55 and Table 2.12. A u^* value of 1 mm (0.04 in.) is used for the critical slip displacement. This value agrees well with the average of the measured slip displacements shown in Table 2.10 and with the previously reported slip displacements by Taljsten (1997). Material properties of CFRP, adhesive and concrete strength used in the analyses are given in Table 2.11. It can be observed that there is a reasonably good agreement between the model predictions and the experiments.

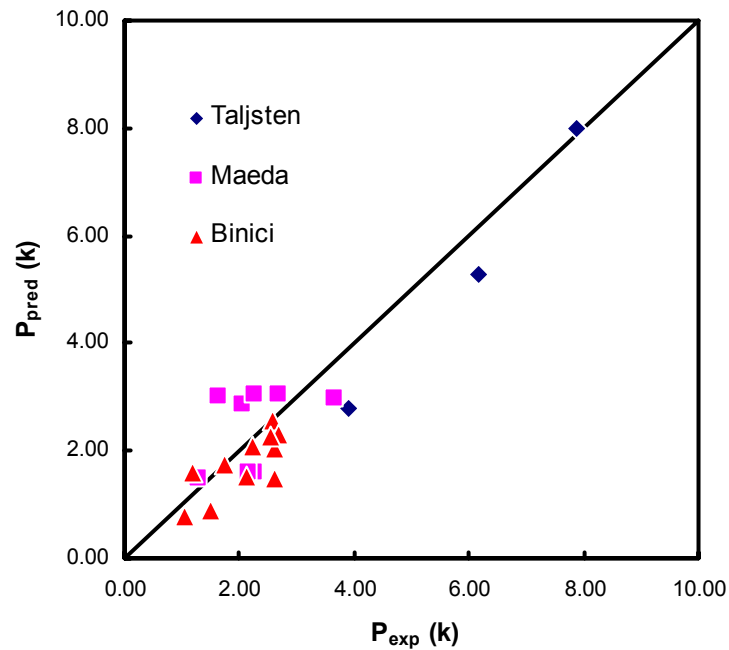


Figure 2.55 Anchorage Strength Comparisons of Model Predictions with Experimental Results

However great uncertainty associated with actual CFRP thickness, t_f , and width, b_f , concrete surface tensile strength, and critical slip displacement, u^* , affect the model predictions resulting in a high standard deviation. The model predictions together with the experimental results can be better studied by examining Figure 2.56. This figure indicates that up to the critical length, l_{cr} , anchorage strength increases linearly with increasing anchorage length. However, beyond the critical length, anchorage strength remains approximately constant with increasing anchor lengths. It is possible to observe that the model predicts the experimental trend in an accurate way as the experimental data points are nicely scattered around the model predictions.

The implications of the anchorage study presented above on punching shear strengthening of flat plates can be summarized as follows:

Table 2.12 Comparisons of Model Predictions with Experiments

Researcher		Anchorage	Analysis		Comparisons	
Name	Specimen	Boded Length, l_d (in.)	Critical Bond Length, l_{cr} (in.)	P_{pred} (k)	P_{exp} (k)	P_{exp} / P_{pred}
Tajsten	C100 50 A	4.0	16.6	2.79	3.89	1.39
	C200 50 A	8.0	16.2	5.27	6.18	1.17
	C300 50 A	12.0	15.8	7.99	7.89	0.99
Maeda et. al.	M1	3.0	6.3	1.50	1.30	0.87
	M2	6.0	6.3	2.87	2.07	0.72
	M3	12.0	6.2	3.03	2.69	0.89
	M4	3.0	9.8	1.60	2.25	1.40
	M5	6.0	9.8	3.00	1.64	0.55
	M6	3.0	8.8	1.59	2.15	1.35
	M7	6.0	8.8	2.99	3.65	1.22
	M8	27.5	6.1	3.06	2.25	0.73
Binici	C-3	3.5	11.5	0.79	1.04	1.31
	C-7	7.0	11.5	1.62	1.19	0.73
	C-12	12.0	11.5	2.55	2.59	1.02
	C-12CL	12.0	11.5	1.73	1.74	1.00
	P-24	24.0	13.3	2.08	2.25	1.08
	P-18	18.0	13.3	2.03	2.63	1.30
	P-15	15.0	13.3	2.31	2.70	1.17
	P-12	12.5	13.4	2.26	2.53	1.12
	P-3	3.25	13.4	0.89	1.50	1.69
	P-6	6.50	13.3	1.47	2.60	1.77
	P-9	9.00	13.3	1.53	2.12	1.39
Mean						1.13
St. Dev						0.31

i) In order to carry forces at magnitudes that are about half the uniaxial tensile strength of CFRPs, a minimum anchorage length of about 12 in. is required for one inch wide one layer of CFRP strip. This result is verified experimentally and supported by the analytical study presented in Appendix B.

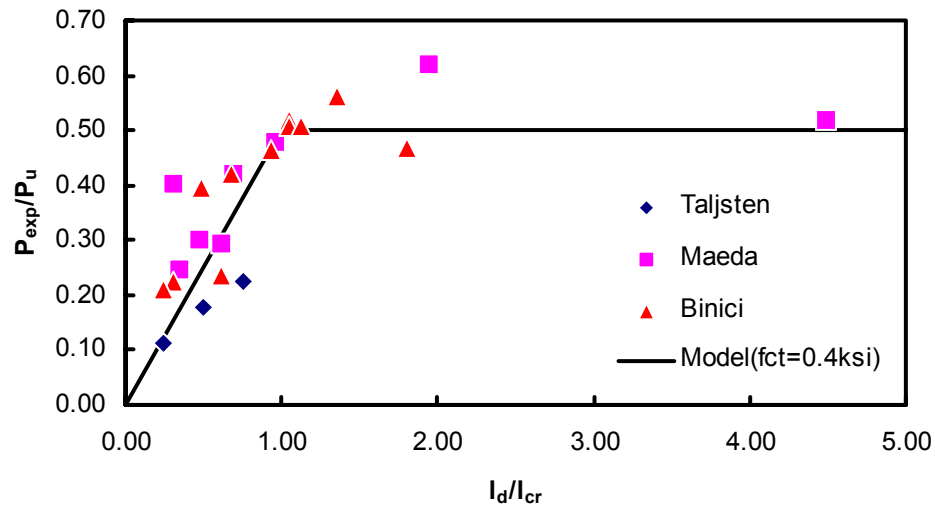


Figure 2.56 Critical Anchorage Length Concept

Moreover, this length is similar to the critical length, above which further increase of anchor length will not result in increased anchorage strength according to the results of experiments and analyses.

ii) The critical anchorage length is proportional to the stiffness of CFRP strips (Equation (2.5)). Therefore, for 1 in. wide CFRP strips that are bonded on concrete surface, using more than one layer is likely to increase the required anchorage length to more than 12 in.

iii) Due to bending of the slab, additional stresses on CFRP anchors develop (especially on the tension side of the slab). These stresses, in addition to those induced by the vertical legs acting as shear reinforcement, should be considered if C-Shape anchors are used. Otherwise the effectiveness of vertical legs will be lost prior to reaching the suggested strain limit of 0.004.

iv) When C-Shape anchors are used, it is necessary to modify the suggested CFRP strain limit (0.004) in vertical legs depending on the provided anchorage length. An anchorage strength model (such as the one presented in Appendix B) can be used to compute the effective strain limit for a given

anchorage length. This strain limit will probably be smaller than the suggested strain limit (0.004) for anchorage lengths smaller than the critical anchorage length. Subsequently, the area of vertical CFRP reinforcement can be determined based on the revised effective strain limit. When anchorage of CFRPs is performed by overlapping them, these calculations are not needed and the effective strain limit of 0.004 can safely be used to determine the amount of vertical CFRP reinforcement. The design procedure that is discussed in Chapter 5 makes use of this strain limit. Hence, CFRP anchorage is assumed to be provided by CFRP overlaps (i.e. CFRP to CFRP bonding).

v) Other form of anchorage methods such as fan anchors at the ends of CFRP vertical legs can also be used in punching shear strengthening applications. However, experimental verification using concentrically loaded slab tests similar to those presented in this chapter are required to show that anchorage strength does not jeopardize the effectiveness of the proposed strengthening scheme.

2.8.5 Capacity Loss at Punching Failure

An important aspect of punching shear failure of slab-column connections is the capacity loss at punching failure. Sudden loss of capacity at a single connection is likely to increase the demands on the neighboring connections. This may result in punching failure of the neighboring connections leading to a progressive collapse of the floor system. When capacity loss is reduced, it may be possible to decrease the additional demands on the neighboring connections due to a single punching failure.

An examination of the load-deformation behavior of specimens (Figures 2.15 and 2.16) shows that significant loss of load carrying capacity occurred upon punching failure. Immediately after punching failure, the primary resistance left in the slab is believed to be dowel action (bending resistance of reinforcing bars),

since the longitudinal reinforcement did not yield at inclined crack locations. At this stage, the inclined crack was wide enough such that aggregate interlock could be neglected. In addition, the compression side of the slab had already failed and there was no resistance left at this location to provide any further capacity. When further displacements were imposed on the specimens after punching failure, load carrying capacity of the specimens tended to increase (specimens A4-1, A4-2, A4-3, A6 in Figure 2.15 and specimens B4 and B6 in Figure 2.16). At large slab deformations, bending resistance of the reinforcement may decrease due to yielding of steel reinforcement. Furthermore, reinforcing bars start acting as hangers in tension (bending resistance changes to tension resistance). Load carrying capacity at large slab deformations can be significantly different than the capacity immediately following punching failure. As explained in Section 1.4.4.1, tension reinforcement rips out at these large deformations, and residual capacity is provided by the well anchored compressive bars, if there is any. The discussions presented in this section are valid only for the capacity loss immediately following a punching failure. Further experiments are required to observe the behavior of connections at large slab deformations.

A quantitative measure of dowel force is required to estimate capacity loss of the tested slabs following punching failures. Bauman and Rüsç (1970) tested beams specially designed to measure the dowel force of the flexural reinforcement as shown in Figure 2.57. The dowel force was determined as the load at which a splitting crack opened along the reinforcement layer. Based on their experimental results, they proposed the following expression to compute the dowel force:

$$V_d = l_c b_n f_{ct} \tag{2.6}$$

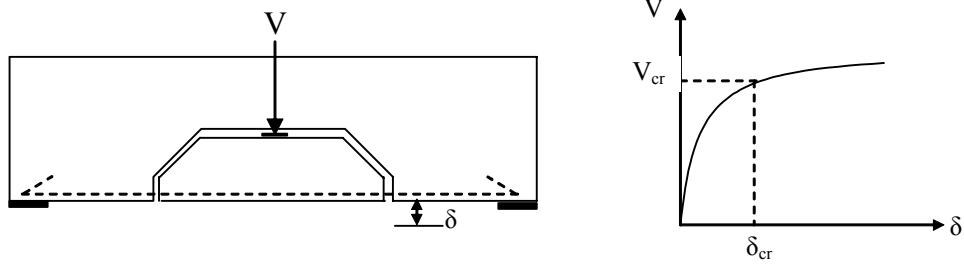


Figure 2.57 Dowel Force Tests by Bauman and Rusch (1970)

where b_n is the effective width of the beam at the level of reinforcement and f_{ct} is the tensile strength of concrete. The characteristic length, l_c was empirically given as follows:

$$l_c = \frac{14.3 d_b}{\sqrt[3]{f_{c,cube}}} \quad (2.7)$$

where d_b is the reinforcement bar diameter, $f_{c,cube}$ is the cube compressive strength of concrete. The expression was adjusted such that it yields l_c in centimeters. The proposed expression was modified by Hamadi and Regan (1980) and later used to estimate dowel forces in two-way slabs by Hallgren (1996). The modified formula is given as:

$$V_d = 4.12 d_b^{2/3} b_n \sqrt[3]{f_{c,cube}} \quad [\text{N}] \quad (2.8)$$

in which d_b is the reinforcement bar diameter [mm], $f_{c,cube}$ is the cube compressive strength [MPa] and can be approximated as $f_{c,cube} = 1.25 f_{c,cylinder} = 1.25 f_c'$. For a two-way reinforced concrete slab, b_n can be calculated using the following expression:

$$b_n = b_d \left(1 - \frac{16 \rho d}{\pi d_b} \right) \quad [\text{mm}] \quad (2.9)$$

where b_d is the length of the perimeter of the critical section at which dowel action is expected to take place. However, if the reinforcing steel intersecting the

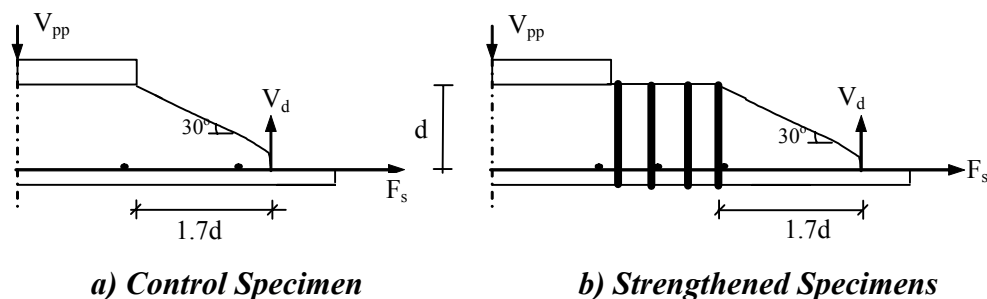
inclined shear crack yields, then the dowel action reduces considerably, and Equation (2.8) can not be applied. Since yielding of flexural reinforcement was not observed outside the shear reinforced zone, Equations (2.8) and (2.9) can be used to compute the dowel forces across the inclined shear crack for the test specimens.

As explained in Section 2.7.3 the inclined crack was observed at about an angle of 30 degrees for the control specimen at the face of the loading area and for the strengthened specimens, A4-1, A4-2, A6, A8, B4, B6, and B8, outside the shear reinforced zone (Figures 2.31, 2.32). Based on this observation, dowel force can be assumed to occur at a critical perimeter, b_d , located about $1.7d$ away from the loading area or from the outermost shear reinforcement (Figure 2.58).

Specimen A4-4 was the only specimen where steel plates were not used to anchor the longitudinal bars. It can be observed that capacity following punching failure of this specimen was actually lower than that of Control-1 (Figure 2.15). In addition, the load carrying capacity of the specimen decreased with increasing displacements. In order to investigate the reason behind this, the required anchorage length of No.6 bars was calculated using the following ACI 318-02 expression:

$$l_d = \frac{3}{40} \frac{f_y}{\sqrt{f_c'}} \left[\frac{\alpha\beta\gamma\lambda}{\left(\frac{c + K_{tr}}{d_b} \right)} \right] d_b \quad (2.10)$$

in which f_y is the yield strength of the reinforcement, f_c' is the concrete compressive strength in psi, d_b is the bar diameter, c is the cover based on centerline bar dimensions, and K_{tr} is the transverse reinforcement ratio index.



a) Control Specimen

b) Strengthened Specimens

Figure 2.58 Locations of Dowel Forces

The factors α , β , γ , and λ are the reinforcement location factor, coating factor, reinforcement size factor, and lightweight aggregate concrete factor, respectively. For the No. 6 bars, the required anchorage value can be computed as about 23 in. for $f_c' = 4100$ psi. On the other hand, the available anchorage length is equal to the distance from the place where dowel action occurs (Figure 2.58) to the edge of the slab. Hence, the available anchorage length was only about 17.5 in. Based on this analysis, it is possible to observe that longitudinal reinforcement was not properly anchored in order to obtain reliable information on capacity loss at punching failure. The response shown in Figure 2.13, where the load carrying capacity decreased for increasing displacements after punching failure occurred, is an indication of possible bar slip. As a result, capacity loss calculations at punching failure based on Equation (2.8) are not presented for this specimen. However, it is important to note that No. 6 bars were successfully developed at the critical moment and shear sections prior to punching shear failure. Although this specimen provided valuable information up to the occurrence of punching shear failure, results obtained in the descending branch are not comparable to those obtained in other tests.

The measured capacity losses at punching failure, V_1 , estimated capacity losses at punching failures V_{1e} , and V_1 to V_{1e} ratios are given in Table 2.13. The loss of capacities at punching failure was computed by subtracting the capacities

immediately after punching failure from the ultimate loads. In addition, capacity loss ratios of V_l to V_u are given in Table 2.13. The top surfaces of specimens after failure are shown in Figure 2.38 and Figure 2.39. These figures indicate that specimens A8, B4, B6, and B8 experienced inclined cracks that terminated at the edge of the slabs. Slabs with these asymmetric failure surfaces and those with inclined cracks that terminated at slab boundaries are also indicated in Table 2.13.

For specimen Control-1, capacity dropped by 70% following punching failure. For specimen Control-2 (with integrity steel), this loss was about 50% of the ultimate load. This shows that use of integrity steel decreases the capacity loss however, a significant loss of capacity still can occur. For strengthened specimens A4-1, A4-2, A4-3, A4-4 and A6, capacity loss ratio (V_l/V_u) was similar to that of specimen Control-1. For strengthened specimens A8, B4, B6 and B8, this ratio was smaller than that of Control-1 specimen and ranged from 0.25 to 0.6.

The measured capacity losses at punching failure (V_l) and calculated capacity losses at punching failure (V_{lc}) were in agreement for specimens Control-1, Control-2, A4-1, A4-2, A4-3, and A6. This confirms the fact that dowel forces were the dominant forces providing resistance immediately after punching failure. For specimens A8, and B8 the computed dowel forces were about half of the measured capacities after punching failure. This shows that as the number of CFRP perimeters was increased and inclined crack locations were close to the slab edges, additional strength was mobilized besides the dowel action. The measured capacity losses for specimens with these boundary effects (especially specimens A8 and B8) may not reflect the actual capacity losses expected in slab-column connections due to specimen size limitations. The additional capacity due to edge effects for specimens A8 and B8 can be estimated as the difference between the measured capacity immediately following punching failure and the computed dowel force. Therefore, the experimental results obtained for these

specimens require special attention in understanding the effect of the strengthening scheme on capacity loss at punching failure. It is important to realize that capacity of specimens with these boundary effects should not be relied upon to reach conclusions on the capacity of the connections at large deformations.

The increases in load carrying capacities immediately following a punching failure were well reflected with the increase in computed dowel forces as shown in Table 2.13. These capacities of the strengthened specimens tended to increase with increase in number of CFRP perimeters. This effect was primarily due to the increase in the number of reinforcing bars contributing to the resistance following a punching failure as the failure was shifted away from the loading area. In addition, externally installed CFRP stirrups helped to prevent stripping out of the bars. When the number of bars at the critical punching section was increased the ratio of capacity loss at punching failure to ultimate capacity decreased.

It should be appreciated that capacity of the upgraded test specimens after punching failure was solely provided by the tension bars. At large slab deformations, tension bars can still strip out leaving the connection without any

Table 2.13 Summary of Capacity Losses at Punching Failure

Specimen Name	Ultimate Load V_u (k)	Capacity Following Punching Failure V_{pp} (k)	Capacity Loss at Punching Failure $V_l = V_u - V_{pp}$ (k)	Capacity Loss Ratio V_l/V_u	Computed Dowel Resistance V_d (k)	V_d/V_{pp}	Estimated Capacity Loss $V_{lc} = V_u - V_d$ (k)	V_{lc}/V_l	Inclined Shear Crack Terminating at Slab Boundary
Control 1	110	31	79	0.72	33	1.04	78	0.98	No
Control 2	114	56	57	0.50	51	0.91	63	1.09	No
A4-1	133	37	96	0.72	40	1.09	92	0.97	No
A4-2	149	39	110	0.74	40	1.04	109	0.99	No
A4-3	139	39	100	0.72	40	1.04	99	0.99	No
A4-4	135	26	109	0.81	NC*	NC*	NC*	NC*	No
A6	161	46	115	0.72	48	1.05	113	0.98	No
A8	166	125	41	0.25	56	0.45	110	2.67	Yes
B4	170	61	109	0.64	51	0.84	119	1.09	Yes
B6	169	79	90	0.53	62	0.78	107	1.19	Yes
B8	175	131	44	0.25	73	0.56	102	2.32	Yes

*: Not computed

residual capacity. Therefore, use of the proposed strengthening procedure to increase residual capacity of slab-column connections at large deformations needs further investigation.

The capacity loss at punching failure, in addition to the desired performance level and cost efficiency (previously discussed in Sections 2.8.1 and 2.8.2), is the crucial indicator in selecting the appropriate strengthening pattern, amount of material and stirrup configuration.

2.8.6 A Simple Model to Calculate Punching Shear Capacity

2.8.6.1 Model by Theodorakopoulos and Swamy (2002)

Theodorakopoulos and Swamy (2002) proposed a simple mechanical model to predict punching shear capacity of slab-column connections without any shear reinforcement. The model considers the free-body diagram around the slab column connection area at the stage where inclined crack has formed and its propagation is prevented by the compression zone (Figure 2.59). According to this model, the total shear resistance of a slab column connection without shear reinforcement can be computed as follows:

$$V_u = V_c + V_a + V_d \quad (2.11)$$

where V_u is the punching shear capacity, V_c is vertical component of the concrete resistance provided in the compression zone, V_a and V_d are the resistances provided by the aggregate interlock and dowel action, respectively. In reality, these components do not remain as isolated quantities, but exist together and their maximum values are not reached at the same time of loading. The aggregate interlock force is activated only after the formation of the inclined crack and the model, discussed herein, neglects this because of large separation of the crack faces as observed in tests ($V_a = 0$). The failure is assumed to occur when splitting

failure occurs along lines AA' and BB' in the compression zone (Figure 2.59). Thus, the model assumes that punching shear failure is the splitting failure of the compression zone at the ultimate load.

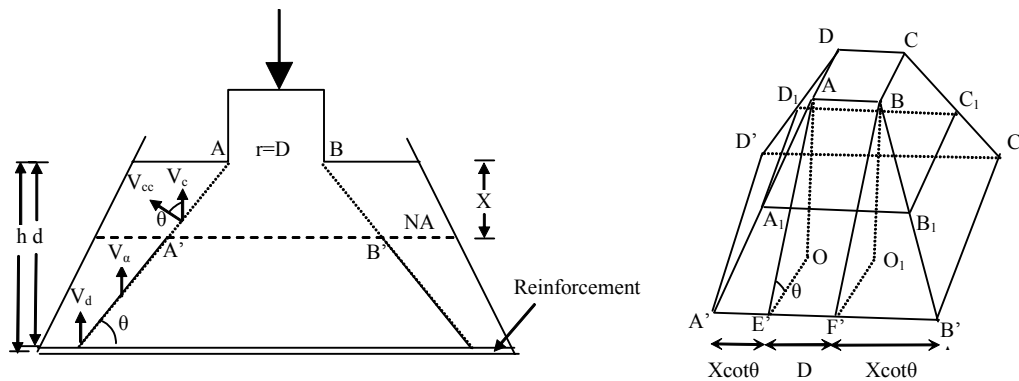
Concrete resistance above the neutral axis, V_{cc} is computed by multiplying the splitting tensile strength of concrete by the failure area as shown in Figure 2.59. For square columns this expression simplifies to:

$$V_{cc} = 4(X \cot \theta + D) \frac{X}{\sin \theta} f_{ct} \quad (2.12)$$

where X is the depth of neutral axis, D is the column size, θ is the assumed angle of crack, and f_{ct} is the splitting tensile strength of concrete. The vertical component of V_{cc} can be calculated using Equation (2.13).

$$V_c = 4(X \cot \theta + D) X \cot \theta f_{ct} \quad (2.13)$$

Based on a literature review, Theodorakopoulos and Swamy (2002) concluded that the dowel action is proportional to the perimeter of the location of the dowel force similar to that presented in Section 2.8.3. They preferred to



$$\begin{aligned} AO &= X \\ AB &= r = D \\ A'B' &= X \cot \theta + r + X \cot \theta \\ A_1B_1 &= 1/2 X \cot \theta + r + 1/2 X \cot \theta \\ AE' &= X / \sin \theta \end{aligned}$$

Area of Compression Zone:

$$\begin{aligned} A_c &= (A_1B_1C_1D_1) \\ A_c &= [4(X \cot \theta + D)] X / \sin \theta \end{aligned}$$

Figure 2.59 Freebody Diagram for Punching Shear Model

combine the two terms V_c and V_d based on an average critical perimeter located $1.5d$ away from the column (as in BS 8110). Resulting expression for ultimate punching shear strength is given as follows:

$$V_c = b_p X \cot \theta f_{ct} \quad (2.14)$$

where b_p is the critical perimeter located $1.5d$ away from the column face, assumed inclined crack angle, θ , is 30° and f_{ct} is taken as $0.27 f_c'^{2/3}$ [N-mm].

One of the most important features of this model is its attempt to compute the depth of neutral axis (X in Equation (2.14)) in a rigorous way. Figure 2.60 shows the two cracks, inclined shear crack, and flexural crack at the critical section of the slab. The mode of failure of the slab column connections, shear or flexure, is strongly influenced by the amount of reinforcement and the neutral axis depth. Theodorakopoulos and Swamy (2002) assumed that for slabs failing in flexure with extensive reinforcing bar yielding, neutral axis depth of shear critical section, X_s , is similar to the depth based on flexural critical section, X_f . For such slabs, they concluded that most of $f_{c,cube}/\rho f_y$ values of these slabs range from 6 to 8 (7.5 to 10 for $f_{c,cylinder}$). Assuming an average $f_{c,cube}/\rho f_y$ value of 7, and computing X_f based on flexural theory as explained below, X_s is simply calculated as:

$$X_s = 0.25 d \quad (2.15)$$

where d is the effective depth of the slab. For all other slabs, where $X_f \neq X_s$, a harmonic mean is used to compute the average neutral axis depth:

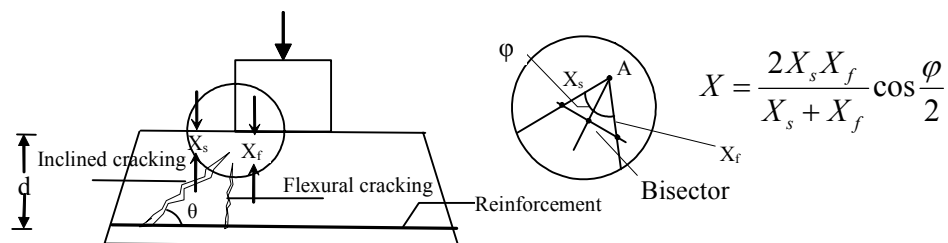


Figure 2.60 Depths of Compression Zones Corresponding to Cracks

$$X = \frac{2X_f X_s}{X_f + X_s} \quad (2.16)$$

The validity of this expression can be observed trigonometrically as shown in Figure 2.60. As the angle between the two cracks approaches zero, the depth of compression zone located at the bisector reduces to that given by Equation (2.16). In addition, Equation (2.16) agrees with the fact that when the amount of reinforcement approaches zero, the depth of neutral axis tends to zero. When the section is heavily reinforced ($X_f \gg X_s$) the neutral axis depth tends to $2X_s$. In contrast, the arithmetic mean does not yield meaningful results.

Theodorakopoulos and Swamy (2002) computed the depth of flexural critical neutral axis depth using classical RC beam theory with the assumed stress-strain behavior for concrete and steel as shown in Figure 2.61. Considering equilibrium of the section, X_f can be obtained for a section with tension reinforcement only by using:

$$X_f = \frac{\rho f_s}{f_{c,cube} \alpha_1} d \quad (2.17)$$

$$\alpha_1 = 0.85 \left(1 - \frac{1}{3} \frac{\varepsilon_o}{\varepsilon_{cu}} \right) \quad (2.18)$$

In Equation (2.18), f_s is the steel stress at the section, α_1 is the equivalent rectangular block parameter, ε_o and ε_{cu} are the strains as shown in Figure 2.61.

The procedure to compute punching shear capacity according to their model is as follows: First, X_f and X_s are calculated using Equations (2.15) and (2.17). Then, mean depth of neutral axis, X , is found using Equation (2.16). Finally, punching shear capacity is computed using Equation (2.14).

Theodorakopoulos and Swamy (2002) verified their model using results from concentrically loaded slabs without any shear reinforcement. The average of the ratio of calculated capacity to experimental capacity was 0.93 with a standard

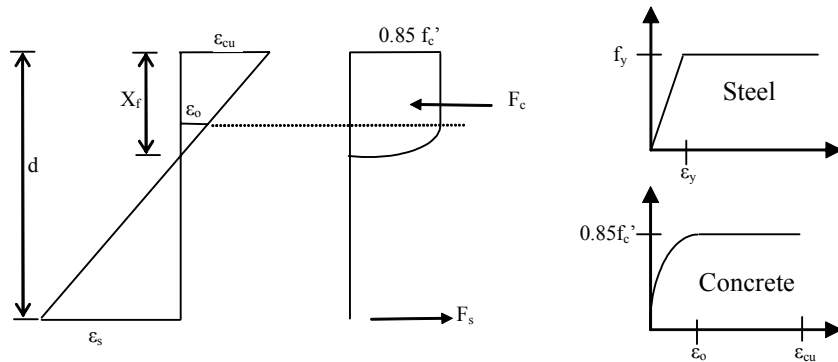


Figure 2.61 Computation of N.A. Depth According to Flexural Theory

deviation of 0.14 for 60 specimens tested by various researchers. Inspired by the simplicity and accuracy of the model, this model with the modifications explained below was used to predict the punching shear strength of test specimens.

2.8.6.2 Modified Model

Following modifications are made to the model presented above:

1- Rectangular stress block parameters of ACI 318-02 are used to compute the depth of neutral axis based on flexure (X_f). For ultimate concrete strain, ϵ_{cu} equal to 0.003, X_f can be computed as follows:

$$X_f = \frac{\rho f_s}{0.85 f'_c \beta_1} d \quad (2.19)$$

where f'_c is the uniaxial compressive strength from cylinder tests, and β_1 is the stress block parameter. Based on this expression, for $f_{c,cube}/\rho f_y$ values between 6 and 8, X_f ranges from approximately $0.2d$ to $0.25d$. In order to be consistent with the original model, no modification to X_s is made and it can be calculated using Equation (2.15).

2- Splitting tensile strength of concrete is computed using the following generally recognized expression:

$$f_{ct} = 6\sqrt{f'_c} \quad (2.20)$$

3- Instead of using Equation (2.14) with a critical perimeter approach, the concrete and dowel contributions are computed separately. According to this V_c is computed using Equation (2.13) and V_d , is computed using Equation (2.8) and (2.9) where b_d is computed at the location of the dowel force. Then the punching shear strength is computed by adding these terms as in Equation (2.11). However, for slabs with $f'_c/\rho f_y$ values greater than 6, dowel contribution can be neglected, since extensive yielding is expected to occur in the flexural reinforcement. The contribution from aggregate interlock is also assumed to be equal to zero in this modified model.

4- For slabs strengthened using CFRPs, the model is extended to incorporate the effect of CFRP acting as shear reinforcement. Based on test observations presented in the previous sections, two failure modes are assumed for the strengthened slabs. First one is the failure inside the shear reinforced zone considering an inclined crack with an angle of 30° (Figure 2.62.a). Equation (2.11) can be modified for this case as follows:

$$V_u^i = V_c^i + V_d^i + V_{FRP} \quad (2.21)$$

$$V_{FRP} = nmA_{FRP}\varepsilon_{FRP_e} E_{FRP} \quad (2.22)$$

where V_{FRP} is the force carried by CFRP crossing the assumed inclined crack, n is the number of vertical CFRP legs used in a perimeter, m is the number of CFRP perimeters crossing the inclined crack, A_{FRP} is the area of vertical FRP reinforcement per hole, ε_{FRP_e} is the effective strain limit for FRP, and E_{FRP} is the Elastic Modulus of FRP. In addition, V_c^i can be computed using Equation (2.13). Based on observations from strain measurements presented in Section 2.7.2.3 and further discussed in Section 2.8.2, FRP strain limit is taken as 0.004 for the

ultimate state when CFRP and concrete contributions are effective. V_d^i is computed at the location of the dowel force as in Figure 2.62.a.

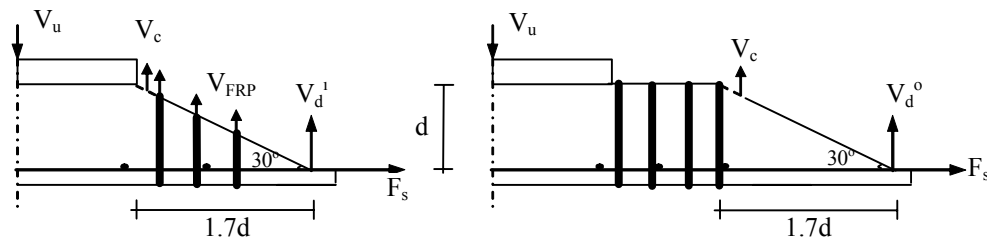
Second failure mode is the failure outside the shear reinforced zone with a similar crack angle (Figure 2.62.b). For this case dowel forces and concrete resistance in the compression zone are computed using a larger perimeter. For Pattern A specimens V_c^o can be calculated using:

$$V_c^o = 4\left(X \cot \theta + \sqrt{2}L + D\right)X \cot \theta \left(\frac{1.7d}{L}\right)^{1/2} f_{ct} \quad (2.23)$$

where L is the distance from the face of the loading area to the outermost shear reinforcement. As explained in Section 1.4.4, ACI 318-02 and BS-8110 consider the decay in shear strength as the distance from the column face increases. This can be seen in Figure 2.63 for the test specimens where b is the length of the outermost shear reinforcement perimeter. The factor $(1.7d/L)^{1/2}$ is incorporated in Equation (2.23) to consider this effect.

For pattern B specimens, the following expression is used to compute the punching capacity outside the shear reinforced zone.

$$V_c^o = 4\left(X \cot \theta + 2L + D\right)X \cot \theta \left(\frac{1.7d}{L}\right)^{1/2} f_{ct} \quad (2.24)$$



a) Inside Shear Reinforced Zone

b) Outside Shear Reinforced Zone

Figure 2.62 Failure Modes for Strengthened Specimens

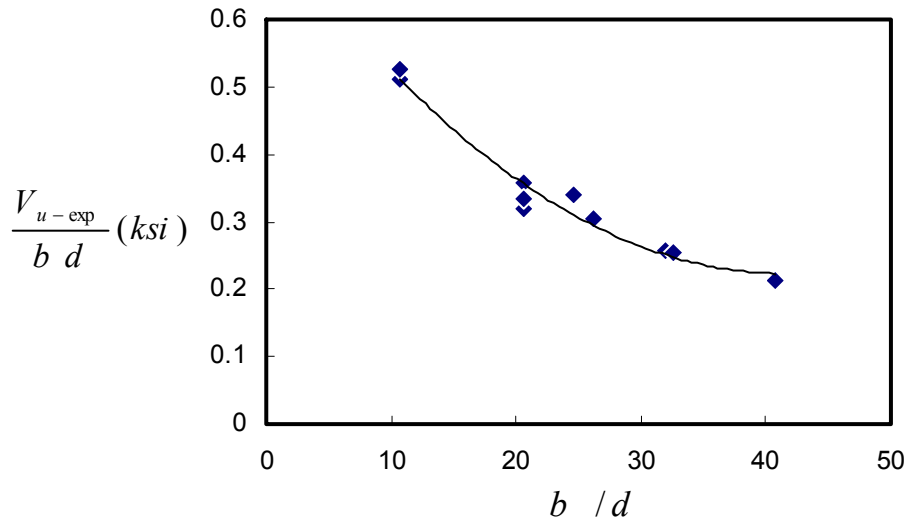


Figure 2.63 Decay of Shear Strength outside the Shear Reinforced Zone

Calculation of X is similar to that given in the no shear reinforcement case (First failure mode as discussed above). The punching shear capacity is the minimum of the two capacities computed inside and outside the shear reinforced zone:

$$V_u = \min(V_c^i + V_d^i + V_{FRP}, V_c^o + V_d^o) \quad (2.25)$$

2.8.6.3 Comparison of Computed Capacities with Test Results

The comparisons of capacities computed using the modified model and test results are presented in Table 2.14. The ratio of model predictions of capacity to observed ultimate loads had a mean of 1.06 with a standard deviation of 0.08. Thus, the model was capable of estimating the ultimate capacity of tested slabs accurately. In addition, the failure modes of all specimens except specimen A4-1 were predicted correctly. This model can capture the failure inside the shear reinforced zone for specimen A4-3 when insufficient amount of CFRP is used. The failure mode of specimen A4-1 was not predicted accurately because the model assumes that detailing of CFRP stirrups is performed correctly, i.e.

diagonal CFRP stirrups exist (Sections 2.8.2 and 2.8.3), and failure takes place based on the load carrying capacities of the two regions. In other words, different anchorage types and associated problems are not modeled.

In order to put the model and results in perspective, $f'_c/\rho f_y$ values are plotted against normalized concrete contribution, V_c^o/V_{c-max} for specimen Control-1, A4 and B4 (Figure 2.64). It is important to note that V_{c-max} used in the vertical axis is the concrete contribution of specimen Control-1. As long as CFRP amount is sufficient, V_c^o can be accepted as the punching shear capacity of specimens A4 and B4. Following observations can be made based on this plot:

i) The model accounts for the effect of flexural reinforcement ratio. Punching shear capacity is limited and further increase of reinforcement ratio does not affect this capacity.

ii) In order to achieve punching shear capacity of a strengthened specimen, sufficient amount of CFRP should be installed in order to ensure that V_c^o can be reached prior to failure inside the shear reinforced zone. Figure 2.64 illustrates that the required CFRP contribution decreases with decreasing flexural reinforcement ratio.

iii) Strength increases that can be obtained using pattern B (up to 2 times the capacity without strengthening as shown in Figure 2.64), are higher than the strength increases that can be obtained with the use of Pattern A (up to 1.75 times the capacity without strengthening as shown in Figure 2.64). This fact is well reflected in the model.

The modified model presented above is simple, yet accurate. It can predict the failure locations and load carrying capacities accurately. It takes into account the failure of the compression zone in a splitting mode, dowel forces, the

geometry including the inclined crack, and the excessive forces carried by CFRP shear reinforcement.

Table 2.14 Comparisons of Model Predictions with Test Results

Specimens	V_{u-exp} (k)	Observed Failure Location	V_{inside} (k)	$V_{outside}$ (k)	V_{u-calc} (k)	V_{u-calc} / V_{u-exp}	Predicted Failure Location
Control-1	110	-	-	95.8	95.8	0.87	-
Control-2	114	-	-	114.4	114.4	1.01	-
A 4-1	133	Inside/Outside	249.4	157.6	157.6	1.18	Outside
A 4-2	149	Outside	172.6	157.6	157.6	1.06	Outside
A 4-3	139	Inside	136.4	157.6	136.4	0.98	Inside
A6	161	Outside	211.0	166.5	166.5	1.03	Outside
A8	166	Outside	211.0	178.4	178.4	1.07	Outside
B4	170	Outside	200.5	180.1	180.1	1.06	Outside
B6	169	Outside	238.9	174.9	174.9	1.03	Outside
B8	175	Outside	232.5	191.6	191.6	1.09	Outside
						mean :	1.06
						stdev :	0.08

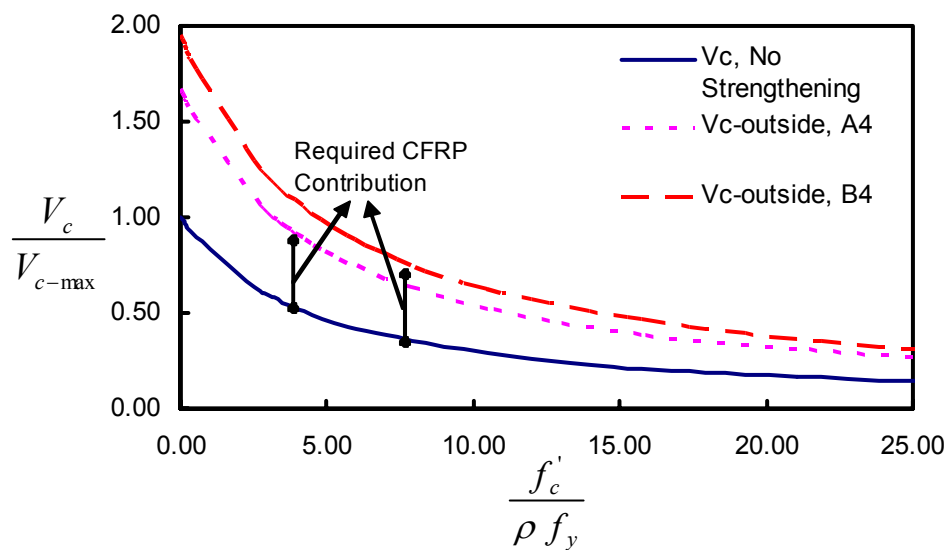


Figure 2.64 Concrete and Required CFRP Contributions

CHAPTER 3

Punching Shear Strengthening of Eccentrically Loaded RC Flat Plates

3.1 GENERAL

The application of the strengthening method developed in Chapter 2 to interior slab-column connections transferring monotonic shear and unbalanced moment are discussed in this chapter. For this purpose, an experimental program was conducted on four half scale reinforced concrete flat plates loaded eccentrically at the center. The objectives of the experimental program were:

- To study the effect of unbalanced moment on punching shear capacity of slab-column connections,
- To study the effectiveness of two different shear reinforcement patterns using CFRPs developed in Chapter 2 for slab-column connections transferring unbalanced moment and shear,
- To examine the effect of support conditions on the punching shear capacity of test specimens simulating RC flat-plate systems.
- To propose design recommendations for the strengthening method for slab-column connections under the action of shear and unbalanced moment based on existing design provisions.

3.2 TEST SPECIMENS

The test specimens in this phase of the experimental program consisted of four slabs, two of which were strengthened with CFRPs. The slab specimens (40"x40"x3") were approximately half scale representatives of the test specimens presented in Chapter 2. The isolated slab-column connection tests that are

discussed in this chapter are believed to simulate the behavior of the interior slab-column connection area of the prototype building shown in Figure 2.1.

In general, unbalanced moments are transferred between slabs and columns in the following cases:

- 1) At interior connections under gravity loads that are different on adjacent spans,
- 2) At interior connections of exterior slab panels,
- 3) At exterior connections,
- 4) At interior and exterior connections when the flat plate system is subjected to gravity forces and laterals loads due to wind or earthquake.

Unbalanced moments can significantly reduce the punching shear capacity of slab-column connections due to increased shear stresses in the slab around the connection region. Therefore, it is necessary to investigate the validity and effectiveness of the strengthening scheme proposed in Chapter 2 for slab-column connections transferring unbalanced moment.

In this phase of the experimental program, longitudinal reinforcement ratios of bottom and top reinforcement were chosen as 1.2% and 0.7% respectively to give an effective depth of 2.25 in. These amounts were obtained from the design of the prototype floor considering the gravity load and the unbalanced moment due to design lateral forces following IBC 2000 requirements and fall in the typical range of values (0.5-1.2%) that are commonly used in existing flat-plate buildings. An unbalanced moment to gravity shear ratio that is equal to approximately the length of column side was found to represent the actual demand on interior slab-column connections for high gravity load cases successfully. Furthermore, the effects of different gravity load patterns on adjacent spans, flat plate and column geometry on unbalanced moment demands in interior slab-column connections are evaluated in detail for the prototype floor

system (Section 3.6). In addition, Elstner and Hognestad (1956) reported that eccentricities smaller than half the column size have negligible effects on the concentric punching shear capacity, whereas eccentricities equal to the column size may significantly reduce the punching shear capacity. Based on these investigations, it was decided to set the eccentricity equal to the column size.

Two of the four specimens had no shear reinforcement, whereas the other two specimens were strengthened with CFRPs using the information obtained from the test results presented in Chapter 2. One of the control specimens (CC), i.e. with no strengthening, was loaded concentrically, and the other control specimen (CE) was loaded with an eccentricity equal to the column size. The other specimens (A4E, and B4E), i.e. the specimens strengthened using CFRPs were loaded with same eccentricity used for specimen CE. Based on the preliminary calculations of shear capacity, it was found that four CFRP perimeters would be enough to shift the failure mode from shear dominated to flexure controlled. Therefore, Patterns A and B with four CFRP perimeters were selected as the strengthening patterns from previous chapter for specimens A4E and B4E. Another important difference between specimen B4E and the other three specimens CC, CE, and A4E was the support conditions. Specimens CC, CE, and A4E were simply supported parallel to the direction of moment transfer and free on the opposite edges. On the other hand specimen B4E was simply supported on four sides. The different boundary conditions for upgraded specimens provided a basis of comparison to evaluate the effect of boundary conditions on punching shear resistance.

Preparation of the specimens and strengthening procedure were similar to those that were discussed in Section 2.4. Due to scaled size of the specimens 1/2-in. PVC pipes were used to provide vertical holes for CFRP wrapping. The pipes were removed after curing and ends of the holes were chamfered to eliminate

sharp corners. CFRP strips, impregnated with epoxy, were wrapped such that closed loops in the form of stirrups were formed within the shear reinforced region. The spacing between these closed CFRP stirrups was kept equal to $d/2$. Bottom CFRP plates were used to seal the holes prior to filling them with epoxy. The specimen details including amount of eccentricity, support conditions, CFRP perimeter and amount are shown in Figure 3.1. Table 3.1 presents the test matrix including the test specimens and variables. The specimen details are illustrated together with the test setup in Figure 3.2.

Material properties of CFRPs were similar to those described in Section 2.3, whereas the average concrete strength at 28 days was found as 3500 psi from uniaxial compression cylinder tests. Steel reinforcement was Grade 60 with yield stress of 66 ksi from uniaxial tension tests.

Table 3.1 Details of Specimens and Test Matrix

TEST MATRIX	Test Specimens			
Test Variables	CC	CE	A4E	B4E
CFRP Pattern	-	-	A	B
Number of CFRP Layers per Hole	-	-	2	2
Eccentricity (in.)	0	6	6	6
Support Conditions	2 Sides SS	2 Sides SS	2 Sides SS	4 Sides SS

SS: Simply Supported

1 layer corresponds to 3/4" wide and 0.04 in. thick CFRP strips.

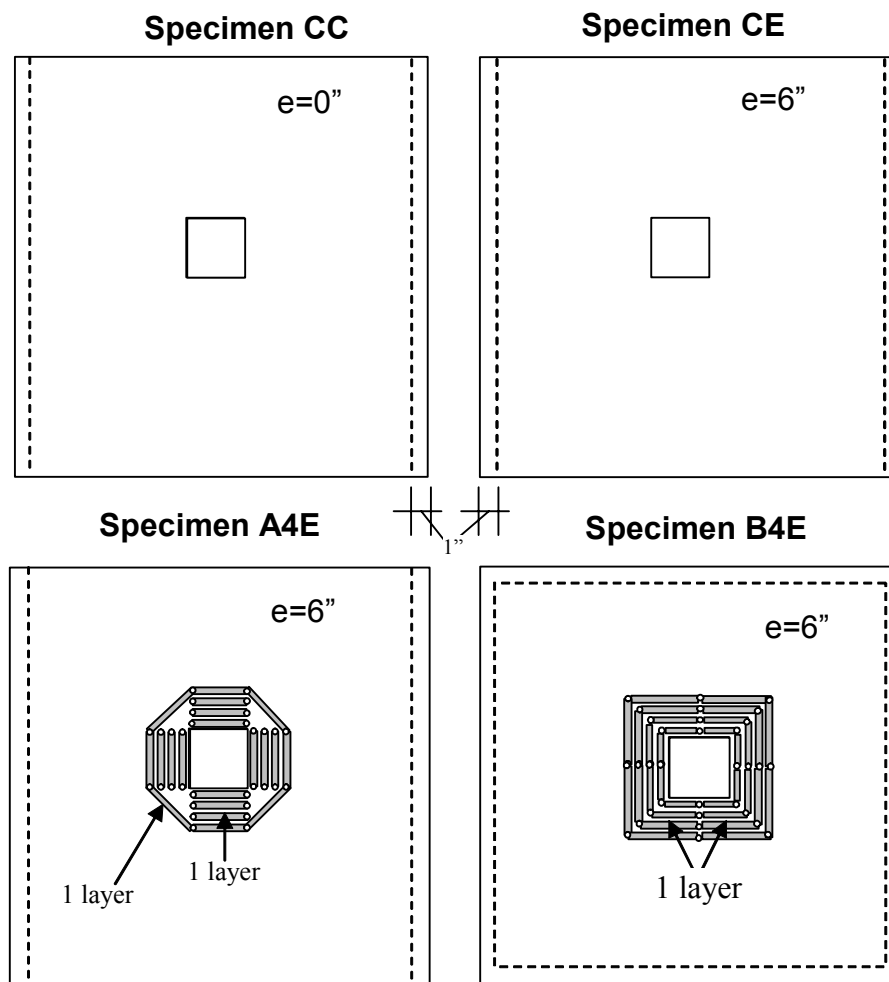


Figure 3.1 Details of Test Specimens (Plan View)

3.3 INSTRUMENTATION AND TESTING

In order to apply shear and unbalanced moment, an eccentrically loaded steel column with an overhang was used (Figure 3.2). The steel column was bolted to the slab through bolt holes which were left during casting. Concrete under the base plate of the steel column was leveled to ensure a smooth horizontal surface. A similar assumption as discussed in Section 2.5 was made; i.e. as long as the failure took place outside the shear reinforced zone or the base plate, the

detailing of the joint region did not affect the capacity of the specimens. The eccentricity was kept constant throughout each test which implies proportional application of unbalanced moment and shear. This simulates proportional increase in gravity load on adjacent spans of the interior slab-column connection in an actual building. However, as discussed in Section 3.2, eccentricity was chosen without paying attention to the loading history and the moment to shear ratio was kept equal to the column size throughout the test. This is believed to represent the unbalanced moment demands on some existing slab-column connections.

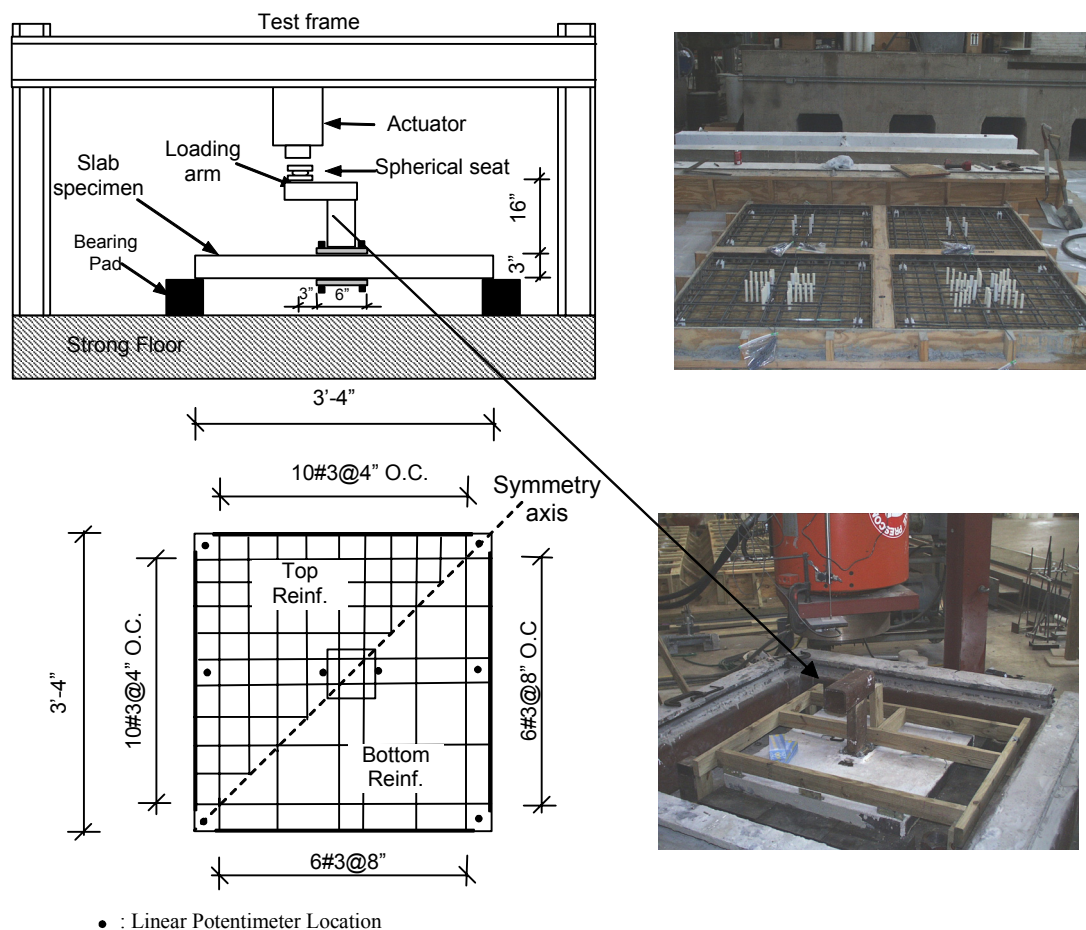


Figure 3.2 Instrumentation, Reinforcement Details, and Test-Setup

Testing of the specimens in this phase of the experimental program was conducted in a similar way to that explained in Section 2.5. Since it was not possible to use the same supports consisting of rollers sandwiched between steel plates due to the smaller size of the specimens, bearing pads were used to simulate the simply supported edges (Figure 3.2). Prior to testing, all the specimens were set on these elastomeric bearing pads. The reaction frame, used in the testing of concentrically loaded specimens, was used for these specimens. A spherical seat was placed between the actuator and the steel overhang to avoid uneven application of the load. Load measurements were taken through the load cell connected to the actuator. Specimens were tested in a displacement controlled mode with an average displacement rate of 0.01 mm/sec. Linear potentiometers (Figure 3.2) were used to measure the displacement of the slab at every displacement increment. Electrical resistance strain gauges attached to reinforcing bars and concrete strain gauges bonded to the compressive surface of the slab were used to monitor the strains. The actual locations of the strain gauges are shown while presenting the individual test results.

3.4 TEST RESULTS

This section presents the results of the experiments on eccentrically loaded flat-plate specimens. Load-deformation characteristics, measured strains in concrete, steel and observed crack patterns are given followed by the discussion of the test results.

3.4.1 Load-Deformation Results

Complete load versus central deflection behavior of the test specimens are shown in Figure 3.3. Center deflections shown on these plots represent center deflections relative to supports. The comparisons of the load deformation response for all of the specimens are shown in Figure 3.4 up to a central

displacement of 1.6 in. Table 3.2 presents a summary of the load carrying capacity and deformation results of the tests. Also, the ratio of load carrying capacity to flexural strength computed based using yield line analyses are given in this table.

Figure 3.5 presents the assumed yield line mechanisms and governing expressions for the flexural capacities. Flexural capacity of Specimen CC was computed based on a yield line pattern under the action of a concentrated load, whereas this capacity was modified for the action of unbalanced moment for specimens CE and A4E. The yield line capacity of Specimen B4 was computed

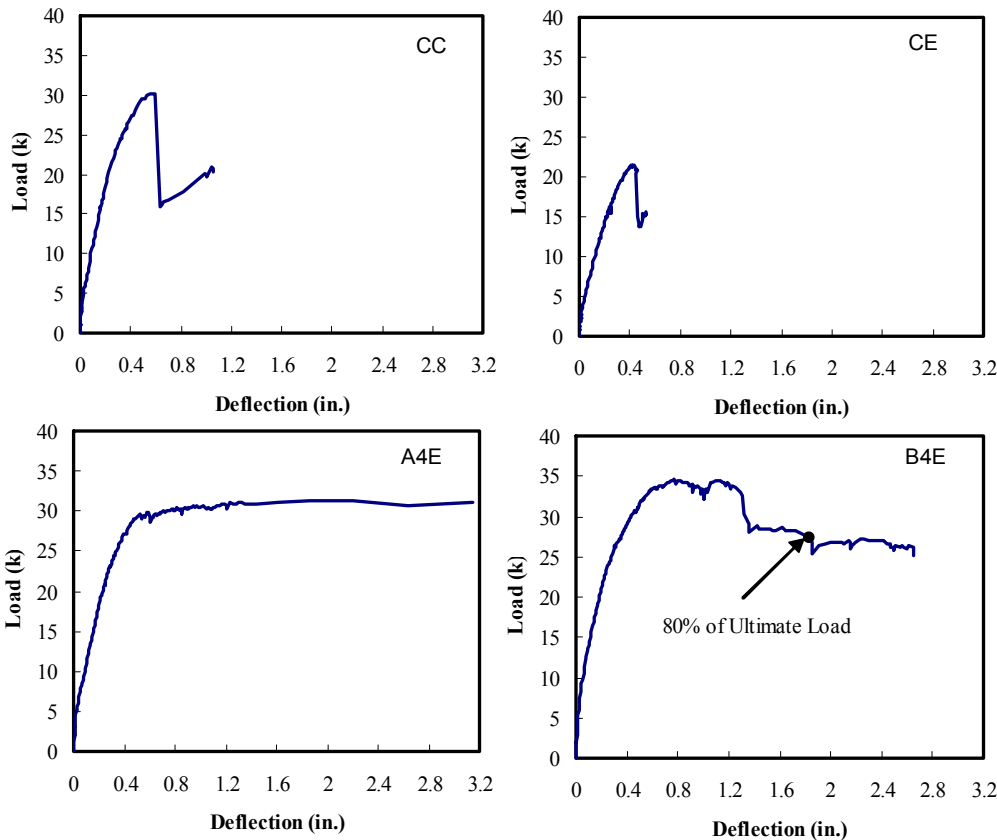


Figure 3.3 Load Deformation Characteristics of Test Specimens

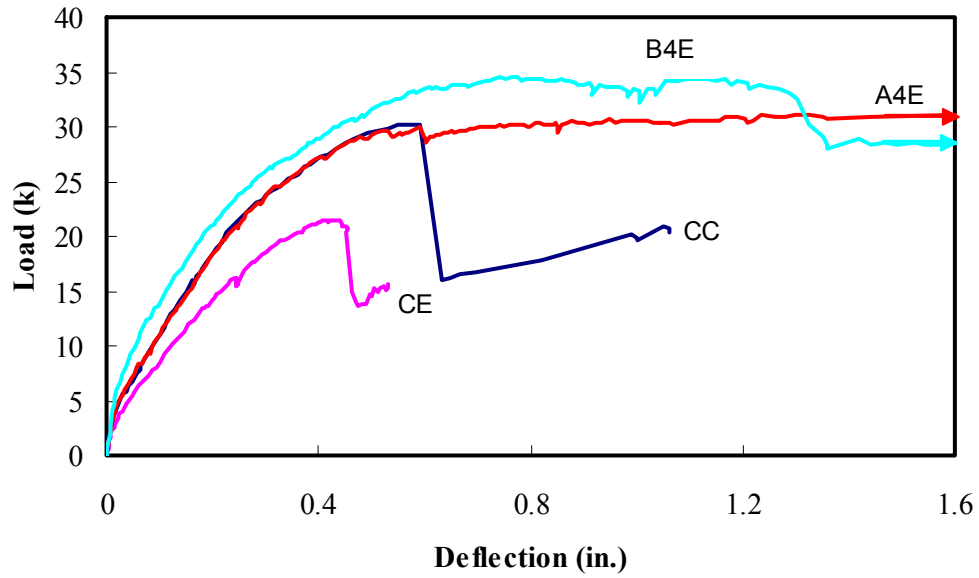


Figure 3.4 Load Deformation Comparisons of Test Specimens

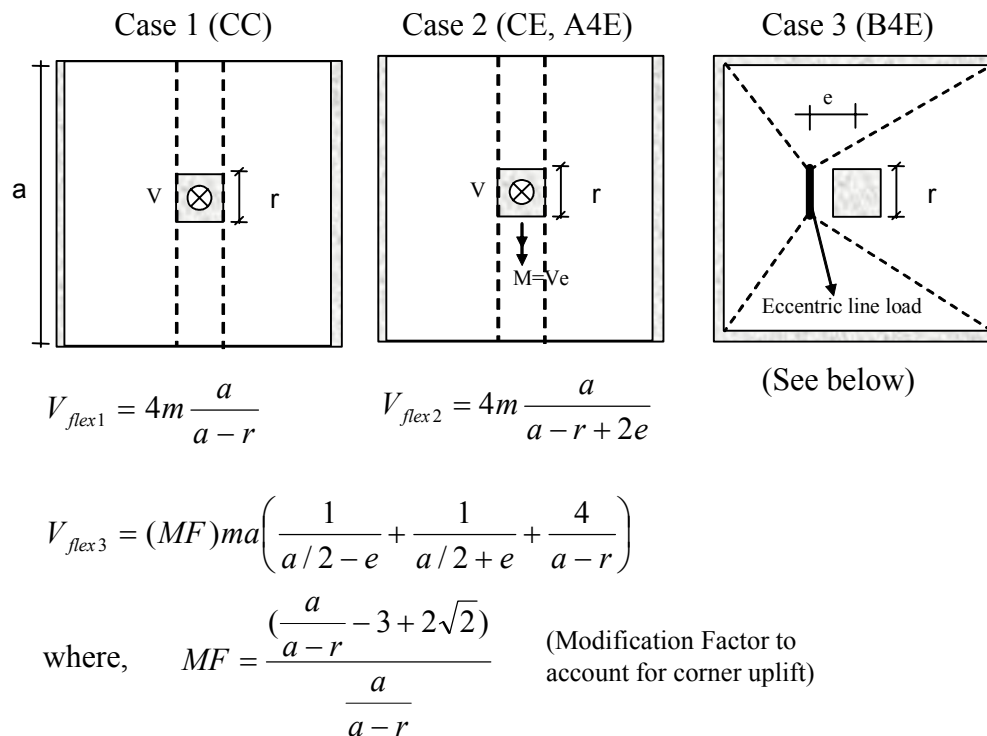
Table 3.2 Summary of Test Results

Specimens	V_{cr} (k)	V_u (k)	M_u (k-in)	Failure Mode	V_{flex} (k)	V_u/V_{flex}	V_u/V_{u-CC}	V_u/V_{u-CE}
CC	3.1	30.2	173.7	Punching	29.9	1.01	1.00	1.40
CE	2.2	21.5	123.6	Punching	23.8	0.90	0.71	1.00
A4E	3.2	31.1	178.8	Flexure	23.8	1.31	1.03	1.45
B4E	4.2	34.6	199.0	Extensive flexural yielding followed by punching	29.7	1.16	1.15	1.61

V_{u-CC} , V_{u-CE} : Load carrying capacity of specimens CC and CE, respectively.

by assuming a line load applied eccentrically on a slab where corners were tied down. This assumed yield line mechanism, shown in Figure 3.5, was modified to account for the uplift by using a modification factor as suggested by Elstner and Hognestad (1956). The value of the modification factor was taken as the ratio of the flexural capacity of the concentrically loaded square slab (with same geometry) considering uplift to the flexural capacity of the concentrically loaded square slab without any uplift. This modification approximately takes into account the effect of corner uplift for the eccentrically loaded slab whose flexural capacity is computed without considering uplift of the corners.

The results presented in Table 3.2 show that although flexural capacity based on yield line analysis was reached for specimen CC, punching failure took



Note: Above expressions were derived by assuming a collapse mechanism as shown above and equating internal and external work.

Figure 3.5 Governing Yield Line Mechanisms

place in a brittle mode. This result agrees well with the previous findings for specimens A8, B4, B6 and B8 (Table 2.6). When combined unbalanced moment and shear act on the slab-column connection (Specimen CE), it was observed that load carrying capacity decreases about 30% compared to the pure shear transfer case. Upon strengthening with patterns A and B with four CFRP perimeters, the load carrying capacity compared to specimen CE increased about 45 and 60%, respectively. More importantly, a ductile failure was observed for specimens A4E and B4E. Punching failure was not observed for specimen A4E whereas punching failure took place at about a central displacement of 1.4 in for specimen B4E. The post punching load carrying capacity for specimen B4E was about 80% of its load carrying capacity and the behavior was stable up to a displacement of about 2.7 in. The load carrying capacity of specimens A4E and B4E were about 30 and 15% more than their computed flexural capacities, respectively. As stated in Section 2.6.2.1 and previously shown in Figure 1.5, Criswell (1974) argued that the required strength to obtain full formation of a flexural mechanism is about 25% more than the computed yield-line mechanism. The observed over strength values for Specimens A4E and B4E are in good agreement with Criswell's conclusions.

3.4.2 Concrete and Steel Strain Measurements

Strain measurements on concrete surface and longitudinal reinforcement versus applied load are presented in Figure 3.6 to 3.9. In addition, the locations of the strain gauges that functioned properly throughout the tests are illustrated with each plot in these figures. Measured concrete compressive strains are plotted on the negative strain axis whereas tensile steel strains are plotted in the positive strain axis. It can be observed that strain increases were almost

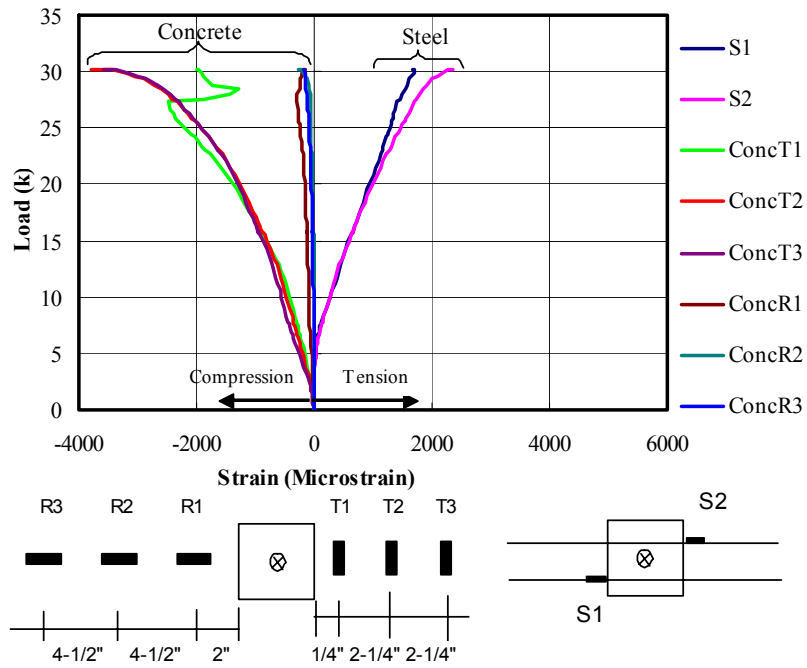


Figure 3.6 Strain Measurements for Specimen CC

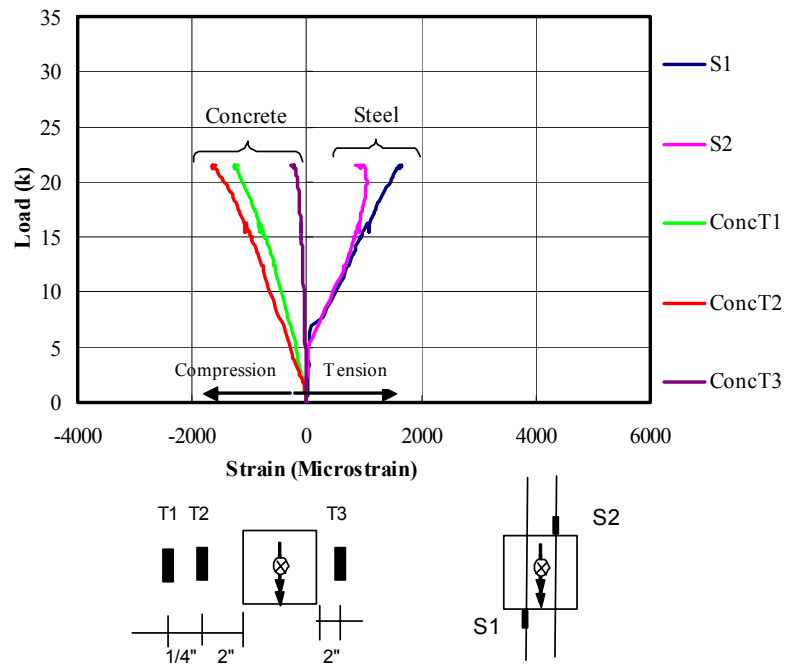


Figure 3.7 Strain Measurements for Specimen CE

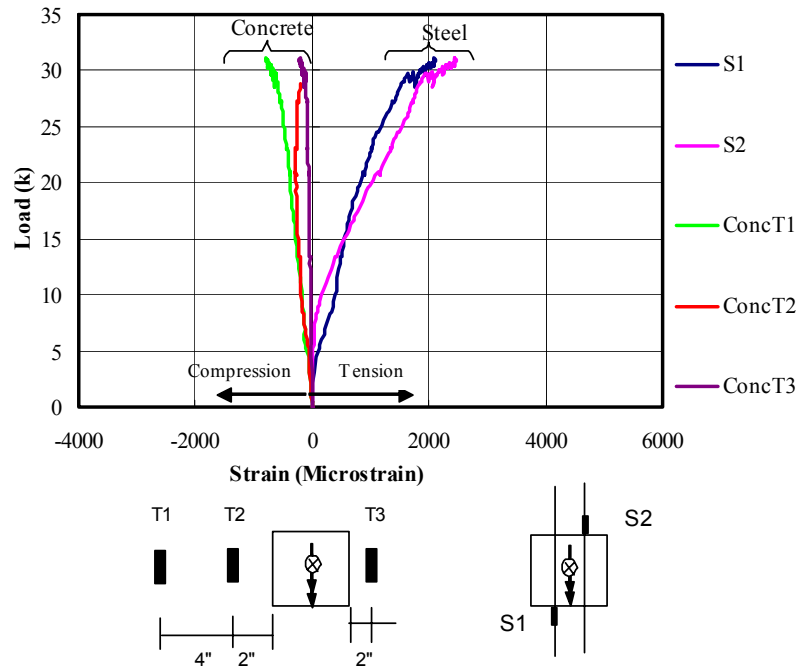


Figure 3.8 Strain Measurements for Specimen A4E

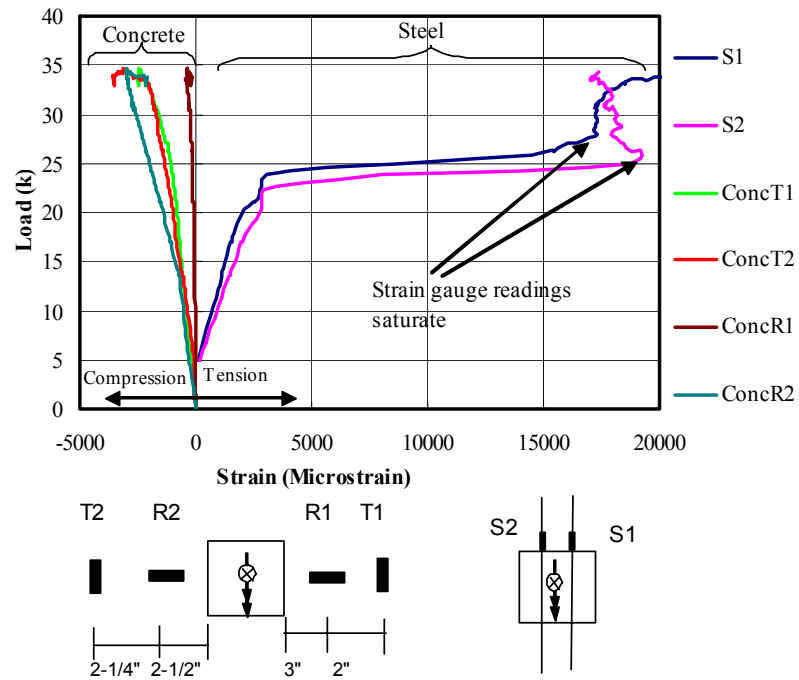


Figure 3.9 Strain Measurements for Specimen B4E

proportional applied load increases, followed by localization of the strains close to the failure loads. Tangential concrete strains were always greater than the radial concrete strains for cases where both strains are measured. This result agrees with the measured concrete strains presented in Section 2.6.2.2. For specimens CE and A4E, concrete radial strain measurements were not available.

Yielding in the longitudinal reinforcement was observed in all of the specimens except specimen CE. The maximum concrete and steel strains in the tangential direction measured at the ultimate load are shown in Table 3.3. The maximum compressive strain reached at the ultimate load for specimen CC was 0.0038, which is very close to the generally accepted ultimate uniaxial compressive strain for concrete. The maximum compressive strain at the ultimate load of specimen Control-2 from the previous phase of the experimental program was about 0.002. This shows that amount of reinforcement is an important factor that influences the maximum tangential strain. In the presence of the unbalanced moment, the maximum compressive tangential concrete strain (Specimen CE) was about 50% of the value observed in specimen CC. The maximum tensile steel strain that is reached in the direction perpendicular to the moment transfer was below yielding for specimen CE. This strain measurement for specimen B4E was well above the yielding value (1.7%). This shows that when proper shear reinforcement in the form of CFRPs was used, for two sides simply-supported specimen, punching failure was eliminated and one-way flexural yield line mechanism was obtained. However, when four sides of a specimen were simply supported, punching failure eventually took place due to the presence of high tangential strains (two-way action).

Table 3.3 Maximum Measured Strains

Specimen	V _u (k)	Maximum Tangential Concrete Compressive Strain	Maximum Steel Tensile Strain
CC	30.2	0.0038	0.0024
CE	21.5	0.0016	0.0017
A4E	31.1	0.0008	0.0025
B4E	34.6	0.0036	0.0173

3.4.3 Crack Patterns and Failure Modes

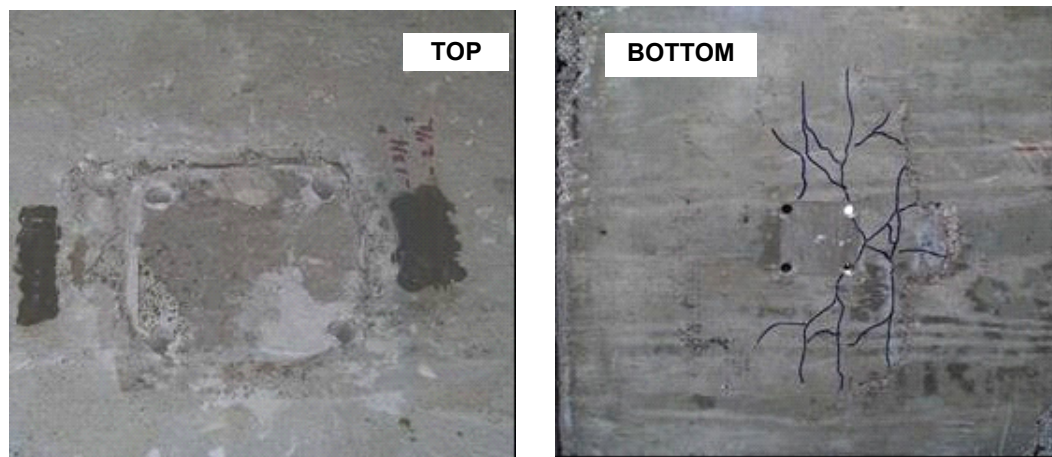
Figure 3.10 and Figure 3.11 show the top and bottom surfaces of specimens after testing. The holes that were used to connect top and bottom steel base plates can be seen in these pictures. Figure 3.10 illustrates that that punching failure occurred locally around the connection area for specimens CC and CE and slab-column connection under the steel base plate remained relatively undamaged. Cracking on the bottom surface was more concentrated on the side where unbalanced moment was acting for specimen CE (marked lines in Figure 3.10). For specimens CC and CE, failure took place in a brittle punching mode when the steel column was pushed into the slab locally around the connection area.

Specimen A4E did not experience punching failure. Significant yielding was observed followed by the initiation of crushing of concrete parallel to the direction of moment transfer between the connection and the free edge (Figure 3.11). Cracking on the bottom of specimen A4E was consistent yield line pattern assumed to compute the flexural capacity (Figure 3.5). The test was terminated when the maximum stroke of the actuator was exhausted. The specimen was subjected to a maximum central displacement of about 3.1 in. and the permanent displacement of the specimen upon unloading was about 2.5 in. There was no

sudden loss of strength in the post-elastic range of the load-deformation response of specimen A4E although very large deformations were imposed (Figure 3.3).



Specimen CC



Specimen CE

Figure 3.10 Top and Bottom Surfaces of Specimens CC and CE after Failure



Crushing of concrete

Specimen A4E

Punching outside of CFRP reinforcement



Crushing of concrete

Specimen B4E

Figure 3.11 Top and Bottom Surfaces of Specimens A4E and B4E after Failure

Specimen B4E experienced punching failure after extensive yielding of flexural reinforcement. Failure initiated with crushing of concrete initiating from the corner of the outermost shear reinforcement perimeter and extending to the corner of the slab specimen (Figure 3.11). Then, punching failure occurred in a brittle manner with a sudden loss of strength (Figure 3.3) outside the shear reinforced zone. The punching crack on the top surface was observed on the side where unbalanced moment was producing additional compressive stresses on the section. Punching shear crack was not observed on the opposite side of the shear reinforced zone. Cracks seen on bottom surface of the specimen (Figure 3.11) agree well with the yield line mechanism extending from the corner of the column to the corner of the specimen.

3.5 DISCUSSION OF TEST RESULTS

3.5.1 Stiffness

Stiffness characteristics of the specimens can be observed in Figure 3.4. According to this figure, there was an elastic range up to first cracking followed by a segment in the loading curve where stiffness was equal to the stiffness of the cracked section. The cracked stiffness of specimen CC was higher than that of specimen CE. This difference can be attributed to the additional demand imposed on the slab-column connection due to the unbalanced moment at the section where cracking initiates. In addition, the cracking load was smaller for specimen CE in comparison to specimen CC (Table 3.2). On the other hand, post cracking stiffness of specimen A4E was similar to that of specimen CC, and higher than the stiffness of specimen CE. The bottom CFRP sheets used on the tension side of A4E (Figure 3.11) were responsible for the increase in the post cracking stiffness.

For serviceability purposes, deflection of one-way members can be computed using an effective stiffness approach. ACI 318-02 recommends using

an effective moment of inertia based on the research reported by Branson (1965), which is shown in Equation (3.1).

$$I_e = \left(\frac{M_{cr}}{M_a} \right)^3 I_g + \left[1 - \left(\frac{M_{cr}}{M_a} \right)^3 \right] I_{cr} \quad (3.1)$$

where I_e is the effective stiffness, M_{cr} is the cracking moment, M_a is the maximum moment at the stage where deflection is computed, I_g is the gross moment of inertia, and I_{cr} is the cracked moment of inertia of the section.

Two way-slabs can be modeled as planar frames using the effective beam width method. The effective beam width factors, α , is obtained by applying a unit moment on the slab-column connection of the idealized two-way plate system and on the equivalent beam (Figure 3.12). Then the equivalent beam width is adjusted such that same joint rotations are achieved for the two systems. Analytical solutions or linear finite element analysis results based on classical plate theory are used to obtain the effective beam factors (Pecknold 1975, Allen and Darvall 1977). The effective beam factors based on this procedure do not include the cracking of the RC slabs; hence they require further modifications to incorporate cracking. Pan and Moehle (1988) suggested using $\left(\frac{1}{3}\right)\alpha$ to account for cracking of the slab in the analysis. It is also possible to estimate the effective stiffness with of the slab system by combining the effective beam width factor with an effective stiffness (Luo and Durrani 1995). This leads to using a stiffness of EaI_e for the equivalent beam with the same span.

For specimens CE and A4E, the procedure outlined above was performed to estimate the stiffness and deflections of the slabs at various loading stages. Effective beam width factor for the slab geometry of the test specimens simply

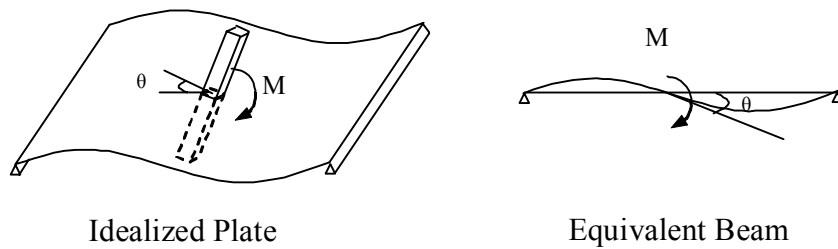


Figure 3.12 Equivalent Beam Idealization

supported on both opposite sides was obtained using the results of Pecknold's elastic solution and simpler expressions recommended by Luo and Durrani (1995), where the joint region is assumed to be rigid. For specimens CE and A4E, an effective beam width factor of 0.75 was obtained, and this factor was verified using a linear elastic finite element analysis with plate bending elements. The deflections of the slab were then estimated by performing a linear elastic analysis for the equivalent beam with the effective stiffness given in Equation (3.1). The results of predictions up to a displacement of 0.3 in. and the experimental results of specimens CE and A4E are compared in Figure 3.13. The only difference between the two analyses was the incorporation of the CFRP bottom sheets in the calculation of cracking moment, M_{cr} , and cracked moment of inertia, I_{cr} for specimen A4E. Figure 3.13 illustrates that elastic analysis of the equivalent beam with an effective stiffness gave reasonable estimations of deflections up to about $\frac{3}{4}$ of the load carrying capacities of the specimens. Beyond a deflection of about 0.2 in. the stiffness of the slabs were significantly overestimated. However the method is reliable in estimating the deformations in the serviceability range. The effective stiffnesses, $(\frac{1}{3})\alpha EI$, proposed by Pan and Moehle (1988) are also given in Figure 3.13. It can be seen that this "secant approach" underestimated the stiffness of the test specimens at small displacements and overestimated it for

large displacements. However, it provided a reasonable estimate of stiffness with a simpler approach.

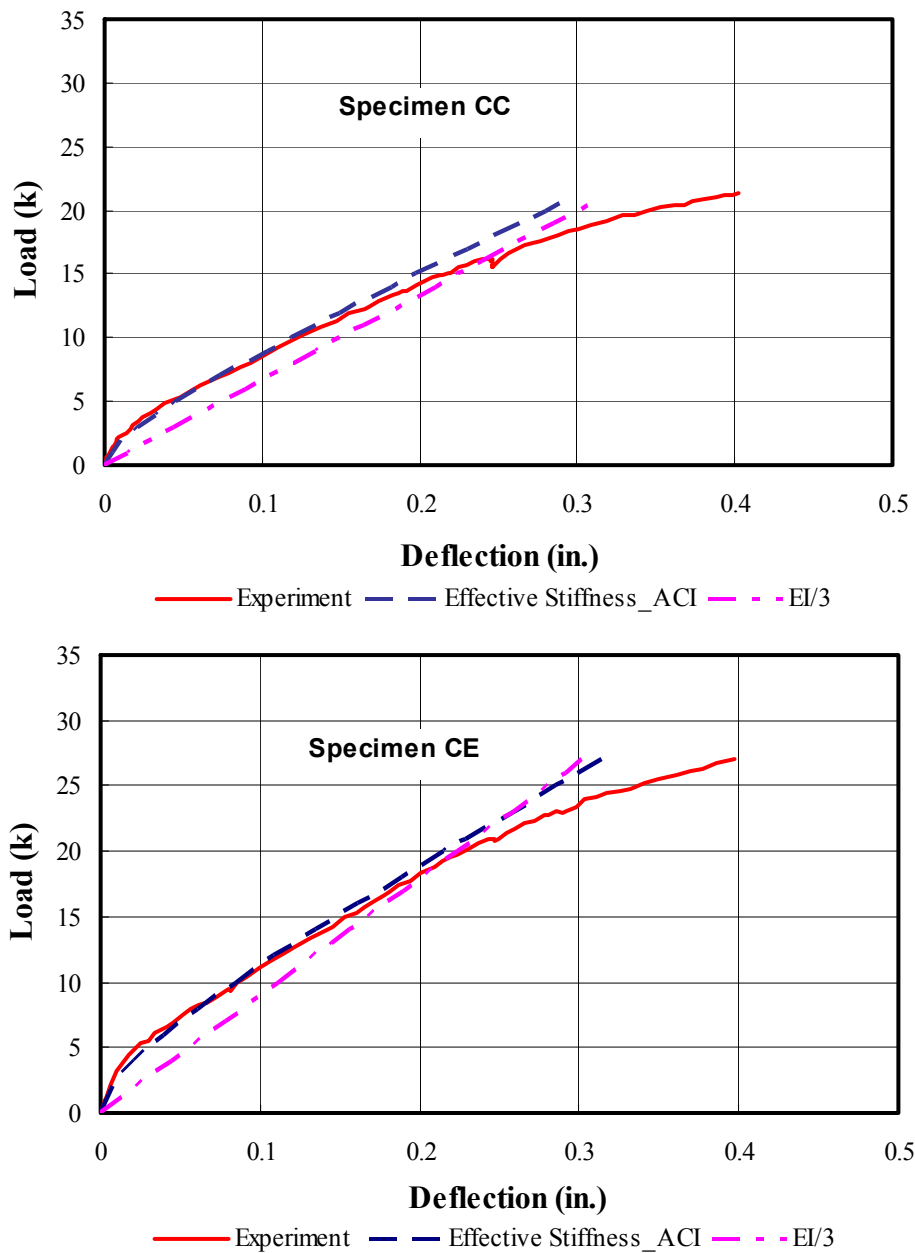


Figure 3.13 Stiffness Estimations of Specimens CC and CE

The selection of the stiffness values for the planar frame analysis of two-way slab systems is very crucial, especially for lateral load analysis. The predicted deformations are very sensitive to the selection of the stiffness values for the equivalent beam. ACI expression given in Equation (3.1), which is recommended for use in deflection estimations of one-way members, together with the use of equivalent beam method provides reasonable estimations for slab deformations.

3.5.2 Strength and Ductility

The capacities of specimens CC and CE were dictated by their shear strength. The load carrying capacities of strengthened specimens A4E and B4E were governed by the flexural capacities of the slabs. Flexural capacities of specimens were presented in Section 3.4.1. Punching shear capacities of these specimens can be calculated using the eccentric shear stress model recommended in ACI 318 Standard for design of slab column connections under the action of shear and unbalanced moment. The effect of CFRP stirrups acting as vertical shear reinforcement on the shear capacity of the slab column connections can be considered by replacing the v_s term with v_{FRP} term in Equation (1.15) as follows:

$$v_n = v_c + v_{FRP} = 2\sqrt{f'_c} + \frac{A_{FRP}\epsilon_{FRP_e}E_{FRP}}{b s} \quad (3.2)$$

where A_{FRP} is the area of FRP per perimeter, E_{FRP} is the Elastic Modulus of FRP used, s is the spacing of external CFRP stirrups, b is the critical perimeter located $d/2$ from the face of the column (Figure 1.14), and ϵ_{FRP_e} is the maximum permissible strain in FRP, which can be taken as 0.004 (Section 2.8.2). Then the load carrying capacity of the test specimens can be computed by:

$$v_n = v_c + v_{FRP} = \frac{V_u}{b d} + \frac{\gamma_v M_u}{(J/c)} \quad (3.3)$$

where V_u and M_u are the shear force and unbalanced moment acting on the slab-column connection, respectively, b is the critical perimeter located $d/2$ from column face, c is the column size perpendicular to moment transfer, J is analogous to the polar moment of inertia (Equation (1.19)), and γ_v is shear transfer coefficient which is equal to 0.4 for square columns. Setting M_u equal to $(V_u e)$ in Equation (3.3) and rearranging the terms yields the shear capacity of the strengthened specimens as follows:

$$V_u = \frac{(v_c + v_{FRP})}{\left(\frac{1}{b_o d} + \frac{\gamma_v e}{J/c}\right)} \quad (3.4)$$

Shear capacities computed using Equations (3.2) and (3.4), flexural capacities calculated using yield line analyses, experimental ultimate loads and failure modes are presented in Figure 3.14. It can be observed that shear and flexural capacity estimations were on the conservative side. For specimens where computed shear capacity was smaller than the flexural capacity, (specimens CC, and CE) punching failure was observed in the experiments. On the other hand, when the computed flexural capacity based on yield line analysis was greater than the shear capacity failure mode was ductile and formation of a flexural collapse mechanism was observed (specimens A4E, B4E). Hence, it is possible to predict the failure mode of the test specimens using the eccentric shear stress model and yield line analysis and selecting the smaller one as the governing failure mode.

Although extensive yielding was observed in specimen B4E, punching failure took place eventually. However, specimen A4E did not experience punching shear failure and the failure mode was flexure. Test results presented in Section 2.7.1 could imply that performance of B4E would be better than that specimen A4E. However, there was an important difference between specimens

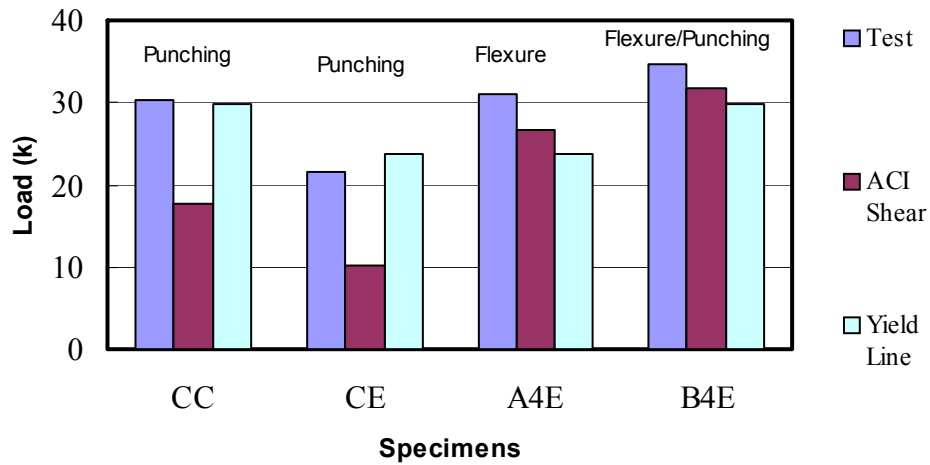


Figure 3.14 Strength Comparisons of Specimens

A4E and B4E that was the support conditions. When only two sides parallel to the moment transfer were simply supported, (specimen A4E) due to small tangential strains on the compressive surface of the slab, (Figure 3.8) one-way flexural failure mode was achieved with the proper placement of CFRP strips and punching shear failure was eliminated. On the other hand, when four sides were simply supported existence of high tangential strains confirmed the presence of two-way action, and punching shear failure eventually took place. The support conditions of the isolated slab specimens were the determining factor for the final failure mode, even though extensive yielding prior to punching took place. In an actual slab-column connection of a flat plate building, due to the existence of the restraint provided by the slab in two directions (Criswell and Hawkins 1974), two way action is likely to be present around the connection area for gravity loading cases; hence this makes the support conditions of specimen B4E more realistic. However, when the main cause of unbalanced moment is lateral loads it is believed that support conditions of specimen A4E are more realistic. These two

cases are considered to be the two limiting cases that can be observed in actual slab-column connections of flat plate buildings.

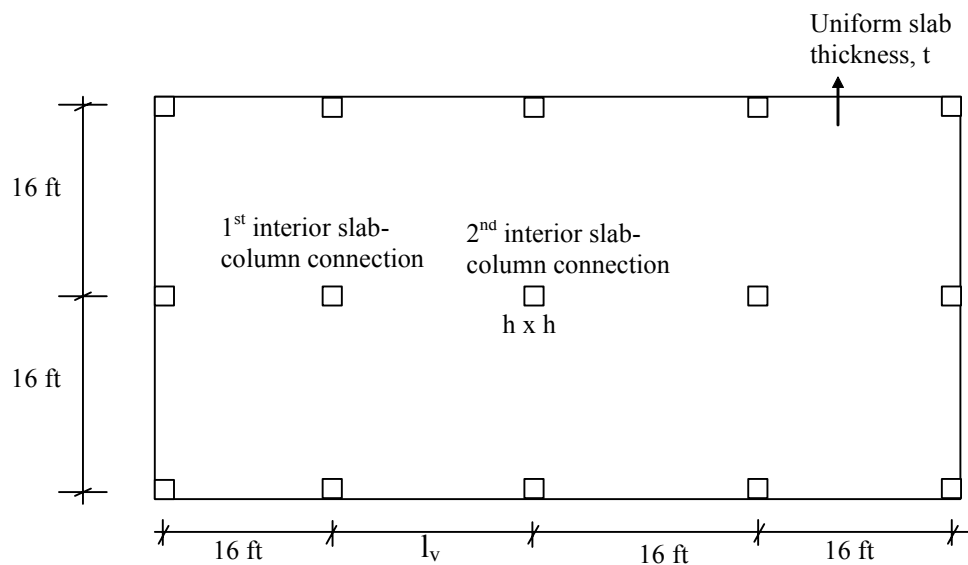
The selection of number of CFRP perimeters for strengthening of slab-column connections under the action of shear and unbalanced moment is not studied in this phase of the experimental program. However, this was investigated in depth in Chapter 2. The design of externally installed CFRP stirrups including the selection of number of shear reinforcement perimeters and calculation of required CFRP cross sectional area is discussed in Chapter 5.

3.6 UNBALANCED MOMENT DEMANDS AT INTERIOR SLAB-COLUMN CONNECTIONS DUE TO GRAVITY LOADS

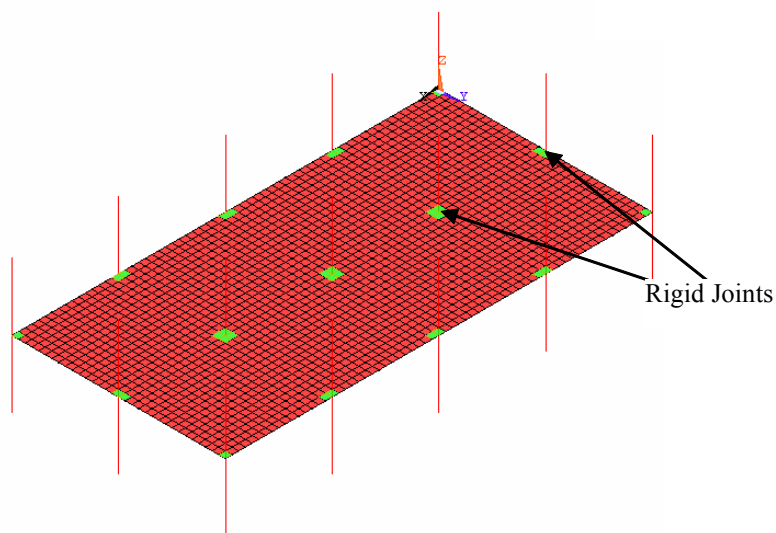
Unbalanced moments can be observed in exterior and/or interior slab-column connections of flat plate buildings due to gravity loads when two adjacent spans are loaded with unequal gravity loads. In addition, different span lengths or column spacing in flat plate structures may result in unbalanced moment transfer at the slab-column connections. In order to quantify the amount of unbalanced moment demands at slab-column connections of existing flat plate buildings, a parametric study was conducted. In this framework, linear elastic finite element analyses were employed to identify the range of unbalanced moment demands.

The floor plan of the prototype building under consideration is shown in Figure 3.15. This building is similar to the prototype floor previously considered (Figure 2.1). Finite element analysis program ANSYS was used for the parametric study. Figure 3.15 illustrates a typical mesh used in the analyses. four-noded shell elements were used to model the slab whereas 3-dimensional beam elements were utilized for the columns. Modulus of elasticity and Poisson's ratio for concrete were taken as 3600 ksi and 0.2, respectively for all the analyses. Slab-column joints were modeled to be rigid by using an increased stiffness

$((E_c)_{joint} = 5(E_c)_{slab})$. The ends of columns were fixed at one story above and below of the floor under consideration. Pattern loading was considered in the



a) Floor Plan of Flat Plate Building Floor



b) Finite Element Mesh

Figure 3.15 Building Floor Plan and Finite Element Mesh

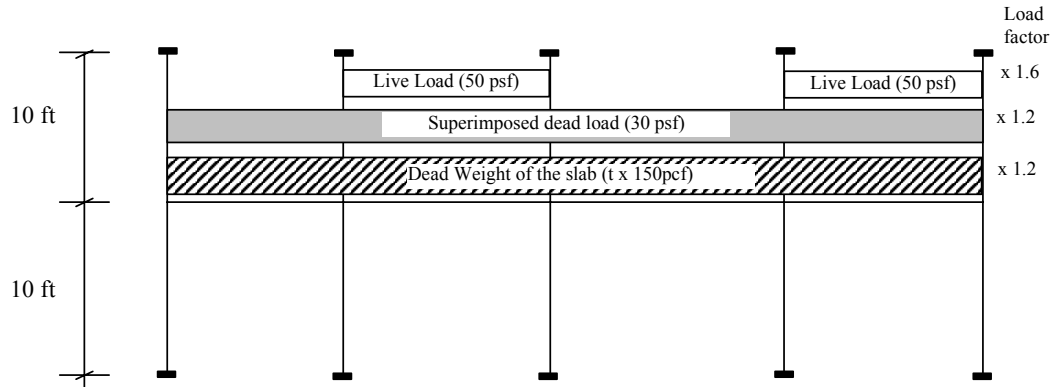


Figure 3.16 Gravity Loading Pattern Used in the Parametric Study

analyses in order to maximize the unbalanced moments in the interior slab-column connections. Loads were selected from ASCE-7-98 (Minimum Design Loads for Buildings and Other Structures) for an office building and the gravity load combination ($1.2D + 1.6L$) from the same document was used in order to obtain factored loads. The details of the pattern loading and applied loads are shown in Figure 3.16.

A parametric study was performed for the building floor using the gravity loading pattern given in Figure 3.16 to estimate the unbalanced moment demands in the interior slab-column connections. The span length measured from column centerline to column centerline was taken to be constant (16 ft) except the variable span length, l_v , for which two span lengths 16 ft and 12 ft are considered. Slab thickness, t , and square column dimensions, $h \times h$, were the other variables

Table 3.4 Details of the Parametric Study

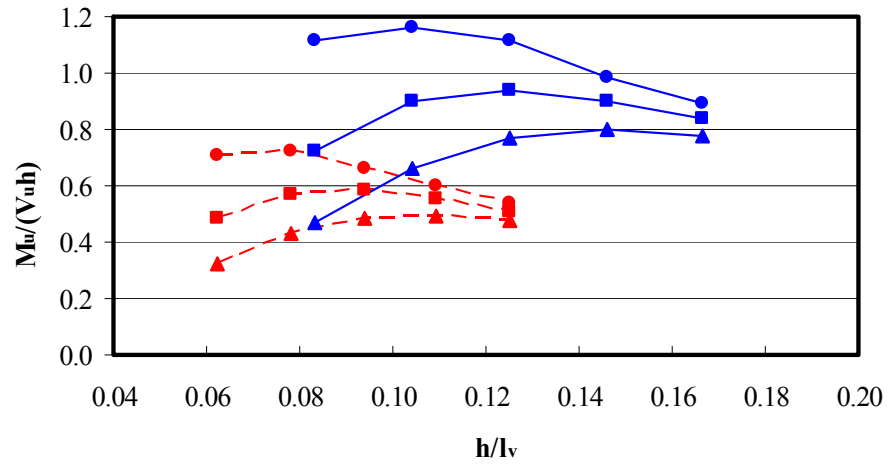
Parameter	Value
Variable Span Length, l_v [ft]	16, 12
Column Dimensions, $h \times h$ [in. x in.]	12x12, 15x15, 18x18, 21x21, 24x24
Slab Thickness, t [in.]	6, 8, 10

parameters in this study. All columns in the flat-plate structure were assumed to have similar cross-sectional dimensions and the story height was taken as 10 ft in all the analyses. The summary of the parameters and their values are shown in Table 3.4.

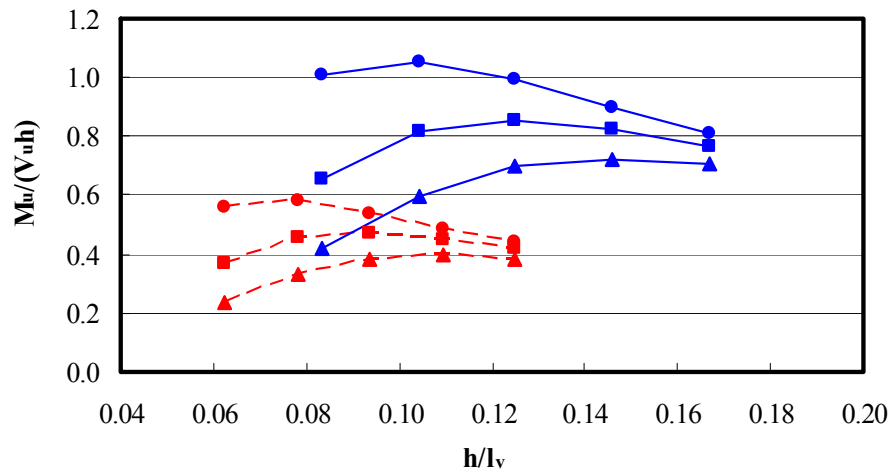
The unbalanced moments in the interior slab-column connections were the values of interest. Two measures were considered to present the results of the analysis. First one is the measure of eccentricity, which is the ratio of unbalanced moment to shear. This eccentricity value was normalized by dividing it with the column dimension, h (i.e. non-dimensional eccentricity = $M_u/(V_u h)$). M_u and V_u were the unbalanced moment and shear force at the slab-column connection due to factored gravity loading pattern as shown in Figure 3.16. Figure 3.17 presents the results of analyses. It can be observed that the presence of a variable span length significantly increased the non-dimensional eccentricity measure at the slab-column connections. In addition, the non-dimensional eccentricities were higher for the flat-plate system with smaller slab thicknesses. A comparison of Figure 3.17.a and 3.17.b reveals that first interior connections were subjected to higher unbalanced moment demands (~10 to 40% higher) compared to second interior slab-column connections.

Second measure for the unbalanced moment demand can be expressed as the ratio shear stress at the critical section due to unbalanced moment to the shear stress at the same section due to gravity shear. Summation of these shear stresses is equal to the effective shear stress at the critical section (Section 1.4.3.1). Shear stress due to gravity shear, τ_V , and shear stress induced by unbalanced moment, τ_M , can be calculated as follows:

$$\tau_V = \frac{V_u}{b_o d} \quad (3.5)$$



a) First Interior Column



b) Second Interior Column

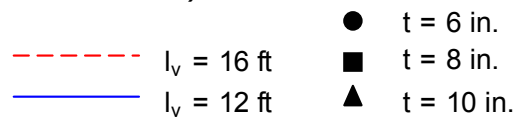


Figure 3.17 Unbalanced Moment Demands in Interior Slab-Column Connections Using Measure of Eccentricity

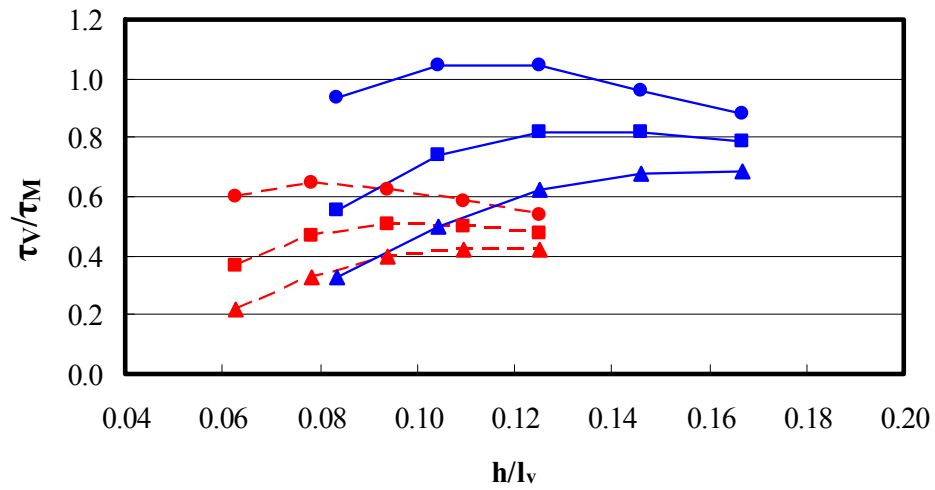
$$\tau_M = \frac{\gamma_v M_u}{(J/c)} \quad (3.6)$$

$$v = \tau_V + \tau_M = \frac{V_u}{b_o d} + \frac{\gamma_v M_u}{(J/c)} \quad (3.7)$$

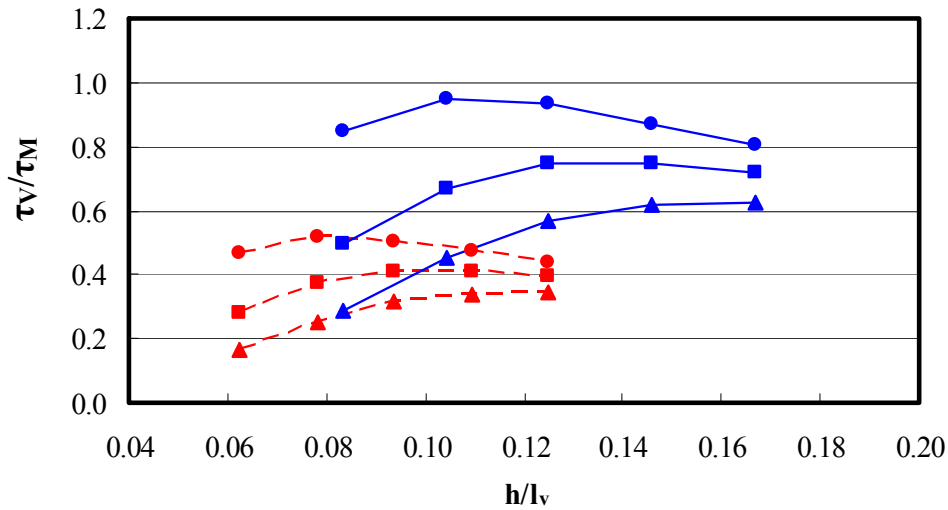
Effects of variable span length, slab thickness, and column size on ratio can be observed in Figure 3.18.

Following observations can be made based on the results of the parametric studies conducted:

- 1- First interior slab-column connections were subjected to higher unbalanced moments in comparison to other interior slab-column connections. The unbalanced moment in first interior slab-column connections could be 40% higher than that of other interior slab-column connections.
- 2- Unbalanced moments were significantly higher in floor systems with unequal adjacent spans. When the length of the first interior span was 12' and all other spans were 16', the unbalanced moment demands were as much as two times greater than a case where all span lengths were equal to 16'.
- 3- The eccentricity, M_u/V_u , varied between 0.3h and 1.2h for the first interior slab-column connection. On the other hand, for the second interior slab-column connection, the eccentricities were lower and ranged between 0.2h to 1.0h depending on l_v and slab thickness.
- 4- Decrease in slab thickness resulted in higher $M_u/(V_u h)$ values for floors with similar spans and column sizes.
- 5- An increase in column dimensions resulted in increases in unbalanced moments up to a certain critical h/l_v ratio. After this critical h/l_w ratio, the



a) First Interior Column



b) Second Interior Column

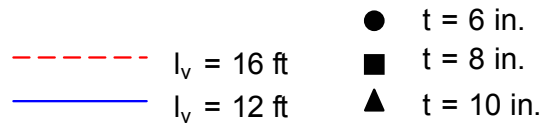


Figure 3.18 Unbalanced Moment Demands in Interior Slab-Column Connections Using Measure of Shear Stresses

unbalanced moments declined at varying rates depending on the slab thickness.

- 6- Shear stresses due to unbalanced moments were as high as those caused by gravity shear. Unequal adjacent spans and pattern loading could result in significant unbalanced moment demands. τ_V/τ_M ratios of slab-column connections ranged between 0.2 to 1.1 depending on the slab thickness, column size and span length.

The results presented above show that flat plate geometry, column dimensions are the important parameters affecting the magnitude of the unbalanced moments. In addition, the parametric study shows that the eccentricity used in the experimental program presented in the previous sections ($M/V = 1.0$ h) is well within the realistic range and closer to the high demand side. Another important deduction is; even in the absence of lateral loads, it is possible to have significant shear stresses due to unbalanced moments (imposed by gravity loads) as high as those caused by gravity shear forces at interior slab-column connections. Therefore, it is necessary to consider the unbalanced moment demands in slab-column connection upgrades of flat plate systems under gravity loads. Gardner et. al. (2002) reported that a design problem, neglecting the unbalanced moments due to pattern loading and unequal spans, had a significant role in the Sampoong Department Store collapse. Hence, for some of the existing flat plate buildings where there is no shear reinforcement around the slab-column connection, effects of unbalanced moments should be calculated carefully during the evaluation and structural upgrade.

3.7 SEISMIC UPGRADE OF SLAB-COLUMN CONNECTIONS

Experimental research and the parametric studies presented in this chapter focused on interior slab-column connections subjected to monotonically

increasing unbalanced moments and gravity shear forces (i.e. constant eccentricity). In the presence of lateral loads due to earthquakes, there are two deviations from this representation. First one is due to the dynamic reversed cyclic nature of the earthquake induced deformations. Such loading impose unbalanced moment reversals at slab-column connections. The accumulated damage at the slab-column connection due to unbalanced moment reversals may be different than those observed in the test specimens presented in Section 3.4.3. Second deviation is due to the loading history during an earthquake. The slab-column connection which is under constant gravity shear is subjected to increasing moment reversals meaning an increase in the imposed eccentricities up to yielding strength of the slab-column connection and subsequent redistribution of forces.

These deviations show that there are considerable differences between slab-column connections subjected to earthquake imposed deformations and the test specimens presented in this chapter. For the strengthening scheme developed during the course of this research to be applied successfully in seismic rehabilitation, physical testing of realistically simulated slab-column connections subjected to unbalanced moment reversals is needed. The influence on gravity shear level on the efficiency of proposed upgrade scheme in seismic applications needs to be evaluated. This part of the experimental program was conducted at the University of Texas at Austin, Ferguson Structural Engineering Laboratory and the details of the experimental program and the results were reported separately (Stark, 2003). Next chapter of this research is devoted to punching shear failure simulations of slab-column connections using nonlinear finite element analyses to focus on the failure mechanisms.

CHAPTER 4

Finite Element Analyses of Concentrically Loaded Flat Plates

4.1 GENERAL

Experimental research on punching shear strengthening of slab-column connections is presented in Chapters 2 and 3. In order to have a better understanding of the slab-column connection behavior, especially the local stress and strain conditions around the loading area resulting in punching shear failure, finite element analyses of the slab-column connections were performed. The models used in the analyses employed simplified treatment of complex concrete behavior under multiaxial state of stress conditions and accurate modeling of geometry and loading conditions. The results of nonlinear finite element analyses performed using the built in features of a commercial software package are summarized in this chapter. Instead, analyses were conducted to achieve the following objectives:

- To develop a nonlinear finite element model that can predict punching shear failure of slab-column connections subjected to concentric shear forces at a reasonable accuracy level.
- To investigate the local stress and strain conditions resulting in punching shear failures around slab-column connections.
- To study the effect of different parameters such as reinforcement ratio, concrete tensile and compressive strength on the overall behavior of the slab-column connections.

- To simulate numerically the effectiveness of the proposed strengthening method in increasing the punching shear capacity of existing interior slab-column connections and investigate the failure mechanism of the upgraded slab-column connections.

4.2 DESCRIPTION OF THE FINITE ELEMENT MODEL

The most appropriate way to simulate the behavior of slab-column connections is to use three dimensional finite element analyses in order to simulate the local triaxial stress conditions and effect of longitudinal and shear reinforcement. The finite element analysis program, ANSYS (1998) was used in this research to simulate the behavior of reinforced concrete slabs patch loaded concentrically at the center.

ANSYS has a dedicated three dimensional finite element, Solid65 for concrete analysis. The element is capable of cracking, crushing, and undergoing plastic deformations. Reinforcement can be defined either as smeared in the element or discretely using three dimensional truss elements (Link8). The eight noded-isoparametric brick element, Solid65, employs linear interpolation functions for the geometry and displacements with eight integration points as shown in Figure 4.1. For all analyses presented here, Solid65 brick elements were used to model concrete behavior, whereas Link8 elements were used to model both longitudinal steel reinforcement and CFRP shear reinforcement discretely. Discrete modeling of the reinforcement was preferred over smeared modeling in order to model the locations of the reinforcement and areas of stress concentrations more accurately.

4.2.1 Concrete Constitutive Model

Solid65 concrete brick element utilizes the Willam-Warnke (1975) failure criterion for concrete where the failure surface for a multiaxial stress-state can be expressed in the following form:

$$\frac{F}{f_c'} - S \geq 0 \quad (4.1)$$

where F is a function of the principal stress state, S is the failure surface expressed in terms of principal stresses and five input parameters and f_c' is the uniaxial compressive strength of concrete. A total of five input stress parameters are required to define the failure surface in function S , which are uniaxial tensile strength, uniaxial compressive strength, biaxial compressive strength, strength from triaxial compression test, and strength from triaxial extension test. The failure surface is as shown in Figure 4.2 in the principal stress space. It can be observed that the failure surface has curved meridians (parabola in this case) and presents symmetry on the deviatoric plane.

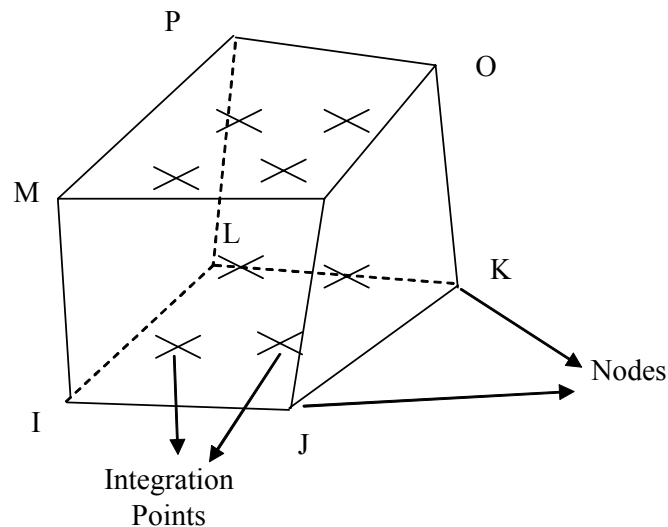


Figure 4.1 Reinforced Concrete Solid65 Element

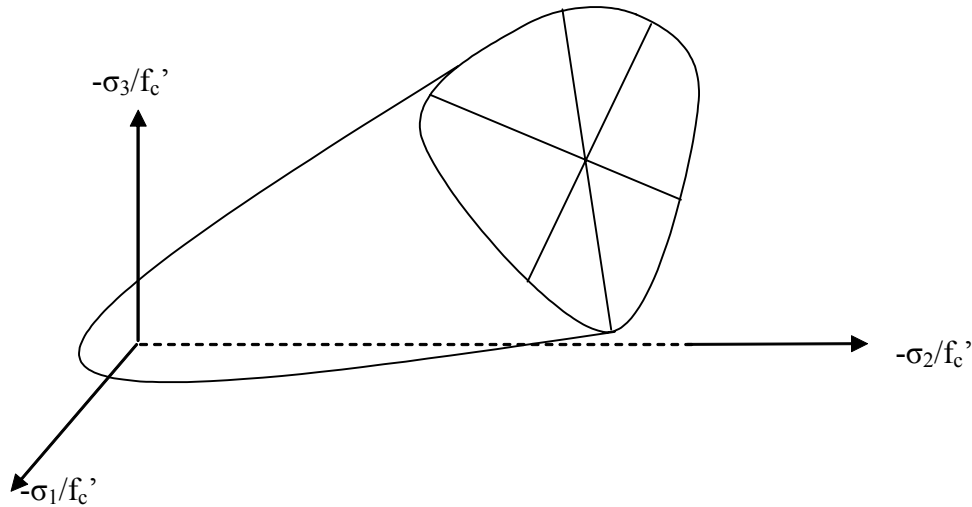


Figure 4.2 3-D Willam-Warnke Failure Surface in Principal Stress Space

The basic assumptions of the material model are as follows:

1. Concrete is initially assumed to be isotropic.
2. Cracking is permitted in three orthogonal directions at each integration point.
3. If cracking occurs at an integration point, it is modeled through an adjustment of the material properties, which treats cracking as a smeared band of cracks rather than discrete cracks.
4. In addition to cracking, concrete may undergo plastic deformations, which can be defined by combining the concrete material model with either a built-in or a user defined plasticity law.

The isotropic stress-strain relationship for concrete in the elastic range is given by:

$$[D] = \frac{E}{(1+\nu)(1-2\nu)} \begin{bmatrix} (1-\nu) & \nu & \nu & 0 & 0 & 0 \\ \nu & (1-\nu) & \nu & 0 & 0 & 0 \\ \nu & \nu & (1-\nu) & 0 & 0 & 0 \\ 0 & 0 & 0 & \frac{(1-2\nu)}{2} & 0 & 0 \\ 0 & 0 & 0 & 0 & \frac{(1-2\nu)}{2} & 0 \\ 0 & 0 & 0 & 0 & 0 & \frac{(1-2\nu)}{2} \end{bmatrix} \quad (4.2)$$

where E is the Modulus of Elasticity and ν is the Poisson's ratio for concrete. The presence of cracking modifies the stress-strain relations of the material model by introducing a plane of weakness in the direction normal to the crack plane, and a shear transfer coefficient β_t , which represents a shear strength reduction factor for those subsequent loads which induce sliding shear along the cracks. Therefore the stress strain relationship for concrete that has cracked in one direction becomes:

$$[D^{ck}] = \frac{E}{(1+\nu)} \begin{bmatrix} \frac{R_t(1+\nu)}{E} & 0 & 0 & 0 & 0 & 0 \\ 0 & \frac{1}{(1-\nu)} & 0 & 0 & 0 & 0 \\ 0 & 0 & \frac{1}{(1-\nu)} & 0 & 0 & 0 \\ 0 & 0 & 0 & \frac{\beta_t}{2} & 0 & 0 \\ 0 & 0 & 0 & 0 & \frac{1}{2} & 0 \\ 0 & 0 & 0 & 0 & 0 & \frac{\beta_t}{2} \end{bmatrix} \quad (4.3)$$

where the superscript ck signifies that the stress strain relationship refers to a coordinate system parallel to the principal stress directions with x^{ck} being perpendicular to the crack direction. As can be observed from Equation (4.3), the material stress-strain relationship is modified by R_t in the direction perpendicular

to cracking, and by β_t for the shear terms. R_t works with adaptive descent and defines the secant slope in the uniaxial tensile stress-strain relationship for concrete as shown in Figure 4.3. In this figure f_t is the uniaxial tensile strength of concrete and T_c is a stress relaxation parameter. The term β_t represents the shear that can be transferred across a crack due to friction, aggregate interlock or dowel action. If the crack closes, then all the compressive stress normal to the crack plane are transmitted across the crack and only a shear transfer coefficient β_c for a closed crack is introduced. Then the corresponding stress-strain relationship for concrete with a closed crack takes the following form:

$$[D^{ck}] = \frac{E}{(1+\nu)(1-2\nu)} \begin{bmatrix} (1-\nu) & \nu & \nu & 0 & 0 & 0 \\ \nu & (1-\nu) & \nu & 0 & 0 & 0 \\ \nu & \nu & (1-\nu) & 0 & 0 & 0 \\ 0 & 0 & 0 & \beta_c \frac{(1-2\nu)}{2} & 0 & 0 \\ 0 & 0 & 0 & 0 & \frac{(1-2\nu)}{2} & 0 \\ 0 & 0 & 0 & 0 & 0 & \beta_c \frac{(1-2\nu)}{2} \end{bmatrix} \quad (4.4)$$

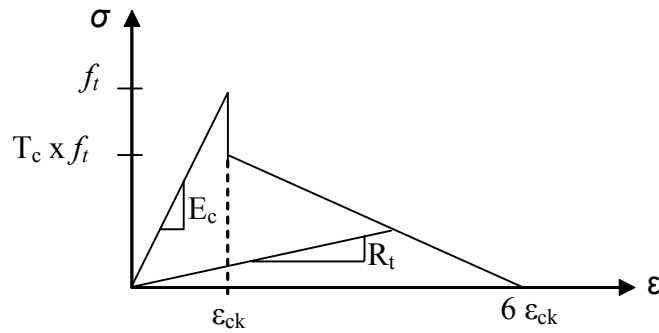


Figure 4.3 Uniaxial-Tensile Stress-Strain Model for Concrete

The built in failure surface in compression for Willam-Warnke (1975) model assumes linear elastic stress-strain relationship until crushing. This, when used without a plasticity law significantly underestimates the deformation capacity of concrete with early crushing of concrete dominating the response (Barbosa and Ribeiro, 1998). On the other hand ANSYS offers a number of rate independent plasticity options that can be used with the reinforced concrete element. One possible candidate is the J_2 plasticity with isotropic hardening, kinematic hardening or combined hardening. The von Mises yield criteria with isotropic hardening reads as:

$$f = \sqrt{J_2} - \sigma(\varepsilon_p) = 0 \quad (4.5)$$

where J_2 is the second stress invariant which can be expressed in terms of principal stresses, σ_1 , σ_2 , and σ_3 :

$$J_2 = \frac{1}{6} [(\sigma_1 - \sigma_2)^2 + (\sigma_1 - \sigma_3)^2 + (\sigma_2 - \sigma_3)^2] \quad (4.6)$$

On the other hand $\sigma(\varepsilon_p)$ is the hardening as a function of equivalent plastic strain, ε_p which can be computed as follows:

$$\varepsilon_p = \sqrt{\sum_{i=1}^6 \sum_{j=1}^6 \frac{2}{3} \varepsilon_{ij}^p \varepsilon_{ij}^p} \quad (4.7)$$

where ε_{ij}^p is the plastic strain component. The yield function given in Equation (4.5) was used for compression behavior of concrete in early finite element models. However, since the function is independent of the magnitude of the hydrostatic stresses, it is not a suitable plasticity model for concrete in compression (Han and Chen 1988).

The second option built in ANSYS for modeling compressive behavior of granular materials is the Drucker-Prager yield criterion, which can be expressed as:

$$f = 3\beta\sigma_m + \sqrt{J_2} - \sigma = 0 \quad (4.8)$$

where β and σ are the material parameters and σ_m is the mean normal stress which can be computed by:

$$\sigma_m = \frac{1}{3}(\sigma_1 + \sigma_2 + \sigma_3) \quad (4.9)$$

Drucker-Prager criterion considers the effect of mean normal stress (i.e. confinement) on the yield function and it is more suitable in modeling concrete behavior in compression than the von Mises criterion (Equation 4.5), which is generally used for metal plasticity. The yield surface for the Drucker-Prager criterion is in the form of a cone that opens along the hydrostatic axis with increasing mean stress as shown in Figure 4.4. For concrete it is well known that the compressive meridians are curved as shown in Figure 4.2 for the Willam-Warnke model. Drucker-Prager model presents a simple approximation for concrete behavior in compression and has been used in various forms by other researchers (Karabinis 1997, Feenstra and De Borst, 1995).

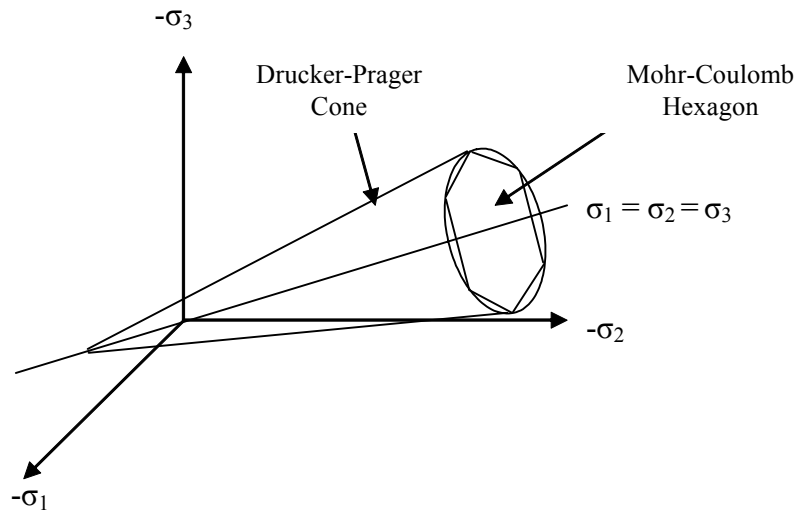
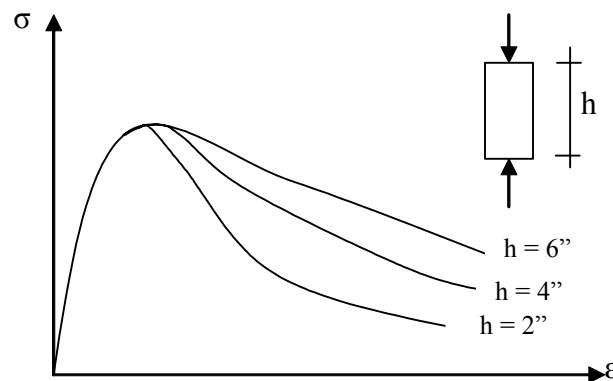


Figure 4.4 Yield Surfaces for Drucker Prager and Mohr Coulomb Criterion

In this study, Drucker-Prager model in its simplest form with an elastoplastic uniaxial stress-strain relationship was used where the material parameters β and σ were calculated by matching the biaxial test data from Kupfer et. al. (1969) (Section 4.2.2). Although this particular form of the Drucker-Prager plasticity model oversimplified the behavior of concrete in compression, it had the advantage of being straightforward with only two material parameters as opposed to some complicated plasticity models (i.e. 24 parameter model by Chen and Mau 1989) and considered the effect of concrete confinement in an approximate fashion. The greatest shortcoming of the current model was the fact that concrete hardening and softening are neglected. Modeling of concrete softening is a current area of research in concrete plasticity (Bazant and Jirasek, 2002) due to the size effect as shown in Figure 4.5 for a uniaxial compressive specimen. The localization of strains and softening regime of concrete from the point of fracture mechanics is beyond the scope of this dissertation. On the other hand, the hardening behavior of concrete beyond the elastic region in compression can be handled easier than that of softening by incorporating a hardening plasticity model. However, ANSYS Drucker-Prager plasticity option does not allow for



**Figure 4.5 Size Effect in Softening Branch of the Uniaxial Compression Test
(Van Mier et. al. 1984)**

a hardening model. Therefore, the current form of the elastoplastic model was used for the simulations, and in fact it is shown that successful simulation of overall reinforced concrete response in the structural level is still possible, despite the aforementioned simplifying assumptions.

In short, the concrete compressive behavior was modeled using elastoplastic Drucker-Prager model whereas the tensile stress-strain behavior was idealized as shown in Figure 4.3. In other words, only tension failure criterion from Willam-Warnke criterion was used together with the Drucker Prager model for compression. The crushing criterion for concrete in compression was imposed by limiting the effective plastic strain, ϵ_p to a value of 0.002. This plastic strain value corresponded to a total strain of 0.003 for the case of uniaxial compression as shown in Figure 4.7 for a concrete strength of 4100 psi. This limiting strain condition, checked at the critical locations on the compressive side of the slabs, was selected based on experimental evidence presented in Chapter 2 and is further consistent with the ultimate strain value of ACI 318-02. The critical location was at the face of the loading area for slabs without any shear reinforcement whereas it was located at the face of the outermost shear reinforcement for the strengthened specimens as shown in Figure 4.6. The critical locations to limit the plastic strains were chosen in the light of experimental evidence for the failed top

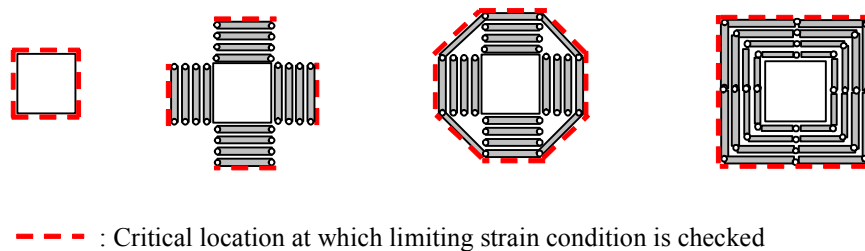


Figure 4.6 Critical Locations for Checking Limiting Strain Condition

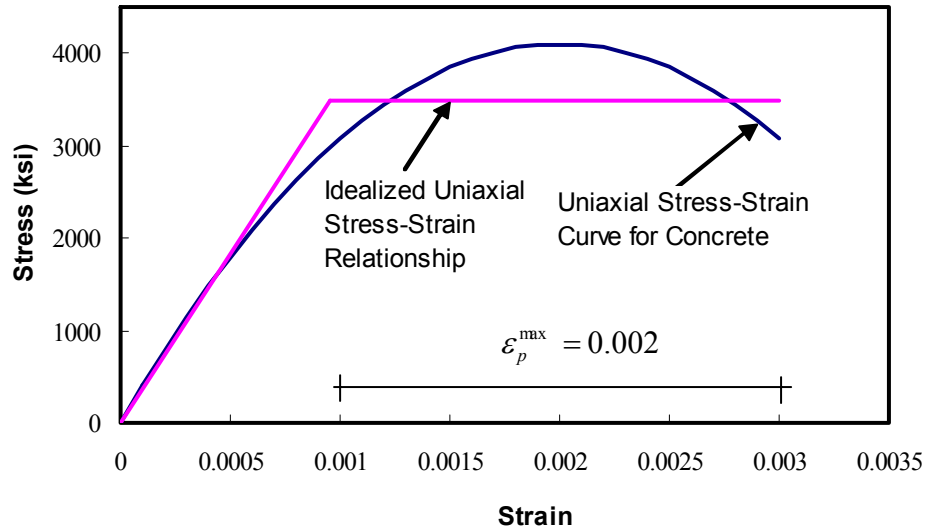


Figure 4.7 Uniaxial Stress-Strain Model for Concrete in Compression

surfaces (Figures 2.35 to 2.38). Since no attempt was made to incorporate the reduced stiffness of elements following significant plastic deformations, i.e. softening, the post punching responses of the slabs were not captured.

4.2.2 Selection of Constitutive Model Parameters for Concrete

Drucker-Prager yield criterion as a smooth approximation to the Mohr-Coulomb criterion can be made to match the latter by adjusting the size of the latter as shown in Figure 4.4 for the compression side. In this way, a smooth function from the Drucker-Prager criterion can be used along with the Mohr-Coulomb parameters that have more physical meaning. Mohr-Coulomb yield criterion in its simplest form can be expressed as:

$$|\tau| = c - \sigma \tan \phi \quad (4.10)$$

in which c is the cohesion and ϕ is the internal angle of friction. Matching two yield criteria on the compressive meridian yields the relationship between the two models.

$$\sigma = \frac{6c \cos \phi}{\sqrt{3}(3 - \sin \phi)} \quad \text{and} \quad \beta = \frac{2 \sin \phi}{\sqrt{3}(3 - \sin \phi)} \quad (4.11)$$

Parameters c and ϕ are the input values to be used with the Drucker-Prager model of the ANSYS plasticity option. In order to obtain these values, Drucker-Prager model was matched against the biaxial test data from Kupfer et. al. (1969) to compute β and σ . This yields the following two equations:

$$\sigma = \frac{1}{\sqrt{3}} \frac{f_{bc} f_c'}{2f_{bc} - f_c'} \quad \text{and} \quad \beta = \frac{1}{\sqrt{3}} \frac{f_{bc} - f_c'}{2f_{bc} - f_c'} \quad (4.12)$$

where f_c' is the uniaxial compressive strength and f_{bc} is the biaxial compressive strength for concrete. Using f_c' from uniaxial compressive tests and setting f_{bc} equal to $1.16xf_c'$, all the necessary input parameters (σ , β , c and ϕ) can be computed. The assumed yield criterion compared with biaxial test data are shown in Figure 4.8. Drucker Prager criterion combined with the tensile failure criterion of the William-Warnke model closely approximates concrete material behavior.

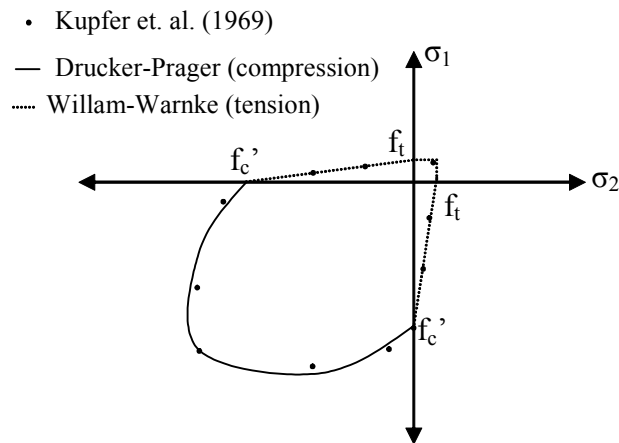


Figure 4.8 Comparison of Biaxial Concrete Strength

A non-associated flow rule, with a potential function similar to the yield function given in Equation (4.8) was used however; β was evaluated using input dilatancy constant, ϕ_f . As reported by Kupfer et. al. (1969) in biaxial tests, there is volume contraction up to 75 to 90% of ultimate compressive strength. Beyond that, the trend is reversed resulting in volumetric expansion of concrete specimen. Dilatation of concrete close to the ultimate strength level is not taken into account in this study, however only volume contraction is modeled. Mirmiran et al. (2000) tested carbon fiber wrapped cylinders subjected to uniaxial compression. They used Drucker-Prager elastoplastic model with a zero dilatancy angle, ϕ_f in modeling the test specimens. Their results showed that reasonable predictions of the volumetric behavior of the specimens can be obtained with a zero dilatancy angle to properly account for shear/compaction phenomenon (Mirmiran et al. 2000). As a result final values of f_c' , f_t , c , ϕ , and ϕ_f as input to ANSYS were 4100 psi, 142 psi, 11.5° and 0°, respectively.

The remaining parameters β_t and T_c were selected based on previously suggested values and parametric studies. β_t represents the amount of shear transfer across a crack due to aggregate interlock and friction and values between 0 and 0.3 have been used in previous studies (Hemmaty 1996, Kachalev, 1998). Using a value of zero totally neglects the shear transfer across a crack and this does not realistically simulate the actual behavior especially for the flexural cracks. A value of 0.3 was used in the current study unless otherwise stated, and its effect on the overall response is investigated for a value of 1.0. It was observed that this parameter has insignificant effects on the stiffness and strength of test specimens. The default value of T_c equal to 1.0 was used where a straight line approximation was made for the tensile strain softening. The area under the softening region also simulated the fracture energy associated with concrete cracking (Bazant and Planas, 1998).

4.2.3 Steel and CFRP Constitutive Model

Steel longitudinal reinforcement was modeled with a bilinear isotropic hardening using von Mises yield criterion as stated in Equation (4.5). Yield strength and modulus of elasticity for steel reinforcement was based on the coupon test results presented previously in Section 2.3. Strain hardening region was not modeled since none of the reinforcing bars in the test specimens experienced strains close to the strain at the onset of strain hardening ($\epsilon_{sh} \approx 0.013$). CFRP strips were modeled using elastic isotropic stress-strain behavior with modulus of elasticity from coupon tests. Three dimensional link (truss) elements with two nodes were used both for steel reinforcement and CFRP strips with aforementioned constitutive models. Idealized uniaxial stress-strain behavior of steel and CFRP are shown in Figure 4.9. It is important to note that the ultimate strain level for CFRP strips was also checked against the ultimate strain from coupon tests at the end of each load step.

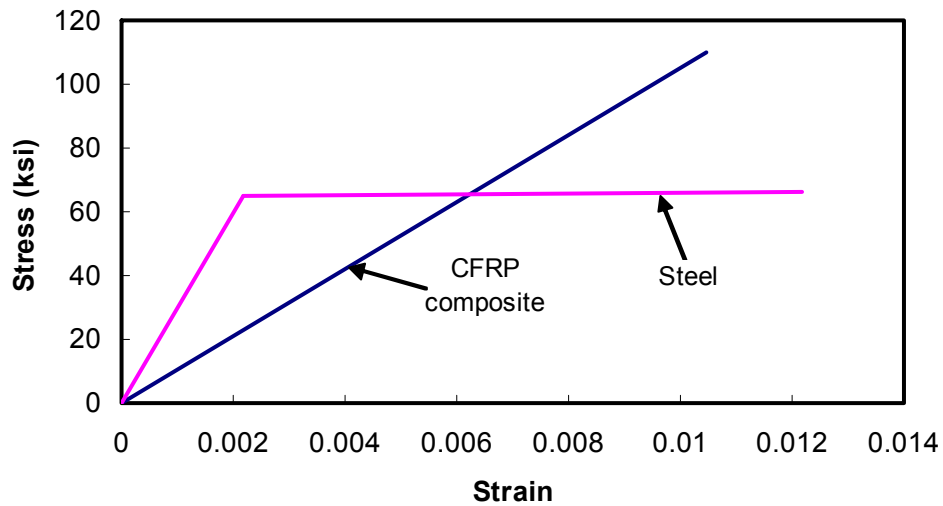


Figure 4.9 Uniaxial Tensile Stress-Strain Models for Steel and CFRP

Perfect bond between the reinforcement (CFRP or steel) and solid concrete elements was assumed. In other words bond slip of the reinforcement was not accounted for in the finite element analyses.

4.2.4 Modeling and Analysis Procedure

Nonlinear finite element analyses of concentrically loaded slabs were performed using ANSYS. The aforementioned constitutive models for concrete, steel and CFRP were used in the finite element analyses. Only quarter of the slab was modeled using symmetry boundary conditions. Two different finite element meshes were used for the mesh sensitivity study (Figure 4.10). First model was meshed using 3"x3"x1.5" solid elements for the quarter model of the slab (Model 1). A total of 676 solid elements were used for this finite element model. Steel reinforcement was modeled using link elements in both directions. Second model consisted of a refined mesh where a finer mesh around the loading area was used. The element sizing and spacing were performed in this second model such that vertical CFRP strips could be modeled precisely (Figure 4.10). This finite element mesh consisted of a total of 1156 solid elements (Model 2). Previous finite element analyses of concentrically loaded reinforced concrete flat plates conducted by Xiao (1998) and Megally (1998) proved that the number of elements along the depth of the slab ranging from three to five were successful in capturing the flexural and inclined cracking. In addition, reasonable program execution times could be obtained without sacrificing from the accuracy. Hence, four elements through the thickness of the slabs were used in both models. Models 1 and 2 were used to simulate the behavior of control specimens. After concluding that mesh size was not significantly affecting the finite element analysis results of the control specimen, Model 2 was used to simulate the behavior of the upgraded specimens.

All the tests were conducted in a displacement controlled fashion. In order to simulate this in the analyses, nodal displacements were imposed to simulate the application of the displacements as explained for the test specimens in Section

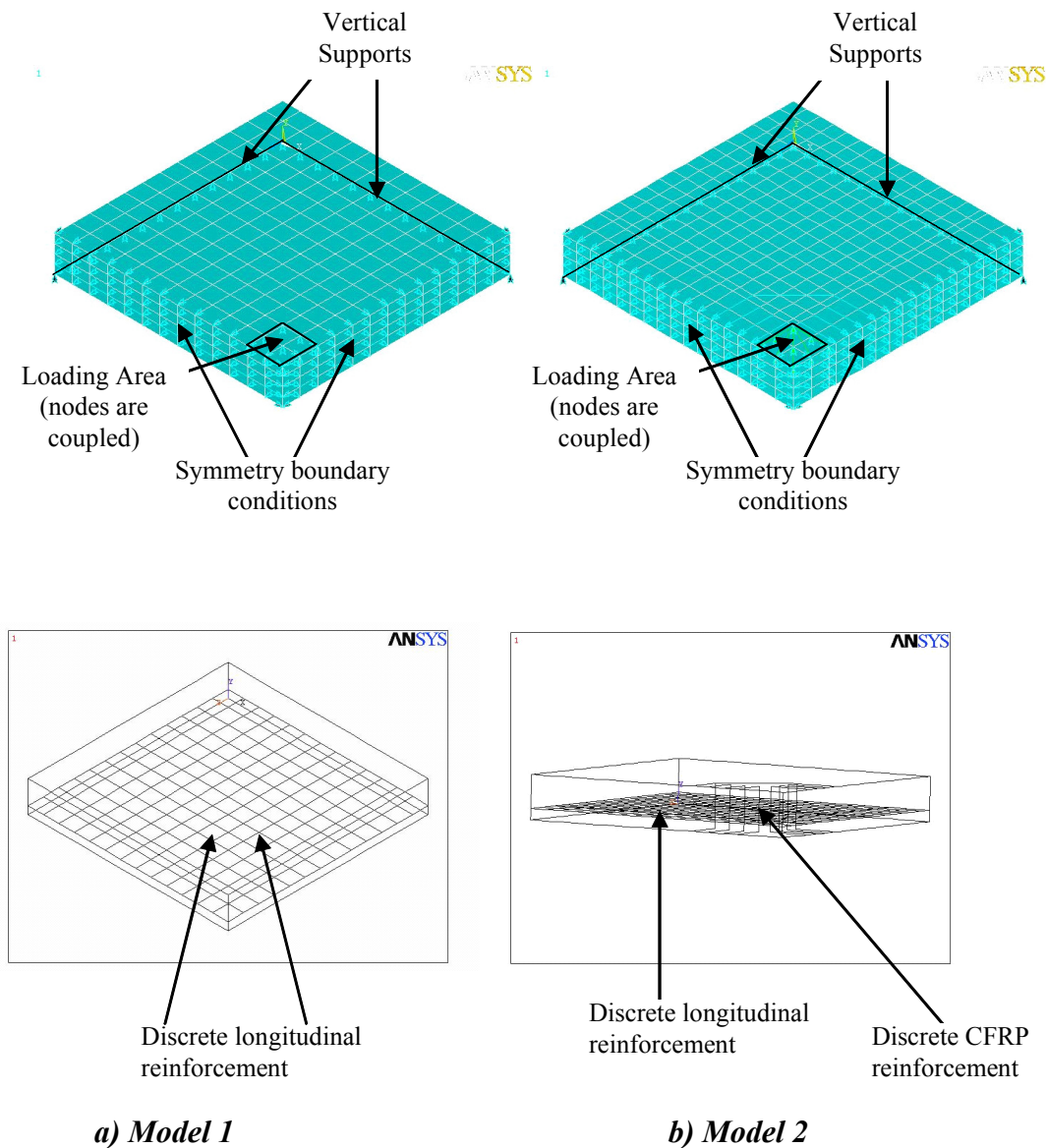


Figure 4.10 Details of Finite Element Meshes

2.5. The nodes on the compressive side of the slab that correspond to the location of the steel loading plate in the experiments were coupled in the vertical direction through the use of constraint equations. Then the displacements were applied in an incremental manner where at each increment several iterations were performed until the convergence criterion was met. Full Newton-Raphson algorithm was applied for the iterative procedure in which tangent stiffness matrix was updated at the beginning of each increment and iteration. Schematics of the incremental procedure can be seen in Figure 4.11. The default convergence criterion of ANSYS is based on satisfying a strict unbalanced force tolerance with an L2 norm where the convergence is assumed to take place for the i^{th} iteration if:

$$\frac{\left(\sum_j (\delta F_j^i)^2 \right)^{1/2}}{\left(\sum_j (\Delta F_j^i)^2 \right)^{1/2}} \leq Tol \quad (4.13)$$

in which Tol is the specified tolerance (default=0.1%), δF_j^i is the unbalanced force at the i^{th} iteration of the j^{th} degree of freedom and ΔF_j^i is the computed value using the following expression:

$$\Delta F_j^i = \Delta F_j^{i-1} + \delta F_j^i \quad (4.14)$$

The preliminary analyses showed that the default force based convergence criterion created convergence problems after onset of first cracking. This agrees well with the observations of Owen and Figuries (1984) where they argued that for nonlinear finite element analysis of concrete, a displacement based criterion was more suitable for cases where nonlinearity due to cracking was concentrated at certain regions of the finite element model. Therefore a displacement based convergence criterion with a tolerance of 0.1% was applied together with a

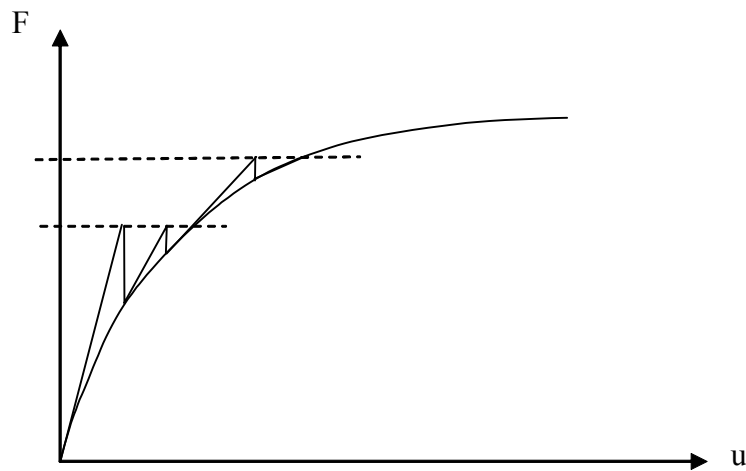


Figure 4.11 Full Newton-Raphson Iteration Schematics

loosened force based criterion where the unbalanced force tolerance was set to 1%. This modification to the default convergence criterion helped to achieve convergence even after extensive cracking and significant plastic deformations took place in concrete.

4.3 ANALYSIS OF CONCENTRICALLY LOADED RC FLAT PLATES WITHOUT SHEAR REINFORCEMENT

This section presents the analyses results of concentrically loaded rectangular reinforced concrete flat plates. First, the results of a sensitivity study is presented to investigate the effect of meshing, shear transfer coefficient, β_t , and the support conditions using the material and geometric properties of specimen Control-1. Then, the detailed results of finite element analysis for specimen Control-1 is presented to provide insight for punching shear failure mechanism and stress conditions at failure. Finally, the results from a parametric study are presented to investigate the effect of different concrete tensile and compressive strength and reinforcement ratio on the behavior of concentrically loaded reinforced concrete flat plates.

4.3.1 Control Specimen

The experimental results of specimen Control-1 specimen were used as a basis for the validation of finite element analysis results. This specimen with longitudinal reinforcement ratio of about 1.76% was not strengthened with CFRP. Finite element analyses were performed using Model 1 and Model 2, with β_t values of 0.3 and 1.0. In addition two support conditions, transverse supports (roller supports) as shown in Figure 4.10 and spring supports along the boundary of the slab were considered. The springs that were attached to the slab edges were stiff in compression and flexible in tension which simulated the actual boundary conditions in tests. The predictions for load versus central deflection curves are compared with the experimental load-deflection curve in Figure 4.12. The ultimate load and deflection predictions of the finite element analyses and the test results are given in Table 4.1. Two meshes used for Model 1 and 2 resulted in similar responses for a β_t value of 1.0. In addition, the analyses results for transverse supported and spring supported slabs were very similar. Hence, the failure mode and the ultimate load carrying capacity of the slab were not influenced by these two types of boundary conditions. Failure occurred locally around the loaded area, and away from the supports.

The effect of variable β_t on the overall response was investigated for two different values 0.3 and 1.0. A β_t value of 1.0 implies full transfer of shear across a crack. It is evident from Figure 4.12 that an increase in β_t value resulted in a stiffer response. However the ultimate load prediction was not significantly influenced by β_t values used in the analysis.

The preliminary analyses results showed that Model 2 with transverse supports at the edges with a β_t value equal to 0.3 could satisfactorily simulate the overall load-deformation response of the control specimen. Therefore the analyses

results (stresses, strains and deflections) from this model were used in the rest of the discussion on Control-1 and strengthened specimens.

In addition to the overall load deformation comparisons, concrete and steel strains obtained from finite element analyses were compared with the experimental results. Figure 4.13 and Figure 4.14 show the steel strain profiles as obtained from the finite element analysis and from experimental measurements. An examination of Figure 4.13 indicates that steel strain trends were correctly predicted; however the predicted values were lower than the experimentally measured strains. This can be attributed to the somewhat stiffer predicted response (Figure 4.12) resulting in underestimation of deflections at the ultimate stage (Table 4.1). A similar observation for concrete tangential strains can be made in Figure 4.14. The maximum tangential strains were underestimated

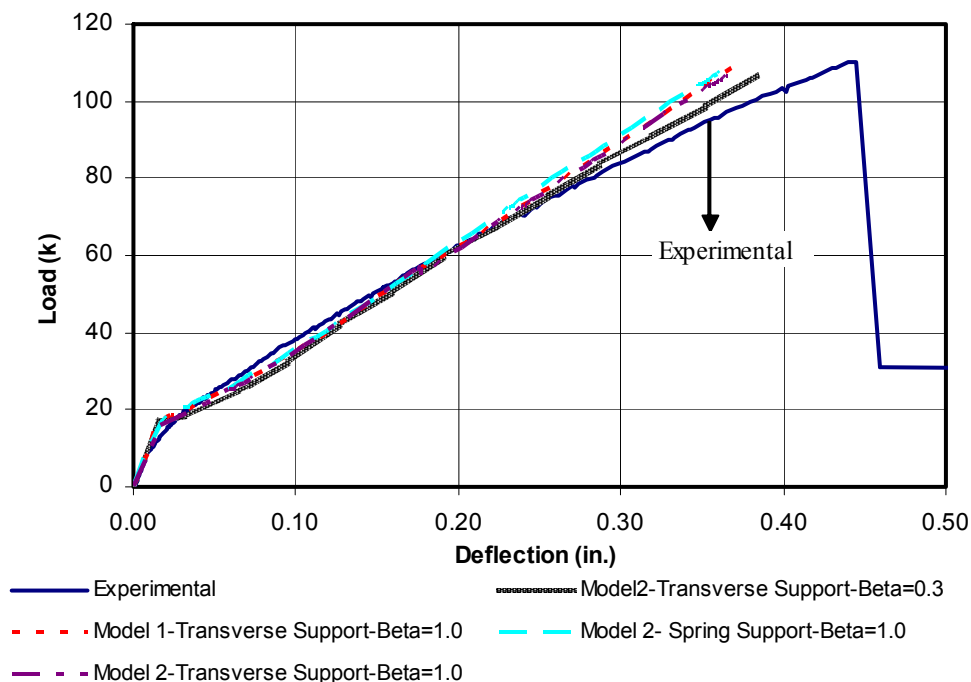


Figure 4.12 Finite Element Analyses Predictions for Control-1 Specimen

especially at locations close to the loading area. The assumed elastic perfectly plastic response of concrete with a Drucker-Prager yield criterion was responsible for the underestimation of the strains. However finite element analysis and experimental results showed similar trends in general.

Table 4.1 Finite Element Analyses Results for Control Specimen

FEA	Model	β_1	Edge Support	Ultimate Load, P_u (k)	Deflection at P_u , Δ_u (in.)	P_u / P_{exp}	Δ_u / Δ_{exp}
1	1	1.0	Transverse	110.62	0.378	1.02	0.87
2	2	1.0	Transverse	108.63	0.373	1.00	0.86
3	2	1.0	Spring	107.16	0.368	0.98	0.85
4	2	0.3	Transverse	106.86	0.384	0.98	0.88

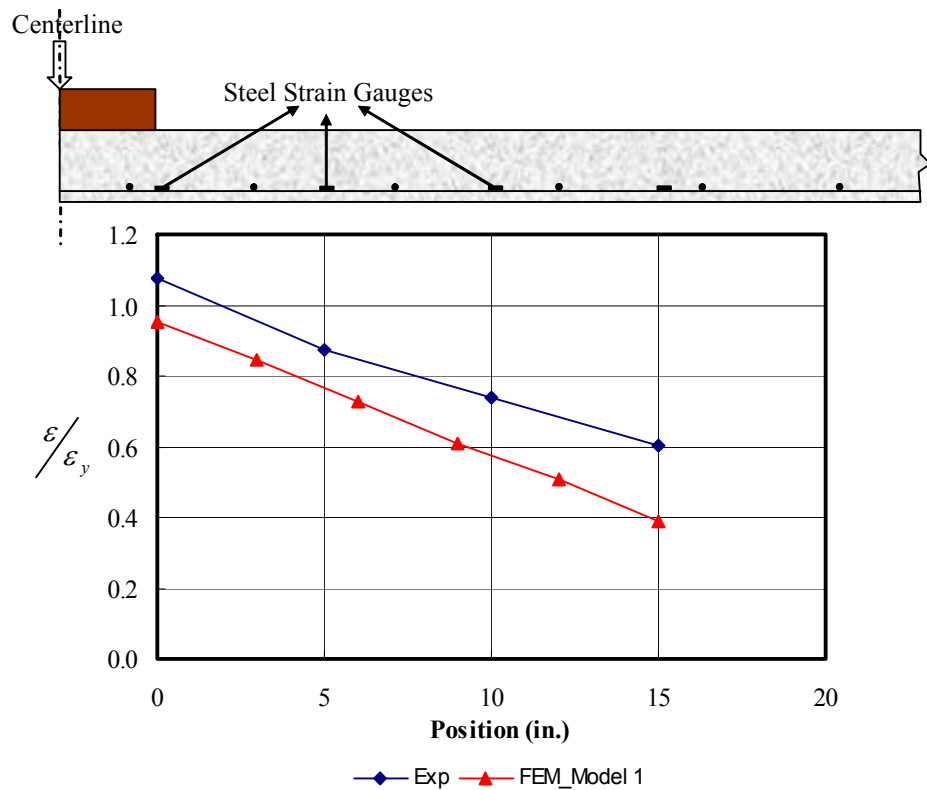


Figure 4.13 Comparisons of Steel Strain Profiles

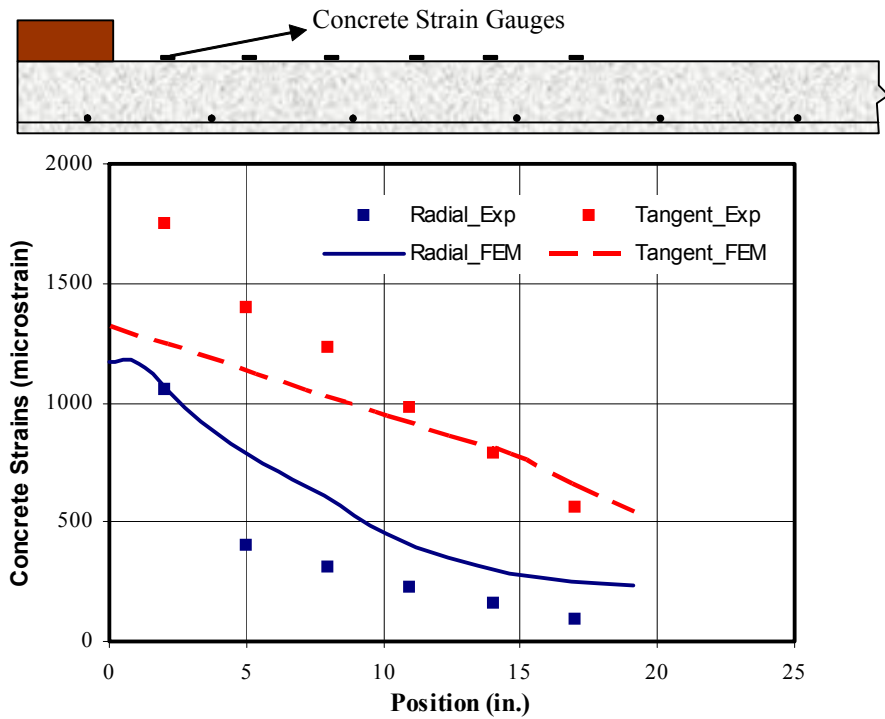
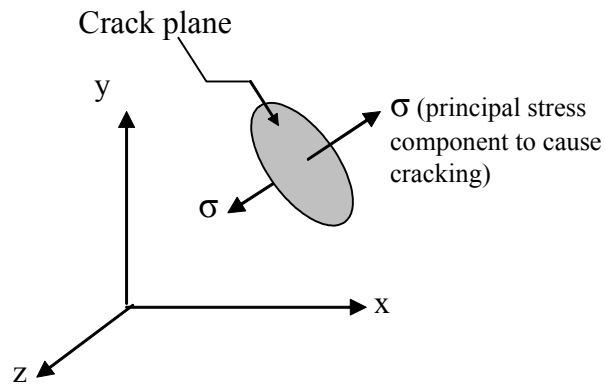
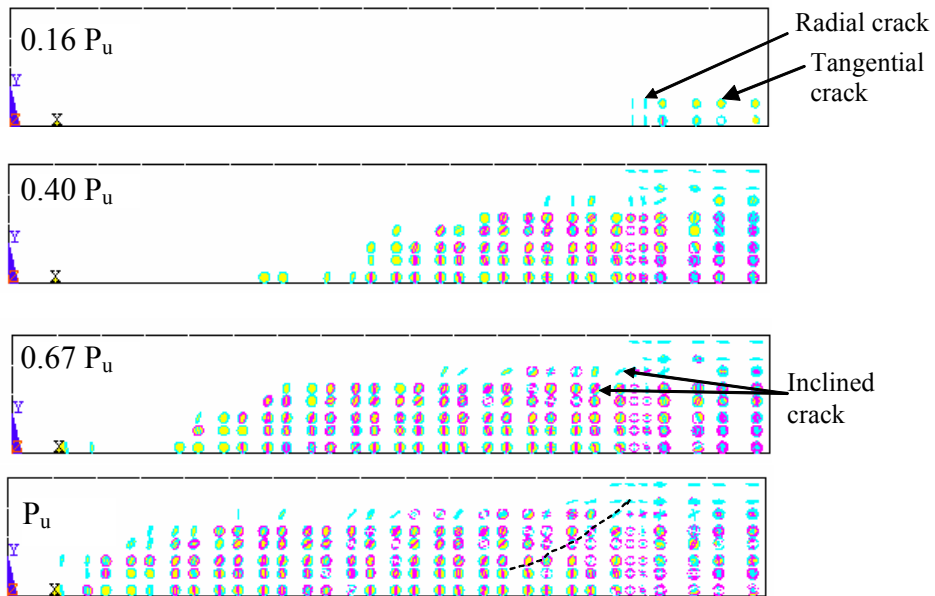


Figure 4.14 Comparisons of Concrete Strain Profiles

Crack patterns can provide valuable information on punching shear failure mechanism. ANSYS provides post processing abilities for crack patterns at any load step. The cracks in the post processing of the results are shown with a circular plane whose normal correspond to the principal stress component that causes cracking (Figure 4.15.a). Figure 4.15.b shows the predicted crack patterns along the symmetry axis for the quarter slab at various load levels. At early stages of loading tangential and radial cracks formed in the tension zone of the slab. Upon further loading, flexural cracks that were essentially perpendicular to the bottom face formed. At about 67% of the ultimate load, first inclined cracks appeared and the cracks at the face of the loading area were observed. At the



a) Crack Plane in global coordinate system



b) Crack Patterns from FEA at different percentage of ultimate load



c) Crack Pattern at Ultimate Load from Experiment

Figure 4.15 Crack Patterns from FEA and Test

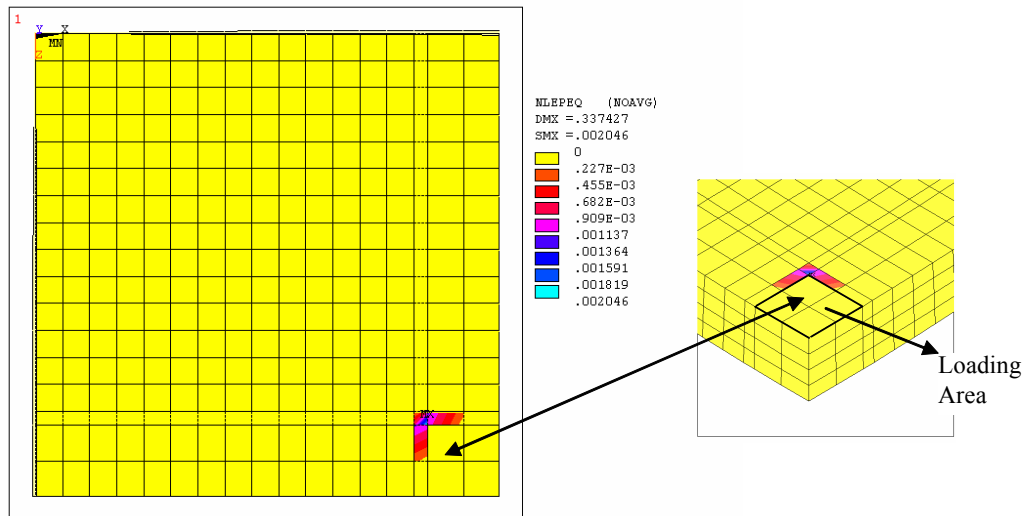


Figure 4.16 Equivalent Plastic Strains at Ultimate Load

ultimate stage, these cracks opened wider and the cracking was in the form of almost horizontal splitting, meaning that the root of the dominant shear crack at the front face of the loading area was in a biaxial state of stress. In other words concrete in the compression zone in front of the loading area had the tendency to separate due to splitting stresses. Figure 4.15.c shows the actual crack pattern, which was observed along the slab cross-section, obtained by cutting the control specimen along the centerline.

The local stress and strain conditions around the patch loaded area can be used to better understand the failure mechanism. Figure 4.16 shows the equivalent plastic strains at the ultimate load. Significant plastic deformations occurred at the corner of the loading area, and the associated plastic strains decayed rapidly with increasing distance measured from the corner. Compressive stresses and associated plastic deformations were more pronounced at locations close to the corners of the loaded area. In order to obtain a better picture of the state of stresses, stress contours for the principal stresses are shown for the region around

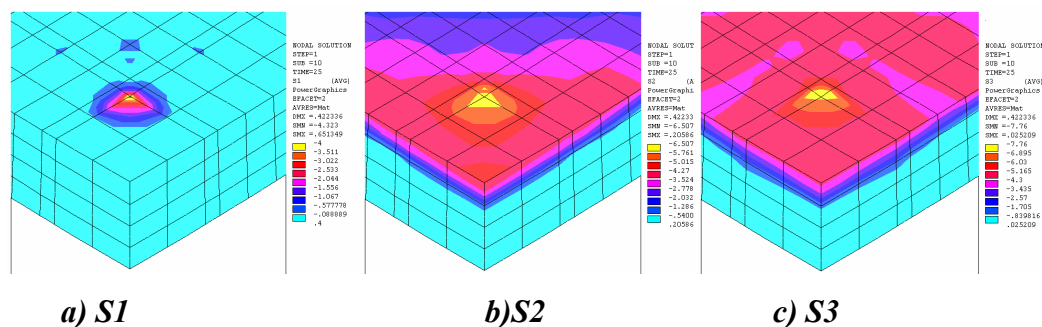


Figure 4.17 Principal Stress Contours from Finite Element Analysis

the loading area in Figure 4.17 ($S1 > S2 > S3$). This figure shows that the principal stresses were highest at the corner. To put these principal stresses in perspective, Figure 4.18 shows the stress profiles along various lines on the compressive side of the slab. All the stresses are scaled by f_c' (assuming $f_c' = -4100$ psi), the concrete compressive strength (positive axis shows compression). At Point B (corner), concrete was in a triaxial state of compression where all three principal stresses were above f_c' . But the highest principal stress ($S1$) decreased sharply from B to A. On the other hand, at point A, cracking took place leaving this location in a biaxial state of stress. The cracking that was observed at point A is shown in Figure 4.15 previously.

The results presented above suggest two consecutive events for failure:

- i) Failure might initiate at the front of the loading area along symmetry axis (Point A) when the splitting cracks in the compression zone, which were almost horizontal, widened significantly (spalling of concrete on the compression side).
- ii) Corner of the concentrically loaded area (Point B) failed due to the lateral propagation of the splitting cracks from Point A to Point B.

The above reasoning based on finite element analyses suggest that for slabs with square columns the horizontal splitting cracks initiate the failure mechanism at the front face of the loading area, whereas the corner is under a triaxial

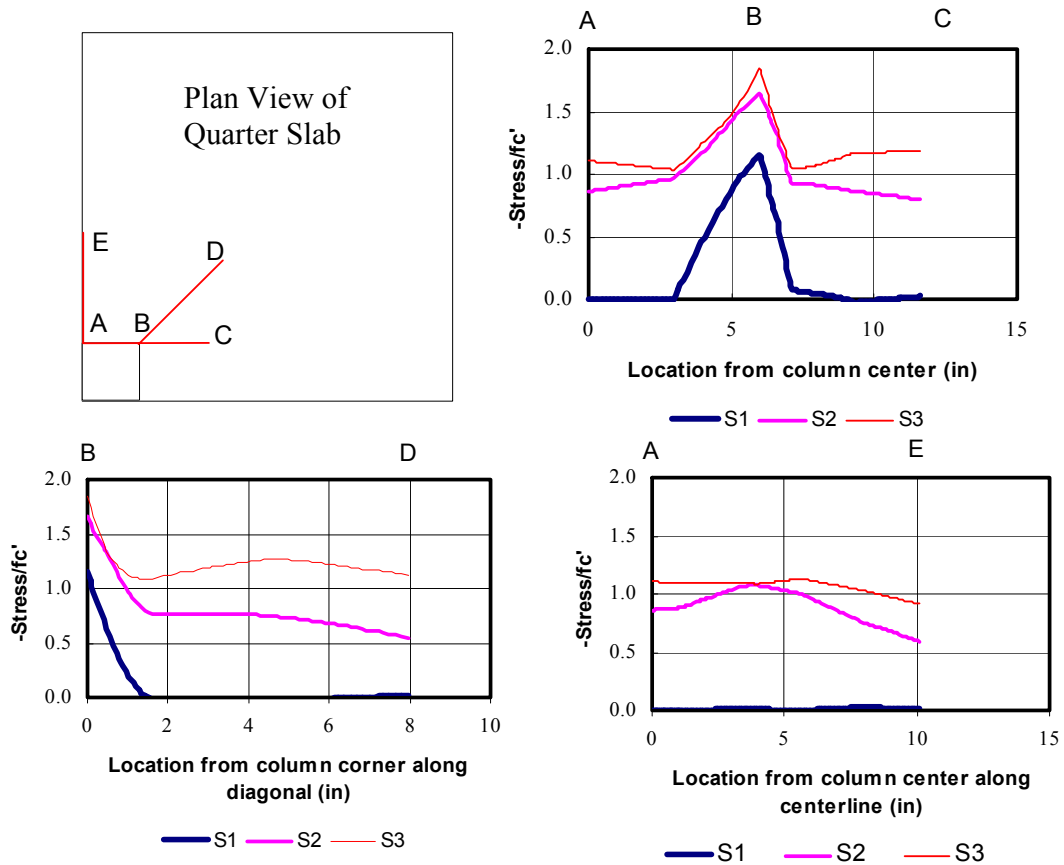


Figure 4.18 Principal Stresses at Ultimate Load

state of stress until this state of stress is lost due to excessive plastic deformation and extensive cracking.

A number of axisymmetric punching shear models have been proposed in the past (Section 1.4.1.2 and 1.4.16) using circular columns for circular slabs. In addition, these models have also been extended to square column cases by using an equivalent circular column concept (Broms 1990, Gomes and Regan, 1999). Vertical deformation contours shown in Figure 4.19 suggest that an axisymmetric approximation is valid for slab deflections. The failure criterion in these models assumed that slab-column interface was under a triaxial state of compression and

failure occurred in a shear-compression mode with a limiting strain condition (Broms 1990, Kinnunen and Nylander 1960). This state of stress agreed well with the state of stress presented for the corner (Point B). On the other hand, it is obvious that generalization of an axisymmetric model for a flat plate supported on square columns does not represent the actual stress distribution, i.e. cracking and failure stress states (especially at the front face, along AB in Figure 4.18).

4.3.2 Parametric Studies

A parametric study was conducted to investigate the effect of longitudinal reinforcement ratio, concrete tensile and compressive strength on the punching shear resistance of concentrically loaded RC slabs. The geometry of the slab used in this study was similar to that of specimen Control-1, and Model 2 was used with the boundary conditions as shown in Figure 4.10. This study facilitated the investigation on the significance of various parameters, which were not taken as test variables in the experimental program, and the influence of these parameters on the slab behavior.

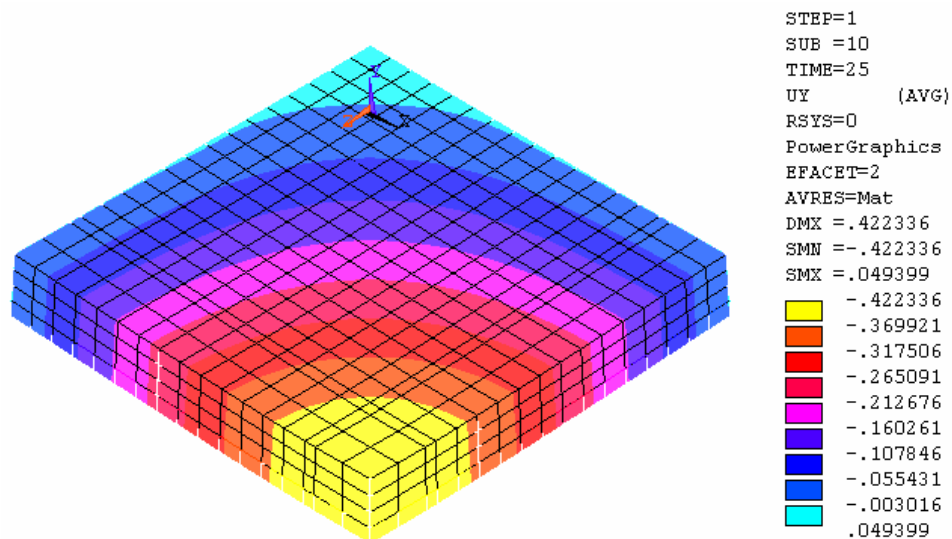


Figure 4.19 Vertical Deformation Contours at Ultimate Load

4.3.2.1 Effect of Longitudinal Reinforcement Ratio

Figure 4.20 illustrates the effect of longitudinal reinforcement ratio on the strength and ductility of flat plates. In these analyses, longitudinal reinforcement ratios ranging between 0.5% and 1.8% were considered. A decrease in reinforcement ratio resulted in lower load carrying capacities. However, deformation capacities of the flat plates increased with decreasing reinforcement ratios. Initiation of reinforcement yielding is marked on all load deformation plots shown in Figure 4.20. As the reinforcement ratio decreased the displacement ductility of the slabs, which can be defined as ultimate displacement divided by yield displacement, increased. Figure 4.21 shows the longitudinal steel strain profile at the ultimate loads of the slabs. Strains reached values well above the yield strain especially for cases where reinforcement ratios were small. The localization of steel strains at the face of the loading area was observed for slabs with low reinforcement ratios. In fact, similar results were also observed for

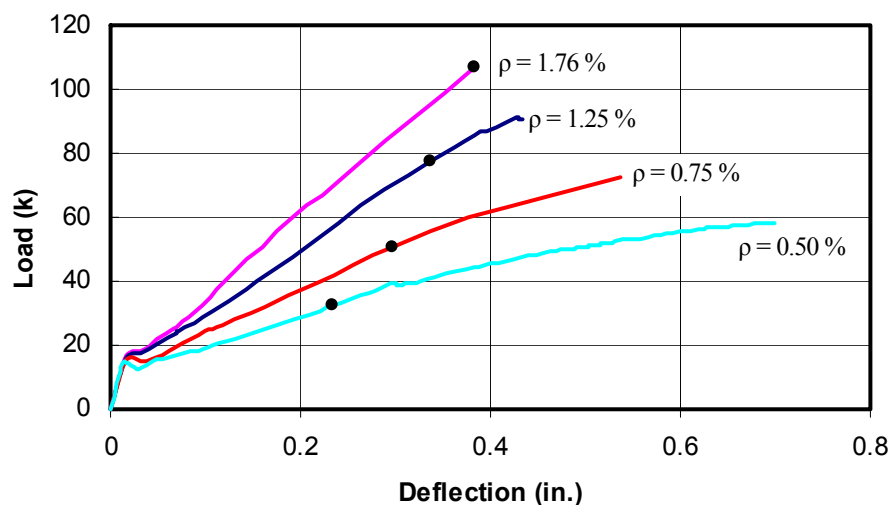


Figure 4.20 Effect of Reinforcement Ratio on the Behavior of Slabs

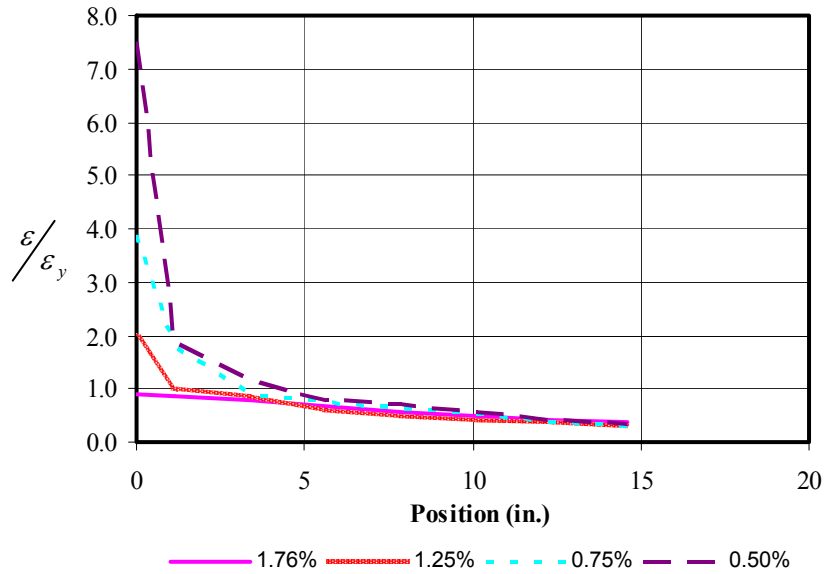


Figure 4.21 Steel Strain Profiles at the Ultimate Loads of Slabs with Different Reinforcement Ratios

strengthened specimens in the experimental program as shown in Figure 2.19. Although significant yielding was observed at the face of the loading area, failure was still in the form punching due to local stress state around the patch loaded area.

4.3.2.2 Effect of Concrete Tensile Strength

Another parameter under investigation was the effect of tensile strength of concrete, f_t , on punching shear capacity. It is well known that f_t value depends on the type of testing (direct tension test, splitting cylinder test or modulus of rupture test), the compressive strength of concrete, concrete design mix, aggregate type and gradation. To investigate the influence of this parameter on punching shear strength three finite element analyses were conducted for specimen Control-1 where f_t was taken as 0.05, 0.1 and 0.15 times concrete compressive strength, f_c' .

These values cover a wide range concrete tensile strength (~ 3.2 to 9.6 times $\sqrt{f'_c}$). All other variables such as compressive strength of concrete, reinforcement ratio were kept the same as those of the control specimen Figure 4.22 shows the predicted load-deformation response of the slabs with different f_t values. Increases in concrete tensile strength resulted in higher ultimate load carrying capacities. When the tensile strength of concrete was taken as $0.15 f'_c$ the capacity increased by about 10% in comparison to the case where f_t was equal to $0.1 f'_c$. Similarly, when f_t was taken as $0.05 f'_c$ capacity decreased by about 9% in comparison to the case where f_t was equal to $0.1 f'_c$. Hence, the use of tensile strength values as high as $9.6 \sqrt{f'_c}$ and as low as $3.2 \sqrt{f'_c}$ resulted in insignificant ultimate load carrying capacity increases. However, for accurate estimations of capacity, the importance of using realistic estimations for tensile strength is appreciated.

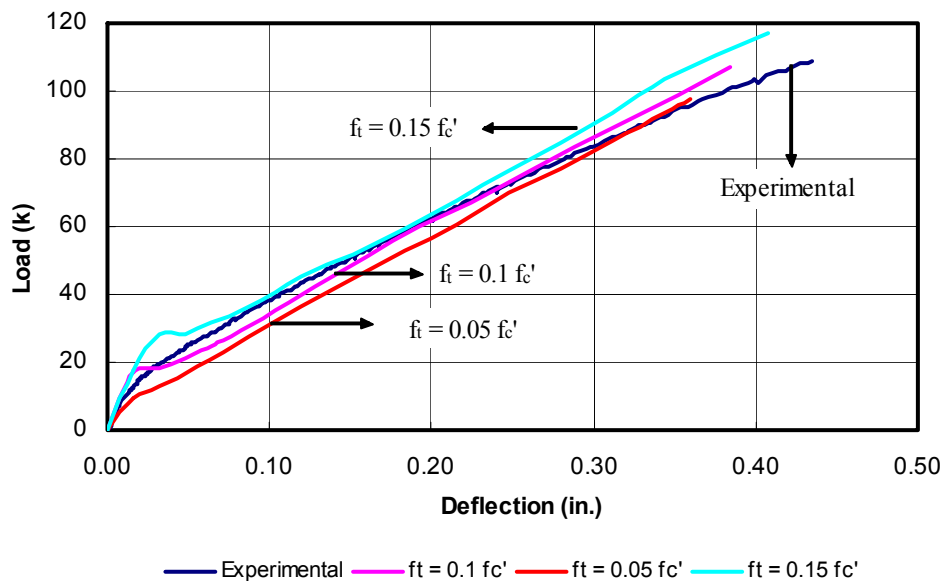


Figure 4.22 Effect of Concrete Tensile Strength on the Behavior of Slabs

4.3.2.3 Effect of Concrete Compressive Strength

The effect of concrete compressive strength on punching shear resistance was investigated through the analyses of the control specimen with compressive strength values of 2000 psi, 4100 psi and 6000 psi. For each case concrete tensile strength was assumed to be 10% of the assigned compressive strength. The load deformation results of the analyses are presented in Figure 4.23. When concrete strength was reduced to half the value that was used in specimen Control-1 the load carrying capacity decreased about 50%. However, a 50% increase in concrete strength resulted in a capacity increase of about only 20%. This result shows that f_c' was one of the most important variables influencing the ultimate load capacity. This was due to the fact that after the formation of the inclined crack the contribution of concrete in the compression zone was highly dependent on concrete strength (as previously shown with a simple model in Section 2.8.6).

The results of the parametric studies are summarized in Table 4.2. In addition to the ultimate load predictions, punching shear capacities computed using ACI 318-02 expressions (presented in Section 1.4.4.1) and flexure capacities based on yield line analyses (Section 2.7.1) are listed in this table for a basis of comparison. ACI predictions for punching shear capacity were safe except for the case where reinforcement ratio was equal to 0.5% (~2.5 times the minimum reinforcement ratio for slabs, 0.18 %). For this analysis ($\rho = 0.5\%$), the flexural capacity estimated using yield line analysis was exceeded by about 15% in the finite element analysis. This was an indication that the mode of failure tended to shift from punching shear to flexural yielding as the reinforcement ratio was decreased below 0.75%.

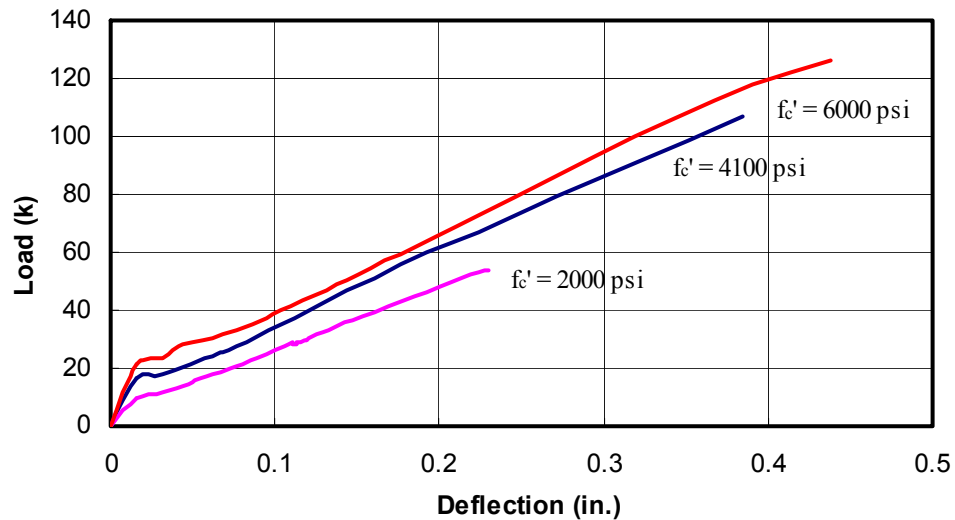


Figure 4.23 Effect of Concrete Compressive Strength on the Behavior of Slabs

Table 4.2 Results of the Parametric Studies

FEA	f'_c (psi)	f_t (psi)	Reinforcement ratio, ρ (%)	Ultimate Load, P_u (k)	P_u / V_{ACI}	P_u / P_{flex}
1	4100	410	1.76	106.9	1.40	0.67
2	4100	410	1.25	90.7	1.19	0.76
3	4100	410	0.75	72.3	0.95	0.97
4	4100	410	0.5	58.2	0.76	1.14
5	4100	205	1.76	97.4	1.28	0.61
6	4100	820	1.76	117.0	1.54	0.73
7	2000	200	1.76	54.0	1.02	0.41
8	6000	600	1.76	126.3	1.37	0.75

4.4 ANALYSIS OF CONCENTRICALLY LOADED RC FLAT PLATES STRENGTHENED WITH CFRP

This section concentrates on the finite element analyses results of RC flat plates strengthened with CFRP. Test specimens from Chapter 2 were used for validation of the finite element analysis results. Strengthening mechanism and local stress conditions resulting in failure of the test specimens were investigated.

Slabs strengthened with four CFRP perimeters using different patterns (A and B) and amounts of CFRP were analyzed in this part of the study. Strengthened specimens with six and eight CFRP perimeters were not included in the finite element analyses, as the strengthening mechanism was similar to those of slabs strengthened with four CFRP perimeters.

4.4.1 Comparisons of Analysis Results with Experimental Results

Finite element analyses results of load versus central deflection behavior of specimens A4-1, A4-2, A4-3, A4-4, and B4 are compared with the experimental results in Figure 4.24 to 4.26. Strengthening patterns and number of CFRP vertical legs of external stirrups are also given in these figures. The summary of the analyses results is given in Table 4.3.

An examination of Figure 4.24 to 4.26 indicates that finite element analyses provided reasonable predictions for stiffness and strength of upgraded specimens. First cracking loads and stiffness after cracking were predicted with reasonable accuracy. This shows that treatment of cracking in the Willam-Warnke model provided realistic estimations for the overall stiffness change during the imposed displacement history. On the other hand, the numerical models underestimated the ultimate load carrying capacities of the test specimens by 2 to 8%. Underestimations of deflections at ultimate loads were more pronounced (10 to 25%). The reason for the underestimations of ultimate loads and deformations was due to the approximate modeling of concrete compressive behavior in the plastic range. The fact that the analyses were performed up to the limiting equivalent plastic strain (0.002) resulted in slight underestimations of the ultimate loads and deformations. In reality, concrete on the compressive side might sustain further plastic strains. This could result in slightly increased load and deformation capacities of the slabs. Inclusion of softening behavior of concrete needs to be

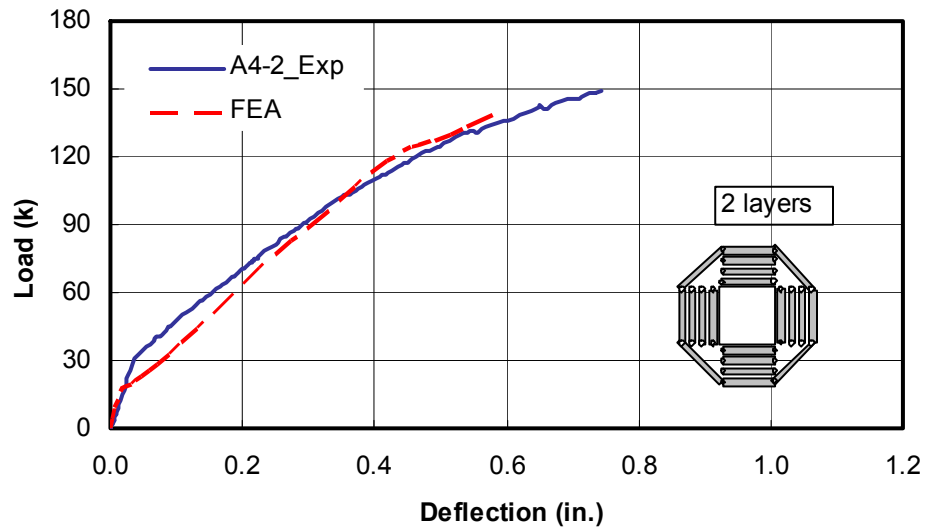
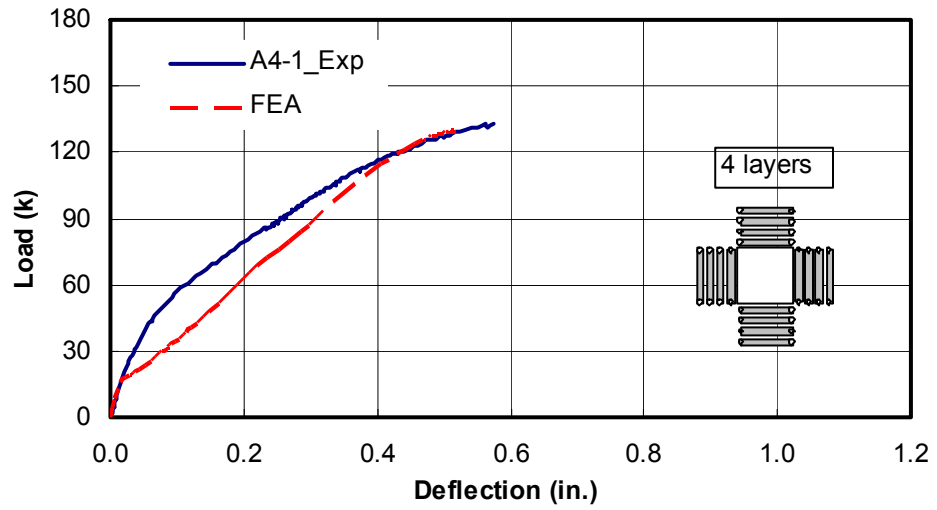


Figure 4.24 Load-Deflection Comparisons of Specimens A4-1, A4-2

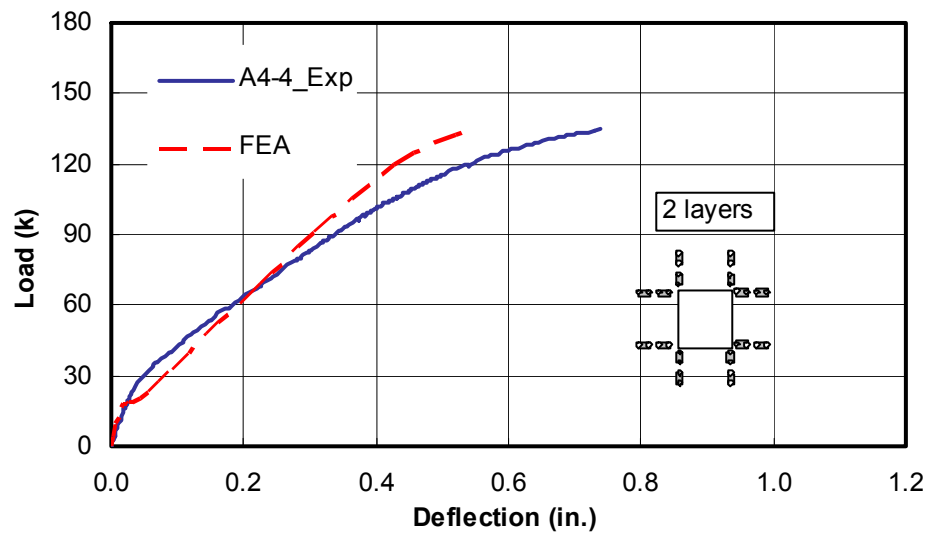
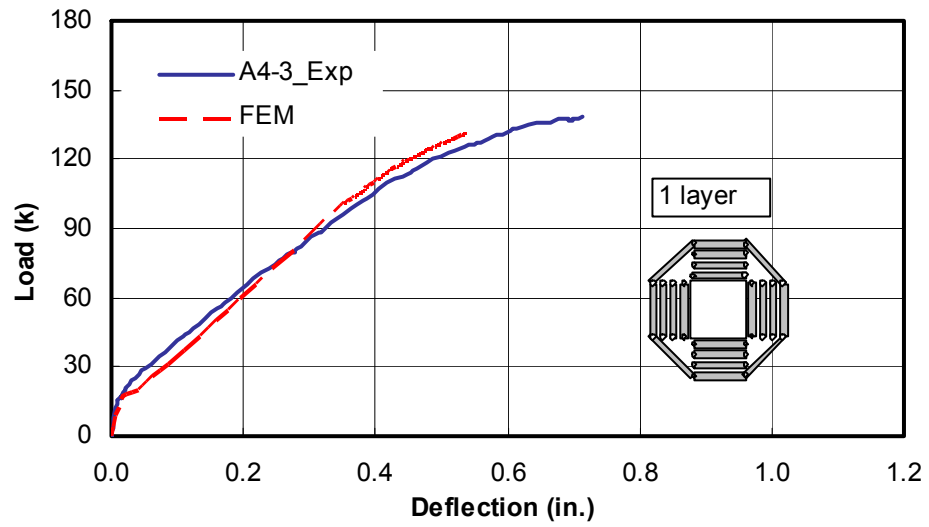


Figure 4.25 Load-Deflection Comparisons of Specimens A4-3, A4-4

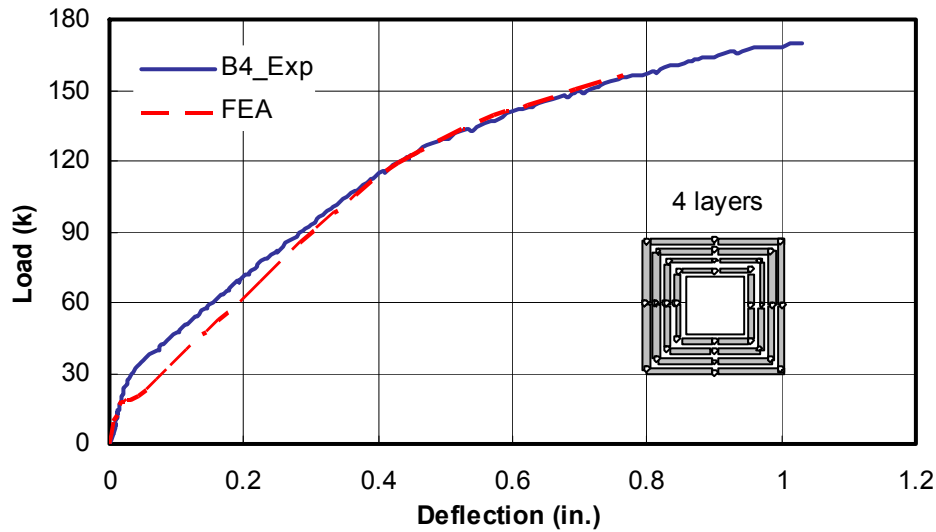


Figure 4.26 Load-Deflection Comparisons of Specimens B4

Table 4.3 Comparisons of Analyses and Experimental Results for Specimens Upgraded in A4 and B4 Configurations

Specimen Name	V_{uFEM} (k)	Δ_{uFEM} (in.)	$\epsilon_{max\ CFRP/FEM}$	V_{uexp} (k)	Δ_{uexp} (in.)	$\epsilon_{max\ CFRP/exp}$	% Error in Ultimate Load	% Error in Ultimate Deformation
A 4-1	130	0.52	0.0016	133	0.58	0.0019	2.3%	10.3%
A 4-2	139	0.57	0.0029	149	0.74	0.004	6.8%	23.0%
A 4-3	131	0.54	0.0041	139	0.71	0.0096	5.4%	23.9%
A 4-4	137	0.55	0.0024	135	0.74	-	-1.4%	25.7%
B 4	156	0.77	0.0021	170	1.03	0.0028	8.1%	25.2%

taken in to account at large strains for more precise estimations of ultimate deformation capacities. However this can only affect the predicted behavior of the slab following the termination of the analyses i.e. deformation levels close to punching shear failure.

The finite element analyses captured the fact that as the amount of CFRP used as shear reinforcement is reduced, the ultimate load carrying capacity decreased (specimens A4-2 and A4-3 in Figures 4.24 and 4.25). In addition, the

analyses confirmed that larger area of strengthening used for B4 resulted in higher ultimate strength compared to other A4 specimens.

Maximum vertical CFRP strain measurements and computed maximum strains from the analyses are shown in Table 4.3. The CFRP strains were significantly underestimated by the finite element analyses. A trend of increase in the vertical CFRP strains with decreasing amount of CFRPs were observed in the finite element analyses. This trend agreed well with the trend of measured CFRP strains from the experimental results. The simplifications made in the modeling of CFRP strips, such as the actual hole geometry, bond between concrete and CFRP, resulted in the differences between measured and predicted strains. However it is possible to say that CFRP strains predicted by the finite element model confirmed the contribution of CFRPs in carrying the excessive shear forces after inclined cracking. This mechanism is studied in the next section.

4.4.2 Cracking and Strengthening Mechanism

Assuming that the ultimate states estimated by the finite element analyses were sufficiently accurate, the predicted cracking patterns can provide valuable information on the failure. Figure 4.27 shows the cracking along the symmetry axis of the specimens at their ultimate loads. For specimen A4-2, section of the slab after failure is also provided. It can be observed that cracks in the compression zone close to the loading area formed in all three specimens; however, the cracks did not widen due to the presence of CFRP reinforcement. For specimen A4-2 failure outside the shear reinforced zone was correctly predicted by the model. When only 1 layers of CFRP was used (specimen A4-3) the cracking of the compressive side of the slab inside the shear reinforced zone was inevitable. This shows that when a sufficient amount of CFRPs was used, a significant stiffness and strength contribution was provided. This delayed the

failure of concrete inside the shear reinforced zone. In this fashion, compressive side of the shear reinforced zone remained relatively undamaged, while failure was shifted outside the shear reinforced region.

Strut and tie models have widely been used in the literature both to conceptualize the transfer of forces and as a design tool (ACI 318-02). The monumental work of Morsch (1909) proposed the original 45° truss model to show the flow of forces in a reinforced concrete beam (Figure 4.28). This figure shows that concrete struts transfer the forces to the nodes, which need to be in equilibrium together with the forces from stirrups and longitudinal reinforcement. Following a similar reasoning, finite element analyses results were used to explain the flow of forces.

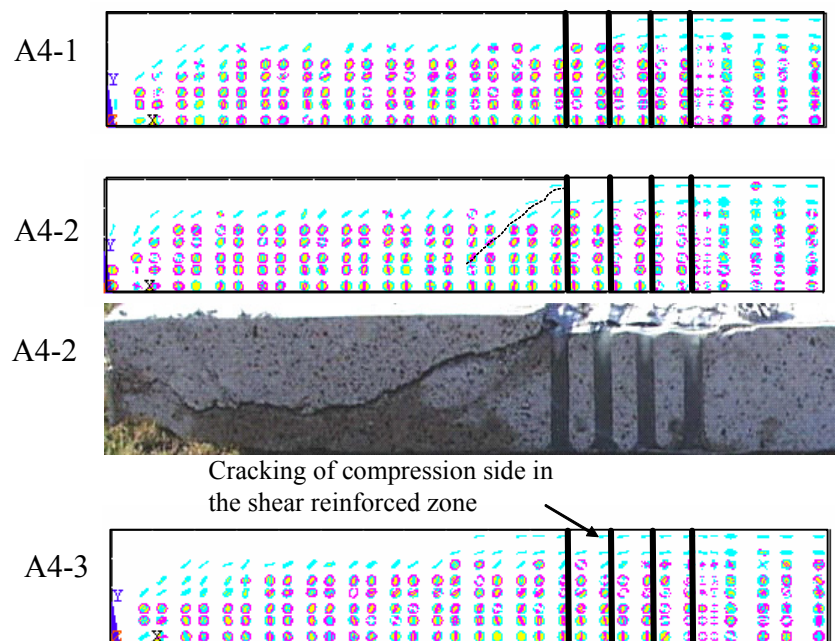
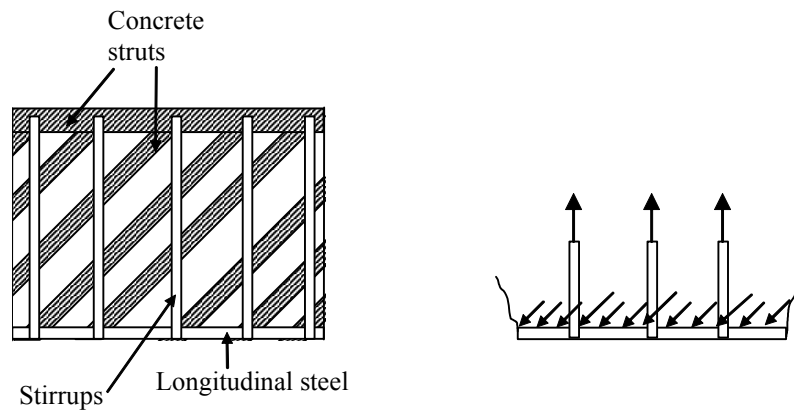


Figure 4.27 Crack Patterns from FEA at Ultimate Loads of Specimens



a) Truss Model

b) Stirrup Forces

Figure 4.28 Mörsch's Truss Model

Figure 4.29 shows the vector plot obtained from finite element analysis for the principal stresses. Strictly following the compression fields (arrows pointing inwards to label principal compressive stresses), struts were drawn and connected to the ties at the nodes. In addition to the longitudinal steel reinforcement and vertical CFRP strips as ties, concrete ties were also required outside the shear reinforced zone for nodal equilibrium. Figure 4.29 presents the strut and tie model constructed following the principal stress directions. It was also assumed that the applied load was distributed to the slab through four nodal forces.

It can be seen that the applied force was transferred by struts that joined to the vertical CFRP ties. CFRP ties carried the vertical component of the transferred force in the shear reinforced zone. Hence, CFRP shear reinforcements acted as stirrups and carried the excessive vertical forces. In the absence of CFRP shear reinforcement, these forces were resisted by concrete ties with significantly lower strength (similar to the region outside the shear reinforced zone). Outside the shear reinforced zone, concrete ties balanced the vertical component of the force

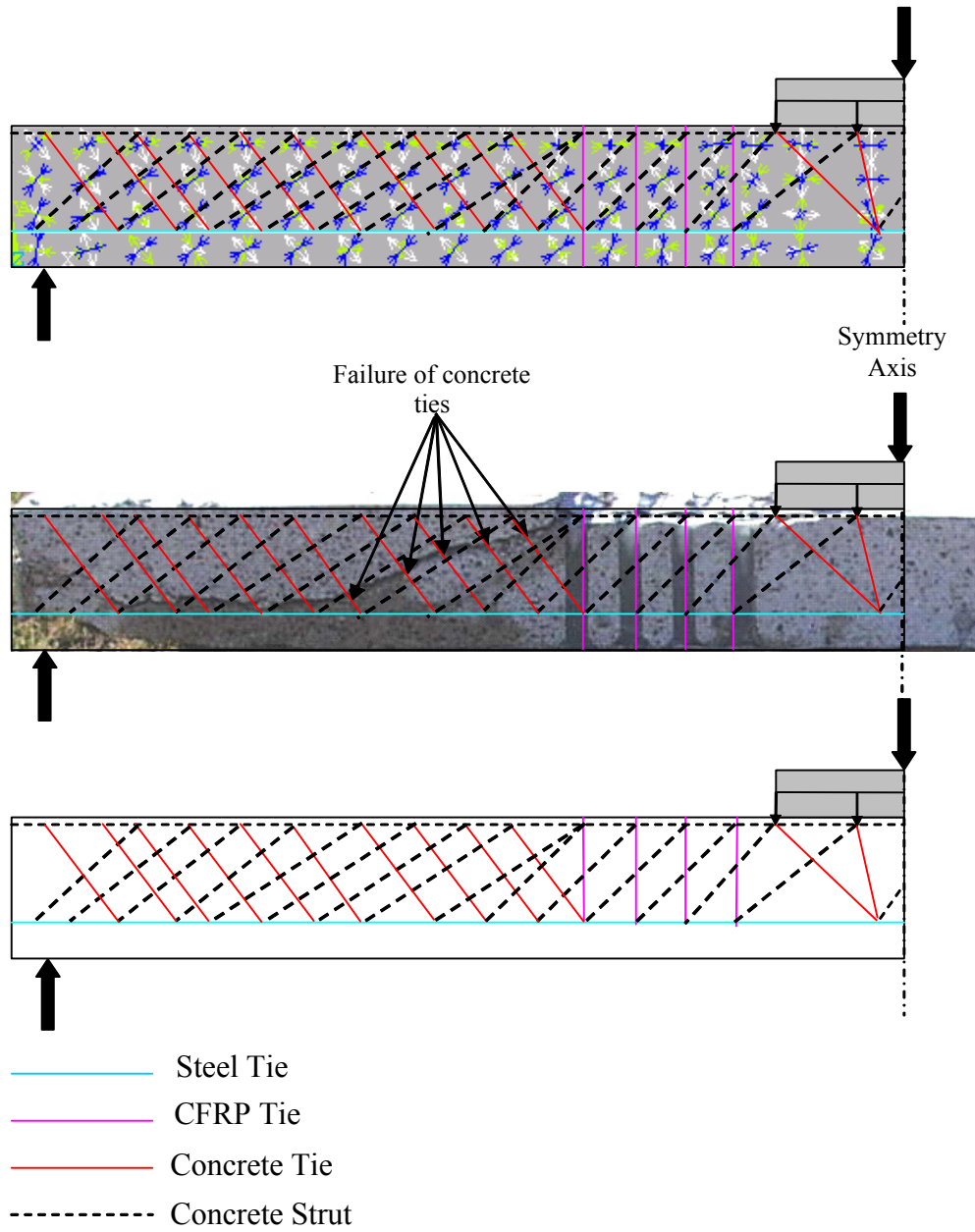


Figure 4.29 *Strut and Tie Analogy Using Principal Stress Directions from Finite Element Analyses*

from the compression struts. As shown in Figure 4.29, the formation of the predominant inclined crack was related to the progressive failure of concrete ties. This supports the fact that punching shear failure is a tension induced failure occurring due to the failure of concrete ties. The region under the loading plate would be the location of the slab-column joint in an actual flat plate system. Therefore, the ties and struts at this region were provided solely to satisfy equilibrium at the nodes. The strut and tie analogy presented in Figure 4.29 provides a visual and conceptual tool for the complex behavior of shear transfer. However, it is not practical to extend this model to three dimensions due to complex interaction of forces and possible complications in quantifying the actual strut and tie capacities that are under multiaxial state of stresses.

4.4.3 Principal Stresses and Failure Surfaces

The maximum and minimum principal stresses around the upgraded region of the specimens are presented in Figure 4.30 to 4.32 for specimens A4-1, A4-2, and A4-3, respectively. In addition, top surfaces of slabs after failure are also provided for each specimen. It can be observed that the corner of the loading area was under a triaxial compressive state of stress for all three specimens similar to that of the control specimen. Failure of the corner was not observed in the experiments and this can be attributed to confinement in this triaxial stress state.

Along the lines of CFRP shear reinforcement locations on the top surfaces of the slab (Figure 4.30), maximum principal stresses (S_1) were compressive but very close to zero (in the order of 0.1 to 0.2 ksi). In addition, the minimum principal stresses (S_3) were compressive and were about 1.5 times of the compressive strength of concrete. It is apparent that there were stress

concentrations along the actually observed failure surfaces. When the dominant inclined crack reached the top surface of the slab, the maximum principal stresses changed from compression to tension. This led to the failure of the top surface along the locations of stress concentration. In fact, the locations of the stress concentrations were similar to the observed “zip-in” failure mode.

For specimen A4-2, finite element analysis results suggested two possible failure-locations on the top of the surface based on principal stress contours:

- 1- Failure surface similar to that observed in A4-1 specimen (Figure 4.30) i.e. occurrence of “zip-in” failure mode,
- 2- Failure outside the shear reinforced zone as shown in Figure 4.27.

Failure of the slab occurred following these paths when the dominant shear crack both widened and increased in length approaching the compression side of the slab.

The maximum and minimum principal stress contours for specimen A4-3 are given in Figure 4.32. In this specimen, failure was spread around and inside the shear reinforced zone. Stress contours for this specimen indicated the presence of critical stress states both inside and outside the shear reinforced zone. Accordingly, failure took place in both locations as shown in Figure 4.32. Since the amount of CFRP stirrups used in this specimen was half of that used in specimen A4-2, significant damage was observed in the shear reinforced zone (Figure 4.27).

In short, it is possible to say that maximum and minimum principal contours at the top surface of the specimens were good indicators for the actual failure surface. However, explanation of more complicated phenomena such as failure of CFRPs at the corners and accurate prediction of strain levels in CFRPs require more detailed modeling of the interface between concrete and CFRPs. Such detailed modeling is beyond the scope of this study.

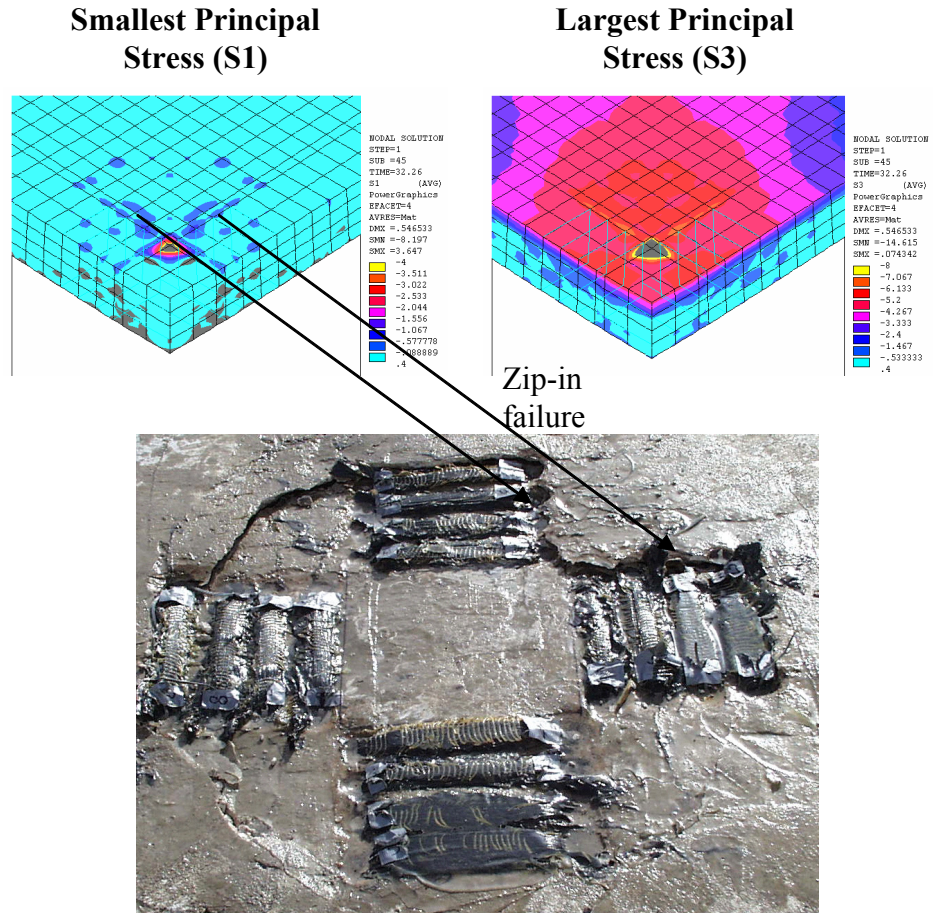


Figure 4.30 Principal Stresses and Failed Surface for Specimen A4-1

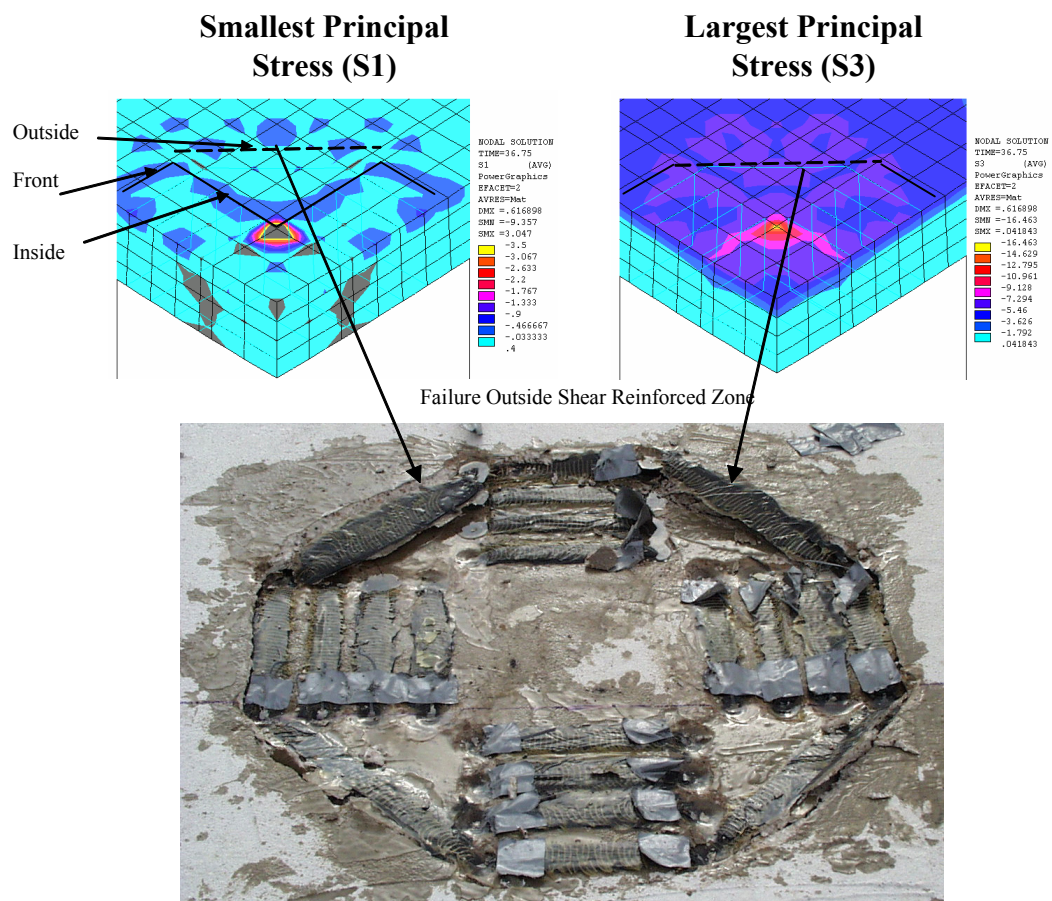


Figure 4.31 Principal Stresses and Failed Surface for Specimen A4-2

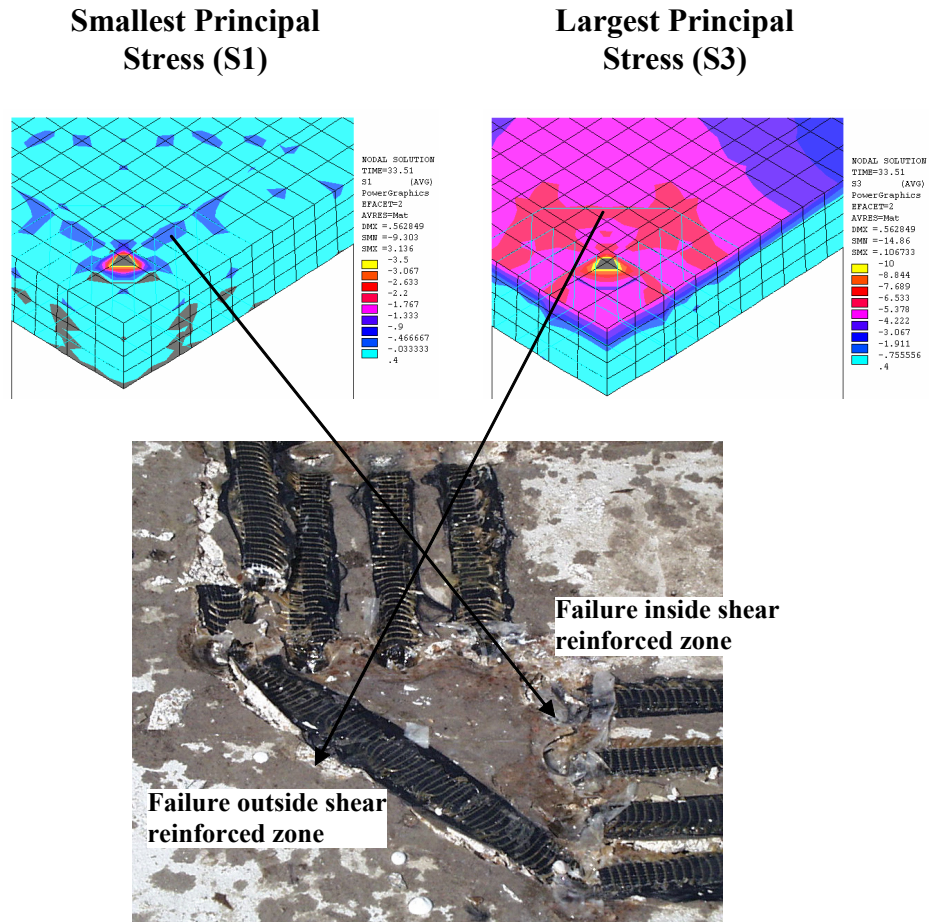


Figure 4.32 Principal Stresses and Failed Surface for Specimen A4-3

CHAPTER 5

Evaluation of Code Requirements and Proposed Design Procedure

5.1 GENERAL

In light of the experimental results, examination of code requirements for punching shear resistance of slab-column connections subjected to pure shear transfer and combined moment and shear transfer is presented in this chapter. Relevant provisions of ACI 318-02, CEB-FIP MC90, CSA-A23.3-94 and BS 8110-97 are included in this discussion. Moreover, a punching shear upgrade design procedure that employs punching shear strength provisions of ACI 318-02 is presented. Strengthening schemes studied in Chapters 2 and 3 are used in this design procedure.

5.2 EXAMINATION OF CODE PROCEDURES AND DESIGN

5.2.1 Pure Shear Transfer

Detailed explanations of the code approaches for punching shear design are presented in Section 1.4.4. A brief summary of ACI 318-02, CEB-FIP MC90, and CSA-23.3-94 provisions for punching shear strength are given below. Unless otherwise stated, all units are given in US Customary Unit System.

5.2.1.1 ACI 318-02

Punching shear strength of slab-column connections without shear reinforcement (or with shear reinforcement for capacity outside the shear reinforced zone) are calculated using the following expressions :

$$v_c = \min \left\{ 4\sqrt{f_c'} ; \left(\frac{\alpha_s}{(b_o/d)} + \frac{1}{2} \right) 4\sqrt{f_c'} ; \left(\frac{1}{2} + \frac{1}{B} \right) 4\sqrt{f_c'} \right\} \text{ [lb-in.]} \quad (5.1)$$

$$v_c = \min \left\{ \frac{1}{3}\sqrt{f_c'} ; \left(\frac{\alpha_s}{(b_o/d)} + \frac{1}{2} \right) \frac{1}{3}\sqrt{f_c'} ; \left(\frac{1}{2} + \frac{1}{B} \right) \frac{1}{3}\sqrt{f_c'} \right\} \text{ [N-mm]}$$

here f_c' is the compressive strength of concrete, d is the average effective depth, B is the aspect ratio of the column section and b_o is the length of the critical perimeter $d/2$ away from the column face (or from the outermost shear reinforcement) as shown in Figure 1.14. The load carrying capacity outside the shear reinforced zone, V_u^o , is calculated by:

$$V_u^o = v_c b_o d \quad (5.2)$$

When stirrups are used as shear reinforcement, the shear capacity inside the shear reinforced zone, V_u^i , is calculated as follows:

$$V_u^i = V_c + V_s \leq 3V_c \quad (5.3)$$

$$V_c = 2\sqrt{f_c'} b d \quad (5.4)$$

$$V_s = A_{sv} f_y \frac{d}{s} \quad (5.5)$$

V_c is the concrete contribution inside the shear reinforced zone, b is the critical perimeter $d/2$ away from the column face in Equation (5.4) (Figure 1.14). V_s is the contribution of stirrups, and A_{sv} , f_y , and s are the total area of the transverse reinforcement, yield strength of steel, and spacing of the stirrups, respectively.

5.2.1.2 CEB-FIP Model Code 90

In addition to the parameters considered by ACI 318-02, CEB-FIP Model Code 90 considers the size effect and the effect of the reinforcement ratio. Equation (5.6) is recommended to compute the punching shear capacity without shear reinforcement (or with shear reinforcement for capacity outside the shear reinforced zone).

$$V_u^o = 0.18 \xi (100 \rho f_c')^{1/3} u d \quad [\text{N-mm}] \quad (5.6)$$

$$\xi = 1 + \sqrt{\frac{200}{d}} \quad (5.7)$$

where ξ is a parameter used to incorporate the size effect, ρ is the flexural reinforcement ratio, and u is the length of the critical perimeter located at a distance of $2d$ away from the column face (or from the outermost shear reinforcement) as shown in Figure 1.17.

Punching shear capacity inside the shear reinforced zone is calculated using Equation (5.8).

$$V_u^i = 0.135 \xi (100 \rho f_c')^{1/3} u d + V_s \quad [\text{N-mm}] \quad (5.8)$$

where u is calculated for the perimeter located $2d$ away from the face of the column and it is given with the following expression for square columns:

$$u = 4(c + \pi d) \quad (5.9)$$

The contribution of the shear reinforcement, V_s can be calculated using a similar expression to Equation (5.5). The maximum capacity associated with concrete crushing at the column face is as follows:

$$V_{\max} = 0.6 (0.5 f_c') \left(1 - \frac{f_c'}{250}\right) (f_c') u_o d \quad [\text{N-mm}] \quad (5.10)$$

where u_o is the perimeter of the loading area or the column.

In order to put the code provisions in perspective, ultimate loads of concentrically loaded slab-column connections without shear reinforcement, previously tested by various researchers (Elstner and Hognestad 1956, Corley and Hawkins 1968, Broms 1990, Regan 1984) and capacities of control specimens tested in this study are compared with the nominal capacities obtained by using the relevant code provisions. The non-dimensional effective shear stresses at the critical perimeter are plotted against the reinforcement ratio for a total of 67 specimens in Figure 5.1 and Figure 5.2. ACI 318-02 provisions do not consider the effect of reinforcement ratio on punching shear resistance however they establish a lower bound to the experimental data. ACI 318-02 provisions for punching shear resistance are meant to be safe and simple; hence they are independent of the flexural capacity. CEB-FIP provisions consider additional parameters such as size effect and flexural capacity for computing the punching shear capacity. The effect of reinforcement ratio on punching shear resistance is considered with cubic root dependence. It is interesting to note that for the practical range of reinforcement ratios (typically 0.5 to 1.0 % used in gravity load design) the effect of reinforcement ratio on punching capacity is not apparent and can therefore be neglected.

5.2.1.3 CSA-A23.3-94

CSA-A.23.3-94 provisions for punching shear resistance of slab-column connections without shear reinforcement (or with shear reinforcement for capacity outside the shear reinforced zone) are similar to the provisions of ACI 318-02 and are presented in Section 1.4.4.2. The code expressions for the contribution of stirrups and SSR to punching shear resistance are given below for comparison:

$$V_n^i = 2.4 \lambda \sqrt{f_c'} b d + \frac{A_{sv} f_y d}{s} \leq 7.2 \lambda \sqrt{f_c'} b d \quad (\text{for stirrups}) \quad (5.11)$$

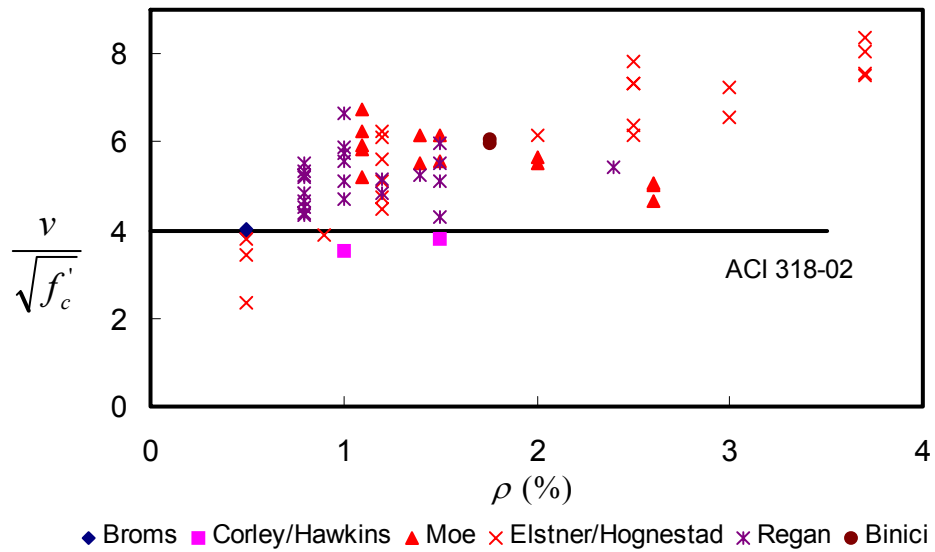


Figure 5.1 Comparisons of ACI 318-02 Provisions with Experimental Data

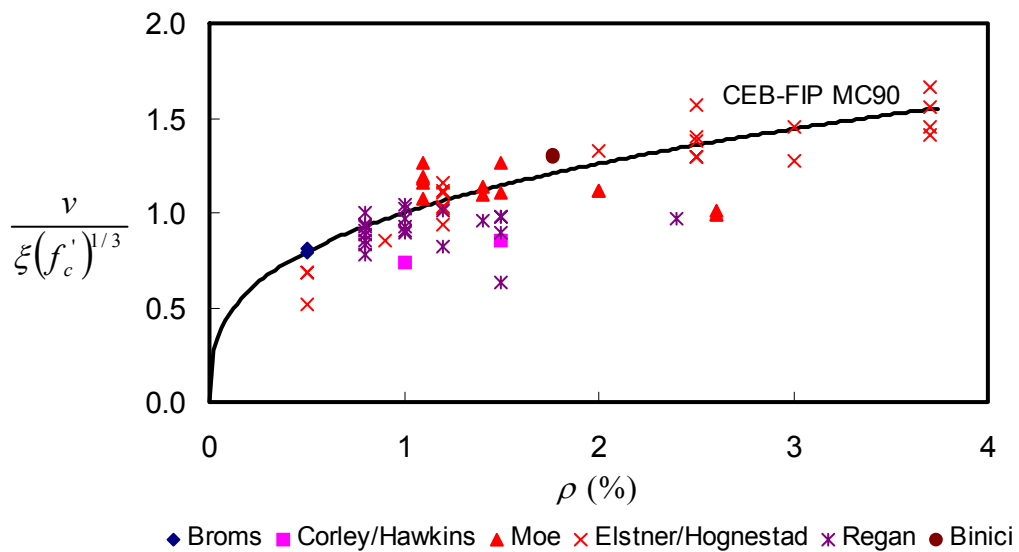


Figure 5.2 Comparisons of CEB-FIP MC90 Provisions with Experimental Data

$$V_n^i = 3.6 \lambda \sqrt{f_c'} b d + \frac{A_v f_y d}{s} \leq 9.6 \lambda \sqrt{f_c'} b d \quad (\text{for SSR}) \quad (5.12)$$

where λ is 1.0, 0.85, and 0.6 for normal weight, semi-lightweight and lightweight concrete, respectively.

Equations (5.11) and (5.12) imply that performance of slab-column connections with SSR are superior in comparison to those with stirrups. The difference can be observed both for concrete contribution inside the shear reinforced zone ($2.4 \lambda \sqrt{f_c'} b d$ vs. $3.6 \lambda \sqrt{f_c'} b d$) and maximum punching shear capacity ($7.2 \lambda \sqrt{f_c'} b d$ vs. $9.6 \lambda \sqrt{f_c'} b d$). This is primarily due to research findings of Ghali and his collaborating investigators, who showed the superior anchorage properties of SSR as discussed in Section 1.4.1.5.

5.2.1.4 Examination of Code Provisions

First, comparisons of computed capacities of test specimens using relevant provisions of ACI 318-02 and CEB-FIP MC90 with the test results are presented in this section. Following that, comparisons of calculated capacities according to CSA-A.23.3-94 and BS 8110-97 with experimental capacities are discussed. For the test specimens strengthened with external CFRP stirrups, capacities inside (V_u^i) and outside (V_u^o) the CFRP reinforced zone were calculated. V_u^o values were calculated using code given shear strength expressions with a critical perimeter located outside the shear reinforced zone (Figure 5.3). The smaller of the two capacities was taken as the punching strength of the test specimens. V_u^i values were calculated using the concrete contribution expressions given in the codes and the following expression for CFRP contribution:

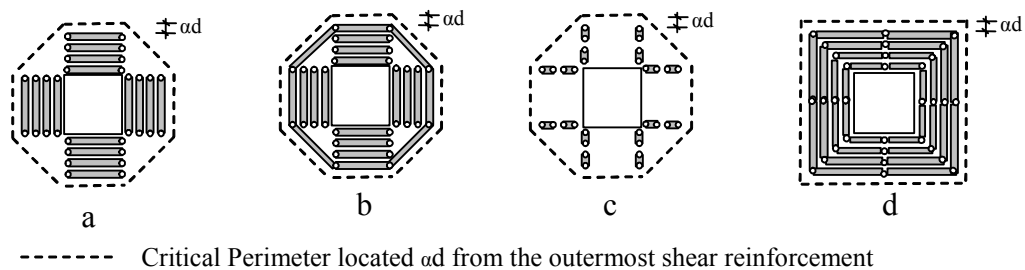


Figure 5.3 Critical Perimeters for Strengthened Specimens (Plan View)

$$V_{FRP} = 0.004 E_{FRP} A_{FRP} \frac{d}{s} \quad (5.13)$$

In Equation (5.13), E_{FRP} is the modulus of elasticity of CFRP used in the tests, A_{FRP} is the total cross sectional area of CFRP per perimeter, and s is the spacing of CFRP reinforcement. This expression is similar to the V_s in Equation (5.5). However, the $(A_{sv}f_y)$ term is replaced with $(0.004 E_{FRP} A_{FRP})$. The useable strain level, (0.004), is established considering the linear elastic and brittle nature of fiber reinforced polymers. Therefore, vertical strains in externally installed CFRP stirrups are limited to 0.004 to calculate CFRP contribution inside the CFRP reinforced zone. As explained in Chapter 2 when higher strains were allowed in vertical CFRP legs, punching shear failure occurred inside the shear reinforced zone due to excessive deformation demands on concrete. In such cases, wide shear cracks diminished concrete contribution to punching shear strength significantly. It is shown in Section 5.2.1.5 that the use of 0.004 strain limit in performing the shear design of all upgraded specimens in this study resulted in safe designs. The use of a lower limiting strain would result in safer designs, and the use of a higher limiting strain would likely result in connection upgrades that are prone to shear failure inside the CFRP reinforced region.

The capacity computed inside and outside the shear reinforced zone, predicted failure location by the two codes, and the ratio of predicted to

experimental ultimate loads are listed in Table 5.1. Since CEB-FIP MC90 accounts for the effect of flexural reinforcement ratio on the punching capacity, the predictions obtained through the use of CEB-FIP MC90 were more accurate for the two control specimens. ACI 318-02 does not take into account the effect of flexural reinforcement on punching shear strength, resulting in simpler and more conservative expressions.

The use of ACI 318-02 provisions for punching shear strength resulted in safe predictions for all the specimens tested in this study. Ratio of experimental to predicted ultimate loads ranged from 1.09 to 2.13 with a mean of 1.40 for all specimens. Computed capacities of control specimens were very conservative because of the exclusion of the effect of reinforcement ratio on punching shear strength. Figure 5.1 clearly illustrates this phenomenon. However, failure locations in all specimens except A4-1, A4-2 and B8 were estimated correctly. A discrepancy was observed for specimen A4-3 for which the computed ultimate strength according to ACI 318-02 provisions was smaller than that of the control specimen. The conservative estimate of concrete strength inside the shear

Table 5.1 Experimental and Computed Punching Shear Strength of Test Specimens (ACI 318-02, CEB-FIP MC90)

Specimen	Experiment		ACI 318-02				CEB-FIP MC 90						
	V_u (k)	Failure Location	V_c^o (k)	V_c^i (k)	$V_{ACI} = \text{Min}(V_c^o, V_c^i)$	Failure Location	V_u/V_{ACI}	V_c^o (k)	V_c^i (k)	$V_{CEB} = \text{Min}(V_c^o, V_c^i)$	Failure Location	V_u/V_{CEB}	
Control 1	110	-	76	-	76	-	1.45	105	-	105	-	1.05	
Control 2	114	-	76	-	76	-	1.50	105	-	105	-	1.08	
A 4-1	133	Inside/Outside	113	146	113	Outside	1.18	144	187	144	Outside	0.92	
A 4-2	149	Outside	113	92	92	Inside	1.62	144	133	133	Inside	1.12	
A 4-3	139	Inside	113	65	65	Inside	2.13	144	106	106	Inside	1.31	
A 4-4	135	Inside	113	92	92	Inside	1.46	144	133	133	Inside	1.02	
A6	161	Outside	127	146	127	Outside	1.27	170	187	170	Outside	0.95	
A8	166	Outside	142	146	142	Outside	1.17	195	187	187	Inside	0.89	
B4	170	Outside	126	133	126	Outside	1.35	184	174	174	Inside	0.98	
B6	169	Outside	147	160	147	Outside	1.15	220	201	201	Inside	0.84	
B8	175	Outside	168	160	160	Inside	1.09	256	201	201	Inside	0.87	
							Mean :	1.40				Mean:	1.00
							Stdev :	0.30				Stdev:	0.14

$V_{\text{max-ACI}} = 114$ k
 $V_{\text{max-CEB}} = 236$ k

reinforced zone, V_c (Equation (5.4)) was responsible for this discrepancy. Hence, for cases where shear reinforcement in the form of CFRP stirrups with proper anchorage, the V_c term, which is the concrete contribution inside the shear reinforced region can be increased. The concrete contributions inside the CFRP reinforced zone computed by using measured vertical CFRP strains (Table 2.8 in Section 2.7.2.3) also support this argument. In this way, more economical designs can be achieved preserving the conservative nature of related ACI 318-02 provisions. The proposed modifications to ACI 318-02 provisions for punching shear upgrade design using externally installed CFRPs are explained in detail in the next section.

The ratio of experimental capacities to the computed capacities using CEB-FIP MC90 ranged from 0.84 to 1.31 with a mean of 1.00. Although CEB-FIP provisions provided a better estimate for the experimental results, these provisions did not estimate the locations of punching shear failure correctly for all specimens except specimens A4-3, A4-4 and A6. This is due to the fact that the critical perimeter constructed $2d$ away from the outermost shear reinforcement resulted in unsafe estimations of the capacities outside the shear reinforced zone.

For specimens A4-1 and A4-2, the locations of punching shear failure were not estimated correctly by either code. Although a smaller amount of shear reinforcement was used in A4-2 in comparison to A4-1, with proper placement of diagonal stirrups that are anchored in alternative directions (Figure 2.36), punching shear failure occurred outside the reinforced region for A4-2. However, punching shear failure penetrated into the shear reinforced zone in specimen A4-1. The code expressions are meant to be used for design of shear reinforcement in the form of stirrups. They relate the area of transverse reinforcement to an increase in punching shear capacity. The use of external CFRP stirrups (placed parallel to the sides of the loading plate and diagonally with proper anchorage)

resulted in an increase in concrete contribution as they helped in controlling width of the cracks in the CFRP reinforced zone. Consequently, increased aggregate interlock along the shear crack and relatively undamaged compression zone contributed to punching shear strength increase. This effect is not considered in the code expressions.

In the design provisions of ACI 318-02 and CEB-FIP MC 90, there is an upper limit on punching shear capacity. Even if substantial amounts of shear reinforcement are used, punching shear strength is limited by this maximum capacity. The upper limit is used to eliminate possible crushing of concrete at the slab-column interface prior to reaching the calculated punching shear capacity. The maximum limit on the capacity inside the shear reinforced zone (V_u^i) given by ACI 318-02 ($3V_c$) was exceeded for Specimens A6 and A8, B4, B6, and B8. This limit was not used in the calculations since crushing was not observed in the test specimens prior to punching failure. However, the maximum values for both codes are presented at the bottom of Table 5.1. For CEB-FIP MC90, maximum capacity did not govern the capacity of the test specimens.

An important observation from Table 5.1 is that punching shear capacity outside the shear reinforced zone was one of the most important factors affecting the ultimate capacity of the test specimens. When properly anchored and detailed CFRP stirrups were used as shear reinforcement, critical punching perimeter was shifted outside the shear reinforced zone. The average shear stresses at the critical perimeter outside the shear reinforced zone are plotted against b_o/d ratios of test specimens in Figure 5.4. This figure also illustrates the reduction in punching shear strength with increasing b_o/d ratios as per ACI 318-02. A similar plot showing the relationship between b_o/d ratios and normalized punching shear strength outside the shear reinforced zone calculated by CEB-FIP MC90 is shown in Figure 5.5. It is apparent that ACI provisions provide a lower bound for the

strength estimations outside the shear reinforced zone and they account for the decrease in shear strength as b_o/d values increase. In fact, this is the main reason

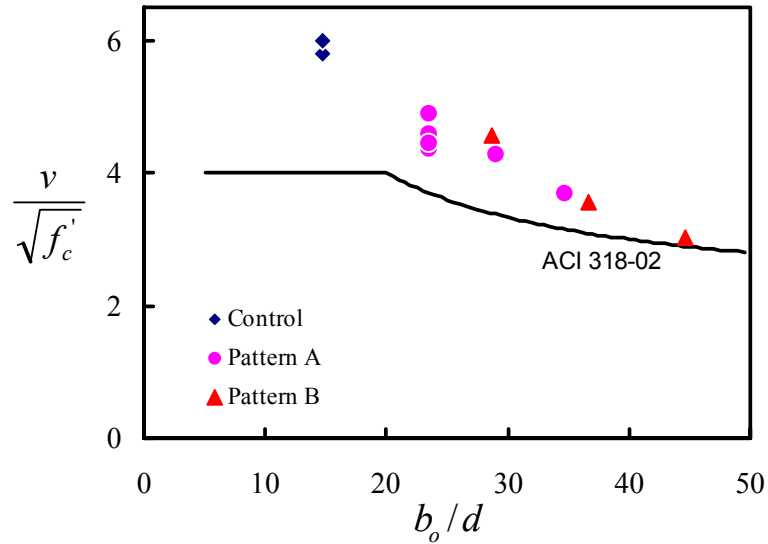


Figure 5.4 Normalized Shear Strength outside the Shear Reinforced Zone and Comparisons with ACI 318-02 Provisions

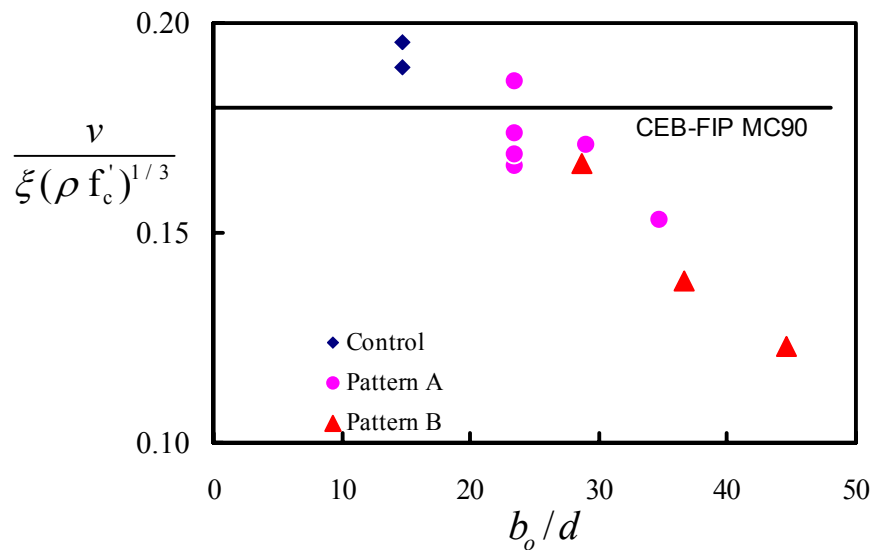


Figure 5.5 Normalized Shear Strength outside the Shear Reinforced Zone and Comparisons with CEB-FIP MC 90 Provisions

why ACI Code estimations for failure locations were accurate. On the other hand, CEB-FIP MC90 does not account for the decrease in shear strength with increasing critical perimeters. As a result, for critical perimeters located $2d$ away from the outermost shear reinforcement, CEB-FIP provisions overestimated the punching shear capacity.

The computed load carrying capacities and estimated failure locations obtained through the use of CSA-A23.3-94 and BS 8110-97 (relevant code provisions given in Section 1.4.4.3) are presented in Table 5.2. In these calculations, Equation (5.13) was used to compute contribution of CFRP shear reinforcement. It can be observed that CSA A23.3-94 estimations of failure locations were similar to those of ACI 318-02. The only unsafe estimate according to CSA-A23.3-94 was observed for specimen A4-1. On the other hand, BS 8110-97 estimations were on the unsafe side except specimens Control-2 and A4-2 (Table 5.2). BS 8110-97 considers similar parameters to those considered in CEB-FIP MC90, i.e. flexural reinforcement ratio, size effect, and concrete strength, resulting in accurate estimations of punching shear strength for cases where no shear reinforcement was used. The fact that BS- 8110-97 suggests to use the same concrete contribution to shear strength term, V_c , inside and outside the shear reinforced region yielded overestimations of punching shear capacity.

The measured and computed punching shear capacities of the test specimens are shown and compared in Figure 5.6. An examination of this figure indicates that ACI Code is the only design code that provided conservative strength predictions for all test specimens.

Table 5.2 Experimental and Computed Punching Shear Strength of Test Specimens (CSA-A23.3-94, BS-8110-97)

Specimen	Experiment		CSA-A23.3-94					BS 8110-97				
	V_u , (k)	Failure Location	V_c^o (k)	V_c^i (k)	$V_{CSA} = \text{Min}(V_c^o, V_c^i)$	Failure Location	V_u/V_{CSA}	V_c^o (k)	V_c^i (k)	$V_{BS} = \text{Min}(V_c^o, V_c^i)$	Failure Location	V_u/V_{BS}
Control 1	110	-	91	-	91	-	1.21	113	-	113	-	0.98
Control 2	114	-	91	-	91	-	1.25	113	-	113	-	1.01
A 4-1	133	Inside/Outside	135	154	135	Outside	0.98	145	222	145	Outside	0.91
A 4-2	149	Outside	135	100	100	Inside	1.49	145	167	145	Outside	1.03
A 4-3	139	Inside	135	73	73	Inside	1.91	145	140	140	Inside	0.99
A 4-4	135	Inside	135	100	100	Inside	1.35	145	167	145	Outside	0.93
A6	161	Outside	153	154	153	Outside	1.06	173	222	173	Outside	0.93
A8	166	Outside	170	154	154	Inside	1.08	202	222	202	Outside	0.82
B4	170	Outside	151	140	140	Inside	1.21	183	208	183	Outside	0.93
B6	169	Outside	176	168	168	Inside	1.01	223	235	223	Outside	0.76
B8	175	Outside	201	168	168	Inside	1.04	263	235	235	Maximum	0.74
$V_{\text{max-CSA}} = 136 \text{ k}$							Mean :	1.24		Mean:		0.91
$V_{\text{max-BS}} = 226 \text{ k}$							Stdev :	0.27		Stdev:		0.10

5.2.1.5 Proposed Design Procedure Using ACI 318-02 Provisions

Based on the above analyses, it can be concluded that punching shear strength provisions of ACI 318-02 can be used in designing slab-column connection upgrades. ACI 318-02 provisions were selected as they provided conservative estimates for punching shear strength of specimens tested in this study. In addition, they were successful in estimating the failure modes and locations of failure in most cases.

The concrete contribution to shear strength (V_c) profiles computed based on strain measurements are shown in Figure 5.7. In addition, concrete contribution given by $2\sqrt{f'_c}$ and $3\sqrt{f'_c}$ are also shown in the same figure. It can be observed that for the specimens tested in this study the concrete contribution can be increased from $2\sqrt{f'_c}$ (ACI 318-02 V_c value for slab-column connections

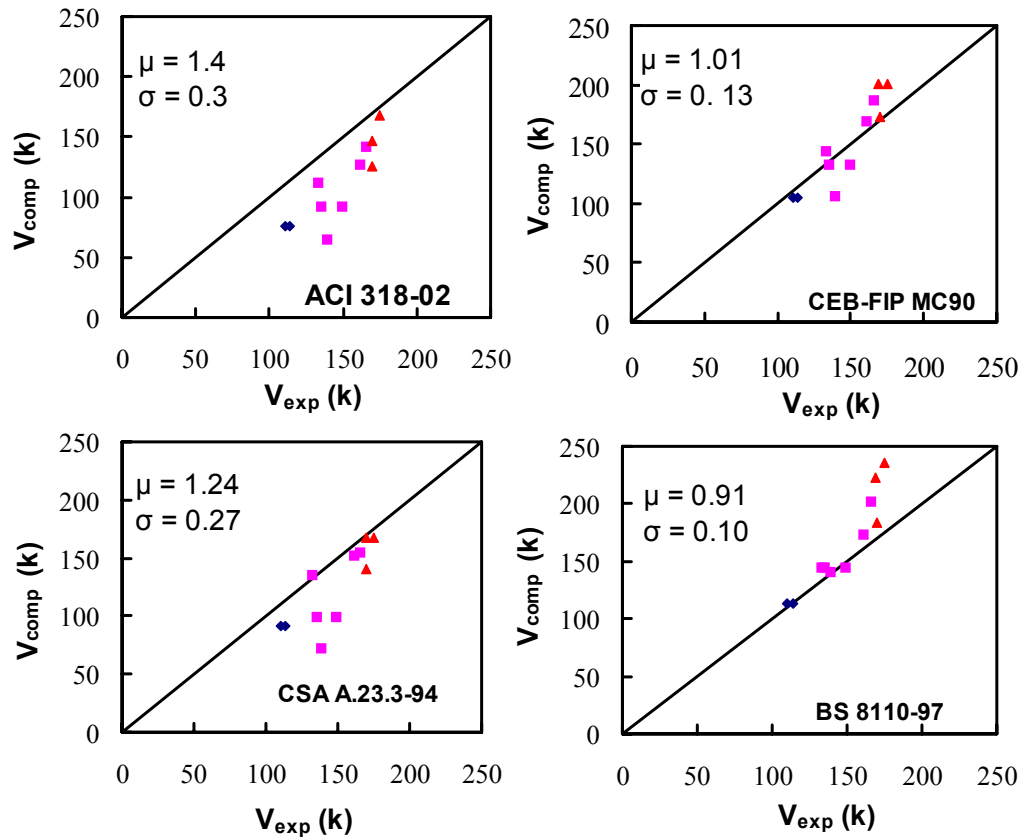


Figure 5.6 Comparisons of Computed and Measured Capacities

with stirrups) to $3\sqrt{f'_c}$. The modified and relaxed form of the concrete contribution still establishes a lower bound for the test data (Figure 5.7). The following expression for concrete contribution inside the shear reinforced zone is proposed as a replacement to Equation (5.4) for slabs strengthened with external CFRP stirrups:

$$V_c = 3\sqrt{f'_c}bd \quad (5.14)$$

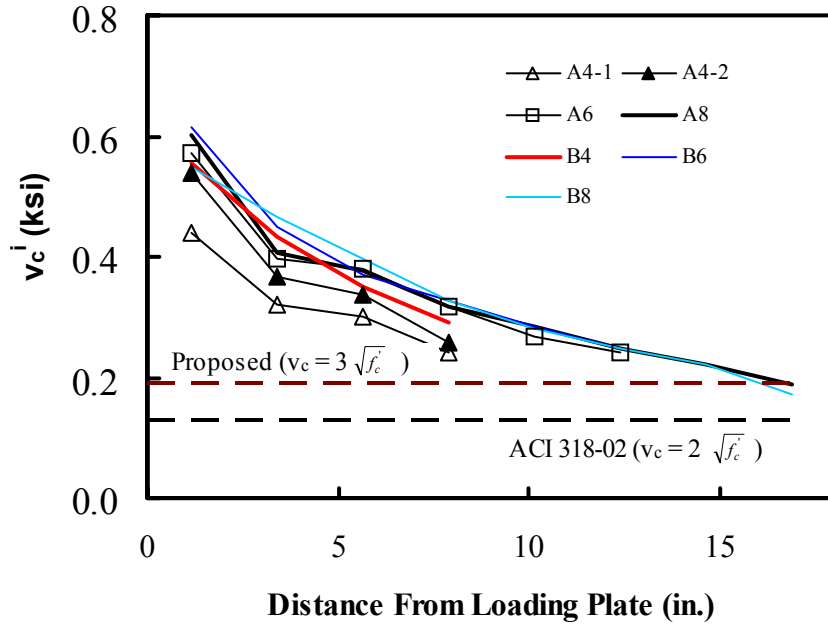


Figure 5.7 Concrete Contribution inside the Shear Reinforced Zone

where b is the critical perimeter located $d/2$ away from the column face. The proposed value of V_c is between the ACI 318-02 V_c value given for connections with stirrups ($2\sqrt{f'_c}$) and the CSA.23.3-94 V_c value recommended for use in connections reinforced with shear stud rails ($3.6\sqrt{f'_c}$).

Assuming that the punching shear capacity can be computed using the critical perimeter located outside the shear reinforced zone, then the required FRP contribution can be computed as follows:

$$V_{FRP} = V_u^o - V_c = v_c b_o d - 3\sqrt{f'_c} b d \quad (5.15)$$

in which v_c and V_c are computed using Equations (5.1) and (5.14), respectively. The critical perimeter located outside the shear reinforced zone is denoted with b_o whereas the critical perimeter located $d/2$ from the column face is given by b . The

experimental and required CFRP contributions per perimeter are presented in Table 5.3. The experimental CFRP contributions were calculated using the strain measurements in vertical legs of CFRP stirrups. The required CFRP contributions were calculated using Equations (5.13) and (5.15). It can be observed that when V_c was computed based on Equation (5.14), and using an outer perimeter located $0.5d$ away ($\alpha=0.5$) from the outermost shear reinforcement as shown in Figure 5.3, CFRP demand and supply were reasonably similar. For specimens strengthened with A4 type CFRP arrangement, the required amount of vertical CFRP was calculated as 2.1 layers per hole using modified ACI 318-02 expressions. This amount is similar to the actual amount of CFRP reinforcement used in specimen A4-2. In fact, this specimen had the optimum amount of CFRP as was shown in Figure 2.35.

Another important modification required is for the maximum punching shear strength, which is given in ACI 318-02 to limit the capacity based on concrete crushing. Since no crushing of concrete is observed inside the shear reinforced zone for any of the specimens, it is reasonable to relax V_{cmax} and use the following expression:

$$V_{cmax} = 8\sqrt{f'_c}bd \quad (5.16)$$

in which b is the critical perimeter located $d/2$ away from the column face. According Equations (5.14) and (5.16), CFRP contribution is limited to $5\sqrt{f'_c}bd$. With this modification, the upper limit on punching shear capacity governs only for specimen B8, with the highest failure load. Therefore Equation (5.16) still provides safe estimates for the maximum punching shear capacity for all the test specimens. In addition the proposed value of V_{cmax} is between the ACI 318-02 V_{cmax} value given for connections reinforced with stirrups ($6\sqrt{f'_c}$) and the

Table 5.3 Comparison of CFRP Amounts: Design vs. Experiments

Specimen	CFRP Contribution Based on Modified ACI 318-02, V_{FRP} (k)	CFRP Contribution from Experiments, V_{FRP} (k)	CFRP layers per leg based on Modified ACI 318-02	Actual CFRP layers per leg in Experiments
Control 1	-	-	-	-
Control 2	-	-	-	-
A 4-1	55.5	52.1	2.1	4.0
A 4-2	55.5	53.9	2.1	2.0
A 4-3	55.5	64.5	2.1	1.0
A 4-4	55.5	53.9	2.1	2.0
A6	70.2	45.1	2.6	3.0
A8	84.8	48.4	3.2	3.0
B4	69.2	65.4	2.6	3.0
B6	89.9	41.3	3.3	4.0
B8	95.1	62.0	3.5	4.0

Each layer is 0.04 in (thickness) x 1in. (width).

CSA.23.3-94 V_{cmax} value given for connections reinforced with shear stud rails ($9.6\sqrt{f'_c}$).

The predictions obtained by using modified ACI 318-02 provisions for punching shear strength of CFRP strengthened slab-column connections are given in Table 5.4. In addition, this table presents ratios of predicted to observed capacities for ACI 318-02 predictions without any modifications (same as those presented in Table 5.1). When modified ACI 318-02 provisions were used, the ratio of predicted to observed capacities ranged between 1.15 and 1.65 (Table 5.4). The average of these ratios was about 1.3 with a standard deviation of 0.16. The proposed modifications resulted in a reduced scatter (standard deviation) with a better correlation of the predicted and computed capacities. Furthermore, the safe nature of ACI 318-02 provisions was not compromised. The predicted and experimental capacities of the test specimens listed in Table 5.4 are presented in

Table 5.4 Capacity Estimations with Modified ACI 318-02 Provisions

Specimen	Experiment		Modified ACI 318-02				ACI 318-02		
	$V_{u,}$ (k)	Failure Location	V_c^o (k)	V_c^i (k)	$V_{pred} = \text{Min}(V_c^o, V_c^i)$	Failure Location	V_u/V_{pred}	V_u/V_{ACI}	
Control 1	110	-	76	-	76	-	1.45	1.45	
Control 2	114	-	76	-	76	-	1.50	1.50	
A 4-1	133	Inside/Outside	113	165	113	Outside	1.18	1.18	
A 4-2	149	Outside	113	111	111	Inside	1.34	1.62	
A 4-3	139	Inside	113	84	84	Inside	1.65	2.13	
A 4-4	135	Inside	113	111	111	Inside	1.21	1.46	
A6	161	Outside	127	165	127	Outside	1.27	1.27	
A8	166	Outside	142	165	142	Outside	1.17	1.17	
B4	170	Outside	126	152	126	Outside	1.35	1.35	
B6	169	Outside	147	179	147	Outside	1.15	1.15	
B8	175	Outside	152	179	152	Maximum	1.15	1.09	
$V_{max-ACI} = 152$ k							Mean :	1.31	1.40
							Stdev :	0.16	0.30

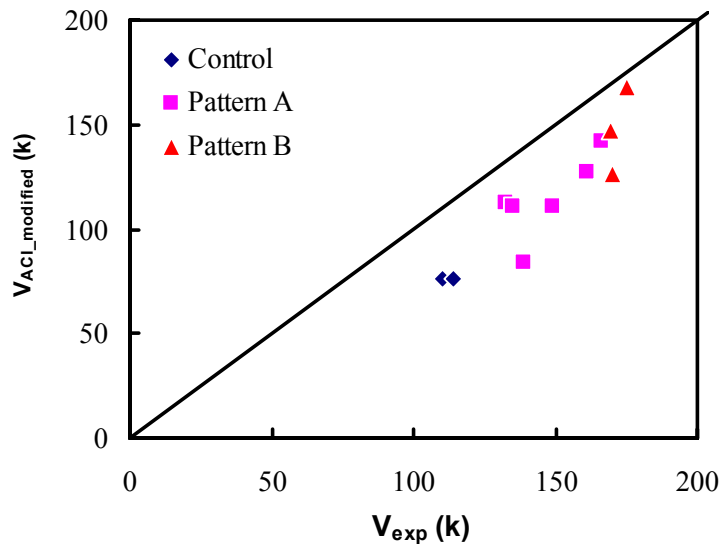


Figure 5.8 Comparison of Modified ACI Estimations with Experimental Results

Figure 5.8. This figure clearly shows that safe designs can be obtained by using the proposed modifications.

The predicted capacity of specimen B8 was controlled by the maximum capacity given by Equation (5.16). This result implies that for slab-column connections (with similar geometry and material properties to the test specimens) strengthened using more than eight CFRP perimeters with pattern B, maximum punching shear capacity, V_{cmax} , governs. Additional experiments for slabs with more than eight CFRP perimeters are required to investigate if crushing of concrete will actually occur inside the shear reinforced zone.

The proposed design procedure given as a flowchart in Figure 5.9 can be summarized as follows:

1. Determine geometric and material properties of the slab-column connection.
2. Confirm that the required punching shear strength is smaller than the maximum permissible punching shear strength, V_{cmax} . If not, reduce the demand by decreasing the gravity load.
3. Compute the required critical perimeter outside the shear reinforced zone such that required punching shear capacity can be achieved.
4. Assume number of perimeters and strengthening pattern.
5. Change number of perimeters until the length of the outer perimeter is greater than that of the computed critical perimeter.
6. Compute required amount of FRP reinforcement per hole.
7. Detail the FRP shear reinforcement. Use closed loops for FRP anchorage overlapped at the slab surfaces. For pattern A, use diagonal stirrups anchored in alternative directions to eliminate punching failure inside the shear reinforced zone. For pattern B use FRP stirrups anchored on the slab surface with CFRP overlaps parallel to the column

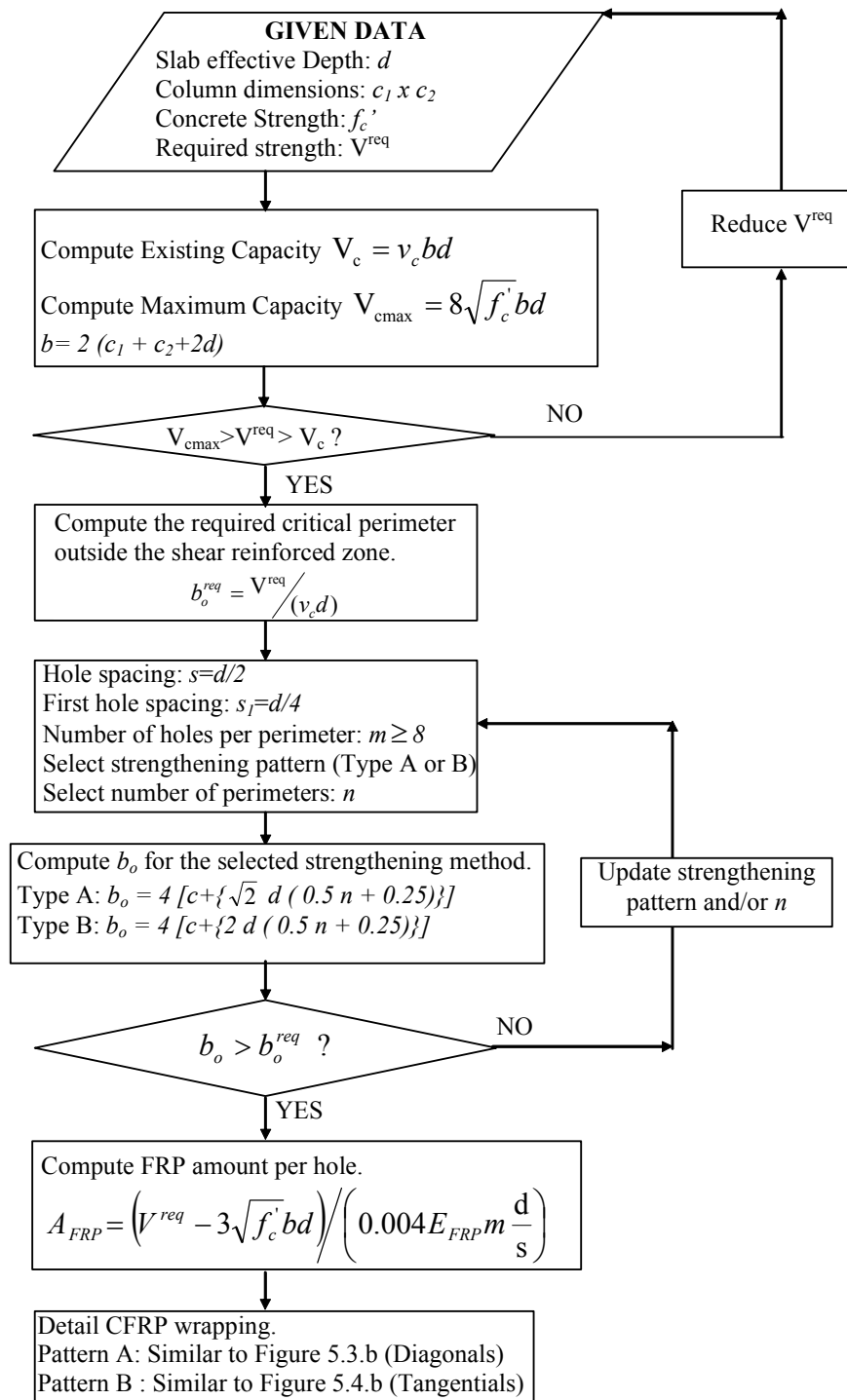


Figure 5.9 Strengthening Design: Pure Shear Transfer

faces. The cross sectional area of diagonal stirrups in pattern A should not be less than half the cross-sectional area of primary CFRP stirrups used in the last CFRP perimeter parallel to the column side. CFRP configurations should be similar to those shown in Figure 5.3-b and Figure 5.3-d.

In order to clarify the procedure a numerical design example is presented in Appendix C.

5.2.1.6 Other Considerations

There are a number of parameters affecting the selection of pattern A or B in slab-column connection strengthening. These parameters are:

1. Relative cost of material to labor.
2. Desired increase in strength with respect to initial strength.
3. Desired post-punching behavior.

Naturally, one of the most important points that will affect the decision process is the cost of the strengthening procedure. For a given level of strength increase selection of Pattern A may require more perimeters than the corresponding number of perimeters with Pattern B. This may increase the labor cost whereas difference in material cost can be insignificant. On the other hand, for lower levels of strength increases, Pattern A may be the optimal solution requiring less labor and material cost.

The detail of the existing slab-column connection, i.e. existence or absence of continuous bottom bars, may affect the decision process. In order to obtain higher resistance immediately after punching failure, more bars contributing to dowel resistance, meaning a larger critical perimeter may be required. The experimental results on capacity loss at punching failure presented in Sections 2.7.1 and 2.8.5 showed that resistance immediately following a punching failure can be enhanced with the proposed upgrade procedure provided

that punching failure (punching pyramid) occurs in the unyielding portions of the slab. In order to obtain increased capacity after a punching failure provided by dowel action of participating tension steel reinforcement, it is required that rebars should be well anchored at the locations of possible dowel action. At large deformations tension steel is likely to strip out and further experimental investigations are required to verify the effectiveness of increased number of tension bars contributing to punching shear resistance.

In cases where increased capacity (immediately following punching shear failure) is required, it is important to ensure that the slab longitudinal reinforcement located outside the shear reinforced zone does not yield. This can be accomplished by comparing the slab moment acting at the critical section with the yielding moment per unit width of the slab (m_y). The moment acting on the critical perimeter can be computed by performing an elastic analysis of the slab. Once this is ensured, the resistance as a result of dowel action can be computed using the equations presented in Section 2.8.5.

In cases where an increased resistance after punching failure is required, the following procedure (Figure 5.10) can be used to enhance the post-punching resistance immediately following a punching failure:

1. Estimate a target capacity immediately after punching failure occurs.
This capacity can be taken as the dowel resistance corresponding to that provided by two continuous compressive bars passing through the column core (similar to ACI 318-02 integrity steel requirement).
2. Estimate punching shear capacity of the strengthened slab-column connection using the procedure explained in Section 5.2.1.5 (Figure 5.8)
3. Compute the length over which longitudinal reinforcement yields (l_y), i.e. the distance between the column and the section where $m=m_y$ when punching shear failure occurs.

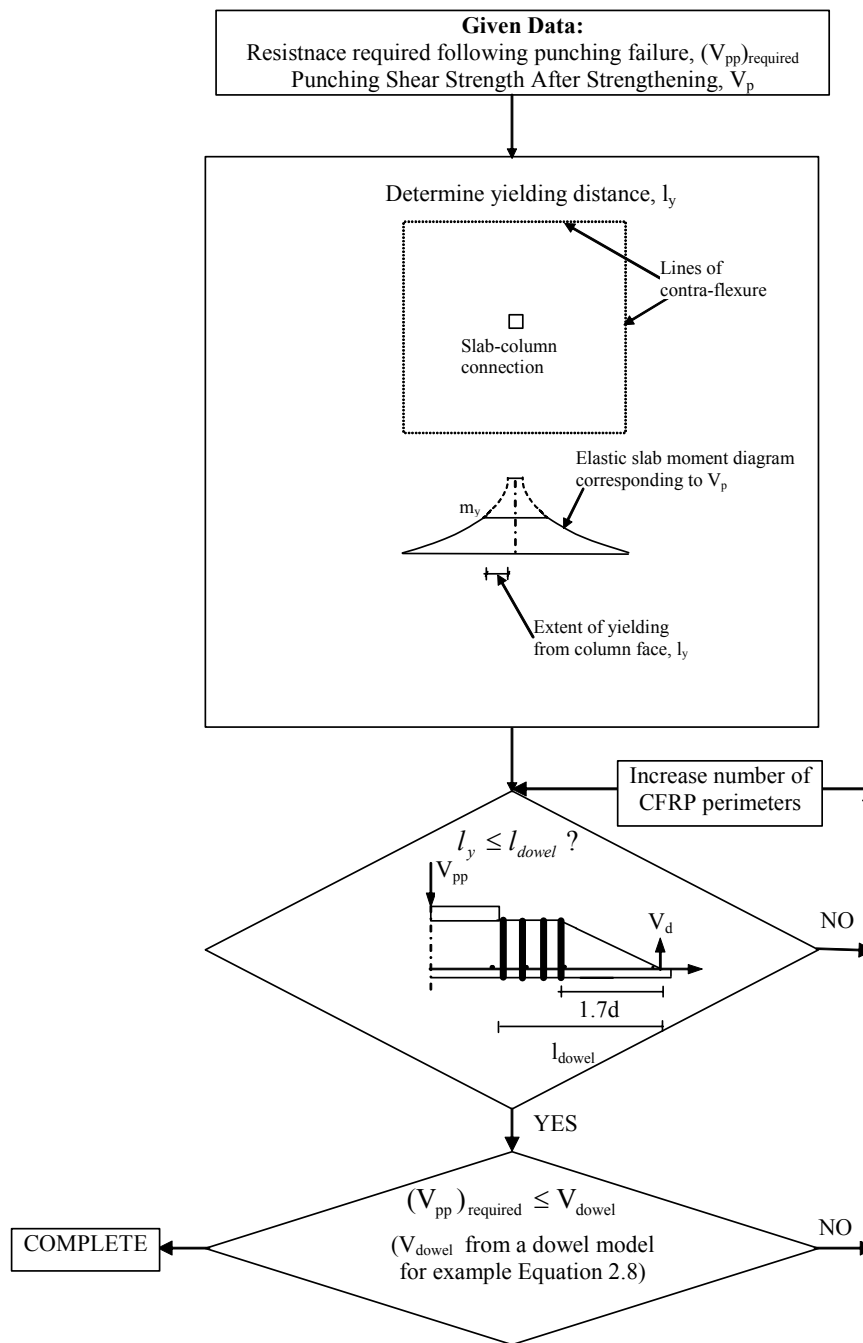


Figure 5.10 A Procedure to Improve Resistance Immediately Following a Punching Failure

4. Check if l_y is smaller than the assumed location of dowel resistance. (Dowel forces can be assumed to act at a distance of $1.7d$ away from the outermost shear reinforcement as shown in Figure 2.58). If longitudinal bars at a section $1.7d$ away from the outermost shear reinforcement are expected to yield, increase the number of CFRP perimeters.
5. Compute the dowel forces, i.e. the post-punching resistance, outside the shear reinforced zone using Equations (2.8).
6. If the dowel resistance is smaller than the estimated resistance, increase the number of CFRP perimeters. In this way, the number of longitudinal bars contributing to dowel resistance will be increased.

The strengthening of individual slab-column connections require selection of FRP perimeters (i.e. size of the shear reinforced zone), design and detailing of FRP amount to achieve desirable performance for punching shear strength and resistance immediately following a punching failure. These issues should be taken into account carefully within a decision framework in the design process, since they influence the performance, cost, and efficiency of the upgrade. Significance of these decisions can be better appreciated in an upgrade project including a large number of slab-column connections.

5.2.2 Combined Shear and Moment Transfer

In this section, ACI 318-02 provisions are used to estimate the capacities of test specimens. Design recommendations for strengthening of slab-column connections using FRPs as shear reinforcement subjected to shear and significant moment transfer are proposed. Even though it is not realistic to base a complete set of design expressions on results of limited number of tests, the applicability of relevant design provisions of ACI 318-02 and derivation of some additional expressions are presented here. In this way, some additional insight is provided to

the behavior of strengthened slab-column connections using the proposed CFRP strengthening technique.

5.2.2.1 ACI 318-02 Provisions

ACI 318-02 provisions for slab column-connections subjected to shear and unbalanced moment transfer are based on the eccentric shear stress model. The model assumes that the unbalanced moment is resisted by flexure and eccentricity of shear as shown in Figure 1.15. Accordingly, shear stress at the critical perimeter located $d/2$ away from the rectangular column is computed using the following expression:

$$v_u = \frac{V_u}{b_o d} + \frac{\gamma_v M_u}{J/c} \quad (5.17)$$

where b_o is the length of the critical perimeter, d is the effective depth of the slab, J is a term analogous to polar moment of inertia, γ_v is the shear transfer coefficient (Equation (1.21)), and c is the distance from the center of the connection to the side of the critical perimeter parallel to the direction of moment transfer. The term J , is computed by:

$$J = \frac{d(c_1 + d)^3}{6} + \frac{(c_1 + d)d^3}{6} + \frac{d(c_2 + d)(c_1 + d)^2}{2} \quad (5.18)$$

in which c_1 and c_2 are cross sectional dimensions of a rectangular column in the direction parallel and perpendicular to the direction of moment transfer, respectively. The maximum shear stress due to combined shear and moment transfer is kept smaller than the shear resistance as a part of the slab-column connection design. Equation (5.19) illustrates the design expression neglecting load and resistance factors:

$$v_u \leq v_n = v_c + v_s \quad (5.19)$$

where v_c is the concrete contribution and v_s is the stirrup contribution (if there is any) to shear strength.

The procedure employed in Section 5.2.1.5 can be extended for slab-column connections subjected to combined unbalanced moment and shear forces. Accordingly, punching shear capacity outside the CFRP reinforced zone can be computed based on a critical perimeter outside the shear reinforced zone. Then the cross-sectional area of vertical CFRP stirrups can be calculated using a critical perimeter located at a distance of $d/2$ away from the column face together with the assumed concrete contribution inside the shear reinforced zone.

This procedure requires calculation of shear stress at the critical section located outside the shear reinforced zone using Equation (5.17). However, ACI provisions do not provide J terms for different geometries of critical perimeters. It can be observed that for specimens strengthened with Pattern A (Figure 5.3), the critical perimeter is in the form of an octagon. The term J can be computed by extending the eccentric shear stress model to octagonal critical perimeter geometry as shown in Figure 5.11. The derivation of the J term for an octagonal perimeter is presented in Appendix D. According to this, J for an octagonal perimeter is calculated using the following expression:

$$\begin{aligned}
 J &= (1/2) c_2 d (c_1 + 2l_1)^2 + (r + 1) l_3 \bar{x} d (c_1 + 2l_1) + \\
 &\quad (1/6) c_1^2 d (r) (c_1 + 2l_1) + (1/6) d^3 (c_1 + 2l_1) \\
 \frac{v'}{v} &= r = \frac{c_1}{c_1 + 2l_3} \tag{5.20} \\
 \bar{x} &= \frac{\{3r l_3 + 2(1-r)l_3\}l_1}{3(1+r)l_3} + \frac{c_1}{2}
 \end{aligned}$$

As can be observed in Equation (5.20), J depends on the ratio of shear stresses v' to v as well as the geometry of the octagonal perimeter. This expression can be

used to compute the shear stress outside the shear reinforced zone for specimens reinforced with pattern A CFRP stirrup arrangement.

On the other hand, for specimens with pattern B CFRP stirrup configuration, J can be computed using Equation (5.18) for a rectangular critical perimeter located outside the shear reinforced zone. Equation 5.21 illustrates a simplified version of Equation (5.18):

$$J = \frac{d(b_1)^3}{6} + \frac{(b_2)d^3}{6} + \frac{d(b_2)(b_1)^2}{2} \quad (5.21)$$

where, b_1 and b_2 are the dimensions of the rectangular critical perimeter constructed outside the shear reinforced zone. b_1 is the dimension parallel to the direction of moment transfer, and b_2 is the dimension perpendicular to b_1 . Using J from Equations (5.20) and (5.21), maximum shear stress at the critical perimeter can be calculated. The maximum shear stress should be smaller than the maximum permissible shear stress for concrete. Equation (5.22) illustrates this requirement:

$$v_u = \frac{V_u}{b_o d} + \frac{\gamma_v M_u}{(J/c)} \leq v_c \quad (5.22)$$

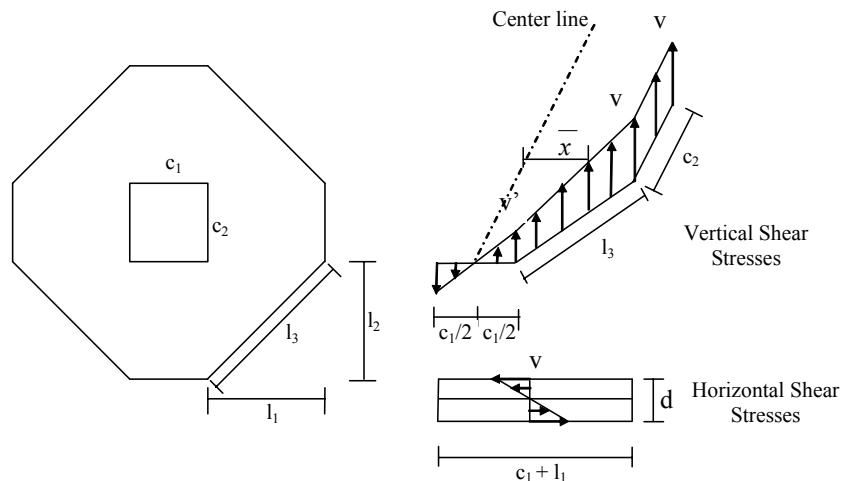


Figure 5.11 Eccentric Shear Stress Model for Octagonal Perimeters

Once the capacity outside the shear reinforced zone is evaluated, the amount of CFRP that ensures punching outside the shear reinforced zone can be found using the following expression:

$$v_u = \frac{V_u}{bd} + \frac{\gamma_v M_u}{(J/c)} = v_c + v_{FRP} = 3\sqrt{f'_c} + \frac{0.004E_{FRP}A_{FRP}}{b_o s} \quad (5.23)$$

J and b in Equation (5.23) are computed for the critical perimeter located $d/2$ away from the column face. The concrete contribution, v_c , and FRP contribution, v_{FRP} , are calculated using the previously proposed values in Section 5.2.1.4.

5.2.2.2 Computed and Experimental Capacities

Punching shear capacities of the specimens subjected to shear forces and unbalanced moments were calculated using the following procedure. For the test specimens strengthened with external CFRP stirrups, capacities inside (V_u^i) and outside (V_u^o) the CFRP reinforced zone were calculated. The smaller of the two capacities was taken as the punching strength of the test specimens (Table 5.5).

Predictions obtained by using ACI 318-02 provisions (with the above modifications) were conservative. The ratio of experimental to predicted ultimate capacities were 1.7 and 2.2 for specimens CC and CE, which were not upgraded using external CFRP stirrups. For strengthened specimens A4E, and B4E, ratios of experimental to predicted ultimate loads were 1.7 and 1.9, respectively. The use of previously modified ACI 318-02 equations resulted in very conservative estimations both for control and strengthened specimens. However, only a limited number of test results are available to assess the performance of the proposed strengthening scheme for slab-column connections subjected to combined shear and unbalanced moment transfer. Only one value of eccentricity (M/V) and four CFRP perimeters in A and B configurations were tested. Based on limited information, it is believed that level of conservatism in upgraded specimens

Table 5.5 Comparison of ACI 318-02 Estimations and Experimental Results

Specimen	V_{u-exp}	V_u^o (k)	V_u^l (k)	$V_{ACI} = \min(V_u^l, V_u^o)$, (k)	V_{u-exp} / V_{ACI}
CC	30.2	17.6	-	17.6	1.7
CE	21.5	9.7	-	9.7	2.2
A4E	31.1	16.3	29.3	16.3	1.9
B4E	34.6	20.2	34.7	20.2	1.7

should be kept similar to that of the control specimens. A design procedure consistent with ACI provisions can still be proposed. In fact, this procedure is an extension of the proposed design guidelines presented in Section 5.2.1.5 for slab column connections subjected to pure shear transfer. However the accuracy of the design equations for slab-column connections subjected to shear and unbalanced moment needs to be further investigated with additional experiments.

5.2.2.3 Proposed Design Procedure Using ACI 318-02 Provisions

The design steps outlined in Section 5.2.1.5 are extended to include the effect of unbalanced moment in addition to gravity shear. Following procedure (or the flowchart in given in Figure 5.12) can be used to clarify the design steps for upgrade of slab-column connections using externally installed CFRPs:

1. Determine geometric and material properties of the connection. Evaluate the target shear and unbalanced moment demand.
2. Confirm that required punching shear strength is within the acceptable range and maximum permissible shear stress is not exceeded.
3. Assume number of FRP perimeters and strengthening pattern.
4. Calculate the effective shear stress (Equation (5.22)) by computing J from Equation (5.20) (Pattern A) or from (5.21) (Pattern B) for a critical perimeter located $d/2$ from the outermost shear reinforcement.
5. Compare v_u with the concrete strength, v_c outside the shear reinforced zone. If $v_u < v_c$ proceed to step 6, otherwise go to step 3.

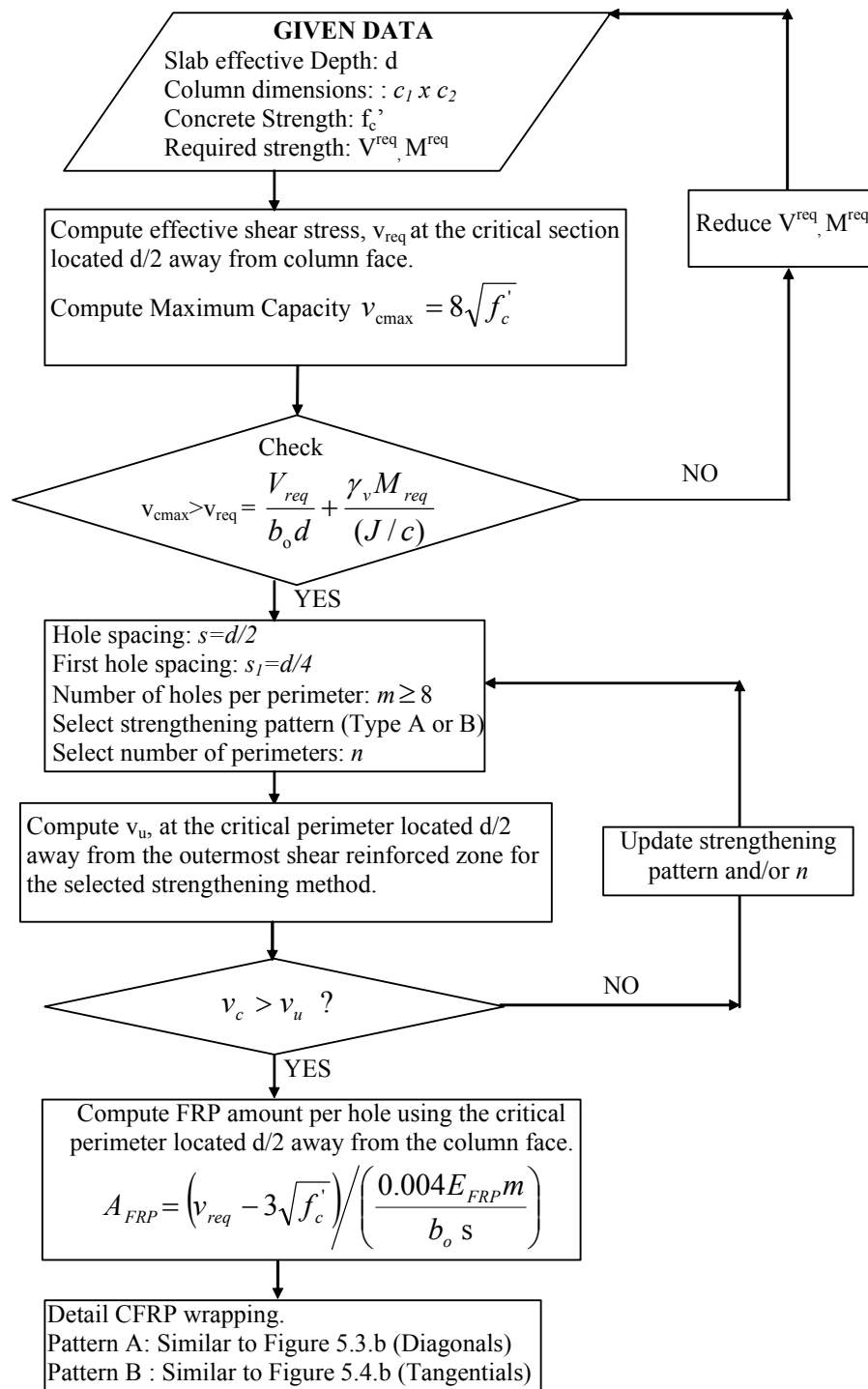


Figure 5.12 Strengthening Design: Shear and Unbalanced Moment Transfer

6. Compute required amount of FRP reinforcement per leg from Equation (5.23).
7. Detail the FRP wrapping similar to that explained in Section 5.2.1.5.

In order to clarify the procedure a numerical design example is presented in Appendix E. The design procedure is similar to that for pure shear transfer case. The difference arises due to the second term in Equation (5.17), which requires the computation of J term. The iterations to find the number of shear reinforcement perimeters are more involved due to the existence of J term in the shear stress expressions. If unbalanced moment is taken as zero, the design procedure reduces down to that presented in Figure 5.9. Therefore the design for pure shear transfer is a special case of the design procedure for slab-column connections subjected to shear and unbalanced moment.

Figure 5.13 shows the comparisons of ultimate load predictions obtained by using the design procedure with the experimental capacities. Computed capacities shown in Figure 5.13 may be considered overly conservative. Considering the limited number of tests on slabs subjected to proportionally increasing shear forces and unbalanced moments, no attempt was made in improving the accuracy of capacity estimations. Instead, the design process proposed for pure shear transfer was extended to incorporate the effects of unbalanced moments.

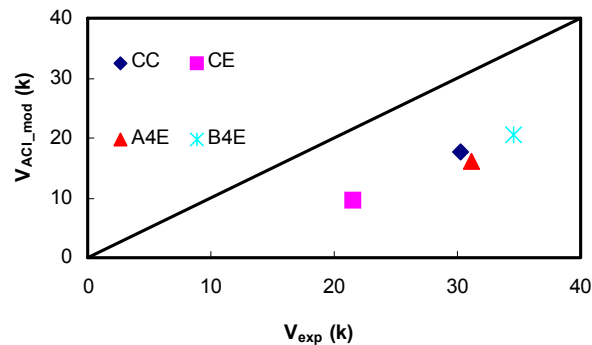


Figure 5.13 Comparison of Modified ACI 318-02 Predictions with Experiments

CHAPTER 6

Summary and Conclusions

6.1 GENERAL

Summary and conclusions of the research are presented in this chapter. Following this, recommendations for future research are addressed.

6.2 SUMMARY

The research presented in this dissertation can be divided into four major parts:

Part 1: Strengthening of Concentrically Loaded Flat Plates (Chapter 2)

First phase of the experimental program focused on the strengthening of reinforced concrete slab-column connections subjected to monotonic shear transfer. Eleven full-scale reinforced concrete slabs, loaded concentrically at the center were tested to develop a strengthening method in which CFRPs were used as shear reinforcement. Nine of the specimens were strengthened with CFRPs, and two control specimens had no strengthening. The effectiveness of two strengthening patterns was investigated. The influence of various external CFRP stirrup arrangements resulting in different sizes of the upgraded region was studied. In addition, the effectiveness of two continuous compressive bars acting as integrity steel was evaluated. Strengthening mechanism, failure modes, and post punching behavior of the test specimens were examined. Simple mechanical models were used to predict the punching shear strength and post punching capacities of the test specimens. A possible anchorage method for externally installed CFRP stirrups was examined through double shear push-out tests and an analytical model was developed.

Part 2 Strengthening of Eccentrically Loaded Flat Plates (Chapter 3)

In order to investigate the performance of strengthened slab-column connections subjected to monotonic shear and unbalanced moment transfer, four reinforced concrete flat plates were tested. Strength, stiffness, ductility, and failure modes of the test specimens were studied and compared with the estimations of simple models. A parametric study was performed for a floor system to investigate the demands on interior slab-column connections for various slab, column and floor geometries.

Part 3 Finite Element Analyses (Chapter 4)

Nonlinear finite element analyses were conducted to study the behavior of strengthened reinforced concrete flat plates. Numerical simulations were performed to provide further insight to the mechanics of load transfer. First, model verification for concentrically loaded flat plates without any shear reinforcement was performed. Then the effect of various parameters on punching shear capacity was discussed. Finally, the analyses of strengthened slabs were presented. Local stress conditions, sequence of cracking were studied. Experimental observations were used to validate the analyses.

Part 4 Code Examinations and Design (Chapter 5)

The design provisions of ACI 318-02, CEB-FIB MC90, CSA A23.3-94 and BS 8110-97 for punching shear design were critically examined using the experimental results from Parts 1 and 2. Findings from the comparative evaluation of various code expressions were used to propose practical design guidelines for the strengthening scheme. The design recommendations were consistent with the design provisions of ACI 318-02. Some modifications to ACI 318-02 provisions were proposed for punching shear strengthening using

externally installed CFRP stirrups such that more economical and safe designs can be achieved.

6.3 CONCLUSIONS

The following major conclusions can be drawn from this study:

1. An effective method for punching shear upgrade of existing reinforced concrete flat plates with the use of CFRPs as shear reinforcement was developed. The proposed method proved to be successful in strengthening the slab-column connections subjected to pure shear, and combined shear and unbalanced moment transfer.
2. Load carrying capacities of deficient slab-column connections following a punching failure were enhanced with the use of the proposed strengthening scheme. Some of the strengthened specimens (A8, B4, B6 and B8) had smaller capacity losses at punching failure than that of a control specimen that complied with integrity steel requirements of ACI 318-02. However significant effects of boundary conditions on post punching capacities were observed for specimens where the inclined cracks terminated close to the slab edges (specimens A8 and B8).
3. The maximum permissible strain in the vertical legs of the CFRP stirrups was found to be approximately 0.004. Experiments showed that when strains greater than 0.004 were measured in CFRP strips (specimen A4-3), concrete contribution inside the shear reinforced zone significantly deteriorated. Subsequently failure occurred inside the shear reinforced zone prior to exhausting shear capacity of concrete outside this zone. When strains smaller than 0.004 were recorded on CFRP legs (specimens A4-2, A6, A8, B4, B6, and B8) failure occurred outside the shear reinforced zone.

4. A previously proposed mechanical model was modified and extended to include the effect of shear reinforcement and dowel action. This model successfully predicted punching shear capacities and failure locations of slab-column connections subjected to pure shear transfer. The modified mechanical model utilizes geometry of the failure surface and employs equilibrium to compute the punching shear capacity.
5. The ratio of ultimate displacement to displacement at first yielding increased from about 1.0 (control specimens) up to 2.6 (pattern B specimens). Tests on specimens subjected to combined shear and moment transfer proved that punching shear failure could be eliminated (specimen A4E) and ductile flexural failure could be obtained when slab-column connections are strengthened by using CFRPs.
6. Nonlinear finite element analyses indicated that CFRP strips worked as vertical members that carried the shear forces transferred by compression struts. The conceptual model based on strut- and tie analogy was capable of reflecting the strengthening mechanism.
7. Results of finite element analyses showed that locations of maximum principal stresses give a good indication of the expected failure surface. In addition, analyses results verified that the amount of CFRP used as shear reinforcement played an important role in controlling cracking inside the shear reinforced zone.
8. The proposed design procedure based on ACI 318-02 provisions can be used for designing slab-column connection upgrades.

Other conclusions of the study are as follows:

1. Use of CFRP strips as closed stirrups increased the strength and deformation capacity of concrete. When CFRP strips were anchored by overlapping them at the compressive side of the slab, the shear reinforced region stayed

relatively undamaged with no shear cracks. As a result punching failure occurred outside the shear reinforced zone.

2. The increase in the number of CFRP perimeters, i.e. the size of the shear reinforced region, resulted in increases in punching shear capacity. In strengthened specimens, the load carrying capacity was limited to the flexural capacity of the slab.
3. In specimens strengthened using Pattern A CFRP placement, when diagonally spanning stirrups were used in addition to those placed parallel to the loading plate, failure was shifted outside the shear reinforced region. This resulted in optimum performance for this CFRP arrangement.
4. For a given number of CFRP perimeters, specimens with pattern B CFRP arrangement had higher capacities than those upgraded using pattern A CFRP stirrup installation. Larger area of the shear reinforced zone in pattern B specimens in comparison to pattern A specimens was responsible for this difference in specimens' performance.
5. ACI 318-02 requirement for integrity steel resulted in smaller capacity losses at punching failure. However, a significant loss of capacity (~50%) was experienced by specimen Control-2 (specimen with integrity steel).
6. The experiments conducted using a self contained setup and an anchorage model used for analysis of these anchorage tests showed that the effective anchorage length for the CFRPs used in this study was about 12 in. Therefore, the required anchorage length upon use of "C- Shape" CFRP shear reinforcement was found to be similar to that provided by the closed loop stirrups in most cases.
7. The parametric study performed for a floor system using linear elastic finite element analyses showed that significant unbalanced moment demands could

be observed in interior slab-column connections under the action of gravity loads alone.

8. Experimental results showed that the concrete contribution, v_c inside the shear reinforced zone could safely be taken as $3\sqrt{f'_c}$ for slabs strengthened using CFRPs in this study. Further experiments are required in order to verify the accuracy of this concrete contribution especially for slabs with lower longitudinal reinforcement ratios.
9. The usable strain level in CFRP vertical legs, 0.004, can be used to compute the cross-sectional area of CFRP stirrups for the upgrade design of the slab-column connections. This strain limit has its basis from experiments conducted in this research. In addition use of this strain limit results in accurate predictions of CFRP design amounts (for specimens A4-2, A6, A8, B4, B6, and B8) when compared to actual values used in the tests. Therefore, using FRP and concrete contributions to punching shear strength, upgrade design can be performed following the critical perimeter approach suggested by ACI 318-02 provisions for punching shear strength calculations.

6.4 RECOMMENDATIONS FOR FUTURE RESEARCH

1. Full scale experiments of slab systems are required to assess the performance of the strengthening scheme containing both interior and exterior slab-column connections, and post punching performance of the connections with details according to older versions of the code. In addition, these tests can provide invaluable information on the internal redistribution of forces in the slab.
2. Other forms of mechanical anchorage schemes for vertical CFRP stirrups can be investigated in order to develop a system that uses CFRP reinforcement more efficiently.

3. The performance of the proposed strengthening scheme should be validated for laterally loaded slab-column connections. The reliability, cost efficiency and seismic qualification of the method should be verified through analytical and experimental studies.
4. Experiments designed specifically to measure dowel resistance in slabs are needed to determine the post punching resistance of the slab-column connections. In this way, realistic modeling of post punching behavior may be possible and reserve capacity of the slab-column connections can be determined more accurately.
5. Nonlinear finite element analyses with realistic material models and concrete-CFRP interface models can be used to study the anchorage behavior of CFRPs used as shear reinforcement in slab-column connections.

APPENDIX A

Vertical CFRP Strains for Specimen A4-2

Measured vertical CFRP strains in the first two perimeters are shown in Figure A.1. CFRP vertical strains in the first perimeters were 0.0014 and 0.0018. Maximum CFRP strains were observed in the second perimeter and they range from 0.0035 to 0.004. According to this, strain gauge readings from locations 3, 4, and 5 at most differ by 15 %. This shows the confidence level on the maximum vertical strain level, which was about 0.004.

Strain Gauge No	Maximum CFRP Strain
1	0.00141
2	0.00177
3	0.00351
4	0.00372
5	0.00401

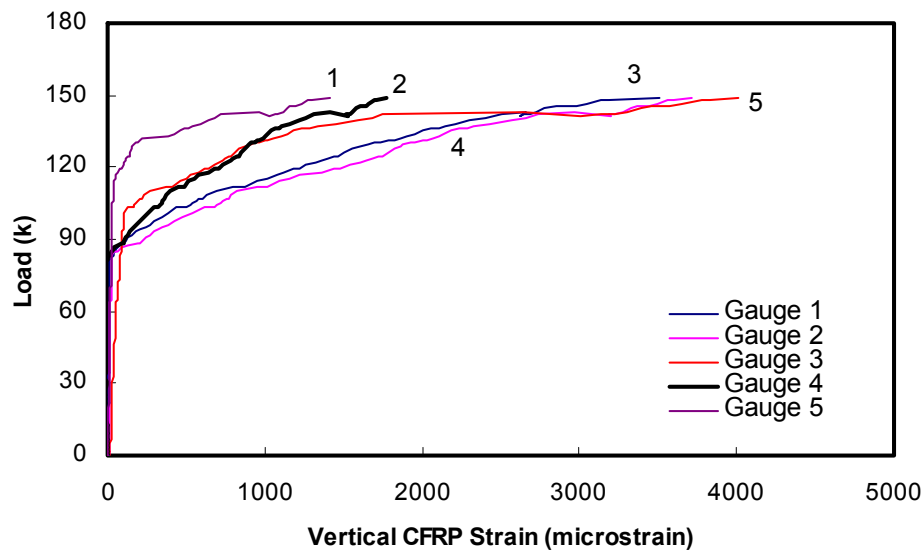
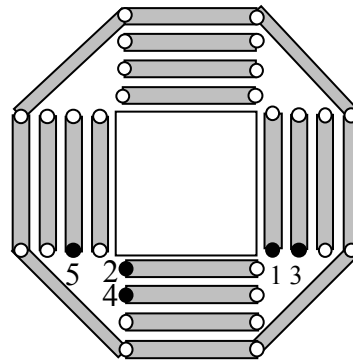


Figure A.1 Vertical CFRP Strains for Specimen A4-2

APPENDIX B

Derivation of Anchorage Length for FRPs Bonded to Concrete

B. 1 General

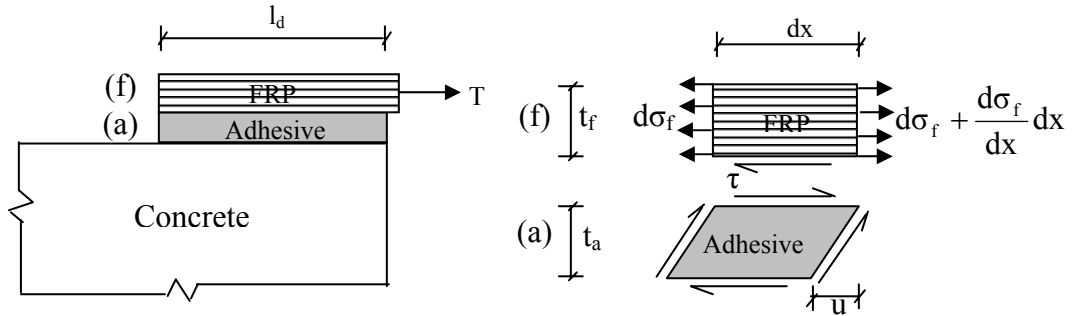


Figure B.1 FRP Bonded to Concrete

The shear stress is related to the displacement through the following equation:

$$\tau = \frac{G_a}{t_a} u \quad (B.1)$$

where :

$$\varepsilon_f = \frac{du}{dx} = \frac{\sigma_f}{E_f} = \frac{t_a}{G_a} \frac{d\tau}{dx} \quad (B.2)$$

From equilibrium of the FRP infinitesimal element:

$$\tau = \frac{d\sigma_f}{dx} t_f \quad (B.3)$$

By differentiating Equation (B.1) twice, Equation (B.4) can be obtained:

$$\frac{d^2 \tau}{dx^2} = \frac{G_a}{t_a} \frac{d^2 u}{dx^2} = \frac{G_a}{t_a} \frac{1}{E_f} \frac{d\sigma_f}{dx} = \frac{G_a}{E_f t_a t_f} \tau \quad (B.4)$$

$$\frac{d^2 \tau}{dx^2} = w^2 \tau \quad (B.5)$$

where ;

$$w^2 = \frac{G_a}{E_f t_a t_f} \quad (B.6)$$

The solution of the Equation (B.5) for the shear stress distribution is:

$$\tau(x) = A e^{wx} + B e^{-wx} \quad (B.7)$$

in which A and B are yet to be determined from the boundary conditions.

As reported by Triantafillou and Deskovic (1991) and Chen and Teng (2001), and also according to the results of Section 2.8.4, failure occurs at the concrete FRP interface due to high shear stresses transferred from FRP to concrete. The descending portion of the shear stress distribution is due to the softening behavior of concrete in shear (Triantafillou and Deskovic, 1991). A qualitative description of shear stress slip distribution is given in Figure B.2. According to this, at a critical slip value, u^* , the anchorage fails. The area under shear stress-slip curve can also be thought as the fracture energy associated with cracking of this region as suggested by Chen and Teng (2001). The elastic solution given in Equation (B.7) can be used to compute the shear stress distribution in the elastic region, whereas for the cracked region a triangular stress distribution is used to approximate the shear stresses.

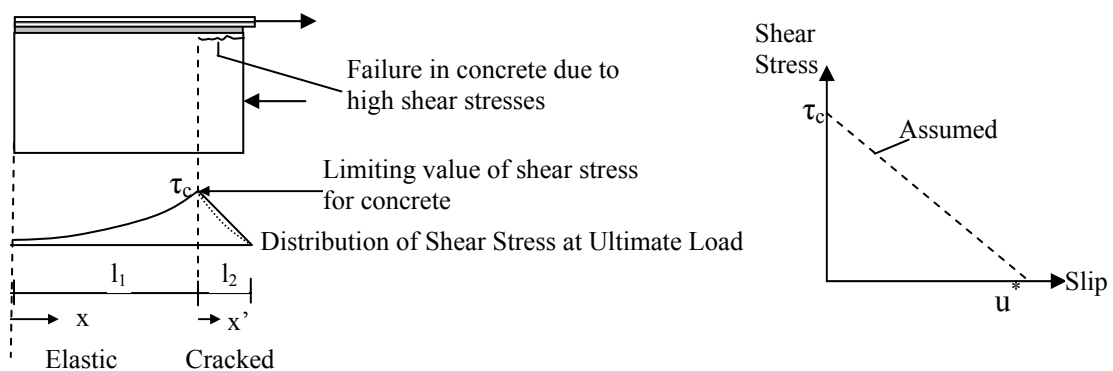


Figure B.2 Failure at Concrete and FRP Interface

Imposing boundary conditions for the elastic region:

$$x = 0 \Rightarrow \sigma = \frac{d\tau}{dx} = 0 \quad (\text{B.8})$$

$$x = l_1 \Rightarrow \tau = \tau_c \quad (\text{B.9})$$

$$A = B = \frac{\tau_c}{e^{wl_1} + e^{-wl_1}} \quad (\text{B.10})$$

Making use of the hyperbolic sine and cosine functions;

$$\sinh wx = \frac{e^{wx} - e^{-wx}}{2} \quad (\text{B.11})$$

$$\cosh wx = \frac{e^{wx} + e^{-wx}}{2} \quad (\text{B.12})$$

the shear stress distribution in the elastic region can be expressed as:

$$\tau(x) = \frac{\tau_c \cosh(wx)}{\cosh(wl_1)} \quad 0 < x < l_1 \quad (\text{B.13})$$

FRP stress distribution can be computed using Equation (B.2):

$$\sigma_f(x) = \frac{E_f t_a w \tau_c \sinh(wx)}{G_a \cosh(wl_1)} = \frac{1}{t_f w} \frac{\tau_c \sinh(wx)}{\cosh(wl_1)} \quad (\text{B.14})$$

FRP stress at $x=l_1$ is given as:

$$\sigma_f(l_1) = \frac{\tau_c}{t_f w} \tanh(wl_1) \quad (\text{B.15})$$

The distribution of shear stress in the cracked region is given as follows:

$$\tau(x') = \tau_c \left(1 - \frac{x'}{l_2}\right) \quad 0 < x' < l_2 \quad (\text{B.16})$$

Considering the equilibrium of the cracked region, stress in FRP can be computed by:

$$\sigma_f(x') = \sigma_f(l_1) + \int_0^{x'} \frac{\tau(x')}{t_f} dx' \quad 0 < x' < l_2 \quad (\text{B.17})$$

$$\sigma_f(x') = \sigma_f(l_1) + \frac{\tau_c}{t_f} \left(x' - \frac{x'^2}{2l_2} \right) + C \quad 0 < x' < l_2 \quad (\text{B.18})$$

The integration constant C is equal to zero due to the boundary condition at $x'=0$.

The boundary condition at $x'=l_2$ yields:

$$\sigma_d = \sigma_f(l_1) + \frac{\tau_c}{t_f} \frac{l_2}{2} \quad (\text{B.19})$$

where :

$$T = \sigma_d b_f t_f \quad (\text{B.20})$$

The critical displacement (slip), u^* at $x'=l_2$, can be computed by integrating the strains and neglecting the contribution from the elastic region.

$$u(x') = \int_0^{x'} \frac{\sigma_f(x')}{E_f} dx' \quad 0 < x' < l_2 \quad (\text{B.21})$$

Assuming slip at $x'=0$ is equal to zero, u^* can be computed as follows:

$$u^* = \frac{l_2}{E_f} \left(\sigma_f(l_1) + \frac{\tau_c}{t_f} \frac{l_2}{3} \right) \quad (\text{B.22})$$

It can be observed that Equations (B.19) and (B.20) suggest that the load carrying capacity of the FRP bonded to concrete increases as the anchorage length is increased. However Equation (B.22) places an upper bound on the load carrying capacity limited by a characteristic displacement. In other words the anchorage strength of the system will increase up to a certain critical length and further increase of anchorage length will not affect the ultimate load carrying capacity beyond a certain length. In fact this aspect of bond behavior of concrete to FRP is significantly different from the bond behavior of internal reinforcement,

for which a bond length can always be designed and full tensile strength of reinforcement can be developed provided that there is sufficient concrete cover.

B. 2 Analysis of Anchorage Behavior for CFRPs Bonded to Concrete

For given anchorage length, l_a , material and geometric properties of CFRP and concrete, the anchorage strength of CFRPs bonded concrete can be computed using the equations presented above with the following simplifications.

Figure B.3 shows the behavior of the tangent-hyperbolic function that appears in Equation (B.15). It can be observed that for wl values greater than 1.5, this function rapidly approaches to 1.0. Using this information, length l_l , along which elastic stress distribution is valid, can be estimated by:

$$l_l = \frac{1.5}{w} \quad (B.23)$$

Hence, the stress on FRP at $x = l_l$ can be approximated as:

$$\sigma_f = \sigma_f(l_l) \approx \frac{\tau_c}{t_f w} \quad (B.24)$$

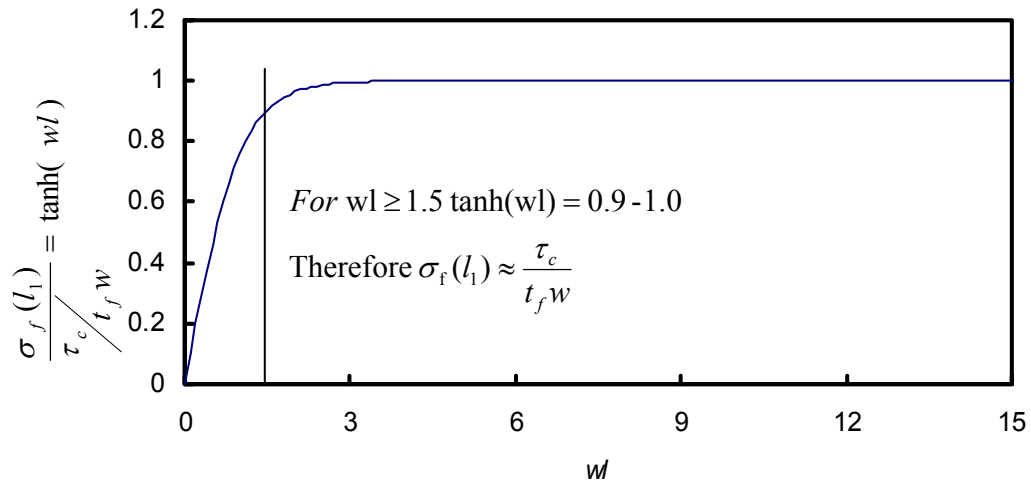


Figure B.3 Effect of wl on FRP Stress “ $\sigma_f(l_l)$ ”

When the anchorage length is sufficiently long, failure occurs due to a limiting slip displacement, u^* , criteriB. The critical length that corresponds to this case can be computed by solving the following quadratic equation for l_{cr} (obtained from Equation (B.22)):

$$u^* = \frac{l_{cr}}{E_f} \left(\frac{\tau_c}{t_f w} + \frac{\tau_c}{t_f} \frac{l_{cr}}{3} \right) \quad (\text{B.25})$$

The solution of Equation (B.25) yields:

$$l_{cr} = \frac{3}{2} \left[\sqrt{\frac{4 u^* E_f t_f}{3 \tau_c} + \frac{1}{w^2}} + \frac{1}{w} \right] \quad (\text{B.26})$$

Then the ultimate load carrying capacity of the anchorage can be computed by combining Equations (B.19) and (B.20):

$$T = \left(\frac{\tau_c b_f}{w} + \frac{\tau_c b_f L_{eff}}{2} \right) \quad (\text{B.27})$$

in which L_{eff} is given as:

$$L_{eff} = \min (l_d - l_1, l_{cr}) = \min \left(l_d - l_1, \frac{3}{2} \left[\sqrt{\frac{4 u^* E_f t_f}{3 \tau_c} + \frac{1}{w^2}} + \frac{1}{w} \right] \right) \quad (\text{B.28})$$

According to the above simplification, l_1 depends only on the properties of the adhesive. With the use of strong adhesives (compared to concrete tensile strength) commonly used in strengthening applications, l_1 values range from $1/4$ to $3/4$ in. Therefore it is possible to further simplify Equation (B.28) by neglecting l_1 when l_1 / l_d ratio is small (~ 0.1 to 0.2). Then the effective anchorage length can be taken as:

$$L_{eff} = \min (l_d, l_{cr}) = \min \left(l_d, \frac{3}{2} \left[\sqrt{\frac{4 u^* E_f t_f}{3 \tau_c} + \frac{1}{w^2}} + \frac{1}{w} \right] \right) \quad (\text{B.29})$$

It can be observed that load carrying capacity of the anchorage increases with increasing anchorage length up to a certain length, l_{cr} . Beyond this critical

anchorage length, ultimate load carrying capacity remains constant and further increase of l_d will only effect the ductility of the anchorage, as the triangular stress distribution (Figure B.2) is shifted and the anchorage failure propagates along length l_d .

The normalized anchorage length is plotted against the normalized load carrying capacity in Figure B.4. It can be observed that the first equation controls up to a certain effective length, l_d , beyond which critical displacement u^* governs the anchorage strength. According to this plot ultimate strength of the anchorage is about half of the ultimate load that can be carried by FRP in direct tension. It should be kept in mid that this figure is plotted for material properties of CFRP and adhesive used in this dissertation together with, a critical displacement, u^* , of 0.04 in (1 mm). The average of the measured slip displacements presented in Table 2.10 is equal to this critical displacement. In addition, this value of critical displacement is within the range of slip values (0.6 to 2.2 mm) that have been observed in anchorage tests performed by Taljsten (1997) and Khalifa and Nanni (2001).

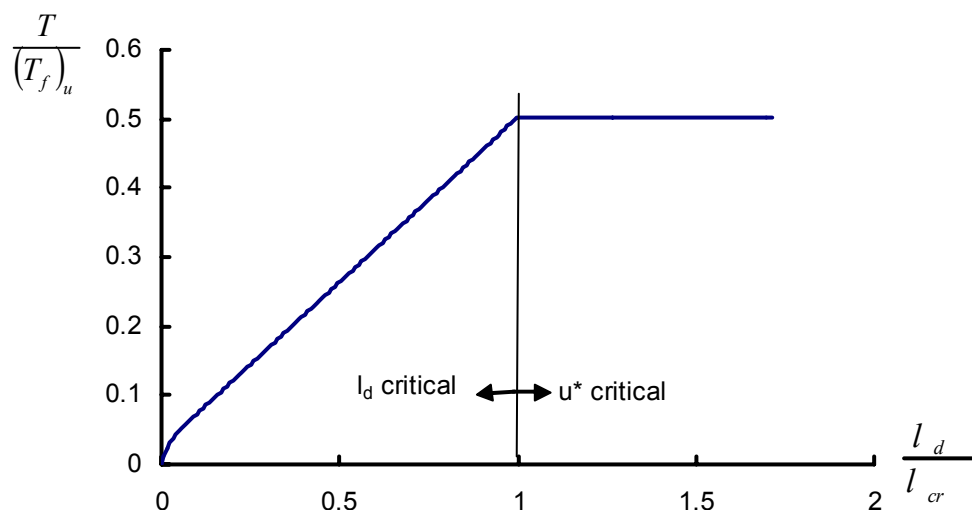


Figure B.4 Effect of Anchorage Length on Ultimate Load Carrying Capacity

B. 3 Design Equation Format for Anchorage of CFRP Bonded to Concrete Surface

For ultimate strength design, the anchorage strength will govern based on the critical length l_{cr} since it is the maximum load carrying capacity that the anchorage can sustain. Equation (B.29) can further be simplified by neglecting the contribution of $1/w$ term for practical range of values of w . Assuming that the limiting shear strength of concrete, τ_c is equal to the splitting tensile strength of concrete ($f_{ct} = 6\sqrt{f'_c}$), the anchorage length required can be computed by:

$$L = \sqrt{\frac{3u^* E_f t_f}{f_{ct}}} = \sqrt{\frac{0.5u^* E_f t_f}{\sqrt{f'_c}}} \quad (\text{B.30})$$

Based on Equation (B.30), the required anchorage length is plotted against the FRP stiffness for different concrete strength values (f'_c) in Figure B.6. It can be observed that there is a trend of increase in anchorage length with increasing FRP stiffness, whereas the relationship between them is non-linear. It can also be observed that the decrease in concrete strength increases the required anchorage length.

The required anchorage length is plotted against the FRP stiffness for different u^* values in Figure B.7. It can be observed that for smaller u^* values, the required anchorage length tends to be shorter which can also be observed in Equation (B.28) through the square root expression. For a critical slip displacement of 0.04 in. (average of the measured maximum slip displacements shown in Table 2.10), the required anchorage length is about 12 in. to achieve the maximum available anchorage strength for the plate stiffness used in the experimental program of this dissertation.

The ultimate load carrying capacity of the anchorage can be computed by using Equations (B.27):

$$T = 3\sqrt{f'_c} L b_f \quad (B.31)$$

where L is given by Equation (B.30), b_f is the width of FRP, and f'_c is the compressive strength of concrete.

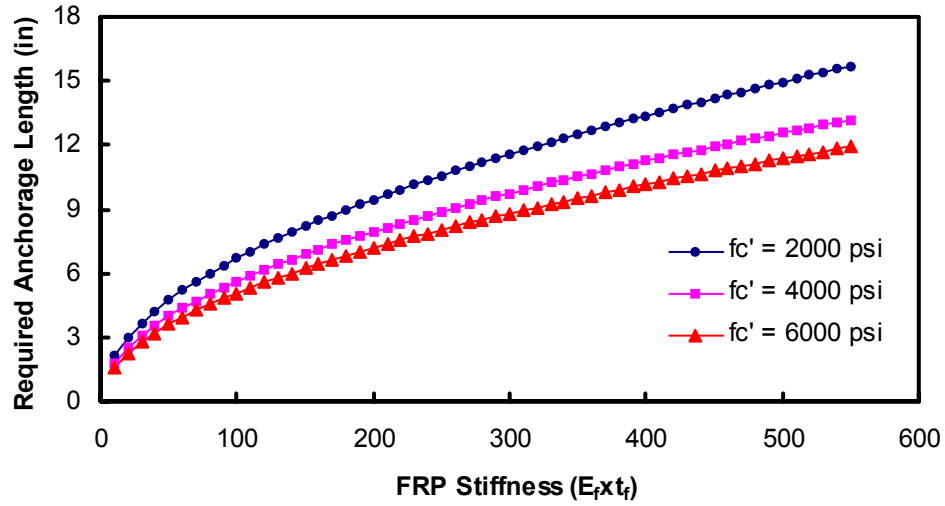


Figure B.5 Effect of Concrete Strength on Required Anchorage Length

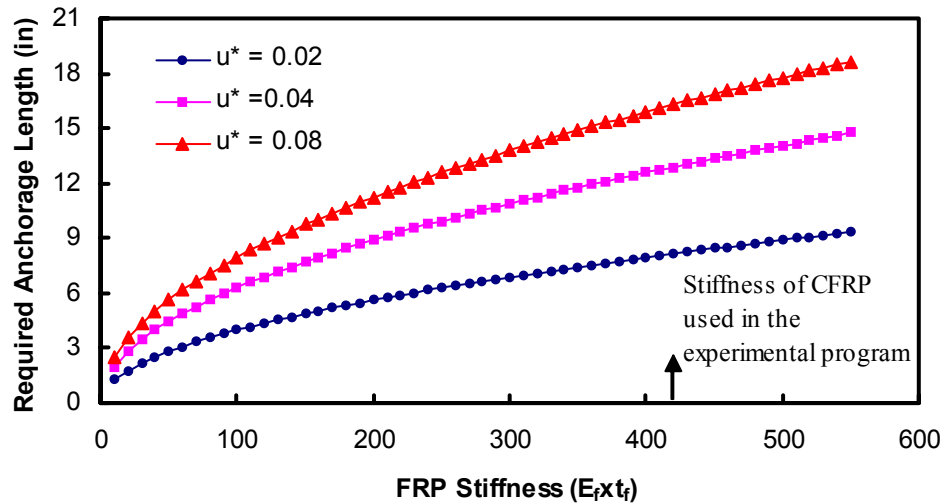


Figure B.6 Effect of Selection of Slip Limit on Required Anchorage Length

APPENDIX C

Design Example for Strengthening of Slab-Column

Connections Subjected to Pure Shear

Given: Column size, $c = 304$ mm ; Slab thickness, $h = 152$ mm ; Concrete strength, $f_c' = 28.3$ MPa ; Flexural reinforcement ratio, $\rho = 1.76$ % ; Effective slab depth,

$d = 114$ mm ; $f_{FRP} = 876$ MPa

Design: Determine the CFRP amount and pattern such that 50% increase in capacity.

1) Existing punching shear capacity:

$$\bullet V_u = \frac{1}{3} \sqrt{f_c'} b_o d = \frac{1}{3} \sqrt{28.3} [4(304 + 114)](114) = 340 \text{ kN}$$

$$\bullet \text{Experiment: } V_u = 494 \text{ kN}$$

2) Punching shear capacity after strengthening:

$$V_u^{st} = 1.5(340) = 510 \text{ kN}$$

3) Assume 6 CFRP perimeters starting $d/4$ away from the column face is required.

$s = d/2 = 57$ mm and first CFRP perimeter located $d/4$ from the column face.

Compute punching shear capacity outside the shear reinforced zone:

$$\bullet \text{Critical perimeter: } b_o = 4[304 + \sqrt{2}(3.25)(114)] = 3310 \text{ mm}$$

$$V_u = \frac{1}{3} \sqrt{f_c'} \left(\frac{10}{b_o/d} + \frac{1}{2} \right) b_o d = \frac{1}{3} \sqrt{28.3} \left(\frac{10}{3310/114} + \frac{1}{2} \right) (3310)(114) = 568 \text{ kN}$$

OK

4) Determine the vertical area of CFRP per hole:

- $V_{FRP} = V_u - V_c = 568 - \frac{1}{6}\sqrt{28.3}(1672)(114)(1/1000) = 400kN$

Area of CFRP per hole is given by:

$$A_{FRP} = \frac{V_{FRP}S}{d\beta f_{FRP}n} = \frac{400000}{2(1/3)(876)(8)} \approx 86mm^2 \text{ required.}$$

Experiment: Specimen (A6), $A_{FRP} = 89 \text{ mm}^2$ (average per hole), $V_u = 721 \text{ kN}$

5) Check V_{max} : $V_{max} = 4\left(\frac{1}{6}\right)\sqrt{28.3}[4(304 + 114)](114) = 676kN \quad \text{OK.}$

APPENDIX D

Derivation of Term “J” For Octagonal Perimeters

The shear stress distribution according to eccentric shear stress model for octagonal perimeters is given in Figure C.1

First the moment at centroid of the connection due to different components of shear stress is calculated. Then term J, analogous to polar moment of inertia, is computed as follows:

$$M_1 = v c_2 d \left(\frac{c_1}{2} + l_1 \right) 2$$

$$M_2 = \frac{1}{2} (v' + v) l_3 \bar{x} d 4$$

$$M_3 = \frac{1}{2} v' \frac{c_1}{2} d \left(\frac{2 c_1}{3} \right) d 4$$

$$M_4 = \frac{1}{2} v \frac{d}{2} \left(\frac{2 d}{3} \right) (c_1 + 2l_1) 4$$

$$\gamma_v M_u "c" = v J$$

$$\gamma_v M_u "c" = \left(\sum_{i=1}^3 M_i \right) (c_1 / 2 + l_1) + M_4 (d / 2)$$

$$J = 2 c_2 d (c_1 / 2 + l_1)^2 + 2 (r + 1) l_3 \bar{x} d (c_1 / 2 + l_1) + (1/3) c_1^2 d (r) (c_1 / 2 + l_1) + (1/6) d^3 (c_1 + 2l_1)$$

$$\frac{v'}{v} = r = \frac{c_1 / 2}{(c_1 / 2) + l_3}$$

$$\bar{x} = \frac{\{3 r l_3 + 2 (1 - r) l_3\} l_1}{3(1 + r) l_3} + \frac{c_1}{2}$$

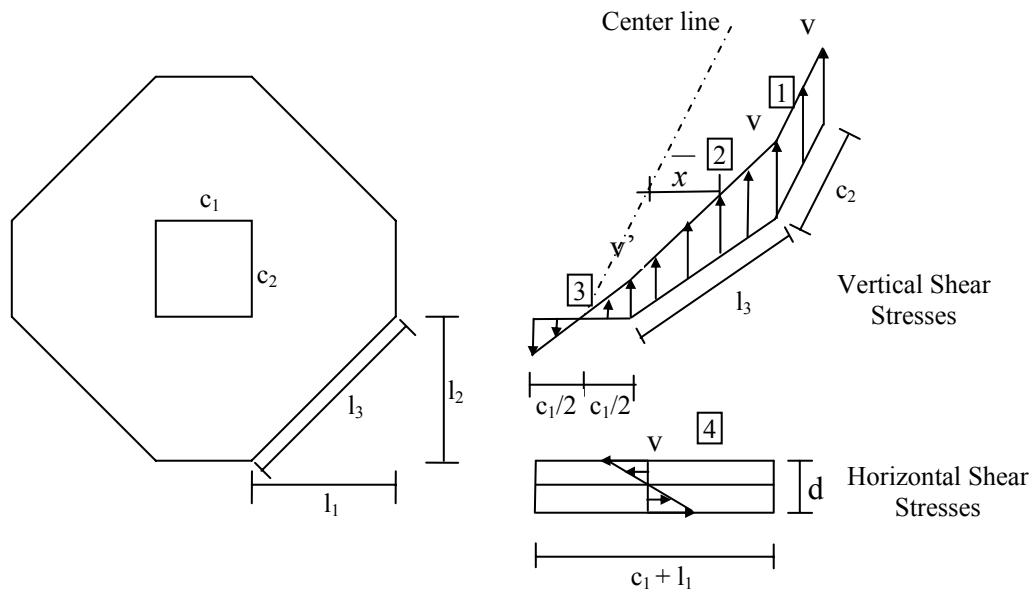


Figure D.1 Eccentric Shear Stress Model for Octagonal Perimeters

In order to recover J for rectangular critical perimeter constructed $d/2$ from the column face:

Set $l_3 = 0$, $l_1 = 0.5d$, $v' = v$

Replace c_2 with $(c_2 + d)$ (First term)

Replace $(c_1)^2$ with $(c_1 + d)^2$ (Third term)

$$J = 2(c_2 + d)d(c_1/2 + 0.5d)^2 + (1/3)(c_1 + d)^2 d(c_1/2 + 0.5d) + (1/6)d^3(c_1 + d)$$

$$J = (1/2)(c_2 + d)d(c_1 + d)^2 + (1/6)(c_1 + d)^3 d + (1/6)d^3(c_1 + d)$$

APPENDIX E

Design Example for Strengthening of Slab-Column Connections Subjected to Combined Shear and Unbalanced Moment

Given: Column size, $c_1 = c_2 = c = 400$ mm; Slab thickness, $h = 180$ mm; Concrete strength, $f'_c = 20$ MPa ; Effective slab depth, $d = 15$ cm ; $E_{FRP} = 71000$ MPa

Design Loads: $V_d = 150$ kN, $M_{un} = 250$ kN-m

Design: Determine the CFRP amount and pattern such that design shear and unbalanced moment can be safely carried according to proposed design procedure based on ACI 318-02 expressions.

- Existing punching shear capacity:

$$v_c = \frac{1}{3}\sqrt{f'_c} = \frac{1}{3}\sqrt{20} = 1.49 \text{ MPa}$$

$$J = \frac{d(c+d)^3}{6} + \frac{(c+d)d^3}{6} + \frac{d(c+d)^3}{2} = 0.0169 \text{ m}^4$$

$$v_u = \frac{V_u}{bd} + \frac{\gamma_v M_u}{(J/c')} = \frac{(150)(1E-3)}{4[0.4+0.15]0.15} + \frac{(0.4)(250)(1E-3)}{\left(\frac{0.0169}{(0.4+0.15)/2}\right)} = 2.08 \text{ MPa}$$

$v_u > v_c$ Strengthening is required.

- Compute maximum punching shear capacity

$$v_{c \max} = \frac{2}{3}\sqrt{f'_c} = 2.98 \text{ MPa}$$
 Retrofit using CFRPs as shear reinforcement is possible.

- Assume pattern A with 4 CFRP perimeters with spacing of CFRP equal to $d/2$. First CFRP stirrup located at a distance of $d/4$ away from the column face.

$l_1 = l_2 = 2.25 d = 0.34 m$ (Distance between the column face and the critical perimeter)

$$l_3 = \sqrt{2} l_1 = 0.48 m$$

$$\frac{v'}{v} = r = \frac{c_1}{c_1 + 2l_3} = \frac{0.4}{(0.4 + 2(0.48))} = 0.30$$

$$\bar{x} = \frac{\{3r l_3 + 2(1-r)l_3\}l_1}{3(1+r)l_3} + \frac{c_1}{2} = 0.40$$

$$\begin{aligned} J &= (1/2) c_2 d (c_1 + 2l_1)^2 + (r+1) l_3 \bar{x} d (c_1 + 2l_1) + \\ &\quad (1/6) c_1^2 d (r)(c_1 + 2l_1) + (1/6) d^3 (c_1 + 2l_1) \\ &= 0.035 + 0.04 + 1.25E - 3 + 6.075E - 3 = 0.076m^4 \end{aligned}$$

(Note that contributions of the last two terms in J expression are negligible.)

$$v_u = \frac{V_u}{b d} + \frac{\gamma_v M_u}{(J/c')} = \frac{1501E - 3}{4[0.4 + 0.48]0.15} + \frac{(0.4)2501E - 3}{\left(\frac{0.07}{(0.4/2 + 0.34)}\right)} = 0.99 MPa$$

$$v_c = \text{Min}\left(\frac{1}{3}\sqrt{20}, \left(\frac{10(0.15)}{4(0.4 + 0.48)} + \frac{1}{2}\right)\frac{1}{3}\sqrt{f'_c}\right) = 1.17 MPa$$

(Strength outside the shear reinforced zone is smaller than design shear stress)

- Compute amount of CFRP in order to avoid failure inside the shear reinforced zone.

Assume 8 CFRP legs per perimeter.

$$\begin{aligned} A_{FRP} &= \left(v_{req} - \frac{1}{4}\sqrt{f'_c}\right) / \left(\frac{0.004E_{FRP}m}{b_o s}\right) \\ &= \left(2.08 - \frac{1}{4}\sqrt{20}\right) / \left(\frac{0.004(71000)8}{4(0.4 + .15)(0.15/2)}\right) = 6.98E - 5 m^2 = 70 mm^2 \end{aligned}$$

Use diagonal strips in the outer perimeter. $A_{diagonal} \geq \frac{1}{2} A_{FRP}$; $A_{diagonal} = 35 mm^2$

REFERENCES

ACI Committee 318. (1963). "Building Code Requirements for Structural Concrete (ACI 318-63)." American Concrete Institute, Farmington Hills, Michigan.

ACI Committee 318. (1989). "Building Code Requirements for Structural Concrete (ACI 318-89)." American Concrete Institute, Farmington Hills, Michigan.

ACI Committee 318. (2002). "Building Code Requirements for Structural Concrete (ACI 318-02)." American Concrete Institute, Farmington Hills, Michigan.

ACI-ASCE Committee 421 (1999). "Shear Reinforcement in Slabs." Joint ACI-ASCE Committee 421.1R-99, 15 pp. Farmington Hills, Michigan.

ACI Committee 440. (2002). "Guide for the Design and Construction of Externally Bonded FRP Systems for Strengthening Concrete Structures." American Concrete Institute, Farmington Hills, Michigan.

ACI-ASCE Committee 326 (1962). "Shear and Diagonal Tension, Part 3, Slabs and Footings." ACI Journal Proceedings, V.59, No.3, pp 353-396

ACI SP-42 (1974). "Shear in Reinforced Concrete." Publication SP-42, American Concrete Institute, Detroit, Michigan.

Aghayere, A. O., and MacGregor J. O. (1990). "Tests of Reinforced Concrete Plates Under Combined In-Plane and Transverse Loads." *ACI Structural Journal*, Vol 87, No. 6.

Allen F., and Darvall, P. (1977). "Lateral Load Equivalent Frame." *ACI, Structural Journal Proceedings*, Vol 74. No.7.

American Society of Civil Engineers (2001). "ASCE 7-98 STANDARD-Minimum Design Loads for Buildings and Other Materials." ASCE, Reston, VA, 352 pp.

ANSYS (1998). "ANSYS 5.6 Theory Manual." Swanson Analysis Systems Inc.

Arduini, M., and Nanni, A. (1997). "Parametric Study of Beams with Externally Bonded FRP Reinforcement." *Struct. J., ACI*, 94(5), 493-501.

Barbosa, A.F. and Ribeiro, G.A. (1998). "Analysis of Reinforced Concrete Structures Using Ansys Concrete Model." *Computational Mechanics, New Trends and Applications*, Idelshon, S., Onate E., Dvorkin E. Editors, Barcelona, Spain.

Bauman, T. and Rüsç, H. (1970). "Versche zum Studium der Verdübelungswirkung dr Biegezugbewehrung eines Stahlbetonbalkens." *Deutcher Ausschuß für Stahlbeton, Heft 210, Ernst&Sohn*, pp. 43-83.

Bazant, Z.P. and Jirasek, M. (2002). "Nonlocal Integral Formulations of Plasticity and Damage: Survey of Progress." *ASCE, Journal of Engineering Mechanics*, Vol. 128, No. 11, November 2002, pp. 1119-1149.

Bazant, Z.P. and Planas, J. (1998). "Fracture and Size Effect in Concrete and Other Quasibrittle Materials." CRC Press, New York, USA, 616 pp.

Branson, D.E. (1965) "Instantaneous and Time-Dependent Deflections on Simple and Continuous Reinforced Concrete Beams." HPR Report No. 7, Part 1, Alabama Highway Department, pp. 1-78.

BS 8110-97 (1997). "Structural Use of Concrete." British Standard Institution, London.

Broms, C.E. (1990). "Punching of Flat Plates- A Question of Concrete Properties in Biaxial Compression and Size Effect." Struct. J., ACI, 87(3), 292-304.

Broms, C.E. (1990), "Shear Reinforcement For Deflection Ductility of Flat Plates." Vol 87, No.6.

Broms, C.E. (2000). "Elimination of Flat Plate Punching Failure Mode." Struct. J., ACI, 97(1), 94-101.

CEB Bulletin. (1985). "Punching Shear in Reinforced Concrete-State of the Art Report." No.168, The International Federation for Structural Concrete, Comitte Lausanne, Switzerland.

CEB-FIP. (1990). "Model Code 1990." Bulletin D'Information No. 203-305, The International Federation for Structural Concrete, Lausanne, Switzerland.

CEB FIP Bulletin. (2001). "Punching of Structural Concrete Slabs." No. 12, Technical Report, 314 pages, The International Federation for Structural Concrete, Lausanne, Switzerland.

Chen, J.F. and Teng, J.G. (2001). "Anchorage Strength Models for FRP and Steel Plates Bonded to Concrete." ASCE, Journal of Structural Engineering, Vol. 127. No.7, pp 784-791.

Chen, B. and Mau, S.T., (1989). "Recalibration of a Plastic Fracturing Model for Concrete Confinement." Cement and Concrete Research 19, pp. 143-154.

Collins, M.P. and Mitchell D. (1990) "Reinforced and Prestressed Concrete Structures." Routledge Publications, 784 pp.

Corley, W. G. and Hawkins, N.M. (1968). "Shearhead Reinforcement for Slabs." ACI Structural Journal Proceedings, Vol.65, No.10.

Corley, G.W. and Jirsa O.J. (1970). "Equivalent Frame Analysis for Slab Design." ACI Journal Proceedings, 67(11), 876-884.

Criswell, M.E. (1974). "Static and Dynamic Response of Reinforced Concrete Slab-Column Connections." ACI Publication SP-42, Shear in Reinforced Concrete, 721-746.

Criswell, M.E. and Hawkins N. W. (1974). "Shear Strength of Slabs: Basic Principle and Their Relation to Current Methods of Analysis." ACI Publication SP-42, Shear in Reinforced Concrete, 641-676.

CSA (1994). "Design of Concrete Structures." Standard CSA-23.3-94, Canadian Standards Association, Rexdale, Ontario, Canada.

Di Stasio, J. S. and Van Buren, M.P. (1960). "Transfer of Bending Moment Between Flat Plate Floor and Column." ACI, Journal Proceedings, Vol.57, No.3, pp299-314.

Durrani, A.J., Du., Y., Luo., Y.H. (1995). "Seismic Resistance of Non-ductile Slab-Column Connections in Existing Flat-Slab Buildings." ACI, Structural Journal, Vol.92. No.4.

Ebead U., Marzouk H. (2002). "Strengthening of Two-Way Slabs Using Steel Plates." Struct. J., ACI, 99(1), 23-31.

Elstner, R.C. and Hognestad, E. (1956). "Shearing Strength of Reinforced Concrete Slabs." ACI, Struct. J., 53(7), 29-59.

Farhey, D.N., Adin, M.A., Yankelevsy, D.Z. (1995). "Repaired RC Flat Slab-Column Connection Subassemblages under Lateral Loading." J. of Struct. Eng., ASCE, 121(11), 1710-1720.

Feenstra, P.H. and De Borst R. (1996). "A Composite Plasticity Model for Concrete." International Journal of Solids and Structures, Vol.33, No.5, pp. 707-730.

Gardner N.J., Huh J., Chung L. (2002) "Lessons from Sampoong Department Store Collapse." Cement and Concrete Composites, 24(2), 523-529.

Grace, N.F., Soliman, A.K., Abdel-Sayed, G, Saleh, K.R. (1999). "Strengthening of Continuous Beams Using Fiber Reinforced Polymer Laminates." ACI Special Publication, SP-188-57.

Gomes, R.B. and Regan, P.E. (1999). "Punching Resistance of RC Flat Slabs with Shear Reinforcement." ASCE, Journal of Structural Engineering, Vol. 125, No. 6, June 1999, pp. 684-692

Hallgren, M. (1996). "Punching Shear Capacity of Reinforced High Strength Concrete Beams without Stirrups." Doctoral Thesis, KTH Stockholm, TRITA-BKN, Bull. Royal Institute of Technology.

Hamadi, Y.D. and Regan, P.E. (1980). "Behavior in Shear of Beams with Flexural Cracks." Magazine of Concrete Research, Vol.32, No.111, pp. 71-78

Han, D.J. and Chen, W.F. (1988). "Plasticity for Structural Engineers." Springer-Verlag, Virginia, USA.

Hassanzadeh G. and Sundqvist H. (1998). "Strengthening of Bridge Slabs on Columns." Nordic Concrete Research 1/1998, No. 21.

Hawkins N. W. (1974). "Shear Strength of Slabs with Shear Reinforcement." ACI Publication SP-42, Shear in Reinforced Concrete, 785-816.

Ghali, A. and Hammil, N. (1992). "Effectiveness of Shear Reinforcement in Slabs." ACI, Concrete International, Vol.14, Issue 1.

Hemmaty Y. (1998) "Modeling of the Shear Force Transferred between Cracks in Reinforced and Fibre Reinforced Concrete Structures." ANSYS Conference, Pittsburg, PA, 1998.

Hwang, S.J. and Moehle, J. P. (1993). "An Experimental Study of Flat Plate Structures Under Vertical and Lateral Loads." Report No. UCB/EERC-93/03, Department of Civil Engineering, University of California at Berkeley.

ISIS CANADA (2001). "Strengthening Reinforced Concrete Structures with Externally-Bonded Fibre Reinforced Polymers." ISIS-M05-00, Spring 2001.

Islam, S. and Park, R. (1976). "Tests on Slab-Column Connections with Shear and Unbalanced Flexure." ASCE Journal of Structural Division, V.102, No.3, pp549-568

JSCE (1997), "Recommendation for design and construction of concrete structures using continuous fiber reinforcing materials", Concrete Engineering Series 23, Ed. A. Machida, Research Committee on Continuous Fibre Reinforcing Materials, Japan Society of Civil Engineers, Japan, 325 p.

Kachalev. D. "Finite Element Modeling of Reinforced Concrete Structures Strengthened with FRP Laminates." Oregon Department of Transportation, Research Report, SPR 316.

Karabinis, A. I. and Rousakis, T.C. (2002) "Concrete Confined by FRP Material: A Plasticity Approach." Engineering Structures, 24, pp. 923-932.

Kinnunen, S. and Nylander, H. (1960). "Punching of Concrete Slabs without Shear Reinforcement." Transaction, Royal Institute of Technology, Stockholm, No.158.

Kupfer, H., Hilsdorf, H.K., Rusch, H. (1969). "Behavior of Concrete Under Biaxial Stresses." ACI Journal, 66(8), pp. 656-666.

Lou., Y.H., and Durrani, A.J., (1995). "Equivalent Beam Model for Flat-Slab Buildings-Part I: Interior Connections." ACI Structural Journal, Vol. 92, No.1, pp. 115-124.

Maeda, T., Asano, Y., Sat, Y., Ueda, T., Kakuta, Y. (1998). "A Study on Bond Mechanism of Carbon Fiber Sheet." Non Metallic (FRP) Reinforcement for Concrete Structures Proceedings, Third international Symposium, JCI, Sappora, pp 279-285.

Malek, A.M., and Saasatmanesh, H. (1998). "Ultimate Shear Capacity of Reinforced Concrete Beams Strengthened with Web-Bonded Fiber-Reinforced Plastic Plates." ACI Struct. J., ACI, 95(4), 343-352.

Martines-Cruzoda, J.A., Qaisrani, A.N., Moehle, J.P. (1994). "Post-Tensioned Flat Plate Slab-Column Connections Subjected to Earthquake Loading" Proceedings, Fifth U.S. National Conference on Earthquake Engineering, Vol. 2, Chicago, Illinois, pp.139-148.

Megally, S. H. and Ghali, A. (1995). "Design Considerations for Slab-Column Connections in Seismic Zones." ACI Structural Journal, Vol.91, Issue 3.

Megally, S. H. (1998). "Punching Shear Resistance of concrete Slabs to Gravity and Earthquake Forces." Ph.D. Dissertation, University of Calgary.

Menetrey P. (1996). "Analytical Computation of the Punching Strength of Reinforced Concrete." Struct. J, ACI, 93(5), 503-501.

Mitchell, D., and Cook, W.D., (1984). "Preventing Progressive Collapse of Slab Structures." ASCE, Journal of Structural Engineering, Vol. 110, No. 7, July 1984, pp. 1513-1532

Mitchell, D., Tinawi, R. and Redwood, R.G. (1990) "Damage to Buildings due to the 1989 Loma Prieta Earthquake-a Canadian Code Perspective." Canadian Journal of Civil Engineering, V.17, No.10, pp 813-834

Mitchell, D., DeVall, R. H., Saatcioglu, M., Simpson, R., Tinawi, R., and Tremblay, R. (1995). "Damage to Concrete Structures due to the 1994 Northridge Earthquake." Canadian Journal of Civil Engineering, V.22, No.4, pp-361-377

Mirmiran, A., Zagers, K., Yuan, W. (2000). "Nonlinear finite element modeling of Concrete Confined by Fiber Composites", Finite Element in Analysis and Design, Vol. 35, pp. 79-96.

Moe J. (1961). "Shearing Strength of Reinforced Concrete Slabs and Footings under Concentrated Loads." Development Department Bulletin D 47, PCA Research and Development Laboratories, Illinois, 130 pp.

Moehle, J.P., Kreger, M.E., Leon, R. (1988). "Background to Recommendations for Design of Reinforced Concrete Slab-Column Connections." ACI Structural Journal. Vol. 85, No. 6, pp. 636-644

Moehle, J.P. and Diebold, J.W. (1984). "Experimental Study of the Seismic Response of a Two Story Flat-Plate Structure." Report No. UCB/EERC-84/08. College of Engineering, University of California at Berkeley.

Mokhtar, A.S., Ghali, A., Dilger, W. (1982). "Stud Shear Reinforcement for Flat Concrete Plates." ACI Journal Proceedings, Vol.82, No.5.

Morrison, D. G., Hirasaga, L. and Sozen, M.A. (1983). "Lateral-Load Tests of R/C Slab-Column Connections." ASCE Journal of Structural Division, V.109, No.11, 2698-2714.

Mosallam A., Kreiner J., Lancey T., Haroun M., Elsanadedy H. (2000). "Experimental and Numerical Analysis of Two-Way Concrete Slabs Repaired with Polymer Composites." ACUN-2 International Composites Conference, Sydney, Australia, February 14-18, 2000.

Mosallam, A.S. and Mosalam, K.M. (2003). "Strengthening of Two-way Concrete Slabs with FRP Composite Laminates." Construction and Building Materials, 17(1), 43-54

Mörsch, E. (1909). "Concrete-Steel Construction." McGraw-Hill Book Company, New York, 368 pp.

NZS 3101 (1995). "Concrete Structures Standard Part 1-The Design of Concrete Structures." Standards, Wellington, New Zealand, 1995.

Oliveria D.R., Melo, S.R., Regan, P.E. (2000). "Punching Strengths of Flat Plates with Vertical or Inclined Stirrups." Struct. J, ACI, 97(3), 485-491.

Owen, D.R.J. and Figueiras, J.A. (1984). "Ultimate Load Analysis of Reinforced Concrete Plates and Shells Including Geometric Nonlinearities." in Finite Element Software for Plates and Shells, Editors, Hinton, E., Owen D.R.J., Pineridge Press, Swansea, UK.

Pan., A. and Meohle., J.P. (1988). "Reinforced Concrete Flat Plates under Lateral Loading: An Experimental Study Including Biaxial Effects." Report No. UCB/EERC-88/16. College of Engineering, University of Californai at Berkeley.

Pecknold, D.A. "Slab Effective Width for Equivalent Frame Analysis." ACI Structural Journal Proceedings, Vol. 72, No.4.

Regan, P.E. (1984). "The Dependence of Punching Resistance upon the Geometry of the Failure Surface." Magazine of Concrete Research, V.6, No. 126, 3-8.

Reddy J. N. (1998). "Theory and Analysis of Elastic Plates." Taylor and Francis, Philedelphia, USA, 540 pp.

Rosenblueth, E. and Meli, R(1986). "The 1985 Earthquake: Causes and Effects in Mexico City." Concrete International: Design&Construction, V.8, No.5, pp-23-34

Seible F., Ghali, A., Dilger, W. H. (1980) "Preassembled Shear Reinforcing Units for Flat Plates." *ACI Journal Proc.*, 77(1), 28-35.

Shehata, I.A.M. and Regan, P.E. (1989). "Punching in R.C Slabs." *Journal of Struct. Eng.*, ASCE, 115(7), 1726-1740.

Talbot, A. N. (1913). "Reinforced Concrete Wall Footings and Column Footings." *Bulletin No.67*, University of Illinois, Engineering Experiment Station.

Taljsten B. (1997). "Defining Anchor Lengths of Steel and CFRP Plates Bonded to Concrete." *International Journal of Adhesion and Adhesives*, 17(4), 319-327

Theodorakopoulos, D. D. and Swamy R. N. (2002) "Ultimate Punching Shear Strength Analysis of Slab-Column Connections." *Cement and Concrete Composites*, V.24, pp 509-521.

Triantafillou, T.C. and Deskovic, N. (1992). "Innovative Prestressing with FRP Sheets: Mechanics of Short Term Behavior." *ASCE, Journal of Engineering Mechanics*, Vol. 117. No.7, pp. 1652-1672.

Triantafillou, T.C. (1998). "Shear Strengthening of Reinforced Concrete Beams Using Epoxy-Bonded FRP Composites." *Struct. J.*, ACI, 95(2), 107-115.

Stark, A. (2003). "Seismic Upgrade of Slab-Column Connections Using Fiber Reinforced Polymers." *M.Sc. Thesis*, University of Texas at Austin, August 2003.

Xiao, R.Y., and O'Flaherty, T. (2000). "Finite-element Analysis of Tested Concrete Connections." *Computers and Structures*, Vol.78, No. 1-3, pp. 247-255.

Willam, K.J. and Warnke, E.P. (1975). "Constitutive Model for the Triaxial Behavior of Concrete." International Association of Bridge and Structural Engineers, Seminar on Concrete Structures Subjected to Triaxial Stresses, Paper III-1, Bergamo, Italy, May, 194, IABSE Proceedings 19.

Zee, H.L. and Moehle J.P. (1984). "Behavior of Interior and Exterior Flat Plate Connections Subjected to Inelastic Load Reversals." Report No. UCB/EERC-84/07, Earthquake Engineering Research Center, university of California at Berkeley, August, 130 pp.

Zhang, W.J., Teng, J.G., Wong, Y.L., and Lu, .T. (2001). "Behavior of Two-Way RC Slabs Externally Bonded with Steel Plate." J. of Struct. Eng., ASCE, 127(4), 390-397.

VITA

Baris Binici was born on September 23, 1976 in Ankara, Turkey, the son of A. Rahmi Binici and Nihal Binici. He graduated from Ataturk Anatolian High School in June 1994 and entered Department of Civil Engineering of Middle East Technical University, Ankara, Turkey. He graduated from Middle East Technical University with the degree of Bachelor of Science. In August 1998, Mr. Binici entered the Graduate School of the University of Texas at Austin. After earning his Master of Engineering Degree in Civil Engineering Department at The University of Texas at Austin (1999, December), he joined the Ph.D Program in Civil Engineering Department at The University of Texas at Austin. His current research interests include mechanics of reinforced concrete and use of fiber reinforced polymers in upgrade of reinforced concrete structures.

Permanent Address: Birlik Mahallesi
2. Cadde 16. Sokak 6/5
Cankaya Ankara

This dissertation was typed by the author.